AN EXPERIMENTAL INVESTIGATION OF A LIQUID FILM ON A HORIZONTAL FLAT PLATE IN A SUPERSONIC GAS STREAM

By

BILLY WAYNE MARSHALL

Bachelor of Science
Louisiana State University
Baton Rouge, Louisiana
1958

Master of Science
University of Missouri at Rolla
Rolla, Missouri
1961

Submitted to the Faculty of the
Graduate College of the
Oklahoma State University
in partial fulfillment of
the requirements for
the Degree of
DOCTOR OF PHILOSOPHY
May, 1971

AN EXPERIMENTAL INVESTIGATION OF A LIQUID FILM ON A HORIZONTAL FLAT PLATE IN A SUPERSONIC GAS STREAM

Thesis Approved:

W. A. Tiederman, Jr.
Thesis Adviser

Paul A. McClaran

J. A. Weibelt

W. B. Brooks

O. D. Durham
Dean of the Graduate College

PREFACE

This research is directed to an investigation of the characteristics of the interface waves formed on a liquid adjacent to the supersonic gas flow created in a hypersonic wind tunnel. These characteristics--the wave speed, wavelength, and the spectral density of the amplitude fluctuation (frequency spectra) of the waves--are correlated as a function of the liquid Reynolds number and thickness for gas Mach numbers of 5 and 7.3. The frequency spectra are calculated by a Fourier analysis of the transient interface wave profile which was measured by a depth gauge mounted in the model surface.

The correlation of the characteristics at each tunnel condition is accomplished by fitting the experimental data to a response surface model with the liquid Reynolds number and thickness as independent parameters. The measured mean wavenumber data are compared for low liquid Reynolds numbers with the results of a linear stability analysis in which an inviscid, supersonic gas flows over a thin, viscous liquid film.

The members of a student's advisory committee provide the essential guidance and encouragement which are necessary for the successful completion of a research project. This is particularly true for this research since the actual experiments were conducted at a location remote from the university campus. My committee, with Dr. John Wiebelt as Chairman, was particularly helpful in this respect. Dr. William G. Tiederman served as the major advisor for the research and provided

extensive guidance and numerous suggestions throughout the entire experimental program. His timely reviews of and comments on the periodic progress reports and initial drafts of the dissertation were also appreciated. Dr. William B. Brooks also provided many helpful suggestions in the formulation of the experiments, and in particular, provided ideas on the design and modifications of the wind tunnel model. Dr. Paul A. McCollum suggested the use of the Fourier analysis which was utilized to calculate the wave frequency spectra and these data provided a significant part of the data reduction.

The experiments were conducted with the support of personnel at Sandia Laboratories in Albuquerque, New Mexico and the research was supported by the United States Atomic Energy Commission. The assistance of the personnel who operate the hypersonic wind tunnel is greatly appreciated. The support and cooperation of Dr. William S. Saric of the Aerofluids Research Department at Sandia are also acknowledged.

Finally, I would like to acknowledge the encouragement, understanding, and sacrifice of my family. Without their assistance and in particular that of my wife, Barbara, who also provided the typing, none of this would have been possible.

TABLE OF CONTENTS

LIST OF TABLES

LIST OF FIGURES

CHAPTER I

INTRODUCTION

There is a long standing scientific interest in waves which appear on the interface of a liquid interacting with an external gas flow. This interest has varied from Kelvin's (1910) study of wave generation on large bodies of water to Chapman and Larson's (1963) discussion of waves on small, originally spherical, glassy objects called tektites. These tektites have been recovered after hypersonic entry into the earth's atmosphere from space. The research reported in this thesis is an experimental investigation of the interface of a liquid film adjacent to a supersonic gas stream and is similar in that respect to the waves on the tektite. In these experiments a blunt, zero-degree wedge with a porous nose tip through which liquid flowed onto the model surface was exposed to Mach 5 and Mach 7.3 gas flows in a hypersonic wind tunnel. The liquid Reynolds number and thickness were varied and the interface wave data was correlated as a function of these liquid parameters.

Practical applications of waves on thin liquid layers adjacent to a supersonic gas flow are generally limited to the entry of objects into the atmosphere at supersonic velocities. Because of the extreme kinetic energy which these objects possess, intense frictional heating is generated and in many cases the objects reach a molten state as in the case of the tektites. The interaction of the molten liquid interface

with the gas flow about the object gives rise to waves on the surface which may grow until debris is stripped from the melt layer. This stripping process is envisioned to be related, in its initial stages at least, to the surface waves formed by the adjacent gas flow. In the event toxic or perhaps radioactive material is involved, the debris size is of particular importance due to its potential fallout onto the earth's surface. The size is thought to be related to the wave characteristics. Interface waves are also of interest for transpiration cooling systems which have been suggested as a means of providing protection for objects during reentry. The principle of operation for these systems is to envelope that portion of the body which is exposed to the severe heating with a liquid film and the technique is most effective when the liquid is not stripped from the body by forces exerted on the liquid by the gas. Again the initial stages of stripping--the removal of mass from the interface in discrete, particulate form--are the waves which appear on the interface.

Of more fundamental interest is an understanding of how the waves which are formed on a liquid interface adjacent to a supersonic gas flow depend on the parameters which characterize the flow. In particular one is interested in knowing the combinations of liquid and gas parameters such as liquid Reynolds number, shear stress, gas Mach number and liquid film thickness for which waves are present on the interface. The dependency of the wave speed, wavelength, and wave frequency on these parameters is also of interest.

The waves on a liquid film are described by the dynamic response of the interface. The analytical study of this dynamic response leads directly to the use of hydrodynamic stability techniques. These

techniques are used to define the regions of stable and unstable behavior of a fluid flow system and to identify the sources of any instabilities. The instabilities evidence themselves as disturbances on the interface which amplify until at some point they become visible as finite amplitude waves.

In a complete analysis the stability of both the liquid and the gas must be considered and the motion of the fluids must satisfy the momentum and the continuity equations. For the simplest case when an infinitesimal two-dimensional disturbance is superimposed onto a parallel flow, the resulting linearized equation for the disturbance in each of the fluids is a fourth-order differential equation. Therefore for the two fluids two fourth-order differential equations and eight boundary conditions and coupling relationships are necessary to completely formulate the problem.

Because of the mathematical complexity of solving this complete system, liquid film stability analyses have been formulated by partially uncoupling the two equations and considering only the stability equations for the liquid. As a result of this uncoupling, the assumption that the velocity components are continuous across the interface is not satisfied and no consideration is given to the stability of the external gas.

There are several linear stability analyses which are related to the problem investigated in this research. Craik (1966) considered the stability of a thin liquid film and included as boundary conditions the expressions derived by Benjamin (1959) for the perturbations in the shear stress and pressure exerted by a subsonic gas flow over the liquid. These perturbations result from the infinitesimal waves which

are assumed to exist on the liquid interface. Miles (1960) considered the stability of a thin film in uniform shear flow. The only effect of the external gas was to produce the mean liquid motion. No perturbation effects in either the gas shear stress or pressure were included in his analysis. Chang and Russell (1965) and Nachtsheim (1970) both considered the stability of a liquid film with an inviscid, supersonic gas flow over the interface. The instability of the liquid resulted from the interaction of the supersonic gas flow with the waves on the interface. The interaction produced a perturbation of the gas pressure and caused a supersonic wave drag to be exerted on the interface. Nayfeh and Saric (1970) also considered the same problem with the addition of a body force oriented at an arbitrary angle to the interface.

However for a viscous, supersonic, external gas precise expressions for the shear stress and pressure perturbations are not known. Because of this inability to specify the complete boundary conditions, the stability analysis for a viscous, supersonic gas flow over a thin film of liquid has not been completed even for the uncoupled formulation of the problem.

Because the precise boundary conditions for the analytical formulation are unknown, the problem has been attacked herein as an experimental investigation. The specific objectives of the experiments were: 1) to characterize the response of a liquid film interface adjacent to an external supersonic gas flow, and 2) to study the dependence of the interface wave properties on the liquid thickness and Reynolds number and on the Mach number and shear stress exerted by the gas on the liquid.

The experiments were conducted in the eighteen inch hypersonic wind tunnel at Sandia Laboratories in Albuquerque, New Mexico. The wind tunnel was operated at three test conditions; two pressures at a free stream Mach number of 5 and one at Mach 7.3. A blunt, zero-degree wedge twelve inches long and six inches wide was used as the test model. A one inch diameter cylindrical nose tip with a 75 degree arc of the cylinder made of porous stainless steel was attached to the front of the model. During an experiment the liquid was forced out of the porous segment by a high pressure expulsion system and was swept back over the model by the forces exerted by the supersonic gas flow.

The data which were observed for the experiments are the mean wave speed, the mean wavelength, the type and shape of the wave, and the frequency spectra of the waves. The interface was photographed with a high speed camera and the wave speed and wavelength data were measured from the movie film.

To measure the frequency spectra of the interface waves, a depth gauge was developed and mounted in the model surface. This gauge measured the instantaneous height of the liquid film by measuring the change in the gauge capacitance as the liquid thickness over the gauge varied. This general technique has been utilized previously to measure the thickness of thin liquid films. However the two specific applications reported by Rogovaya, Olevskii, and Runova (1966) and by Plate, Chang, and Hidy (1969) were unacceptable for these experiments since both would have resulted in a portion of the gauge being located in the supersonic gas flow where it would have created severe disturbances.

The principle utilized in the sensor employed in these experiments is that of an end-effect capacitance variation. The two elements of

the gauge are separated by a 0.002 inch thickness of glass. This small spacing of the sensing elements permitted the gauge to trace the profiles of the individual interface waves. The two Kovar sensing elements were connected to a capacitance bridge circuit which converted the thickness of the liquid above the sensing elements into a voltage for subsequent data analysis. The gauge, mounted with its sensing elements level with the plate surface, was positioned three inches behind the nose tip on the centerline of the model. The output of the capacitance bridge circuit was recorded on an FM tape recorder and the data subsequently digitized and Fourier analyzed to determine the frequency spectra.

As stated previously the objectives of the experiments were to examine the interface wave characteristics as a function of the liquid Reynolds number, the liquid thickness, the gas shear stress, and the free-stream gas Mach number. For a constant gas shear stress condition, the liquid Reynolds number and thickness may be varied independently by control of the liquid viscosity and flow rate. A two by two factorial design with a center point offers a very effective method of selecting the liquid conditions which produce the variation of the liquid Reynolds number and thickness for each gas condition. For the factorial design two levels of Reynolds number and two levels of thickness form the corner points and an intermediate third level of both of the parameters creates the center point. This technique was utilized to select the liquid flow rate and viscosity for five experiments at each gas condition. However because of differences between the anticipated liquid viscosity and that measured for the actual liquid test temperatures and because of uncertainties in the calculated gas shear

stress, the resulting Reynolds number-thickness combinations did not produce the desired factorial design. Therefore the data from these five experiments were combined with that from ten additional experiments at different Reynolds number-thickness combinations at each gas condition and the data for all fifteen experiments were interpreted by using a quadratic response surface model with the Reynolds number and thickness as the independent parameters.

To extend the data and include the effects of independently varying the gas shear stress and Mach number, two levels of shear stress at each of the two levels of Mach number are required. Because of the limitations in the wind tunnel operating range, this complete variation in shear stress and Mach number was not possible and only three gas conditions were utilized. However two different pressure levels at a free stream Mach number of 5 produced two levels of shear stress for constant free stream Mach number. The third gas condition was a Mach 7.3 flow and this condition produced a calculated shear stress level essentially equal to that of the low pressure Mach 5 condition. Consequently, two levels of the free stream Mach number at the lower level of shear were produced. However the higher shear level at the Mach 7.3 condition is not attainable in the facility and as a result the factorial design for the two gas conditions is incomplete. The data are therefore analyzed by considering the effects of the two liquid parameters at each of the three gas conditions. The effects of the different gas conditions are evaluated by comparing data at similar liquid conditions.

Glycerin-water mixtures ranging from 100 percent water to 100 percent glycerin were employed for variation of the fluid viscosity. For

each particular fluid two or three different flow rates were utilized and provided the fifteen tests at each gas condition. The liquid Reynolds number, defined using the flow rate and the liquid viscosity, varied from 0.22 to approximately 360 and the liquid film thickness varied from 0.003 inches to 0.016 inches.

A smooth liquid is not observed at any of the test conditions. For a fixed gas condition the general appearance of the waves on the interface is primarily affected by the magnitude of the liquid Reynolds number. At low Reynolds numbers (near 1 and below) relatively small, three-dimensional, horseshoe-shaped waves are observed. At moderate Reynolds numbers (near 100) the waves are larger and extend for some distance across the model surface. However the shape remains three-dimensional and many different wave sizes are observed. At the highest Reynolds number (>300), the interface appearance is one of intense agitation with the wave speed data difficult and in some cases impossible to obtain. Each of the three gas conditions results in an interface appearance similar to the above. However, for the high pressure (and resulting high shear) Mach 5 gas condition, the surface becomes totally irregular at lower Reynolds numbers than for the other two low shear gas conditions.

The results of the experiments are interpreted by considering the variation of the wave speed, wavelength, and frequency spectra for each of the three gas conditions. At each gas condition the data are fit to a response surface model with the liquid Reynolds number and thickness included as independent parameters. For two gas conditions the model is quadratic and for the third gas condition the model is linear. The logarithm of the Reynolds number is used in both models. By using the

response model technique, the effects of the Reynolds number and thickness are evaluated independently for each of the gas conditions. A comparison of the data for the different gas conditions at similar liquid conditions provides an evaluation of the effects of the gas shear stress and Mach number. The results are summarized in the remainder of this chapter.

At each of the gas conditions, the dimensional mean wave speed depends on both the thickness and the Reynolds number. At the high shear Mach 5 condition, the limited data do not permit as extensive an interpretation as for the other conditions. However the conclusion is made that the wave speed increases with Reynolds number in a manner similar to the increase of wave speed with Reynolds number at the low shear Mach 5 and the Mach 7 conditions. The effect of liquid thickness is not as consistent in that the wave speed decreases with increasing thickness at some Reynolds number values and increases for others. The wave speeds for the Mach 7 and the low shear Mach 5 conditions are not sufficiently different at equivalent liquid conditions to permit a conclusion on which of the two produces higher wave speeds. The wave speeds at the high shear Mach 5 condition are higher than those for the other two conditions.

The dimensionless mean wave speed, formed by normalizing the mean wave speed with twice the mass average liquid velocity, also depends on both the liquid thickness and Reynolds number for each gas condition. The dimensionless speed decreases with increasing Reynolds numbers and for Reynolds numbers above 100 at the Mach 7 condition, the value is less than one. At all other liquid conditions it is larger than one. For a linear velocity profile in the liquid a dimensionless wave speed

value less than one means that the waves are traveling slower than the liquid interface. Similarly a value greater than one means that the waves are traveling faster than the interface.

The mean wavelength also depends on both liquid parameters for the Mach 7 and the low shear Mach 5 conditions. These data were not obtained for the other gas condition. The wavelength increases with Reynolds numbers and reflects the greater distance between the larger waves which occur at the higher Reynolds numbers. The waves also appear to possess larger amplitudes at the higher Reynolds numbers. The waves are always irregularly spaced on the interface and the mean value reflects an average spacing.

The frequency spectra data provide a description of the wave frequencies as a function of the liquid and gas parameters. At all conditions the Fourier analysis of the depth gauge output reveals the presence of a band of frequencies. The results of the analysis are shown qualitatively in Figure 1. At any particular liquid Reynolds number, waves are observed for a range of frequencies and the range is bounded by upper and lower cutoff values. Linear stability analyses of an inviscid supersonic gas flow over a viscous liquid film (viz. Nayfeh and Saric (1970)) predict unstable behavior for waves whose wavenumbers are between two cutoff values. The analyses therefore predict a range of unstable waves which have different wave speeds and wavelengths. Consequently a range of wave frequencies such as that measured in these experiments and illustrated by Figure 1 is qualitatively consistent with the results of the linear analyses. The band of wave frequencies measured in the experiments is the result one would expect if the waves on the interface were unequally spaced, possessed different propagation

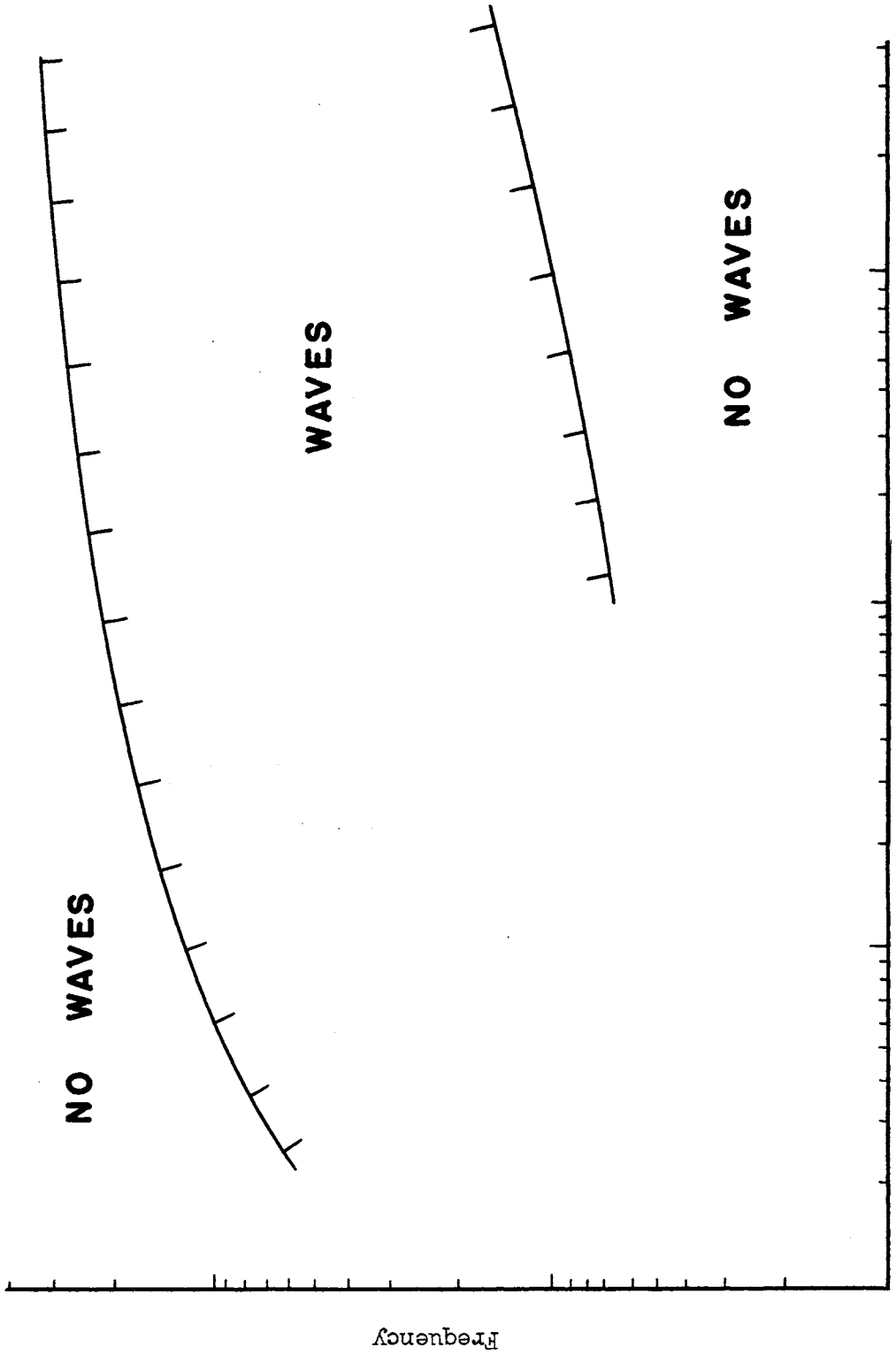

Figure 1. Illustration of Wave Frequency Band

velocities, and varied in size and amplitude. From a study of the photographic film, these characteristics are found to be descriptive of the waves.

The upper cutoff frequency in each band increases with increasing Reynolds number at each of the three gas conditions. Further this upper cutoff occurs at higher frequencies for the high shear Mach 5 condition than for the other two gas conditions. For the high shear Mach 5 condition, the cutoff occurs near 400 Hertz and for the other two gas conditions the cutoff is near 225 Hertz. The higher frequencies at the high shear condition reflect the more agitated state of the liquid.

At all test conditions the spectra data reveal the presence of a dominant wave frequency within the frequency band. The dominant frequency is dependent on both the thickness and Reynolds number of the liquid and increases with increasing Reynolds number at each gas condition. At similar liquid conditions the peak frequency occurs at higher values for the high shear Mach 5 gas condition than for the remaining gas conditions. This is consistent with higher wave speeds observed at the high shear condition. The data for the low shear Mach 5 and the Mach 7 gas conditions are inconclusive on the matter of which results in higher dominant frequencies at similar liquid conditions.

Comparison of the measured wavenumber data with the results of calculations using the linear stability model of Nayfeh and Saric (1970) shows that for low Reynolds number the observed wavenumbers are larger than the predicted lower cutoff wavenumbers. Therefore the waves are disturbances which according to the linear analysis are unstable and

consequently the results from the linear analysis are consistent with these experimental results.

The effect of the higher shear at the high shear Mach 5 gas condition is apparent in all of the data. Higher wave speeds, higher dominant wave frequencies and higher values of the upper cutoff on the frequency band occur for this gas condition than for the other two conditions. In contrast the data for the low shear Mach 5 and the Mach 7 gas conditions are not consistently different at similar liquid conditions. At some liquid conditions the wave speed and frequency data for the Mach 7 condition are greater than the corresponding values for the low shear Mach 5 condition while at other conditions the opposite is true. In addition, 80 percent confidence intervals on predicted data for either of the two conditions includes in most cases the predicted values for the other condition. Since the calculated shear stress is similar for the two gas conditions and the free stream Mach numbers are different, the data suggest that the Mach number does not play a significant role in determining the wave characteristics whereas the shear stress does. However calculations indicate that the Mach numbers at the edge of the boundary layer are equal for all three gas conditions and since the Mach number near the liquid interface rather than that in the free stream may be the controlling influence, no conclusions regarding Mach number effects can be stated.

A description of the test apparatus including the model, the wind tunnel, and the data acquisition systems is presented in Chapter II. Also given are the gas and the liquid test conditions. In Chapter III the mean wave data measured from the photographs are discussed in detail. The mean dimensional wave speed, the mean dimensionless wave

speed, and the mean wavelength data are presented in tabular and graphic form and the data are analyzed to examine their dependency on the liquid parameters and the gas conditions. The dominant wave frequency data and the frequency band data are presented and analyzed in Chapter IV. In Chapter V the data are compared with some results of a linear stability analysis and with other experiments. Finally in Chapter VI a summary of the experiments as well as the conclusions from the data and some recommendations for additional research are presented. For the readers who are interested in the results and conclusions from the research without going into a description of the experiments and the details of the data analysis, a review of Chapter VI should be sufficient.

CHAPTER II

DESCRIPTION OF EXPERIMENTS

Test Facility

The experiments were conducted in the hypersonic wind tunnel at Sandia Laboratories in Albuquerque, New Mexico. The test section of the tunnel is eighteen inches in diameter and is sufficient to provide a uniform flow field over the model sizes used. The tunnel is a pebble bed heated, intermittent, blowdown-to-vacuum type operated with air and has a 48-inch long test section. The facility is designed such that one of six different contoured nozzles may be selected to produce the particular Mach number flow desired. For these experiments the tunnel was operated at Mach numbers of 5 and 7.3. Test times were limited to approximately 45 seconds with one test per hour possible. Facility operating parameters (viz. pressures, temperatures) as well as liquid temperatures and pressure were recorded on the facility computerizer data recording system.

Test Model and Instrumentation

The model configuration chosen for these experiments was a blunt zero-degree wedge. The model modifications necessary to develop the final configuration are given in Appendix B and a sketch of the final model configuration is shown in Figure 2. A one-half inch radius

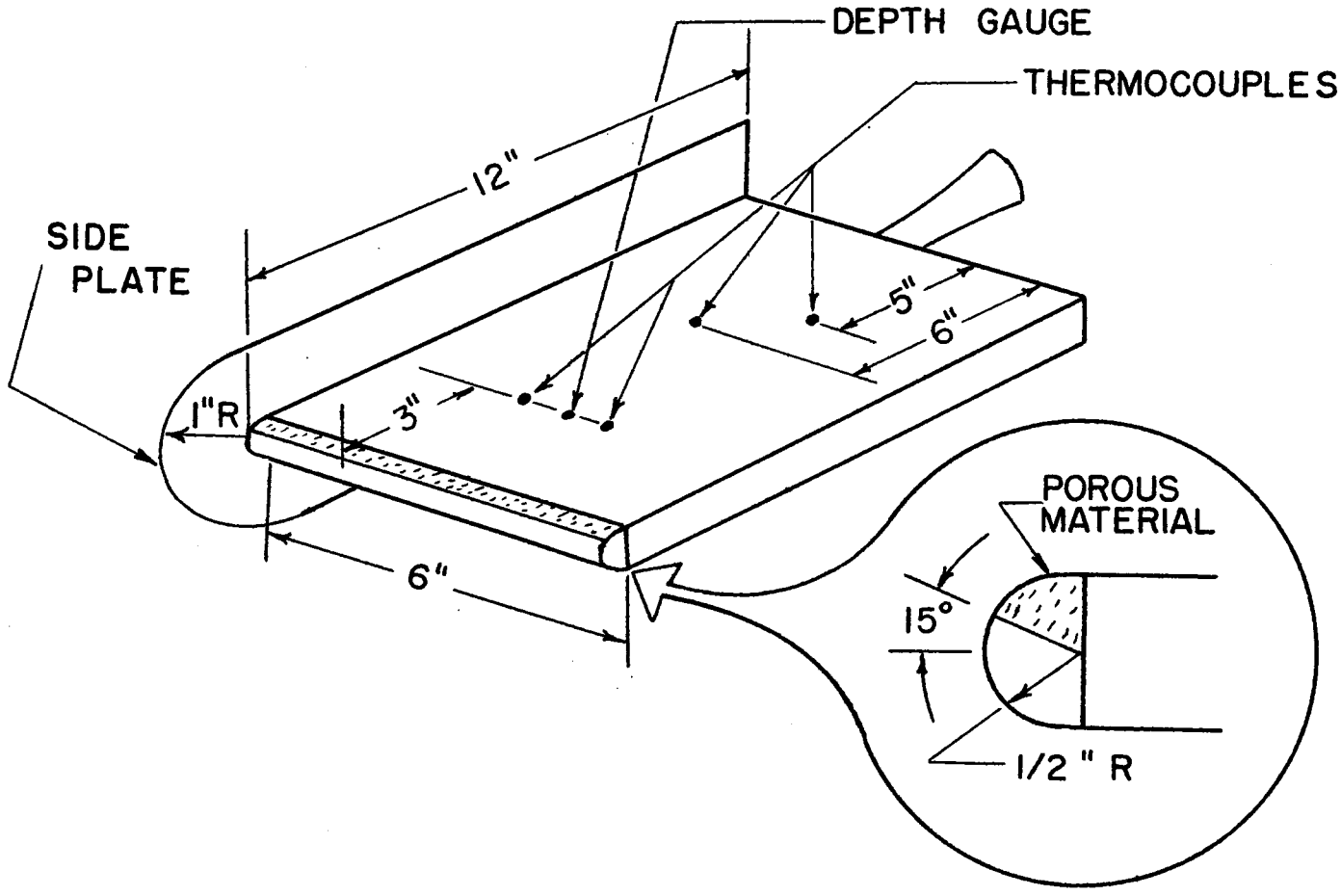

Figure 2. Sketch of Model

cylindrical nose tip is attached to the front of the six inch wide stainless steel plate to make an overall model length of twelve inches. A 75 degree arc of the nose tip, located as shown in the sketch, was made of porous stainless steel and the remainder of the tip was made of non-porous stainless. This area of porous material insured that all of the liquid expelled through the nose tip was confined to one surface of the model. The permeability coefficient of the porous material was 2.5×10^{-10} square inch. The variation in this permeability coefficient was measured and found to be less than 7 percent thus assuring satisfactory uniformity of the tips. Four thermocouples, mounted as shown in Figure 2, measured the liquid temperature and the model temperature. Two of the thermocouples were copper constantan and were mounted in thin copper discs encased in teflon. This teflon insulated the very low mass, high conductivity copper from the plate in order that the thermocouple measure the temperature of the liquid rather than that of the model. The remaining two thermocouples were chromel-alumel and were soldered directly into the plate for measurement of the model temperature.

To provide for two-dimensional liquid flow over as much of the model as possible, side plates (one of which is shown in Figure 2) were attached to the plate. The sides were positioned on the model such that the sharp leading edges were located 0.3 inches in front of the nose tip with equal heights of the sides extending above and below the model. Figure 3 shows an assembled model mounted in the wind tunnel. The porous nose tip was connected through tubing within the model to a high pressure expulsion system which forced the liquid to the model surface. This system consisted of a reservoir, filters, pressure

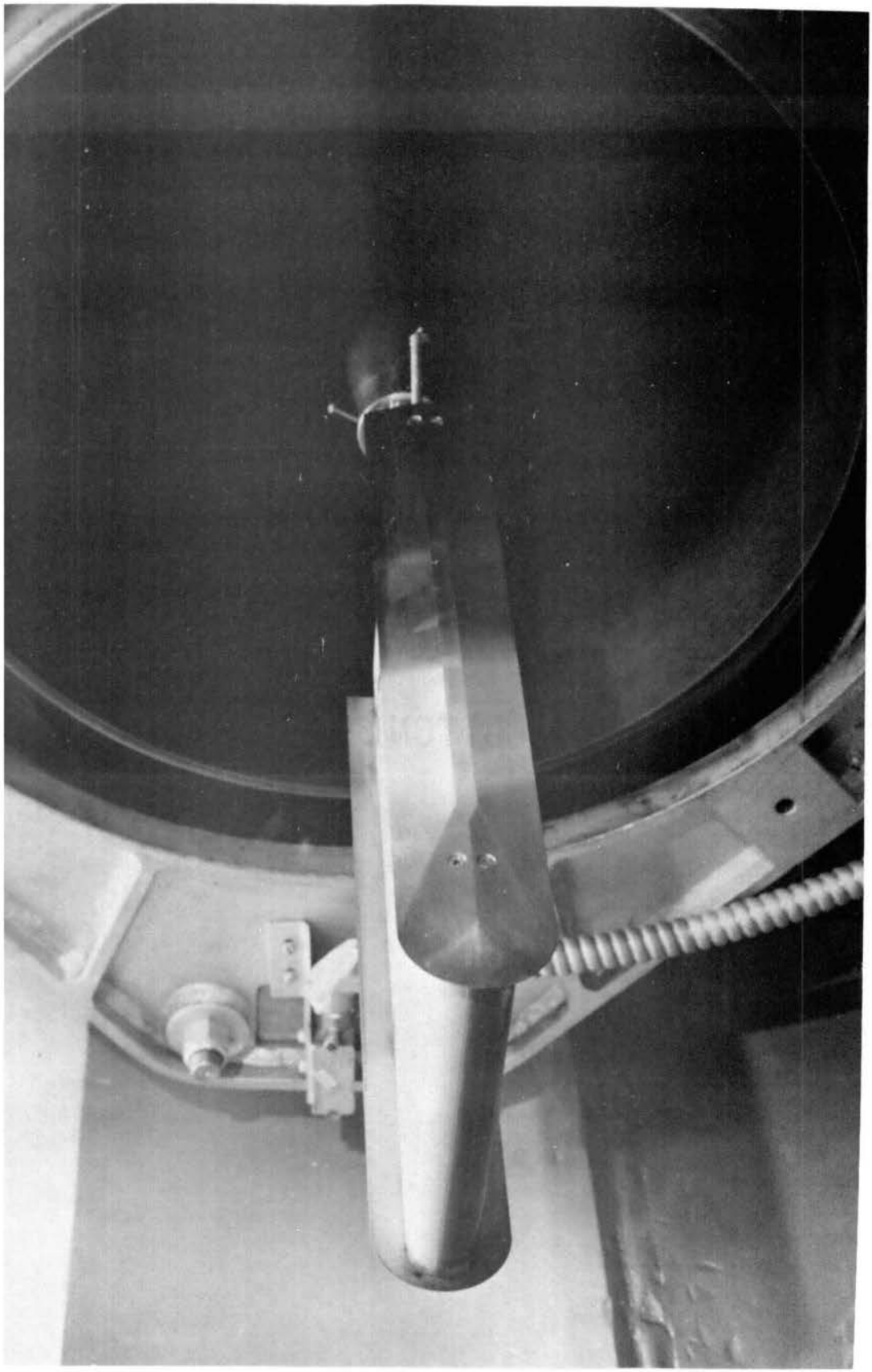

Figure 3. Test Model in Wind Tunnel

sensing equipment and flow rate monitoring equipment. The system was operated at pressures from 35 to 140 atmospheres to prevent either the pressure fluctuations in the tunnel or the pressure distribution in the gas about the nose tip from affecting the flow rate. The flow rate was measured by recording the pressure drop across sharp-edged orifices which were calibrated for fluids of different viscosities.

The thickness of the liquid and the frequency spectrum of the interface waves were measured with a depth gauge mounted in the model. A sketch of the gauge is shown in Figure 4.

The principal of operation of the gauge was that of a change in its capacitance when different thicknesses of a substance were placed upon it. The basic elements of the gauge were two pieces of a conducting material separated by a dielectric substance. The two sensing elements were spaced as closely as possible so that the gauge measure the frequency characteristics of the interface waves. The two metal conductors were made of 0.010 inch thick Kovar and the dielectric material separating them was a .002 inch thick piece of glass. These matetials with similar thermal expansion coefficients were chosen to prevent separation when subjected to the slight heating in the tunnel. The sensing elements of the gauge were mounted into a copper mounting ring with an epoxy which will withstand temperatures of 250 degrees F. The complete gauge was 0.25 inch in diameter and was press-fitted into the model so that its top was precisely level with the surface. The tops of the sensors were polished during fabrication and the entire model surface was polished after the gauge was installed.

Preliminary investigations were conducted with the plate design shown in Figure 4 and a cylindrical design in which the sensing

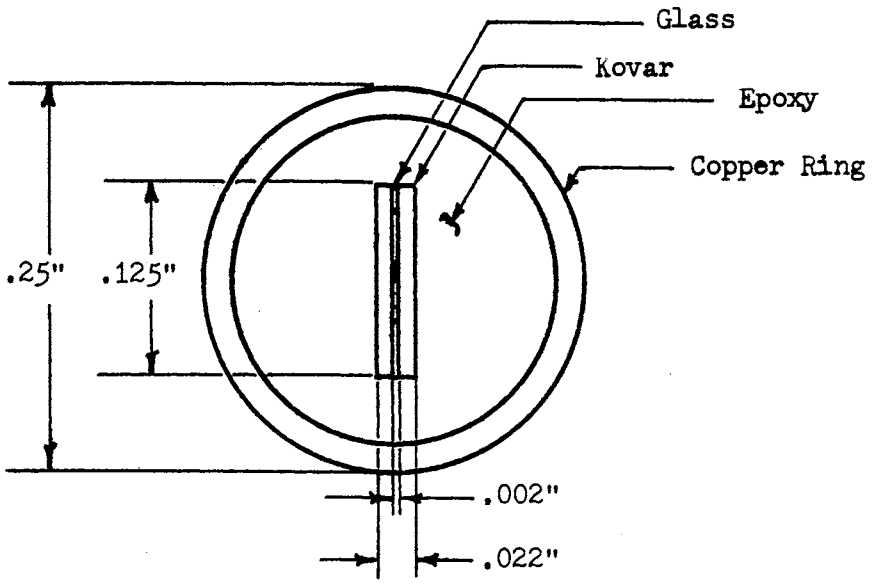

Top View

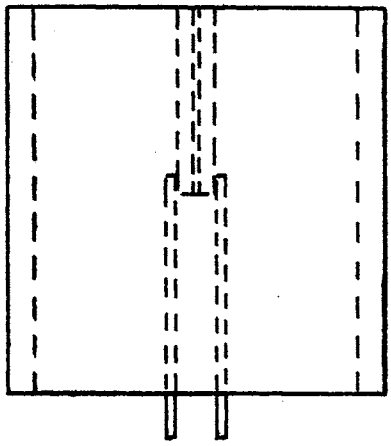

Side View

Figure 4. Depth Gauge Design

elements were two concentric cylindrical elements separated by a thin ring of glass. This development led to the selection of the plate design primarily because the sensing area was smaller and more successful in measuring the transient wave profile of the interface. It was also determined that direct contact of the liquids with the sensing elements caused an eratic signal in the measuring circuit. Because of this the entire model surface, with the gauge installed three inches behind the nose tip along the model centerline as shown in Figure 2, was covered with approximately .002 inches of enamel paint.

The output of the gauge was connected to a 100 kilohertz capacitance bridge by means of a double shielded triaxial cable. This bridge circuit has a stated capacitance resolution to 1 X 10^{-4} picofarads with a frequency response of 10 kilohertz. The bridge consists of a bridge transformer, an adjustable capacitor for nulling out the nominal capacitance of the depth gauge when balancing the bridge, and the capacitance depth gauge. The basic bridge circuit may be understood by referring to the sketch in Figure 5 and considering the following. If the input voltages (E_{in}) across the inductively coupled ratio arms are equal, then the output voltage (E_o) is

$$E_o = \frac{X_t - X_c}{X_t + X_c} E_{in}$$

If $X_t = X_c$, then the output voltage will be zero and a null condition exists. When the depth gauge transducer capacity changes by C_t, the output of the bridge is given by

$$E_o \simeq \frac{C_t}{2X_c} E_{in}$$

provided

$$|C_t| \ll |X_c|.$$

With no liquid on the gauge surface the bridge was balanced using the variable capacitor. When any thickness of liquid was placed on the gauge, its capacitance was altered and the bridge was unbalanced, and the unbalance was converted to voltage. The double shielded triaxial cable connecting the depth gauge to the electronics was necessary in order to measure an extremely small capacitance variation at the end of a long cable. The inner shield of the cable was driven at the same potential as the bridge transformer center tap and minimized the inner conductor to outer shield shunt capacitance. In effect the cable capacitance was removed from the system and only the very small capacitance of the gauge remained to be nulled out in the bridge.

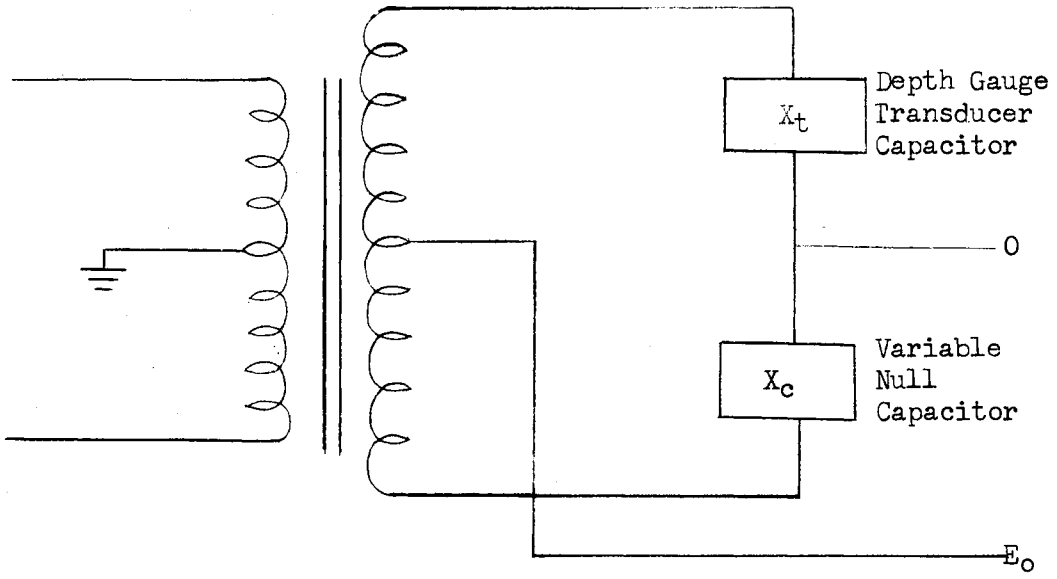

Figure 5. Depth Gauge Bridge Circuit

The output of the capacitance bridge was recorded on a visicorder for continuous monitoring of the gauge operation and on an FM tape recorder for subsequent data analysis. A four channel Ampex model FR 1300 tape recorder operating at 30 inches per second was used to record the gauge output. A time code generator, a 100 kilohertz reference frequency and a 5 volt spin calibration, all of which were necessary for locating the data on the tape in the ensuing digitizing, were placed on the remaining tape channels by the ground station electronics. The data acquisition system was stated to be sensitive to frequencies up to approximately 3 kilohertz. Figure 6 is a photograph of the data acquisition system for the depth gauge and shows the capacitance bridge electronics, the ground station electronics, the FM tape recorder and the visicorder.

The flow characteristics of the liquid over the model and the liquid interface response were recorded with a 16 millimeter and a 35 millimeter camera. The 16 millimeter camera was a Millican model operated at 400 frames per second using color film and the 35 millimeter was a Photosonics camera operated at 300 frames per second using a fine grain black and white film. Six high intensity tungsten lamps were placed around the test section to provide adequate lighting on the liquid interface. The model, which was placed in the tunnel with the test surface horizontal, was observed by placing a front surface mirror outside the tunnel on the window directly above the model. The cameras viewed the interface through this mirror. Figure 7 is a photograph of the model in the tunnel with the cameras, mirror and external lighting shown. Timing marks at a frequency of 1000 per second were placed on the film to provide an accurate means of time resolution and the nose

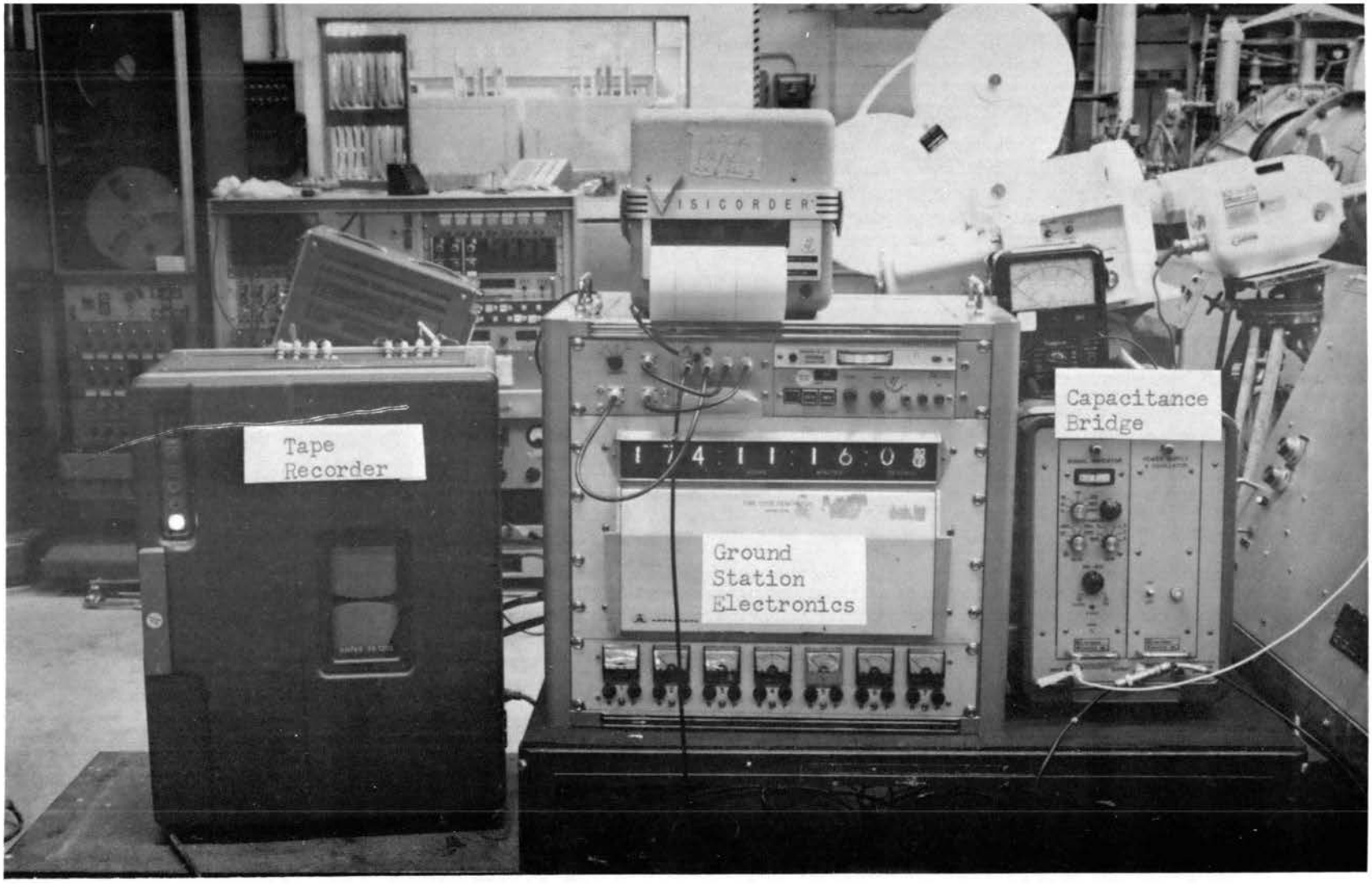

Figure 6. Depth Gauge Data Acquisition System

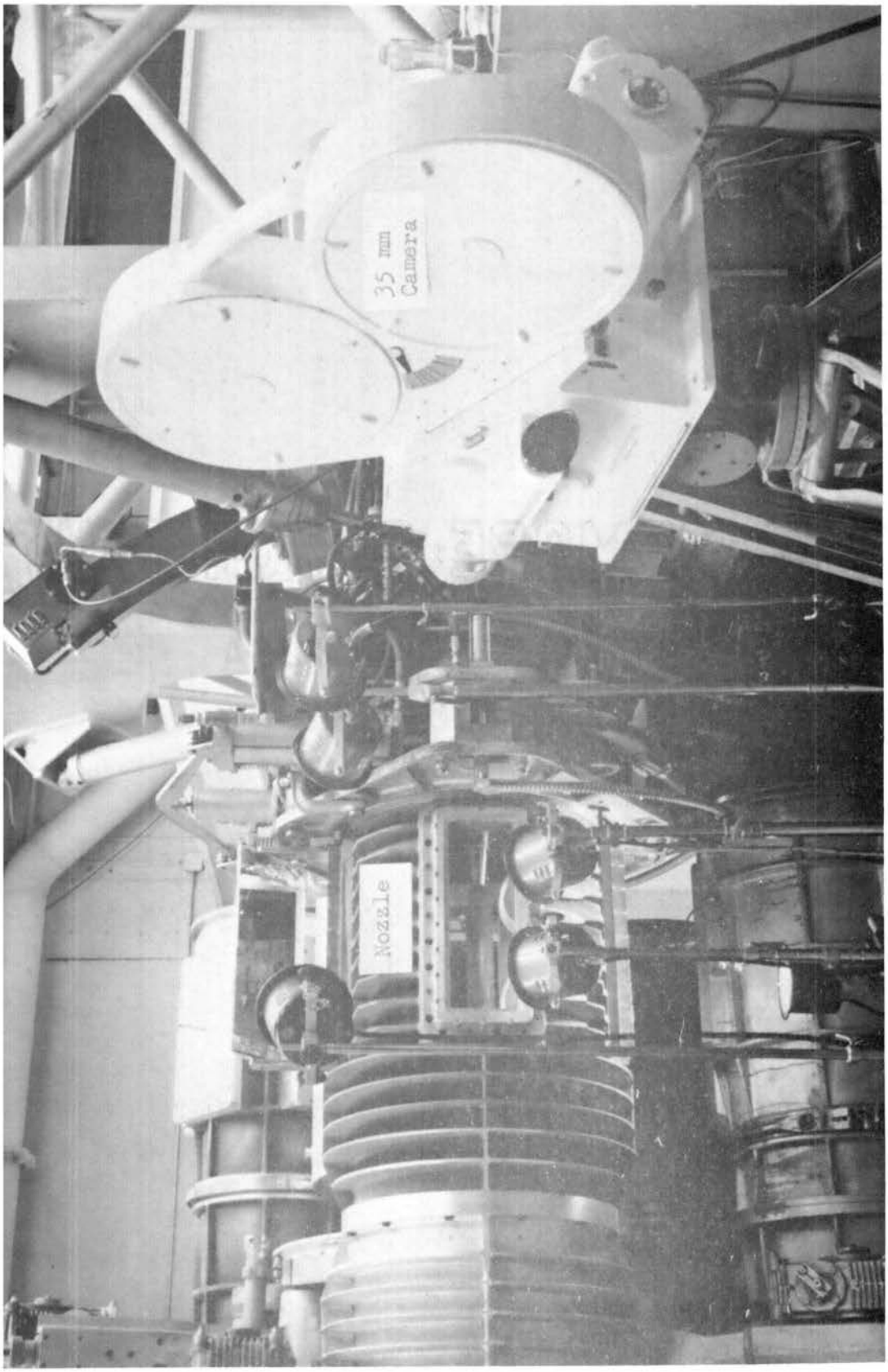

Figure 7. Wind Tunnel Nozzle with Camera and Lights

tip radius provided the dimension reference for length measurements. During each run the facility operating parameters and the temperatures of the liquid and the model were recorded on the tunnel computer data system.

Design of Gas Test Conditions

The purpose of the experiments was to study the characteristics of a liquid interface adjacent to a supersonic gas stream as a function of the liquid parameters and the external gas condition. In a later section the liquid conditions which were varied to permit independent study of the effects of the liquid Reynolds number and thickness are discussed. To include the effects of independently varying the gas shear and the Mach number, a two by two factorial design for these two gas parameters may be formulated. Two levels of shear stress and two levels of Mach number are required to accomplish this. Because of limitations in the range of operation of the wind tunnel, this complete factorial design was not possible. As shown in Table I two pressures at the Mach 5 condition were utilized and the resulting two levels of shear stress at the same Mach number provided one of the required elements of the factorial design. The second Mach number employed was 7.3. The particular gas condition produced a calculated shear stress approximately equal to that of the low pressure Mach 5 flow. Therefore, the effects of Mach number variation at constant shear stress may be evaluated and this variation produced another of the required elements of the factorial design. However, to complete the design a Mach 7.3 shear stress level equal to that at the high pressure Mach 5 gas

condition was necessary and it is this condition which was not possible. As a result the factorial design was incomplete.

TABLE I

WIND TUNNEL CONDITIONS

Tunnel Condition	High Shear Mach 5	Mach 7	Low Shear Mach 5
Mach Number	5.0	7.3	5.0
Total Pressure (atm)	6.8	17.	3.4
Total Temperature (^{o}R)	1400.	1400.	1400.
Reynolds Number ($ft^{-1} \times 10^{-6}$)	.95	.875	.475
Free Stream Velocity (fps)	3680.	3870.	3680.
Free Stream Density ($lb/ft^3 \times 10^3$)	8.61	3.87	4.305

The three nominal tunnel test conditions utilized in these experiments are shown in Table I. The total pressure and temperature were measured during each run while the remaining parameters were calculated using perfect gas relationships. Surveys have been made across the test section to demonstrate the uniformity of the flow at these conditions. The three gas conditions will be referred to throughout the text as the low shear Mach 5 condition, the high shear Mach 5 condition and the Mach 7 condition.

Test Liquids

The liquid film conditions were varied through control of the flow rate and liquid viscosity. For a constant viscosity, the Reynolds number was varied by altering the flow rate. The Reynolds number used to correlate the data from the experiments is defined by the expression

$$R = \frac{2Q}{\nu l} \tag{1}$$

where Q is the flow rate and l is the model width. The flow rate is given by

$$Q = h\, U_m\, l$$

where h is the film thickness and U_m is the mean liquid velocity. In linear stability analyses the Reynolds number is defined by

$$R = \frac{U_i h}{\nu} \tag{2}$$

where U_i is the liquid interface velocity. For a linear velocity profile in the liquid the interface velocity is twice the mean velocity and the Reynolds number defined by equation 1 is the same as that used in the analyses. To secure a wider range of variation in the Reynolds number than could be obtained through variation of the flow rate alone, the viscosity of the liquid was also varied. Glycerin-water mixtures ranging from complete water to complete glycerin were used to provide the viscosity variation. Table II shows the densities and compositions of the mixtures used. For all mixtures blue, green, or black dye was added to the liquid to provide better contrast of the interface for the photographic equipment.

TABLE II

LIQUID PROPERTIES

Liquid Designation	%Water/%Glycerin	Density, lb/ft^3
A	100/0	62.4
B	55/45	69.2.
C	40/60	71.
D	15/85	76.
E	9/91	77.
F	0/100	78.5

Design of Liquid Test Conditions

To study the effects of the liquid thickness and Reynolds number independently, the liquid conditions for the experiments at the three gas conditions may be selected from a two by two factorial design. This design can be implemented by producing the same two levels of the liquid thickness at each of two levels of the Reynolds number and these four conditions form the corner points of the factorial design. An intermediate level of both the Reynolds number and thickness produces a center point and completes the design.

This method was utilized in an attempt to include a factorial design of the liquid conditions for each of the gas conditions. For a constant value of the mean shear stress the liquid Reynolds number and thickness may be varied independently by independent control of the liquid flow rate and viscosity. Based on assumed values of the shear

stress and liquid viscosity and for a linear velocity profile in the liquid, the liquid conditions to implement the factorial design were calculated. However, due to uncertainties in the shear stress and differences between the assumed and actual liquid viscosities, the factorial design was not obtained. The liquid flow rate-viscosity combinations were calculated for the low shear Mach 5 and the Mach 7 gas conditions since they both produce the same nominal shear stress of the model. Because the variations in the viscosity caused the factorial design to be significantly altered, the design was not attempted for the high shear Mach 5 condition. Therefore, the same flow rate viscosity combinations were produced for each of the three gas conditions. Variations in the liquid temperature (and as a result the viscosity) resulted in different Reynolds numbers at similar flow rates for each of the gas conditions.

The liquid flow parameters for each of the three gas test conditions are shown in Table III. The viscosities were determined for the measured nominal liquid test temperatures using a viscometer. In most cases the minimum liquid flow rates are the lowest for which satisfactory model coverage was obtained while the maximum flow rates are the largest obtainable with the expulsion system. Fifteen combinations of viscosity and flow rate were tested at each of the three gas conditions for a total of 45 tests. With the selected viscosity and flow rate conditions the particular gas condition determined the film thickness and liquid velocity.

TABLE III

LIQUID AND GAS TEST CONDITIONS

Test Number	Tunnel Condition	Liquid Flow Rate, gph	Liquid Reynolds Number	Liquid Viscosity $\frac{lb}{ft\text{-}sec} \times 10^4$
1		1.15	.33	404.
2		1.83	.53	404.
3		2.09	.9	256.
4		2.83	1.	323.
5		1.5	2.	80.8
6	High	5.6	4.3	148.
7	Shear	8.	21.	40.4
8	Mach	15.	32.	50.5
9	5	10.	38.	28.2
10		29.	66.	53.8
11		15.	60.	26.9
12		27.	110.	26.9
13		8.	135.	5.4
14		15.5	265.	5.4
15		21.	360.	5.4
16		1.15	.22	605.
17		1.83	.50	444.
18		2.09	.9	269.
19		2.83	1.2	269.
20		1.5	1.4	121.
21	Mach	5.6	3.8	168.
22	7	8.	21.	40.4

TABLE III (Continued)

Test Number	Tunnel Condition	Liquid Flow Rate, gph	Liquid Reynolds Number	Liquid Viscosity $\frac{lb}{ft\text{-}sec} \times 10^4$
23	Mach	10.	34.	33.6
24	7	15.	32.	50.5
25		15.	54.	30.2
26		29.	85.	40.4
27		27.	126.	23.6
28		8.	130.	5.4
29		15.5	260.	5.4
30		21.	360.	5.4
31		1.15	.22	605.
32		1.83	.35	605.
33		2.09	.73	336.
34		2.9	1.0	323.
35		1.5	1.8	94.2
36	Low	5.6	4.	161.5
37	Shear	8.	23.	37.
38	Mach	15.	32.	53.8
39	5	10.	40.	26.9
40		25.	56.	53.8
41		15.	54.	30.3
42		27.	110.	26.9
43		15.	255.	5.4
44		18.3	310.	5.4
45		21.	360.	5.4

Data Reduction

The 35 mm black and white film served as the source of two basic pieces of data. First, the interface behavior was characterized regarding the absence or presence of waves and their type; and second, the wave velocity and wavelength were measured from the film. By using the timing marks placed on the film as a reference time and the nose tip radius as a reference length, the velocity of the wave was measured from the film. A Boscar automatic film reader was employed for this purpose. The image of the interface was projected onto a screen on which were located a set of continuously adjustable cross hairs. Individual waves were located at random with their location traced from frame to frame for several frames and automatically punched onto computer cards. A short program for use on a CDC 6600 computer was written and used to calculate the wave velocity directly from the film reader output cards. From 40 to 80 waves were measured and averaged to determine each mean velocity data point. The mean wavelength data were determined by measuring the number of waves in a known length on the model. All tunnel operating parameters including stagnation pressure and temperature, the liquid parameters such as expulsion system pressure and liquid flow rate, and all model and liquid temperatures were evaluated from the facility data system.

Once steady state conditions were obtained on the model, a six second segment of the output from the depth gauge was taken from the capacitance bridge and recorded on the FM tape recorder system described previously. The six second interval from the continuous tape data was digitized into the proper format and these segments were all placed on a single tape for use in further reduction and analysis.

Based on the depth gauge output from some preliminary experiments, frequencies below 500 Hertz were anticipated. Consequently, a datum point was taken every .001 seconds during the digitizing process. A Fourier analysis of the six second interval of digitized data was performed using a modified Sandia Laboratory library computer program called COAP. For each integral frequency between one and 500 Hertz, the value of the calculated Fourier decomposition of the gauge output was converted from a complex number to a real number by multiplying the number by its complex conjugate. At each frequency this value of the amplitude fluctuation was normalized using the maximum value calculated for each segment of data. From this analysis the frequency spectrum of the waves on the interface was calculated for the different combinations of Reynolds number and thickness of the liquid film.

The output of the depth gauge was also analyzed to determine the mean thickness of the liquid film. From the six second interval of digitized output, approximately 50 data points were randomly selected. The mean of these data was calculated and converted to a voltage using the 5 volt spin calibration placed on the FM tape. The voltage was converted to mean thickness using the depth gauge calibration curves for each fluid which are given along with a description of the calibration technique in Appendix C.

For each experiment the mean thickness of the film was also calculated directly from the particular liquid and gas conditions. A description of this calculation procedure is presented in Appendix D. Briefly, the gas pressure and shear distributions on the model were calculated and imposed as boundary conditions on the liquid film calculations. The liquid conditions, including thickness and interface

velocity, were calculated for each liquid flow rate and property condition using a non-similar, variable property, boundary layer solution modified to include a liquid film. A discussion and comparison of the results of the measurement and the calculations are presented in Appendix D.

CHAPTER III

ANALYSIS OF MEAN WAVE DATA

As described in Chapter II the interface of the liquid film was photographed with a 35 millimeter camera and the movie film was a source for the wave characteristic data. The data which were measured on the photographs were the mean wavelength, the maximum and minimum wave speeds, and the mean wave speed. The movie film also provided an excellent means for describing the general qualitative appearance of the liquid interface.

In this chapter these wave characteristics are presented and discussed. The chapter is divided into two general divisions. First, a description of the appearance of the interface waves at selected Reynolds number and thickness conditions is presented in the section entitled 'Interface Characterisitcs.' Second, the quantitative data in the form of the mean dimensional wave speed, the dimensionless wave speed, and the mean wavelength are presented in the section entitled 'Discussion of Mean Wave Data.' A discussion of each of these three types of data is presented for each of the gas conditions to determine the effects of the liquid Reynolds number and thickness. The data are compared at similar liquid conditions to evaluate the effects of the gas parameters.

Interface Characteristics

A smooth interface was not observed for any combination of liquid and gas flow conditions in these experiments. Finite amplitude waves were observed on the interface during all experiments. Although waves were present at all conditions, there was no evidence to suggest the presence of any discrete particulate entrainment or "stripping" from the liquid film. The waves became visible at a distance of 0.5 to 1 inch behind the leading edge of the model and upon reaching a finite amplitude condition propagated back along the model. The waves appeared to travel at a steady state condition with neither additional growth nor damping visible. No motion of the liquid or the waves to suggest the presence of significant adverse pressure gradients on the model was observed. The liquid appeared in the photographs to be of uniform thickness with perhaps slightly increased thickness near the side walls. No waves moving diagonally across the model were observed. This apparent uniform thickness and the lack of lateral wave motion contributed to the conclusion that no significant adverse pressure gradients were present on the model surface.

For purposes of illustrating the interface appearance, photographs of the experiments at the Mach 7 gas condition were selected because the photographs for this particular gas condition were superior over the range of experiments necessary to illustrate the data.

For the minimum Reynolds number conditions relatively small, three-dimensional, horseshoe-shaped waves covered the model. Figure 8 presents a section of the model near the porous nose tip and illustrates the general interface structure at a liquid Reynolds number of 1 and a film thickness of 0.01 inches. The presence of irregularly spaced

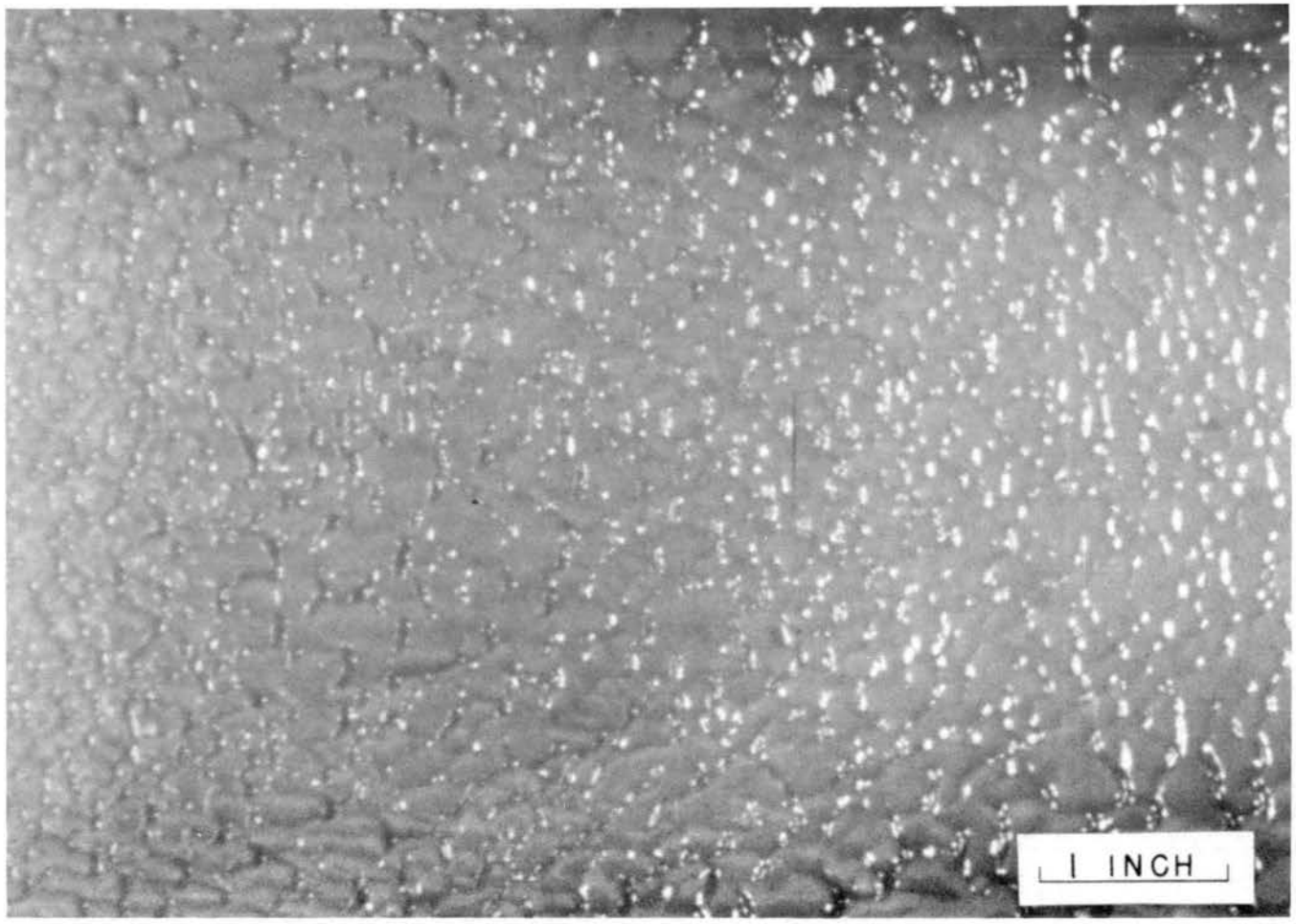

Figure 8. Liquid Interface Structure for Reynolds Number = 1, Mach 7 Gas Condition, h = 0.01 Inches, Flow Left to Right

waves with a lateral span of approximately 0.3 inches is noted. The distance between the leading edge and the trailing edge of the waves is typically 0.1 inches and less.

Figure 9 is a photograph of the interface at a Reynolds number of 88 and a thickness of 0.014 inches. The waves at this condition are larger than those for the previous condition. The lateral span of some of the waves is typically 1 inch and larger and lengths of 0.15 to 0.2 inch are typical of the distance between the leading and trailing edges of the waves. The shape of these waves remains basically three-dimensional and in that respect the waves are similar to the low Reynolds number waves. The presence of many different sizes of waves on the interface can be seen in Figure 9. The waves are also irregularly spaced and in many cases waves interact with other nearby waves.

At higher Reynolds numbers the interface becomes very irregular with the waves moving very fast, rapidly changing shapes, merging with other waves, and in general exhibiting a condition for which the wave speed data were difficult and in some cases impossible to obtain. Figure 10 is typical of the interface appearance at this condition. The Reynolds number for this condition is 360 and the liquid thickness is 0.007 inches. For descriptive purposes the interface may be characterized as chaotic but no stripping or entrainment is visible in the photographic coverage.

For these three examples the external gas condition was the Mach 7 flow and the variation in the liquid interface appearance results from changes in the liquid conditions. The qualitative effects of varying the shear stress and pressure exerted by the external gas on the interface can be seen by comparing Figures 11 and 12. Figure 11 represents

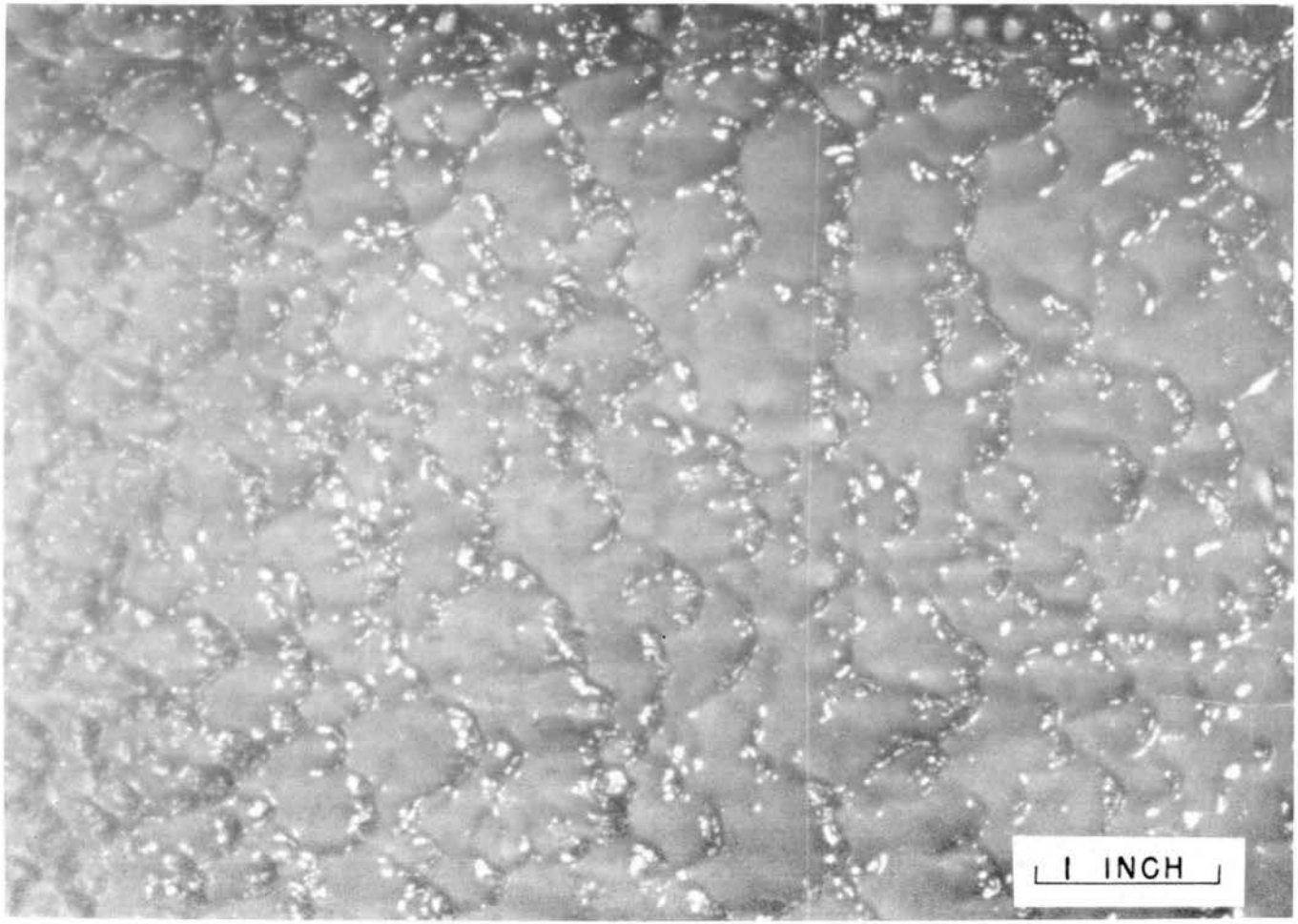

Figure 9. Liquid Interface Structure for Reynolds Number = 88, Mach 7 Gas Condition, h = 0.014 Inches, Flow Left to Right

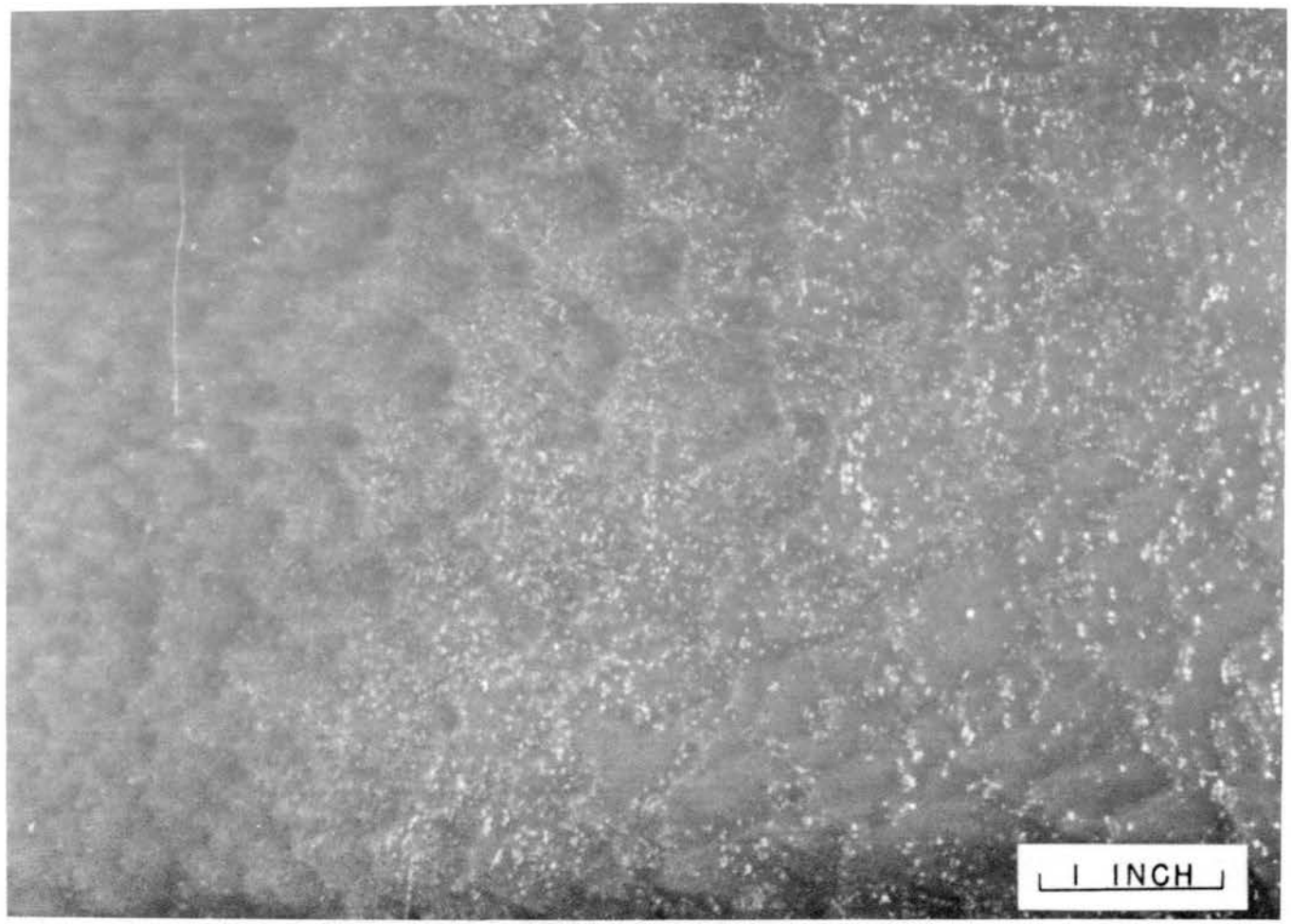

Figure 10. Liquid Interface Structure for Reynolds Number = 360, Mach 7 Gas Condition, h = 0.007 Inches, Flow Left to Right

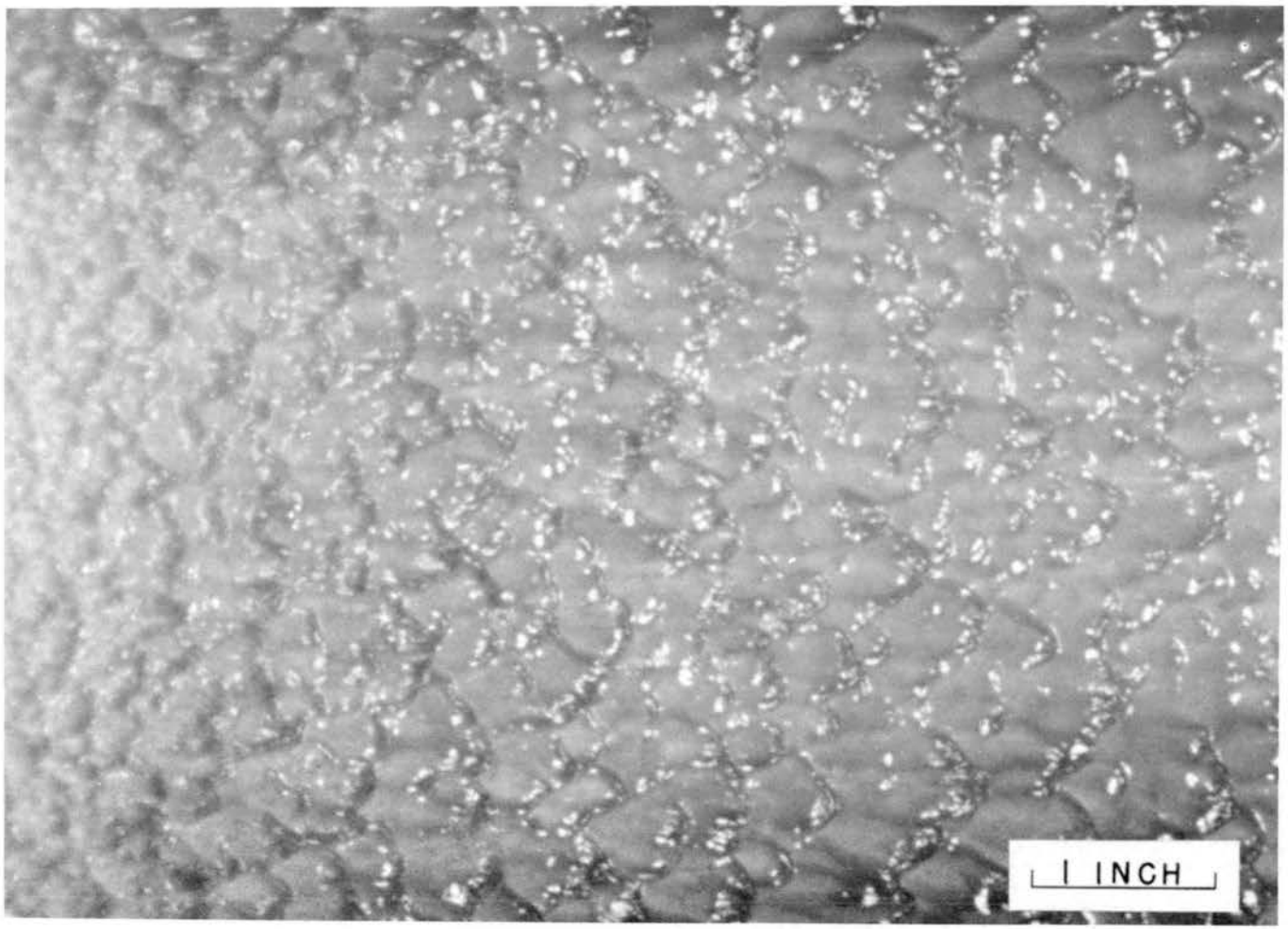

Figure 11. Liquid Interface Structure for Reynolds Number = 56, Low Shear Mach 5 Gas Condition, h = 0.016 Inches, Flow Left to Right

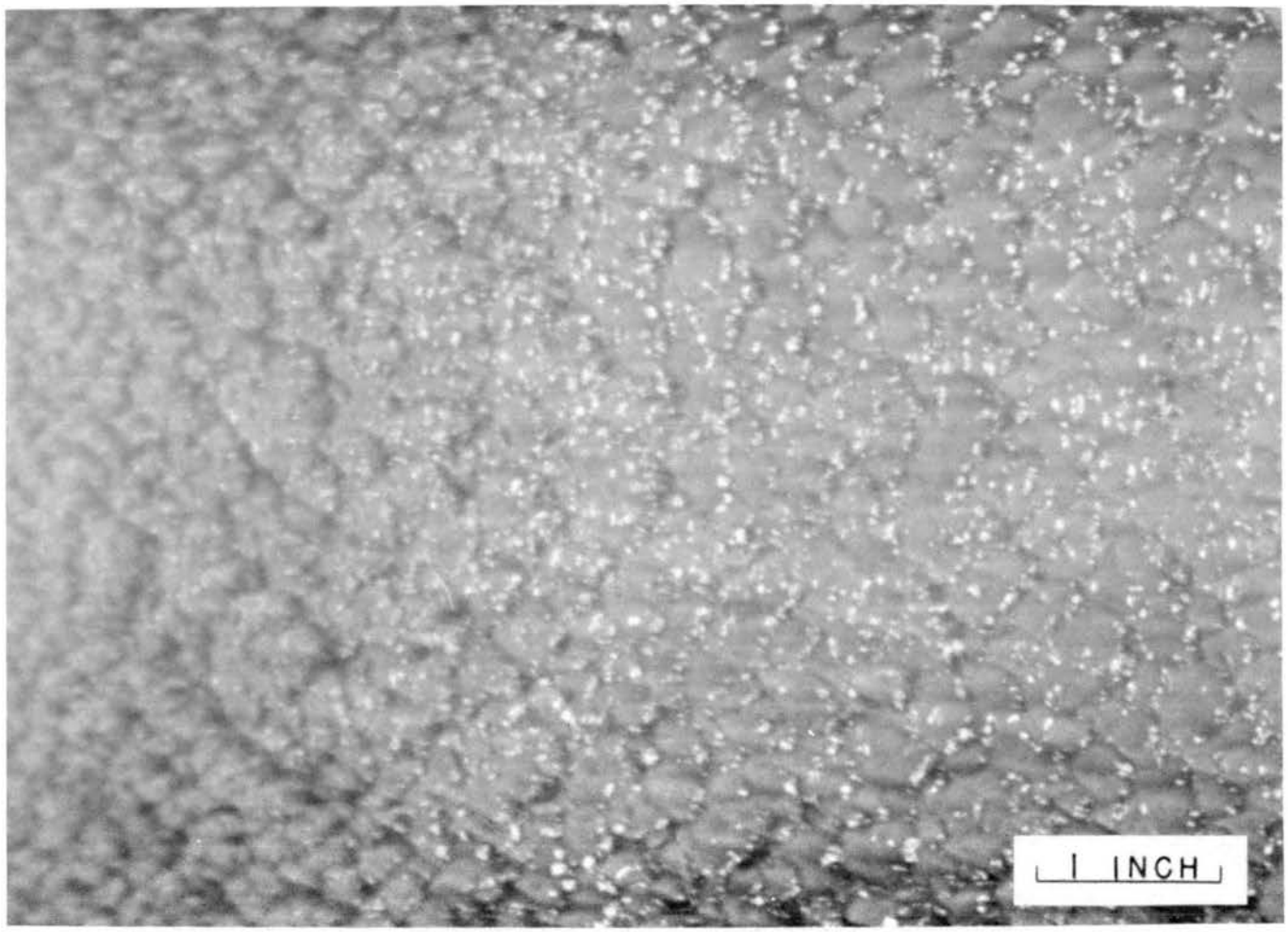

Figure 12. Liquid Interface Structure for Reynolds Number = 60, High Shear Mach 5 Gas Condition, h = 0.013 Inches, Flow Left to Right

the interface response at the low shear Mach 5 condition for a liquid Reynolds number of 56 and a thickness of 0.016 inches. For a Reynolds number of 60 and a thickness of 0.013 inches, Figure 12 represents the interface response at the high shear Mach 5 condition. The higher shear condition results in more numerous, smaller waves along with the general appearance of a more disturbed interface. Since the Reynolds numbers and the thicknesses are approximately equal, the difference in the interface appearance is attributed to the increased shear and pressure of the more extreme Mach 5 condition.

For all of the experiments the waves on the interface do not all travel at the same velocity. Although it is concluded that the majority of the waves move at some particular uniform velocity, examination of the movie film reveals that waves traveling slower than the mean velocity as well as waves traveling faster than the mean velocity are also present. In some cases the faster waves move through slower waves while in other cases the faster waves merge with slower ones. In either event the waves interact and exert some influence on each other.

In summary the waves observed on the interface for all of the liquid-gas combinations are predominately three-dimensional, horseshoe-shaped waves. No distinct two-dimensional waves which extend across the width of the model are observed. The lateral span of the waves as well as the distance between the leading and trailing edges of the waves increases with increasing Reynolds number. The waves are irregularly spaced, are of many different sizes, and generally interact with other nearby waves. This appearance is not surprising and illustrates the random formation of waves with a range of wavelength and wave speed rather than a single frequency wave.

The evolution of the wave shape and the increasing size of the wave are continuous throughout the Reynolds number range studied. No sudden or dramatic changes in the transition from one wave type to another are observed for any Reynolds number-thickness combinations. This orderly transition suggests that if different mechanisms are responsible for the waves at low and high Reynolds number, the different mechanisms are gradually engaged or disengaged as the Reynolds number is changed. It is not apparent from the data that for any particular liquid condition a source of wave generation (i.e., the Tollmein-Schlichting instability) is energized due to exceeding a critical value of any of the liquid parameters.

Discussion of Mean Wave Data

The liquid conditions for the fifteen experiments at each gas condition were selected to permit the independent evaluation of the effects of the liquid Reynolds number and the liquid thickness. The data are analyzed for the two liquid parameter effects by interpreting the wave characteristics for the experiments at each gas condition. The effects of varying the shear stress and the pressure at the Mach 5 flow are evaluated by comparing the data at the two shear levels for similar liquid conditions. The effects of variation in the free stream Mach number at the low shear level are evaluated by comparing the data for the Mach 7 and the low shear Mach 5 gas flows at similar liquid conditions.

The discussion and analysis of the data presented in this section are organized as follows: the matrix of Reynolds number and thickness conditions for each of the gas conditions is presented; the regression

analysis technique used for the data interpretation is discussed; the mean dimensional wave speed is analyzed for each of the gas conditions; the mean dimensionless wave speed data for the three gas conditions are discussed; and finally the mean wavelength data are presented.

Matrix of Liquid Test Conditions

The matrices of the actual liquid conditions for each of the gas conditions are given in Figures 13, 14, and 15. Shown connected by dashed lines in each of the figures are the resulting corner points of the two by two factorial design which was imbedded in the liquid conditions. The conditions for the points were calculated based on assumed values of shear stress and liquid viscosity (or liquid temperature) to provide the regular, rectangular design shown as solid lines on each curve. However, due to differences between the assumed and the experimental values of the shear stress and liquid viscosity, the Reynolds number and thickness varied and the skewed designs which are shown were produced. Since the points in the factorial design varied so significantly from the original design, the data from the four experiments were combined with the other experimental conditions shown on the figures to provide the independent parameters for the regression analyses which were performed on the wave data. As shown in Table III the fifteen experiments at each gas condition were created by six fluid mixtures and fifteen liquid flow rates. These were the same for each gas condition.

Quantitative data for the wave characteristics were not obtained for all fifteen of the conditions at each gas condition due in some cases to the extreme irregular appearance of the interface and in other

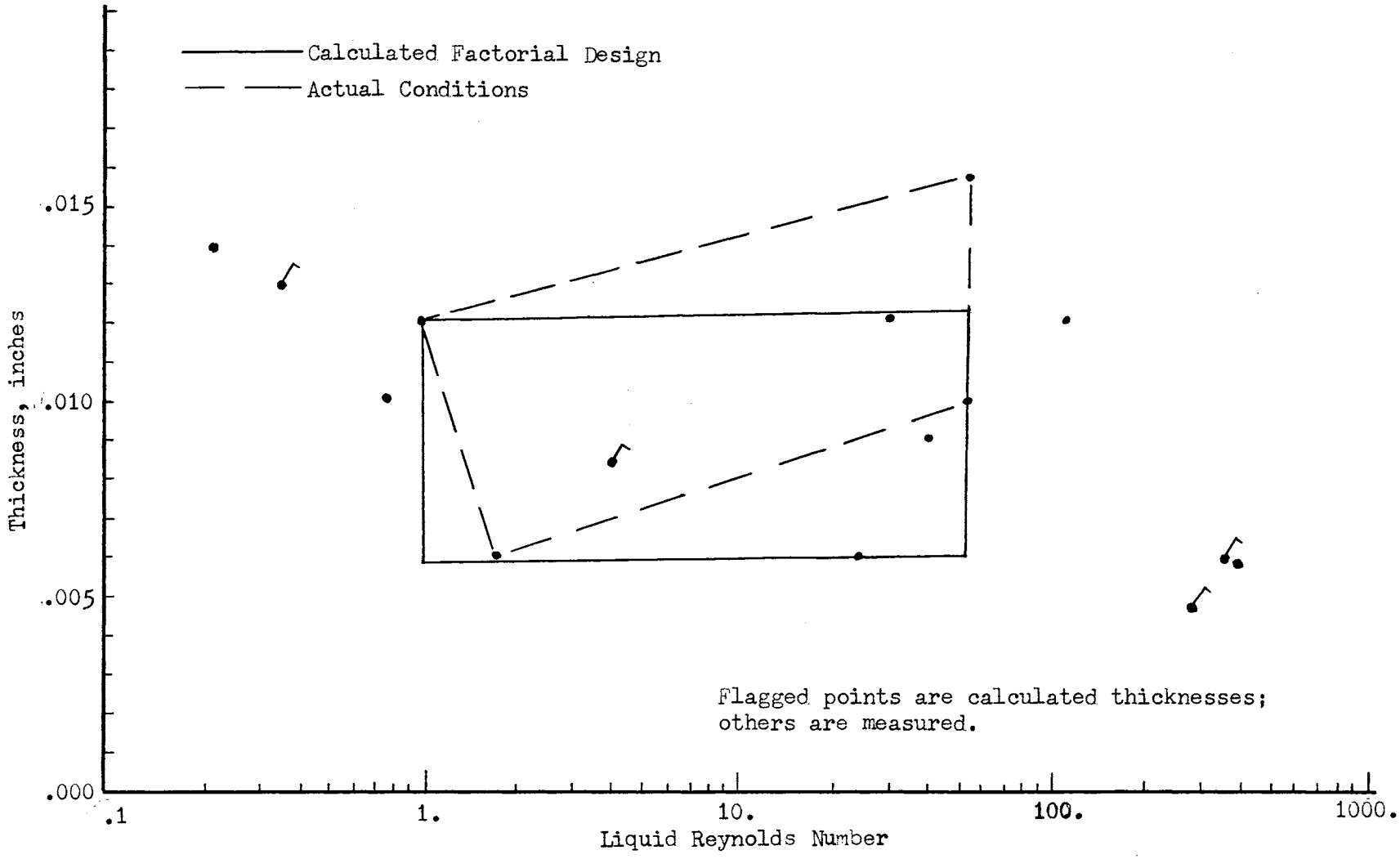

Figure 13. Matrix of Liquid Conditions for Low Shear Mach 5 Condition

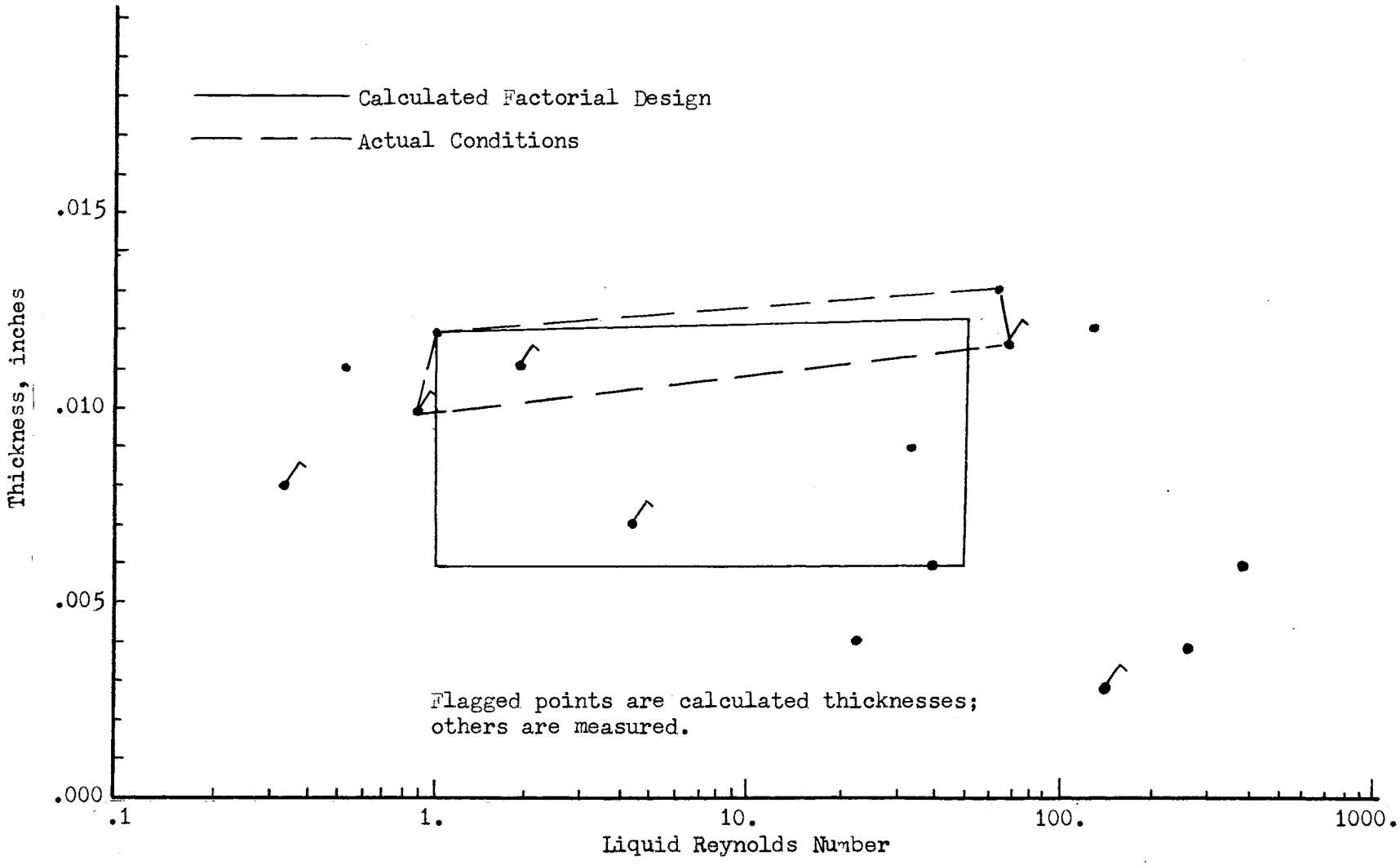

Figure 14. Matrix of Liquid Conditions for High Shear Mach 5 Condition

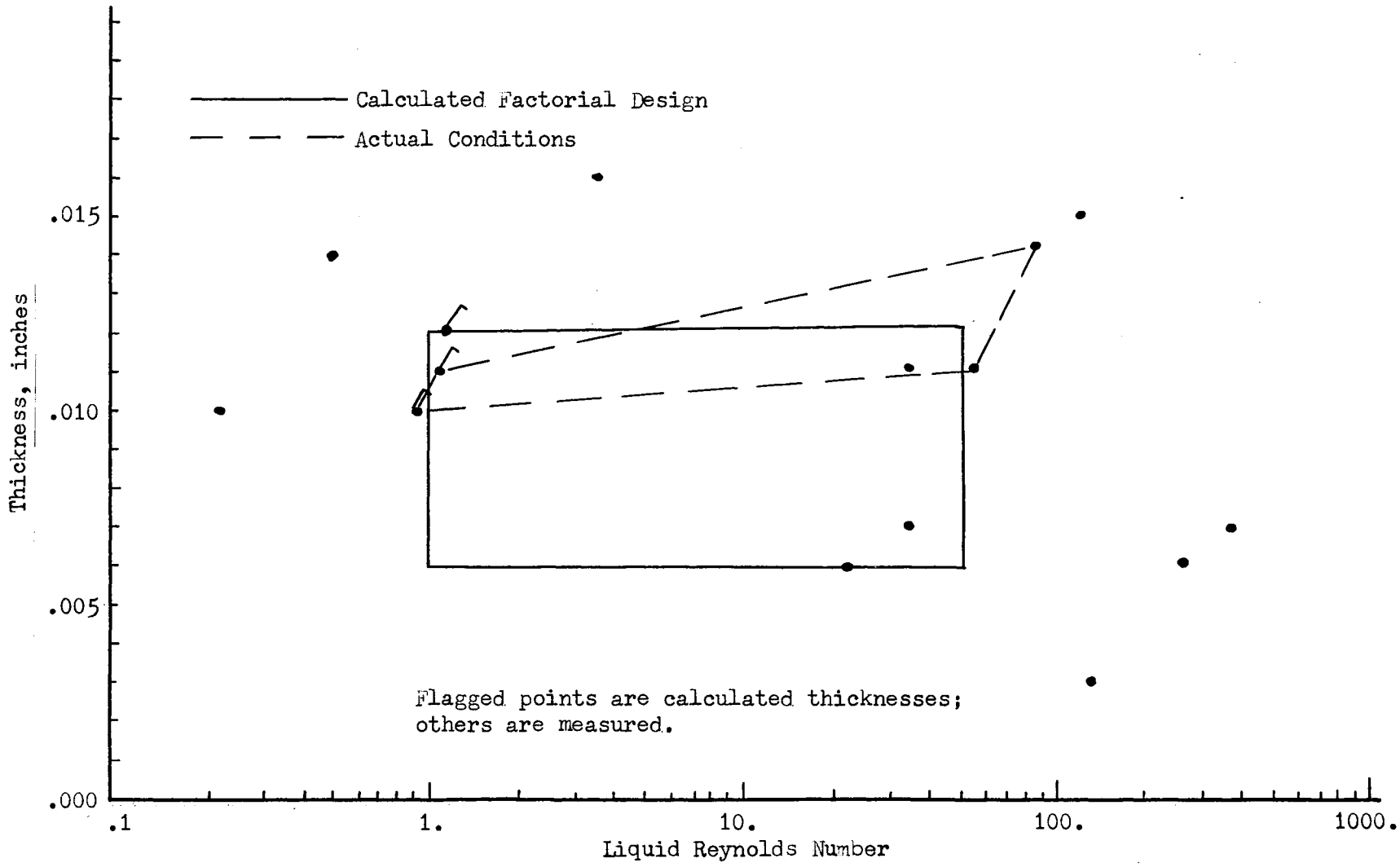

Figure 15. Matrix of Liquid Conditions for Mach 7 Condition

cases to the lack of adequate detail of the waves on the movie film. The particular runs for which data were not obtained are designated in the appropriate tables.

Description of Regression Analysis

For a constant external gas condition any variation in the interface wave characteristics which occurs at different liquid conditions is related to parameters which describe the liquid flow. The parameters employed for this purpose are the liquid Reynolds number as defined by equation 1 and the mean thickness of the liquid film. A general, functional relationship between the wave characteristics and the liquid parameters for a constant external gas condition is

$$f = g(R,h)$$

where f is any of the measured wave characteristics and g is an unknown function. The data are analyzed for each gas condition over the range of Reynolds number and thickness by employing multiple regression analyses to evaluate the unknown function. The data are analyzed for each of the gas conditions by performing the regression analysis on an assumed form of the function g. The assumed model is a fully quadratic equation with the Reynolds number dependency included as a logarithmic term. The model is given by

$$f = b_0 + b_1\hat{h} + b_2\hat{R} + b_3\hat{h}^2 + b_4\hat{R}^2 + b_5\hat{h}\hat{R} + E \qquad (3)$$

where $\hat{h}$ and $\hat{R}$ are normalized liquid thickness and Reynolds number parameters defined for the data at the low shear Mach 5 and the Mach 7 gas conditions by

$$\hat{h} = \frac{h - 0.009}{0.012 - 0.009} \qquad \hat{R} = \frac{\ln R - \ln 8.9}{\ln 56.5 - \ln 8.9}$$

For the high shear Mach 5 gas condition the Reynolds number is normalized using different values to reflect the smaller range of Reynolds number variation and the exact equation for that condition is given later. In the former expression the dimensions of the film thickness h are inches and in the latter lnR indicates the natural logarithm of the Reynolds number. By using these normalized expressions both liquid parameters are constrained to lie roughly between minus 2 and plus 2. In this manner the coefficient of each term in the final fitted equation may be examined to determine its relative importance in causing the variation of the wave characteristics.

The regression analyses were performed by using an existing Sandia Laboratory computer program. The program performs a step-wise regression analysis for fitting the experimental data to the assumed response surface model. As a part of the analysis each coefficient, b_i, in the assumed model is checked to determine if the coefficient is significantly different from zero. The criteria employed is the F-ratio test. Details of this standard test are given in many statistical textbooks, including Snedecor and Cochran (1968).

The F-ratio is defined by

$$F = \left(\frac{\hat{b}_i}{s_{\hat{b}}}\right)^2$$

where $\hat{b}_i$ is the estimated value of each of the various coefficients and $s_{\hat{b}}$ is the estimated variance of each of the coefficients. Both of

these terms are calculated in the regression analysis. To implement the F-ratio test in the computer analysis, a critical F value is assigned for comparative purposes. The program compares each calculated F value with the critical value and retains the coefficients with F-ratio values equal to or greater than the critical value. Coefficients with F values less than the critical value are set equal to zero and the regression analysis is repeated until only those terms with F-ratio values in excess of the critical value are retained in the model. The critical F-ratio value utilized in the analyses was 2.0. This value corresponds to a confidence level of approximately 70 to 80 percent depending on the specific number of degrees of freedom in the error of the final analysis of variance.

The values of the F-ratio terms which are retained in the final model are compared with the distribution of the F-ratio statistic found in numerous statistics textbooks including Snedecor and Cochran (1968). Based on this comparison, a significance level is attached to each coefficient and the particular parameters with a higher significance level may be determined. Also a confidence limit may be placed on the values of the coefficients by multiplying the associated standard error by the t-statistic at the desired confidence level and the error degrees of freedom in the analysis of variance.

The form of the equation is such that the coefficients are not all dimensionless and the ones with dimensions possess the same dimensional units as those of the dependent parameter being examined. Consequently in each case care must be taken to incorporate the terms in the resulting models with the proper units. In all of the analyses the

dimension of the wave speed is feet per second, that of the wave frequency is Hertz, and that of the wavelength is inch.

Dimensional Wave Speed

The general procedure utilized to deduce the mean wave velocity from the photographic film is described in Chapter II. Briefly, the method was one in which the displacement of randomly selected waves was measured from frame to frame and the velocity calculated from the known time interval between frames. From 40 to 80 measurements were made and the mean velocity was calculated as the average of the measured data. Details of the mean wave calculations, together with examples to illustrate the statistical acceptability of the sample size for the data, are given in Appendix F. In order that the location of the wave speed measurements coincide approximately with the position of the depth gauge located three inches behind the nose tip, the velocity measurements were made when the waves were located from two to five inches behind the nose tip.

During the measurement of its speed a wave necessarily travels a finite distance along the model. The curves shown in Figure 92 of Appendix D indicate that the calculated shear stress varies along the model at the location of the velocity measurements. For several of the experiments the wave speed data were examined using regression analyses to determine if the wave speed was a function of the location of the wave and these results are also presented in Appendix F. In all cases the analyses result in some functional relationship between the wave speed and the wave location. In some cases the relationship indicates that the wave speed increases with distance along the surface and in

others the relationship shows a decrease in the wave speed with distance along the surface. However, as shown in the appendix the confidence level associated with the dependence of the wave speed on the location is in most cases relatively low.

Another factor which complicates this analyses of wave speed and wave location is that the waves do not all travel at the same speed and the presence of the different wave speeds contributes to the apparent contradiction in the calculated regression curves. In some cases the speeds of a number of fast waves located toward the back of the region of interest are measured. In other examples more of the faster waves are measured while located toward the front of the region. The result of the former is to show an increase in wave speed with distance while the result of the latter is to show a decrease in the wave speed with distance.

The mean wave speed data therefore represent a mean of the wave speeds in both time and position and also reflect the presence of waves traveling at different speeds. Consequently, the data describe the mean interface response as a function of the mean gas conditions (i.e., shear stress) over the section of the model located two to five inches behind the nose tip. The presence of the different wave speeds together with interaction effects of nearby waves prevents the description of how the wave speed of a specific, individual wave varies as a function of the shear stress along the model interface. The maximum and minimum wave speed data shown in the following tables illustrate the range of different wave speeds which occur on the interface.

Shown in Table IV are the measured mean wave speed, the maximum and minimum wave speed as well as the dimensionless mean wave speed,

TABLE IV

MEASURED INTERFACE DATA FOR LOW SHEAR MACH 5 GAS CONDITION

Reynolds Number	Mean Wave Length, in.	Mean Wave Speed, fps	Maximum Wave Speed, fps	Minimum Wave Speed, fps	Dimensionless Mean Wave Speed	Measured Thickness, in.	Calculated Thickness, in.
0.22	.16	0.4	0.6	0.3	2.8 ∓ .8	.014 ∓ .003	.012
0.35	.17	0.6	0.8	0.5		**	.013
0.73	.2	1.1	1.7	0.7	3.2 ∓ .9	.010 ∓ .002	.011
1.0	.2	1.7	2.5	1.1	4.2 ∓ 1.2	.012 ∓ .003	.013
1.8	.17	0.8	1.3	0.6	1.86 ∓ .53	.006 ∓ .003	.005
4.0*						**	.008
23.	.22	3.2	3.7	2.4	1.25 ∓ .35	.006 ∓ .002	.0086
32.	.27	4.3	4.7	3.5	1.92 ∓ .54	.012 ∓ .002	.012
40.	.25	3.8	4.2	3.4	1.93 ∓ .55	.009 ∓ .002	.009
54.	.3	4.3	4.8	4.0	1.65 ∓ .47	.010 ∓ .003	.009
56.	.29	3.8	4.7	3.5	1.32 ∓ .37	.016 ∓ .003	.017
110.	.35	4.5	5.3	3.9	1.14 ∓ .32	.012 ∓ .003	.012
260.*						**	.005
310.*						**	.006
360.	*	5.4	5.8	4.9	1.15 ∓ .32	.006 ∓ .002	.006

*The missing wave data were not obtained due to inadequate detail on the photographs.

**The measured thickness was not obtained due to excessive gauge null shift.

the calculated and measured mean thickness, and the mean wavelength for the low shear Mach 5 gas condition. Dependence of the mean wave speed on the liquid parameters is apparent from the data presented in the table.

The relationship between the dimensional wave speed and the liquid Reynolds number and thickness was examined by fitting the mean wave speed data to the response surface model given by equation 3. The regression analysis results for the model are given in Table V. The standard deviation of the data from this model is 0.227 and the significant coefficients of equation 3 are shown in Table VI. In this response surface model the units of the thickness in the normalized thickness parameter are inches and those of the wave speed are feet per second. For these data the critical F value of 2.0 used in the regression analysis corresponds to a significance level of approximately 80 percent. Therefore an 80 percent confidence interval is placed on each of the values of the coefficients and these intervals are also shown in Table VI. For all coefficients, the 80 percent confidence interval does not include zero and this is consistent with the higher significance level for each.

The F-ratio is a test of the assumption that the different b coefficients of the assumed model are equal to zero. For the original quadratic equation the regression analysis shows that the mean dimensional wave speed depends on both the film thickness and the Reynolds number. The final form of the equation for the low shear Mach 5 gas condition is

$$U_w = 2.856 + 0.391\hat{h} + 1.424\hat{R} - 0.2087\hat{h}^2 - 0.1265\hat{h}\hat{R}.$$

TABLE V

ANALYSIS OF VARIANCE FOR DIMENSIONAL WAVE SPEED AT LOW SHEAR MACH 5 GAS CONDITION

Source	Sum of Squares	Degrees of Freedom	Mean Square	F-Ratio
Total	35.00	11	0.182	
Regression	34.643	4	8.66	168.5
Error	0.357	7	0.0514	

TABLE VI

MODEL COEFFICIENT VALUES FOR DIMENSIONAL WAVE SPEED AT LOW SHEAR MACH 5 GAS CONDITION

Coefficient	Value and 80% Confidence Interval	Standard Error	F-Ratio	Significance Level
b_0	2.866 ± 0.135	.0917		
b_1	0.391 ± 0.13	.0883	19.57	.996
b_2	1.424 ± 0.096	.0647	484.96	.999
b_3	-0.2087 ± 0.08	.0543	14.74	.99
b_5	-0.1265 ± 0.067	.0451	7.88	.97

It is apparent from the form of this equation that the most significant variation of the wave speed is associated with the linear variation of the logarithm of Reynolds number and that the wave speed increases with Reynolds number. The equation should not be applied outside of the range and combinations of the data shown in Table IV. Specifically, h varies between 0.006 and 0.016 inches and R varies between 0.22 and 360. As an example for a Reynolds number of 1.0 ($\hat{R}$ = -1.183) and thicknesses below the 0.006 inch minimum in the table ($\hat{h}$ = -1.), the predicted wave speed can become negative and this is physically meaningless.

Figure 16 is a plot of the dimensional wave speed versus Reynolds number for thicknesses of 0.006, 0.010, and 0.012 inches. The curves for the three thicknesses were generated using the model given by equation 3 with the values of the coefficients shown in Table VI. Eighty percent confidence intervals for the predicted values using this model include in all cases the observed values and the intervals are shown at the measured data points in the figure. The agreement between the measured data points and the two curves is satisfactory. Since the final form of the model is generated using all of the measured data, this agreement attests to the satisfactory fit of the data to the model. The curves show for each thickness the influence of the Reynolds number. For a constant thickness of 0.006 inches at Reynolds numbers of 1.8, 23, and 360, the mean wave speeds are 0.8, 3.0, and 5.4 feet per second respectively. For a constant thickness of 0.012 inches at Reynolds numbers of 1.0, 30, and 110, the corresponding data are 1.7, 4.3, and 4.5 feet per second. Both examples confirm that the wave speed increases with increasing Reynolds number.

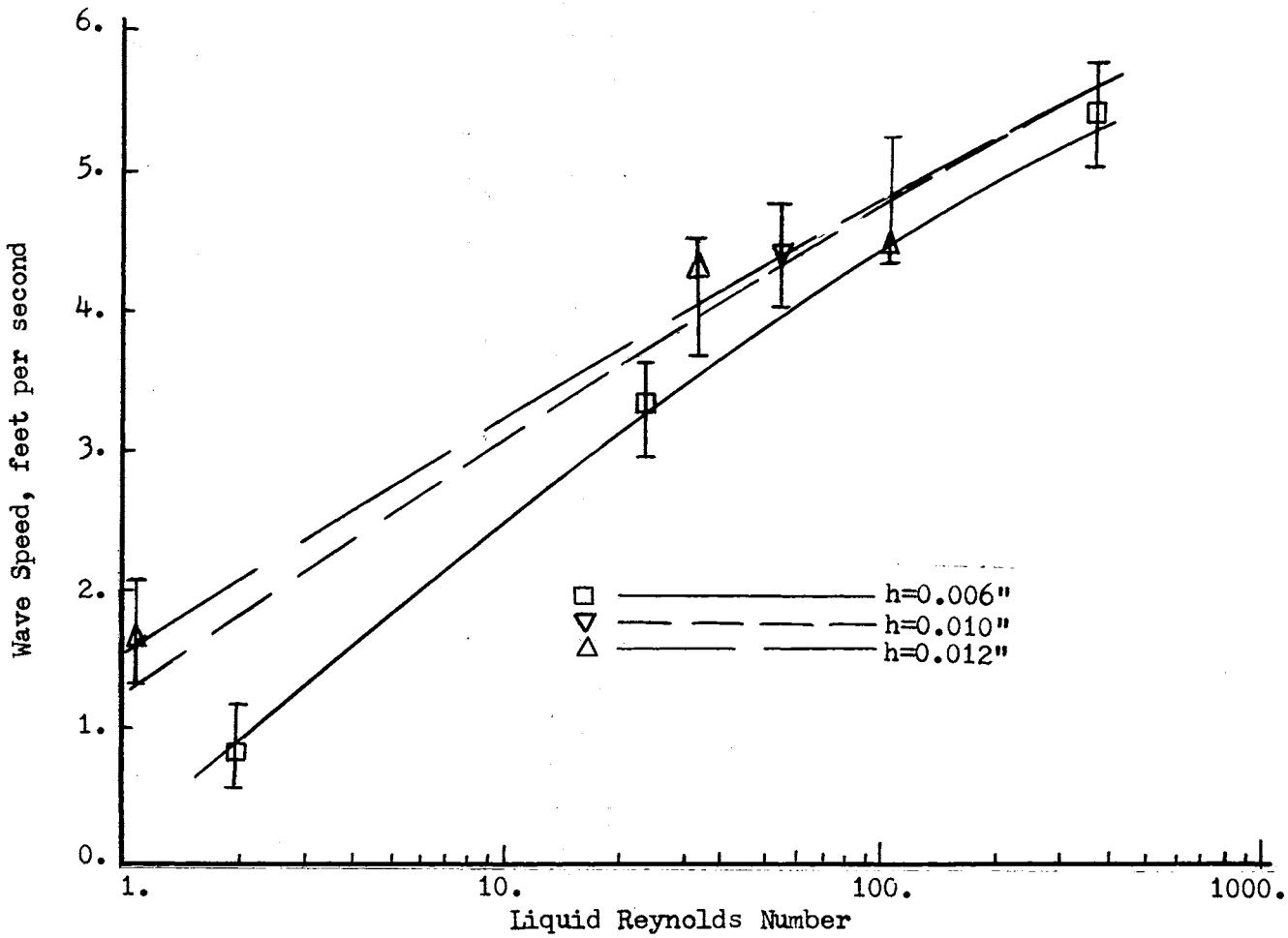

Figure 16. Variation of Wave Speed for Constant Liquid Thicknesses at Low Shear Mach 5 Gas Condition

Figure 17 presents a plot of the mean wave speed as a function of the liquid thickness for Reynolds numbers of 1, 55, and 360. As before the fitted model was used to generate the three curves and the appropriate data taken from Table IV are also shown. The effect of thickness is not as evident or as consistent as the effect of varying the Reynolds number. At each Reynolds number the model predicts that the wave speed increases with thickness for certain values and decreases with increasing thickness values at other values. This trend does not contradict the measured data but additional data are necessary to confirm that this is a real trend. As before the error bars on the curves represent the 80 percent confidence intervals and these intervals include the observed data.

The same liquid flow rate-viscosity combinations were produced at the high shear Mach 5 condition as were produced at the low shear Mach 5 condition just discussed. However, because of the higher shear at this condition, corresponding liquid velocities are somewhat higher and the thicknesses smaller. The measured mean wave speeds for each of the experiments for which the data could be measured are shown in Table VII together with the maximum and minimum values measured in the series of measurements which go to make up each mean velocity. As discussed previously, the liquid conditions for which the interface became too irregular for the wave data to be obtained were found to be a function of the gas condition. For the high shear Mach 5 condition the interface became irregular and chaotic at a liquid Reynolds number above 60. In addition the photographs of some of the experiments at Reynolds numbers less than 60 were not of sufficient detail to permit the

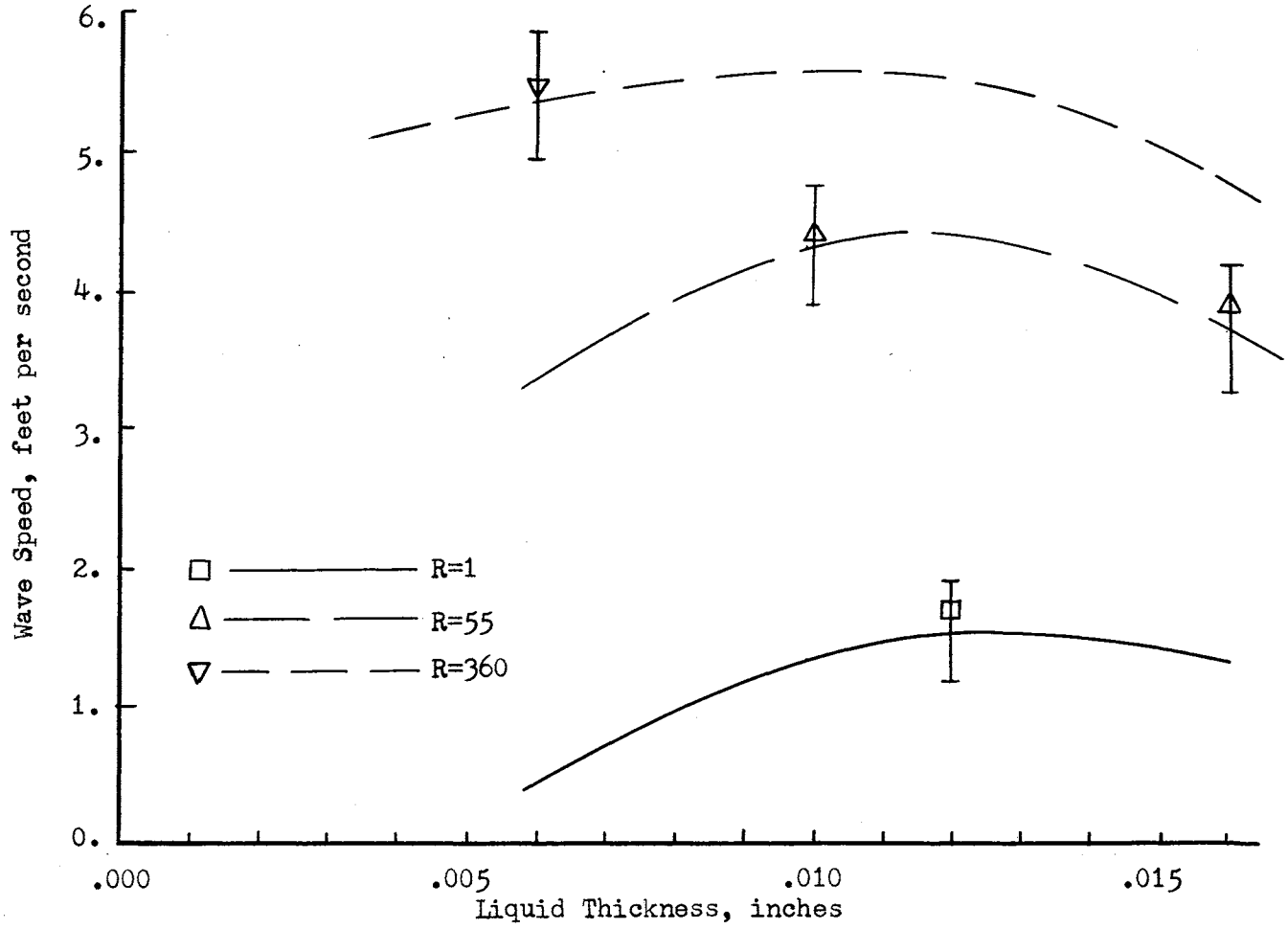

Figure 17. Variation of Wave Speed for Constant Reynolds Numbers at Low Shear Mach 5 Gas Condition

TABLE VII

MEASURED INTERFACE DATA FOR HIGH SHEAR MACH 5 GAS CONDITION

Reynolds Number	Mean Wave Length, in.	Mean Wave Speed, fps	Maximum Wave Speed, fps	Minimum Wave Speed, fps	Dimensionless Mean Wave Speed	Measured Thickness, in.	Calculated Thickness, in.
.33	.15	.9	1.2	.6		**	.008
.53*		1.8	3.3	1.2	4.65 ∓ 1.3	.011 ∓ .001	.01
.9*						**	.01
1.0*	.17	3.3	4.1	3.0	7.83 ∓ 2.2	.012 ∓ .003	.011
2.0*						**	.011
4.3*						**	.007
21.		6.0	6.3	5.6	1.68 ∓ .48	.004 ∓ .002	.006
32.	.22	6.4	6.8	5.8	3.09 ∓ .9	.009 ∓ .002	.01
38.*						.006 ∓ .001	.007
60.	.23	5.0	6.0	4.3	1.24 ∓ .35	.013 ∓ .002	.014
66.*						.012 ∓ .002	.009
110.*						.012 ∓ .002	.011
135.*						**	.003
265.*						.004 ∓ .001	.005
360.*						.006 ∓ .002	.006

*The missing wave data were not obtained due to inadequate detail on the photographs.

**The measured thickness was not obtained due to excessive gauge null shift.

measurement of the data. Consequently, only a limited amount of wave speed data was obtained.

The wave data are given in Table VII and suggest that the dimensional wave speed increases with increasing Reynolds number. To verify this and to determine if the data also depend on the thickness, the regression analysis technique described previously was utilized. However because only five data points were obtained, a model with not more than four unknown coefficients can be used. For this condition the model is

$$U_w = b_0 + b_1\hat{h} + b_2\hat{R} + b_3\hat{h}\hat{R} + E$$

where $\hat{h}$ is the normalized liquid thickness defined previously and $\hat{R}$ is defined by

$$\hat{R} = \frac{\ln R - \ln 4.5}{\ln 60 - \ln 4.5} \quad .$$

For the limited Reynolds number range for this gas condition, this normalization constrains the parameter to lie between minus one and plus one. This equation is a linear model with interaction of the two liquid parameters. The results of the regression analysis are shown in Table VIII. Because of the minimum degrees of freedom in the error term of the analysis of variance, the assumed critical F-ratio value of 2.0 corresponds to a confidence level of only 60 percent. The standard deviation of the data from the model is 0.283 and the values of the significant coefficients, including 60 percent confidence intervals, are given in Table IX. The regression analysis retains all coefficients; however the significance levels of all four coefficients are lower than those for the low shear Mach 5 condition. This result is

TABLE VIII

ANALYSIS OF VARIANCE FOR DIMENSIONAL WAVE SPEED
AT HIGH SHEAR MACH 5 GAS CONDITION

Source	Sum of Squares	Degrees of Freedom	Mean Square	F-Ratio
Total	14.84	4	3.71	
Regression	14.76	3	4.92	61.3
Error	0.08	1	0.08	

TABLE IX

MODEL COEFFICIENT VALUES FOR DIMENSIONAL WAVE
SPEED AT HIGH SHEAR MACH 5 GAS CONDITION

Coefficients	Value and 60% Confidence Interval	Standard Error	F-Ratio	Significance Level
b_0	2.74 ± 0.55	0.389		
b_1	1.49 ± 0.618	0.489	9.3	.80
b_2	4.56 ± 0.91	0.658	48.1	.91
b_3	-3.155 ± 1.03	0.748	17.8	.88

due to the very limited data available for the analysis. The final form of the fitted model for the high shear Mach 5 condition is

$$U_w = 2.74 + 1.49h + 4.56R - 3.155hR.$$

As for the previous low shear Mach 5 data, the wave speed is affected more strongly by the variation in the liquid Reynolds number as is shown by the larger coefficient for the normalized Reynolds number term in the fitted model. Use of the final equation is restricted to the range of parameters for these experiments and therefore is of more limited use than the model for the low shear Mach 5 condition.

Careful examination of the form of the model for different liquid conditions reveals some interesting and perhaps questionable features. At a Reynolds number of 21.3 the wave speed is independent of the thickness. At constant Reynolds numbers below 21.3 the wave speed increases with increasing thickness and at Reynolds numbers above 21.3 it decreases with increasing thickness.

At a thickness of 0.0133 inches the wave speed is independent of the Reynolds number. At thicknesses below this value the wave speed increases with increasing Reynolds number. Since the model is restricted to use in the range of these particular experimental conditions and the maximum thickness was 0.013 inches, the wave speed therefore increases with increasing Reynolds number at constant thickness.

A comparison of the observed wave speed data with the predicted values from the fitted model reveals extremely close agreement. The largest difference between the predicted and measured values is 0.203 feet per second. Because of the limited data with which to work, this

very close agreement is obtained even though the model appears to be unsatisfactory for predicting values other than at the measured conditions as was shown in the preceeding paragraphs.

Therefore the conclusions from the regression analysis of the data at this condition is limited to those of accepting or rejecting at the appropriate confidence level the hypothesis that the wave speed depends on the thickness and Reynolds number. Specifically, the linear regression analysis shows that the wave speed depends on both the liquid thickness and Reynolds number with an 80 to 91 percent confidence level.

The third gas condition utilized was the Mach 7 condition shown in Table I. The same liquid flow rate-viscosity combinations as those reported for both Mach 5 conditions were also produced for this condition. The measured wave data for the experiments at this gas condition are shown in Table X.

The mean wave speed data together with the maximum and minimum values measured are shown in the table. As for the other gas conditions the mean dimensional wave speed varies as a function of the liquid conditions. The regression analysis technique was employed to fit the data to the different thickness-Reynolds number combinations shown in the table. Similar to the low shear Mach 5 condition, the data were fit to the model given by equation 3. The results of the regression analysis are shown in Table XI. For the 8 degrees of freedom in the error term of the regression analysis, the assumed critical F value corresponds to a confidence level of 81 percent. The standard deviation of the data is 0.3582 and the values of the significant coefficients are given in Table XII along with 80 percent confidence intervals on

TABLE X

MEASURED INTERFACE DATA FOR MACH 7 GAS CONDITION

Reynolds Number	Mean Wave Length, in.	Mean Wave Speed, fps	Maximum Wave Speed, fps	Minimum Wave Speed, fps	Dimensionless Mean Wave Speed	Measured Thickness, in.	Calculated Thickness, in.
.22	.18	.4	.5	.3	2. ∓ .57	.01 ∓ .002	.0127
.5	.21	.7	1.0	.5	3.22 ∓ .92	.014 ∓ .002	.013
.9	.19	1.3	1.9	.7		**	.01
1.2	.26	1.7	2.5	1.2		**	.011
1.4*						**	.012
3.8	.37	3.1	3.5	2.3	5. ∓ 1.4	.016 ∓ .002	.0136
21.	.34	3.9	4.2	3.3	1.65 ∓ .47	.006 ∓ .002	.008
32.	.41	3.9	4.3	3.6	1.54 ∓ .43	.007 ∓ .002	.0076
34.	.41	3.6	4.0	3.3	1.49 ∓ .42	.011 ∓ .002	.012
54.	.45	3.8	4.0	3.3	1.5 ∓ .42	.011 ∓ .002	.0092
85.	.4	3.3	3.9	2.2	.89 ∓ .25	.014 ∓ .003	.013
126.	.42	4.1	4.72	3.57	1.05 ∓ .3	.015 ∓ .003	.010
130.*		4.3	4.6	2.9	.905 ∓ .25	.003 ∓ .002	.0033
260.*		4.6	4.8	4.2	.84 ∓ .24	.006 ∓ .002	.0046
360.*		4.7	5.2	3.7	.932 ∓ .26	.007 ∓ .003	.006

*The missing wave data were not obtained due to inadequate detail on the photographs.

**The measured thickness was not obtained due to excessive gauge null shift.

TABLE XI

ANALYSIS OF VARIANCE FOR DIMENSIONAL WAVE SPEED AT MACH 7 GAS CONDITION

Source	Sum of Squares	Degrees of Freedom	Mean Square	F-Ratio
Total	21.51	11	1.96	
Regression	20.48	3	6.83	53.2
Error	1.03	8	.128	

TABLE XII

MODEL COEFFICIENT VALUES FOR DIMENSIONAL WAVE SPEED AT MACH 7 GAS CONDITION

Coefficient	Value and 80% Confidence Interval	Standard Error	F-Ratio	Significance Level
b_0	3.13 ± 0.253	.1809		
b_2	1.063 ± 0.121	.0867	150.3	.999
b_4	-0.225 ± 0.112	.08	7.94	.975
b_5	-0.107 ± 0.094	.0672	2.54	.85

each coefficient. In all cases this interval does not include zero and reflects the higher significance levels of each coefficient.

The results of this regression analysis show that the coefficients of both the linear and quadratic thickness terms are not different from zero at the 81 percent confidence level. The coefficient of the interaction term $\hat{h}\hat{R}$ is significantly different from zero; however, the F-ratio test produces a lower significance level for this term than for either the linear or the quadratic Reynolds number terms.

The final form of the response surface model for the Mach 7 gas condition is

$$U_w = 3.13 + 1.063\hat{R} - 0.225\hat{R}^2 - 0.107\hat{h}\hat{R}.$$

Comparison of the values of the coefficients confirms that the data depend more on the Reynolds number terms than on the interaction term and also shows that the linear Reynolds number term accounts for the greatest effect on the wave speed. Figure 18 is a plot of the mean wave speed as a function of Reynolds number for liquid thicknesses of 0.006, 0.007, and 0.011 inches. The curves are calculated using the final form of the model. The mean wave speed data for the corresponding thicknesses are also plotted and the error bars represent 80 percent confidence intervals for predicted data based on this model. The agreement between the curves and the data illustrate the satisfactory fit of the model to the data. These curves show that the wave speed increases with Reynolds number at constant thickness. As an example for a constant thickness of 0.006 inches and Reynolds numbers of 21 and 260, the wave speed is 3.9 and 4.6 feet per second respectively. Also at a constant thickness of 0.011 inches and Reynolds numbers of 34 and

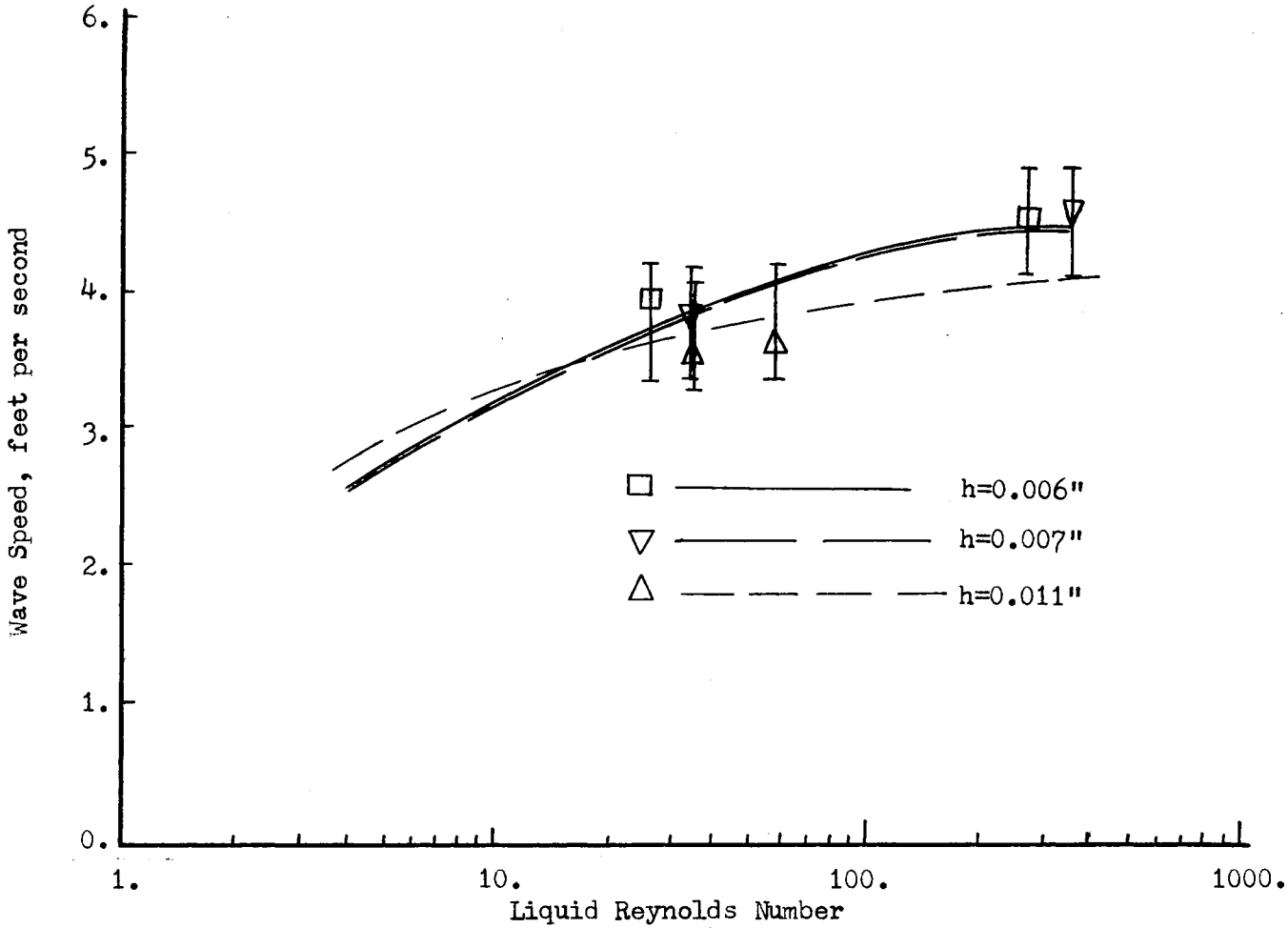

Figure 18. Variation of Wave Speed for Constant Liquid Thicknesses at Mach 7 Gas Condition

54, the wave speed is 3.6 and 3.8 feet per second respectively. For each of these thickness values the wave speed increases with Reynolds number.

Figure 19 is a plot of mean wave speed versus film thickness for liquid Reynolds number of 0.5, 33, and 260. The curves are calculated using the fitted model and appropriate data points from Table X are also shown to illustrate the agreement of the measured data and the model.

For the two experiments at Reynolds numbers of 32 and 34, the resulting thicknesses are 0.007 and 0.011 inches. If these two Reynolds numbers are for comparative purposes assumed equal, the effect of thickness change at constant Reynolds number is isolated. For these two thicknesses the wave speeds are 3.9 and 3.6 feet per second respectively and suggest that the wave speed decreases slightly with increasing thickness at constant Reynolds number. This result is consistent with the curve for a Reynolds number of 33 shown in Figure 19. At higher Reynolds numbers an increase in thickness also produces a decrease in the wave speed for any constant Reynolds number. At lower Reynolds numbers the model indicates that the thickness effect is reversed and the wave speed increases with increasing thickness at constant Reynolds numbers.

In the preceding paragraphs of this section the effects of the liquid Reynolds number and thickness on the mean wave speed were discussed individually for each of the three gas conditions. The effects of the gas condition on the mean wave speed can be evaluated by comparing the data at similar liquid conditions and different gas conditions. The final models for the Mach 7 and the low shear Mach 5

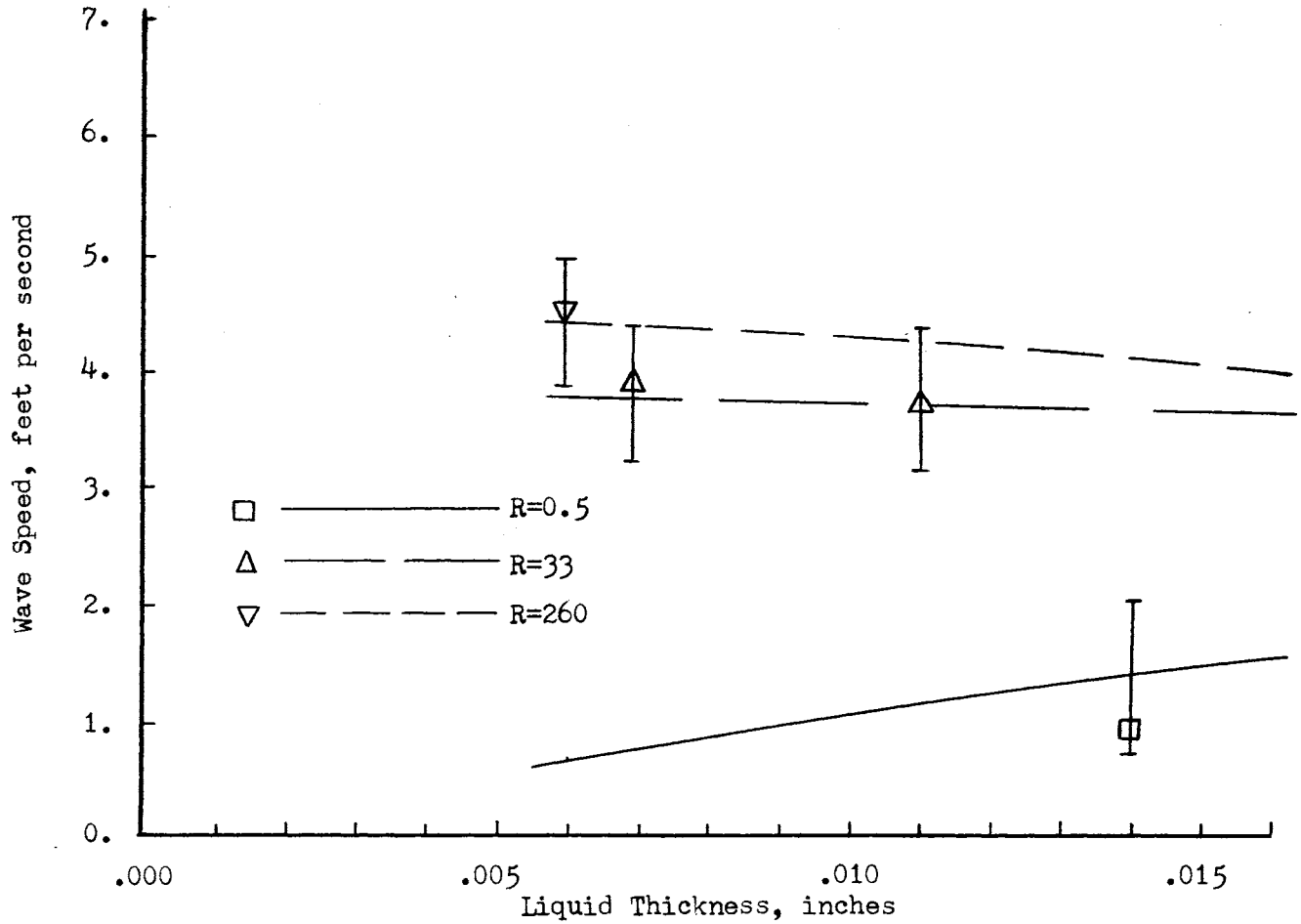

Figure 19. Variation of Wave Speed for Constant Reynolds Numbers at Mach 7 Gas Condition

conditions are not similar in form and therefore suggest that the effects of the thickness and Reynolds number are not similar. However comparisons of the particular forms of the final equations are not as meaningful as comparing the predicted trends from the models for conditions typical of these experiments. To make these comparisons, curves representing each of the models together with appropriate data are most effective. Figure 20 presents the mean wave speed for a liquid thickness of 0.012 inches as a function of Reynolds number for the low shear Mach 5 and Mach 7 conditions. The high shear Mach 5 curves and data are not included in this comparison because of the limited data obtained at that condition. The curves in Figure 20 for the two gas conditions are calculated using the final forms of the response surface models discussed in the previous sections. Shown also on this figure are three measured data points at the low shear Mach 5 gas condition. No data for a thickness of 0.012 inches were obtained at the Mach 7 gas condition but the comparisons presented in the preceding paragraphs confirm the acceptable fit of the data to the model in this range of thickness. For a selected thickness the liquid conditions are constant for a fixed Reynolds number value and the variation in wave speed is therefore due to the variation in the gas condition. Comparison of the data from the two gas conditions reflect the effects of the variation in the gas condition at approximately equal shear stress. At Reynolds numbers below 3 the model predicts higher wave speeds for the Mach 7 condition while at higher Reynolds number the low shear Mach 5 condition produces a higher wave speed.

The effects of the gas conditions on the mean wave speed for similar liquid conditions may be evaluated at a second liquid thickness by

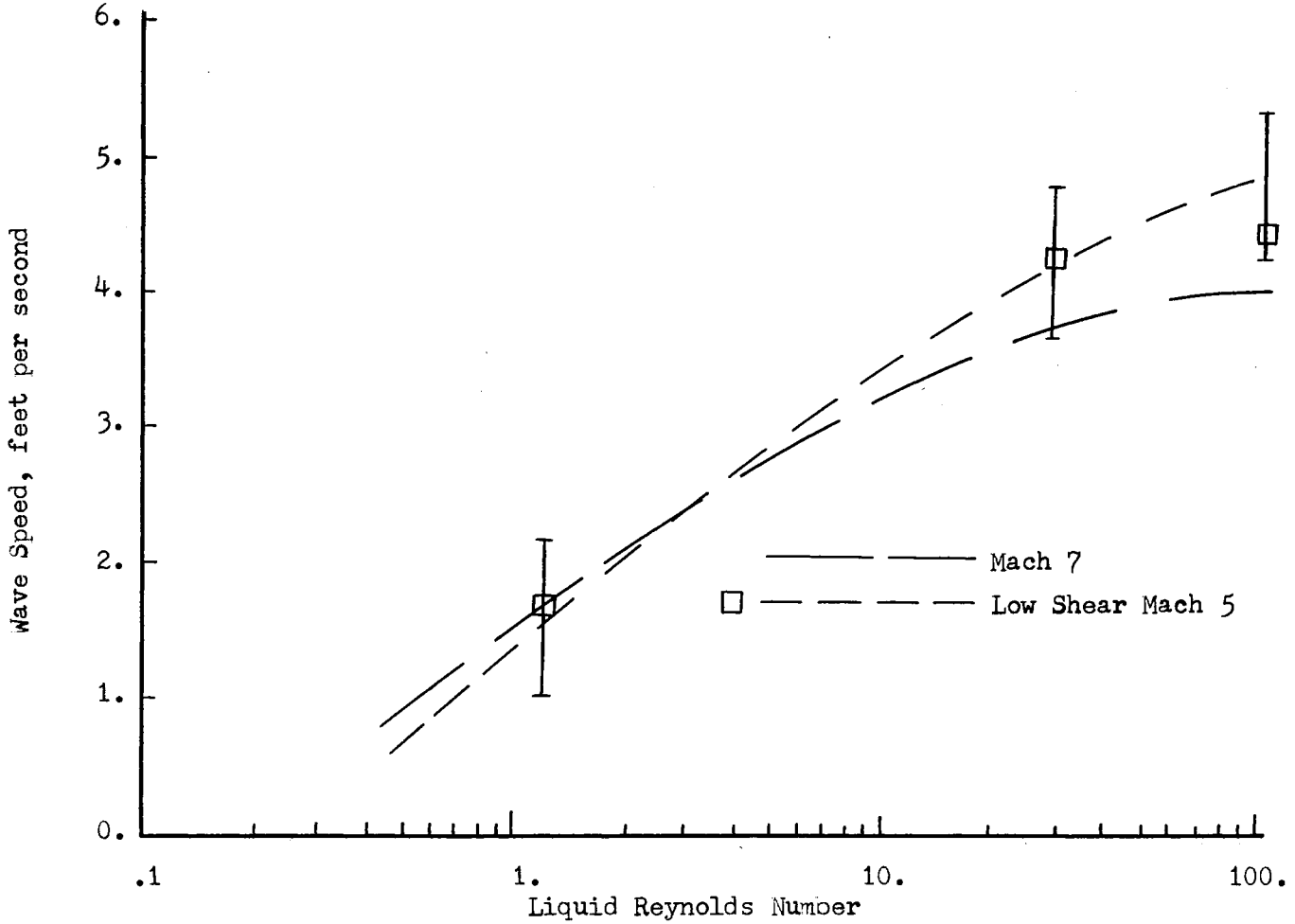

Figure 20. Comparison of Wave Speed for Different Gas Conditions at Similar Liquid Conditions, h = 0.012 Inches

considering Figure 21. As for the previous figure, curves are shown for low shear Mach 5 and Mach 7 gas conditions and present the wave speed as a function of Reynolds number. The curves are constructed using the fitted model equations for a liquid thickness of 0.006 inches. Shown also on the figure are data points for both gas conditions which illustrate the satisfactory fit of the model to the data. The data and curves at the Mach 7 and the low shear Mach 5 show that the wave speed is higher for the Mach 7 condition at Reynolds number below about 70 while the wave speed is lower for the Mach 7 condition at higher Reynolds numbers.

Figure 22 is a plot of the mean wave speed versus thickness for the same two gas conditions at a Reynolds number of 32. Data points for each of the gas conditions are also shown. As in the previous two figures the wave speeds for the two conditions are nearly equal at similar liquid conditions with the curves crossing at intermediate values of the thickness.

In summary the effects of the liquid parameters and the gas conditions on the mean wave speed are evaluated. At the low shear Mach 5 condition the mean wave speed depends on both the liquid Reynolds number and thickness. The F-ratio tests suggest the dependence on the Reynolds number may be accepted at a higher level of confidence. Because of the limited data at the high shear Mach 5 condition, a linear response surface model was used. The regression analysis indicates that the data depend on both the thickness and Reynolds number. In the range of thicknesses for these experiments, the wave speed increases with increasing Reynolds number at constant thickness. The analysis of the Mach 7 data also reveals that the data are dependent on both the

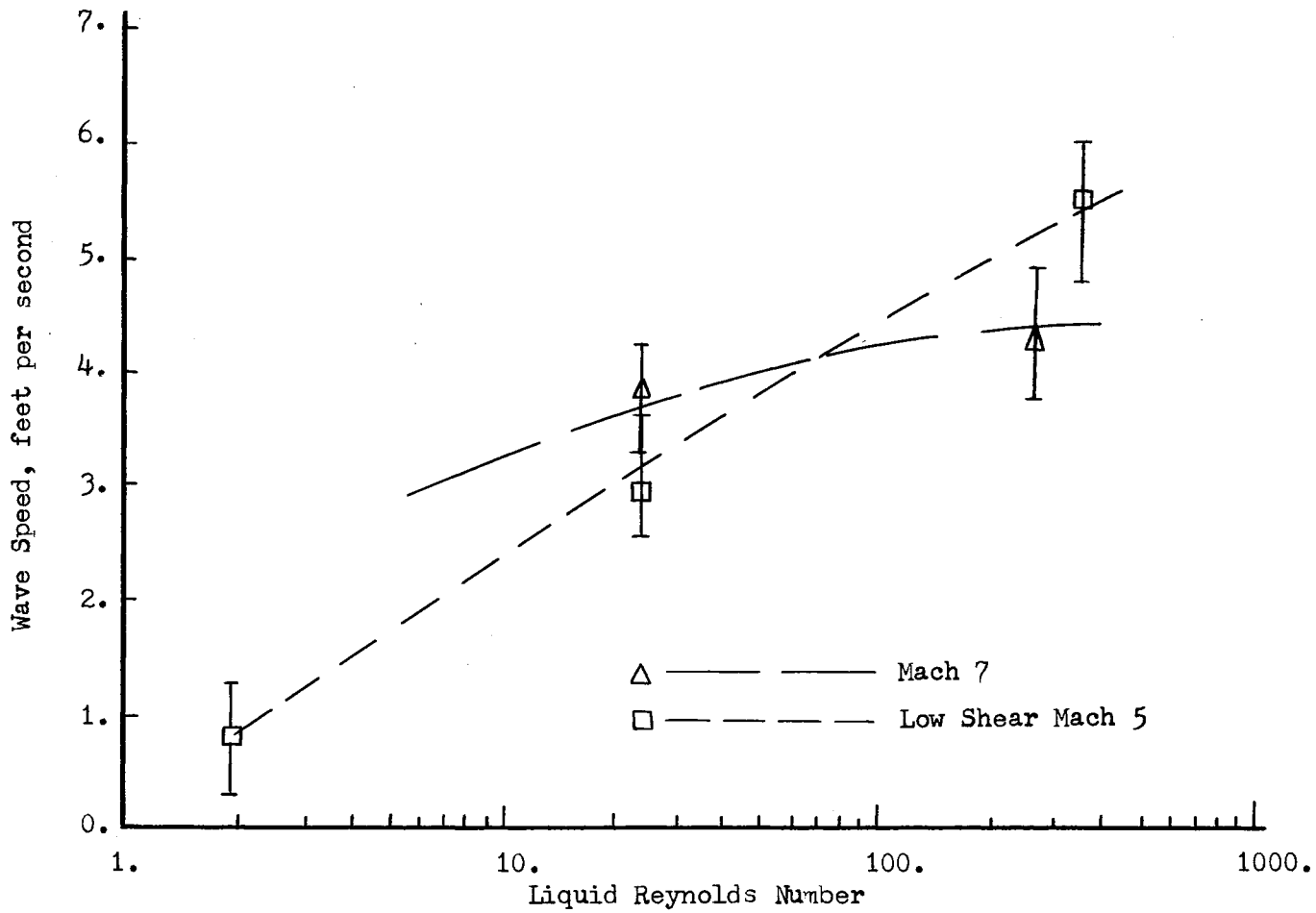

Figure 21. Comparison of Wave Speed for Different Gas Conditions at Similar Liquid Conditions, h = 0.006 Inches

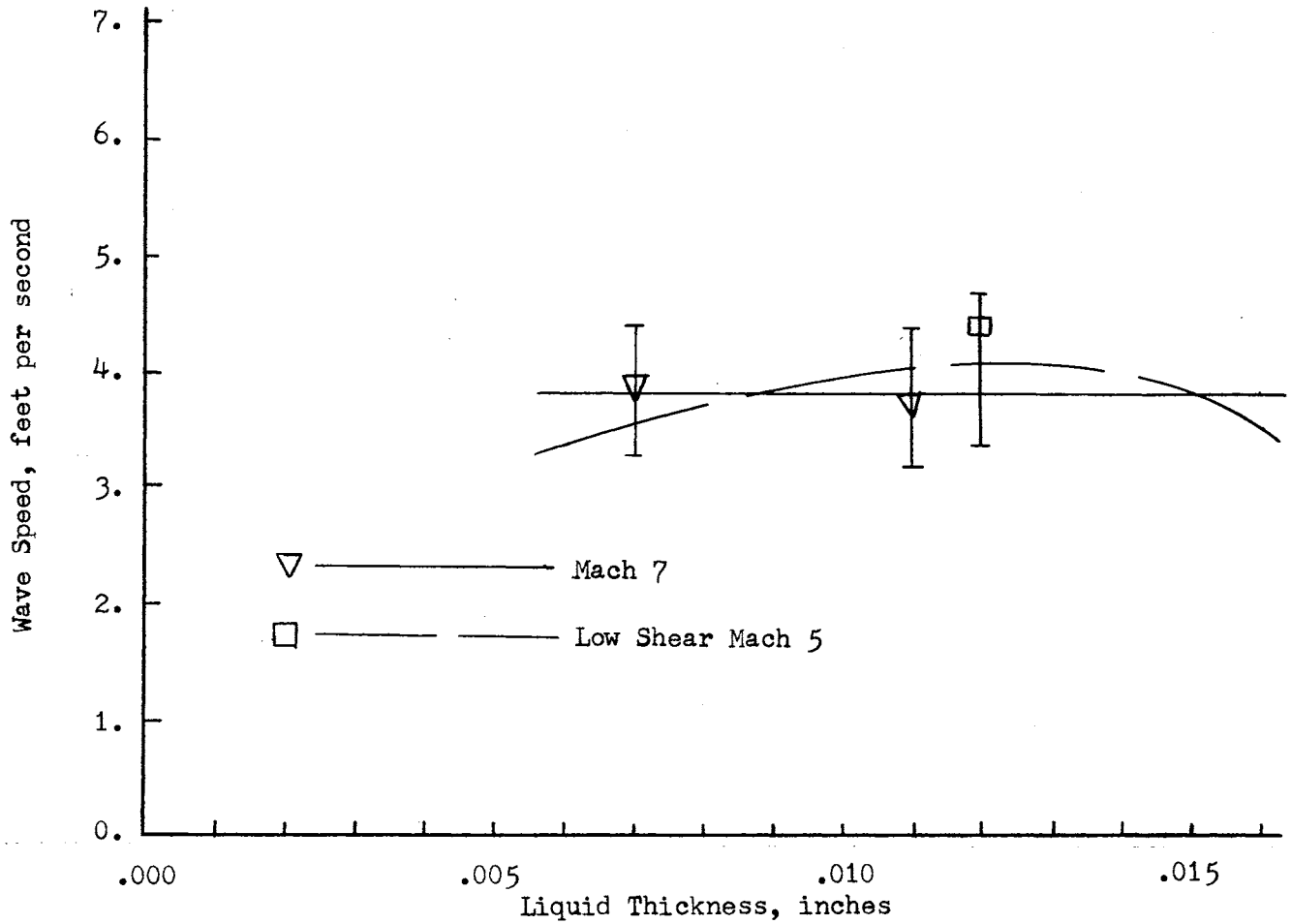

Figure 22. Comparison of Wave Speed for Different Gas Conditions at Similar Liquid Conditions, R = 32

Reynolds number and thickness. The mean wave speed for all conditions increases with increasing Reynolds number at constant thickness. The regression analyses show that the wave speeds at the Mach 7 and the low shear Mach 5 condition are not sufficiently different to allow any conclusion regarding which condition produces the higher wave speeds.

Since at some liquid conditions the Mach 7 condition produces the higher speed while at others the reverse is true, one concludes that the gas Mach number is not a parameter which significantly affects the liquid wave speeds. However, calculations made with the boundary layer analysis described in Appendix D show that, due to the blunt body effects of the model, the Mach numbers at the edge of the boundary layer are equal for the Mach 5 and the Mach 7 gas flows. Because these Mach numbers are equal, any conclusions regarding the effects of the gas Mach number must be reserved until additional experiments are performed which produce a wider range of Mach number variation.

Dimensionless Wave Speed

The dimensionless wave speed is also utilized to characterize the liquid interface. As the liquid Reynolds number varies for the different experiments, the liquid velocity also varies. Therefore to incorporate this variation into the data, the dimensionless wave speed is formed by dividing the measured wave speed by twice the mass average liquid velocity. The dimensionless wave speed is given by

$$C = \frac{U_w}{2U_m} . \qquad (4)$$

In this equation U_w is the dimensional mean wave speed and U_m is the

mean liquid velocity calculated from the expression

$$U_m = \frac{Q}{hl}$$

where Q is the volumetric flow rate, h is the liquid thickness and l is the model width. For a linear profile in the liquid the interface velocity is twice the mean velocity and the wave speed is for that case non-dimensionalized using the interface velocity. In portions of the data analyses which follow the distinction of waves which possess a dimensionless speed greater or less than one will be made. The data will be further interpreted as waves which are moving faster or slower than the interface velocity. For this interpretation the assumption of a linear velocity profile is therefore implicit.

The dimensionless wave speed data for the low shear Mach 5 condition are given in Table IV. These data were fit to the response surface model given by equation 3 and the results of the regression analysis are given in Table XIII. The confidence level corresponding to the assumed critical F-ratio of 2.0 is approximately 80 percent for this analysis. The standard deviation for the model is 0.5756 and the statistically significant coefficients, including 80 percent confidence intervals, are given in Table XIV. The coefficients b_5 and b_4 which correspond to the interaction term and the quadratic Reynolds number term are not significant. Of the remaining terms the dependence of the data on the linear variation of the logarithm of the Reynolds number term is accepted at a higher probability as indicated by the higher significance level as shown in Table XIV. The final form of the response surface is

$$C = 2.336 + 0.346\hat{h} - 0.551\hat{R} - 0.264\hat{h}^2 .$$

TABLE XIII

ANALYSIS OF VARIANCE FOR DIMENSIONLESS WAVE SPEED AT LOW SHEAR MACH 5 GAS CONDITION

Source	Sum of Squares	Degrees of Freedom	Mean Square	F-Ratio
Total	9.544	10	.9544	
Regression	7.225	3	2.4085	7.27
Error	2.319	7	.3313	

TABLE XIV

MODEL COEFFICIENT VALUES FOR DIMENSIONLESS WAVE SPEED AT LOW SHEAR MACH 5 GAS CONDITION

Coefficient	Value and 80% Confidence Interval	Standard Error	F-Ratio	Significance Level
b_0	2.336 ± 0.331	0.235		
b_1	0.346 ± 0.31	0.22	2.47	.8
b_2	-0.551 ± 0.203	0.144	14.53	.99
b_3	-0.264 ± 0.217	0.154	2.92	.82

Since the wave speed C is dimensionless for this model, all coefficients are also dimensionless. The limits for the use of this equation are the thickness-Reynolds number conditions shown in Table IV and in no event is a negative value of the wave speed meaningful. By comparing the values of the coefficients in this equation it is apparent that the data are more affected by variations in the Reynolds number than in the thickness and that the dimensionless wave speed decreases with increasing Reynolds number.

Figure 23 is a plot of the dimensionless wave speed as a function of the Reynolds numbers for thicknesses of 0.006 and 0.012 inches. The curves are constructed using the final response surface model. Two data points for each thickness are also shown and these points illustrate the satisfactory fit of the data to the model. The error bars on the curves are 80 percent confidence intervals on predicted data using this model and these intervals include the appropriate measured quantities for all of the experiments. At both thicknesses the dimensionless wave speed decreases with increasing Reynolds number at constant thickness.

Figure 24 is a plot of the dimensionless wave speed as a function of the thickness for Reynolds numbers of 55 and 1 with three data points shown for comparison. For both Reynolds numbers the model predicts that the dimensionless wave speed increases slightly with increasing thickness at lower thickness values and predicts a decrease with increasing thickness at thicknesses above 0.010 inches. However additional experiments are necessary to confirm this type of dependence. The 80 percent variations of the model coefficients will alter the curves more significantly than these slight changes.

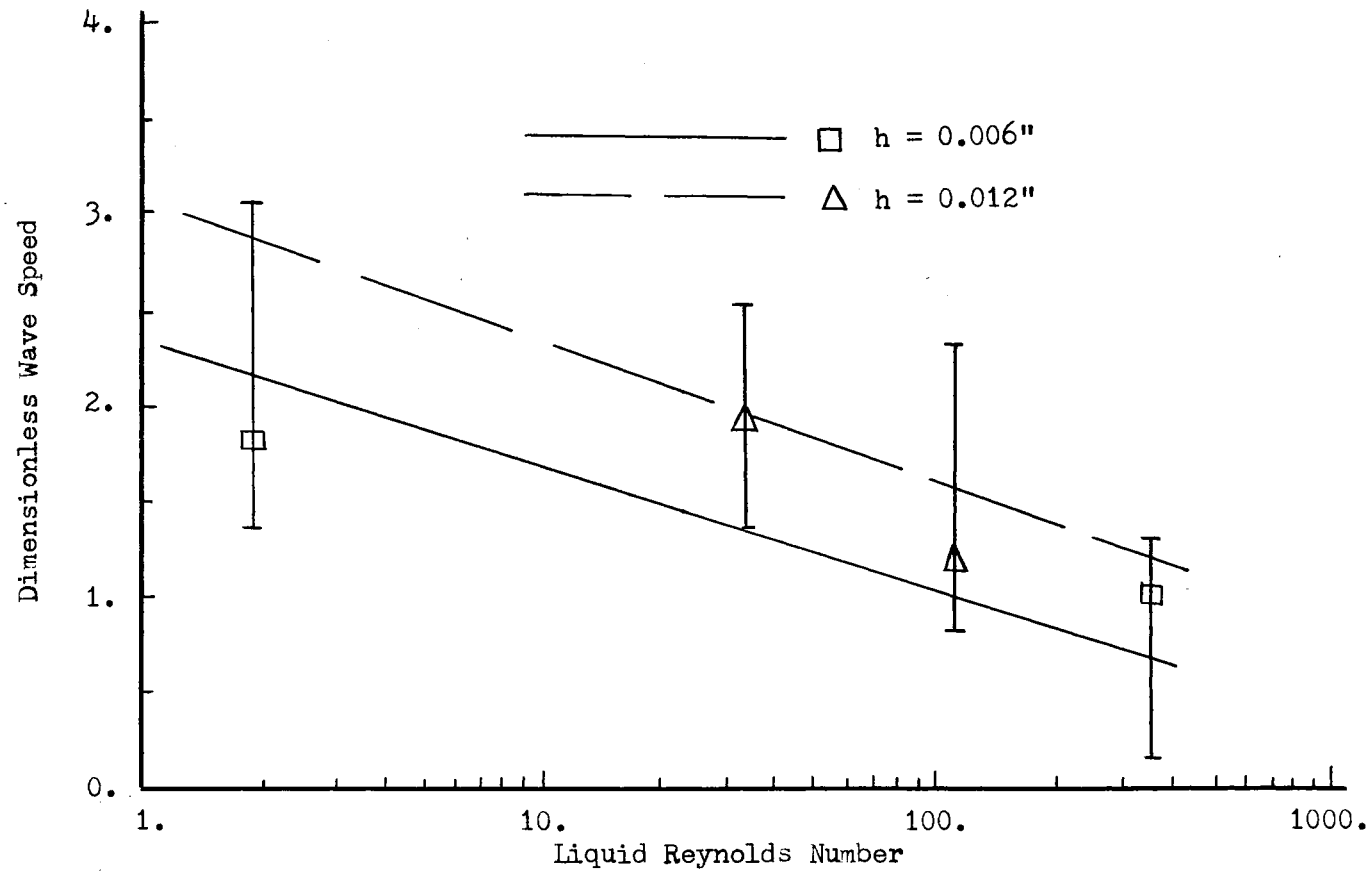

Figure 23. Variation of Dimensionless Wave Speed for Constant Liquid Thicknesses at Low Shear Mach 5 Gas Condition

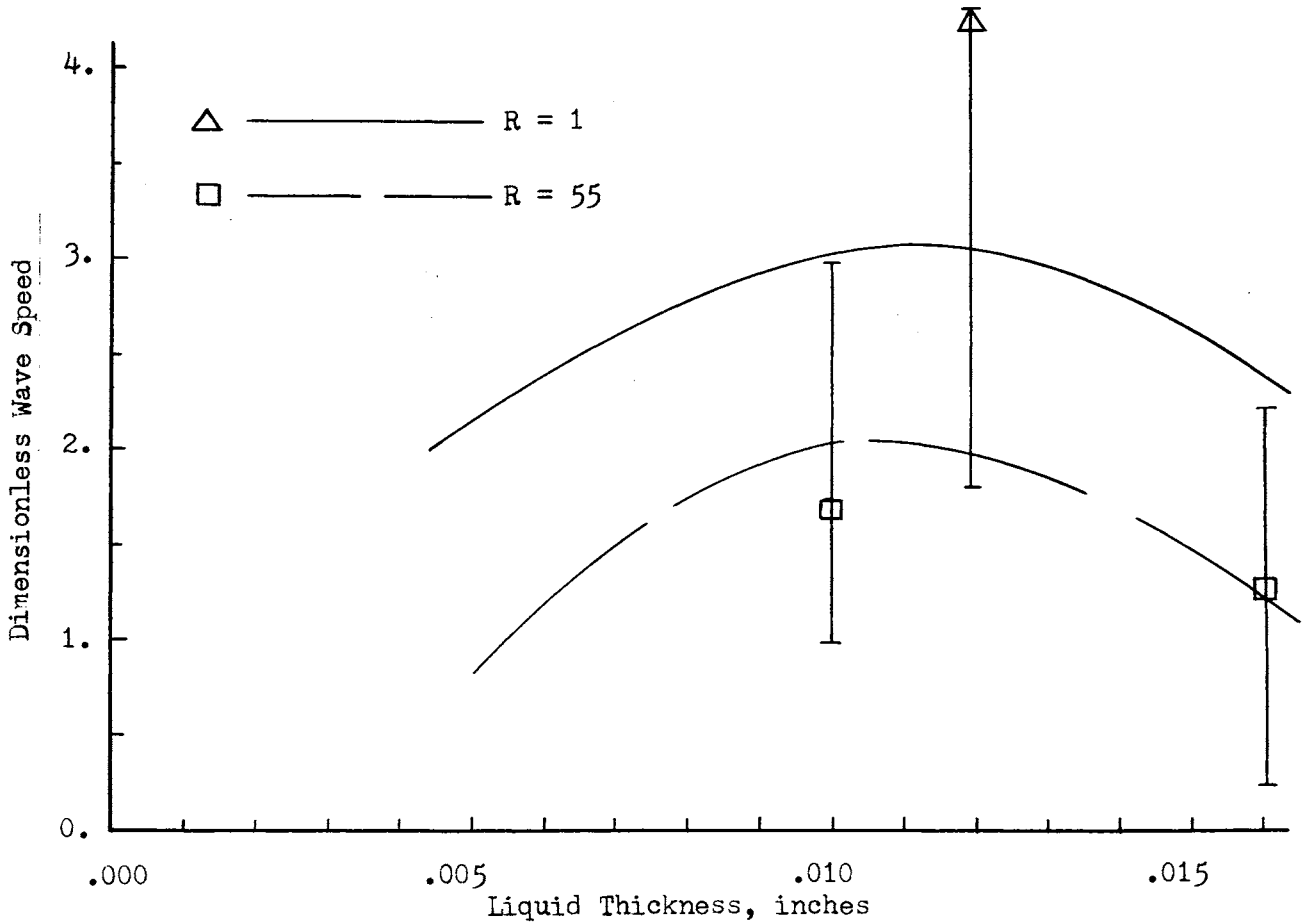

Figure 24. Variation of Dimensionless Wave Speed for Constant Reynolds Numbers at Low Shear Mach 5 Gas Condition

The dimensionless wave speed data for the high shear Mach 5 condition are shown in Table VII. Because of the limited data at this condition, the linear model described in the preceding discussion of the high shear Mach 5 dimensional wave speed data was utilized. The regression analysis results are given in Table XV. For these data the F-ratio of 2.0 assumed in the regression analysis corresponds to a confidence level of only 60 percent due to the minimum value of the error degrees of freedom. The standard deviation of the data from the model is 0.357 and the significant coefficients together with 60 percent confidence intervals on each value are given in Table XVI. For this model the thickness, Reynolds number, and the interaction term are all retained and all are significant at a confidence level well in excess of the 60 percent cutoff value. However because of the limited data the error degrees of freedom is only one, its minimum value; and the significance level is generally less than that calculated for the other two gas conditions. As for the previous models this equation will predict negative values for some combinations of $\hat{h}$ and $\hat{R}$ and therefore its use is restricted to the range of liquid parameters shown in Table VII. The final form of the model is

$$C = 0.38 + 5.19\hat{h} + 3.92\hat{R} - 7.57\hat{h}\hat{R}.$$

This model is very similar to that for the dimensional wave speed at this gas condition and has some of the same features. At a Reynolds number of 26.6 the wave speed is independent of the thickness. Above this Reynolds number the wave speed decreases with thickness and below the value it increases with thickness. Although the model predicts the measured data satisfactorily (a maximum of 0.26 difference), a 95

TABLE XV

ANALYSIS OF VARIANCE FOR DIMENSIONLESS WAVE SPEED
AT HIGH SHEAR MACH 5 GAS CONDITION

Source	Sum of Squares	Degrees of Freedom	Mean Square	F-Ratio
Total	28.46	4	7.11	
Regression	28.332	3	9.45	73.8
Error	.128	1	.128	

TABLE XVI

MODEL COEFFICIENT VALUES FOR DIMENSIONLESS WAVE SPEED
AT HIGH SHEAR MACH 5 GAS CONDITION

Coefficient	Value and 60% Confidence Interval	Standard Error	F-Ratio	Significance Level
b_0	0.38 ± 0.68	0.492		
b_1	5.19 ± 0.85	0.618	70.6	.93
b_2	3.92 ± 1.14	0.831	22.3	.85
b_3	-7.57 ± 1.30	0.944	64.2	.92

percent confidence interval for the prediction of a future observation from the model reflects an error margin of approximately $\pm$ 6 for all data points. This extremely large confidence band reflects the limited data upon which the model is constructed. In effect about the strongest conclusion which can be made from these data is that the wave speed does depend on the liquid parameters at approximately a 90 percent confidence level and that it decreases with increasing Reynolds number.

The dimensionless mean wave speeds for the Mach 7 gas condition are shown in Table X. Examination of these data suggests that the dimensionless wave speed decreases with the increasing Reynolds number. The regression analysis described previously for the low shear Mach 5 condition was also performed using these data. The results of the regression analysis are given in Table XVII. The confidence level corresponding to the assumed critical F-ratio of 2.0 is 81 percent for this analysis. The standard deviation of the model is 0.552 and the values of the coefficients in the fitted equation including 80 percent confidence intervals are given in Table XVIII. For this model the coefficients of both the film thickness and the Reynolds number terms are significant at approximately the same confidence level and the response surface equation is

$$C = 1.8 + 0.816\hat{h} - 0.319\hat{R}^2 - 0.614\hat{h}\hat{R}.$$

As for the previous models this relationship should not be utilized outside the range and combinations of thickness and Reynolds numbers shown in Table X since it is apparent from the form of the equation that negative wave speeds can be predicted under some combinations of thickness and Reynolds number.

TABLE XVII

ANALYSIS OF VARIANCE FOR DIMENSIONLESS WAVE SPEED AT MACH 7 GAS CONDITION

Source	Sum of Squares	Degrees of Freedom	Mean Square	F-Ratio
Total	16.411	11	1.492	
Regression	13.973	3	4.658	15.29
Error	2.438	8	.3047	

TABLE XVIII

MODEL COEFFICIENT VALUES FOR DIMENSIONLESS WAVE SPEED AT MACH 7 GAS CONDITION

Coefficient	Value and 80% Confidence Interval	Standard Error	F-Ratio	Significance Level
b_0	1.80 ± 0.501	0.282		
b_1	0.816 ± 0.201	0.142	33.1	.997
b_4	-0.319 ± 0.174	0.123	6.7	.97
b_5	-0.614 ± 0.167	0.118	27.4	.995

Figure 25 is a plot of the dimensionless wave speed as a function of Reynolds number for thicknesses of 0.006 and 0.011 inches. For both of these thicknesses the measured wave speed decreases with increasing Reynolds number and the model generally predicts this trend. Measured data for each of these thicknesses are shown for comparison with the response surface model. The error bars on the curves are 80 percent confidence levels on the values predicted by the fitted model.

The effects of the external gas condition on the dimensionless wave speed are evaluated by comparing the data at constant liquid conditions. Similar to the dimension wave speed results, the equation for the low shear Mach 5 and the Mach 7 conditions are different in detail for this dimensionless wave speed data. The conclusions to be drawn from a comparison of the data must be made from a comparison of the trends and predictions of the equations over the range of the liquid conditions rather than from a term by term comparison of the fitted equations. Curves representing each of the models are an effective way to compare the overall trends and effects predicted by the models. Figure 26 presents the dimensionless wave speed as a function of Reynolds number for a thickness of 0.006 inches for the Mach 7 and the low shear Mach 5 condition. Measured data are also plotted. It is apparent that the low shear Mach 5 condition and the Mach 7 condition produce virtually the same dimensionless wave speeds on the interface.

In summary the regression analyses show that the dimensionless wave speed is dependent on the liquid Reynolds number and thickness for all three gas conditions. The wave speed decreases with increasing Reynolds number for both the Mach 7 and the low shear Mach 5 conditions. The limited data at the high shear Mach 5 condition are utilized in a

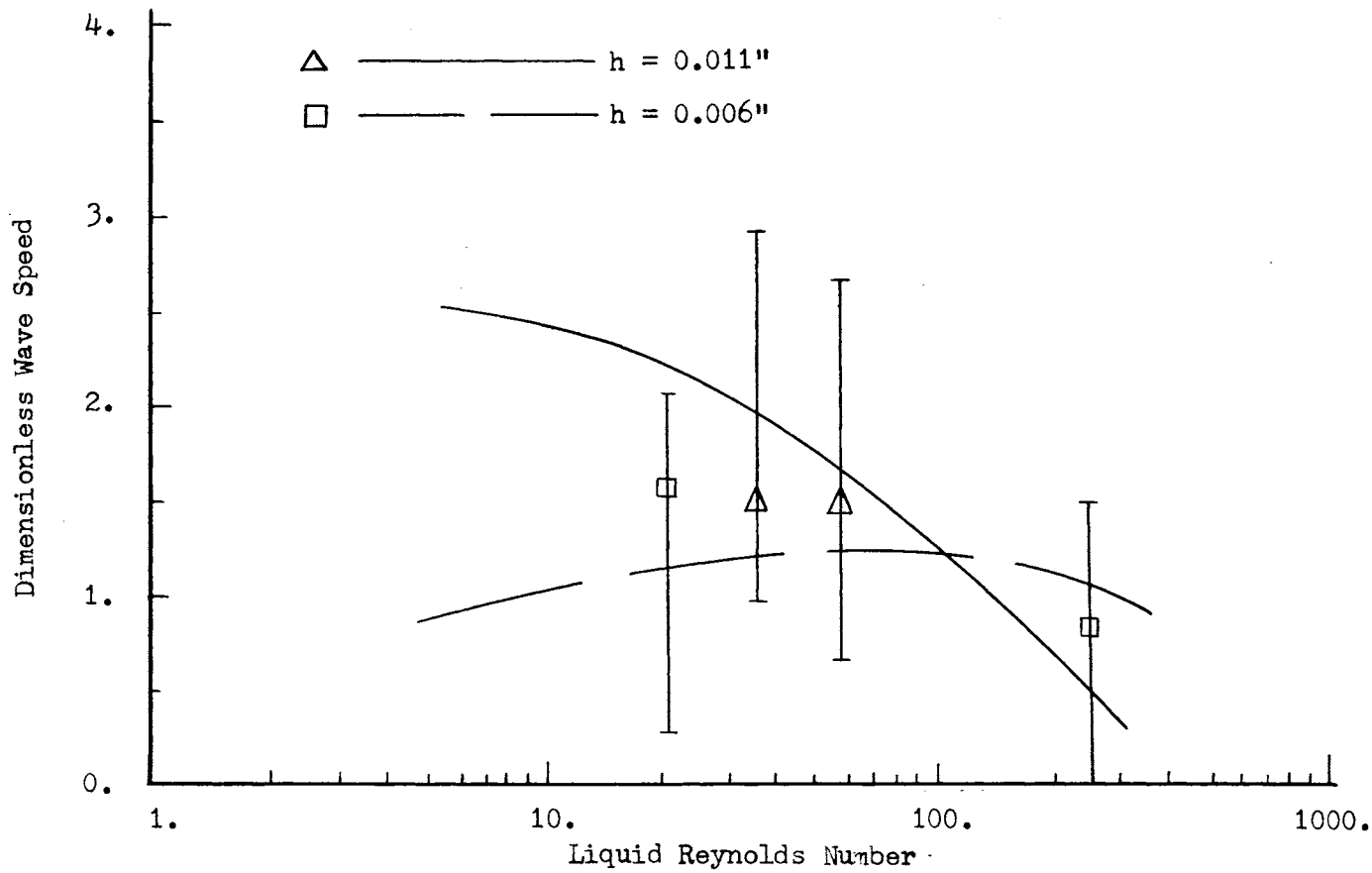

Figure 25. Variation of Dimensionless Wave Speed for Constant Liquid Thicknesses at Mach 7 Gas Condition

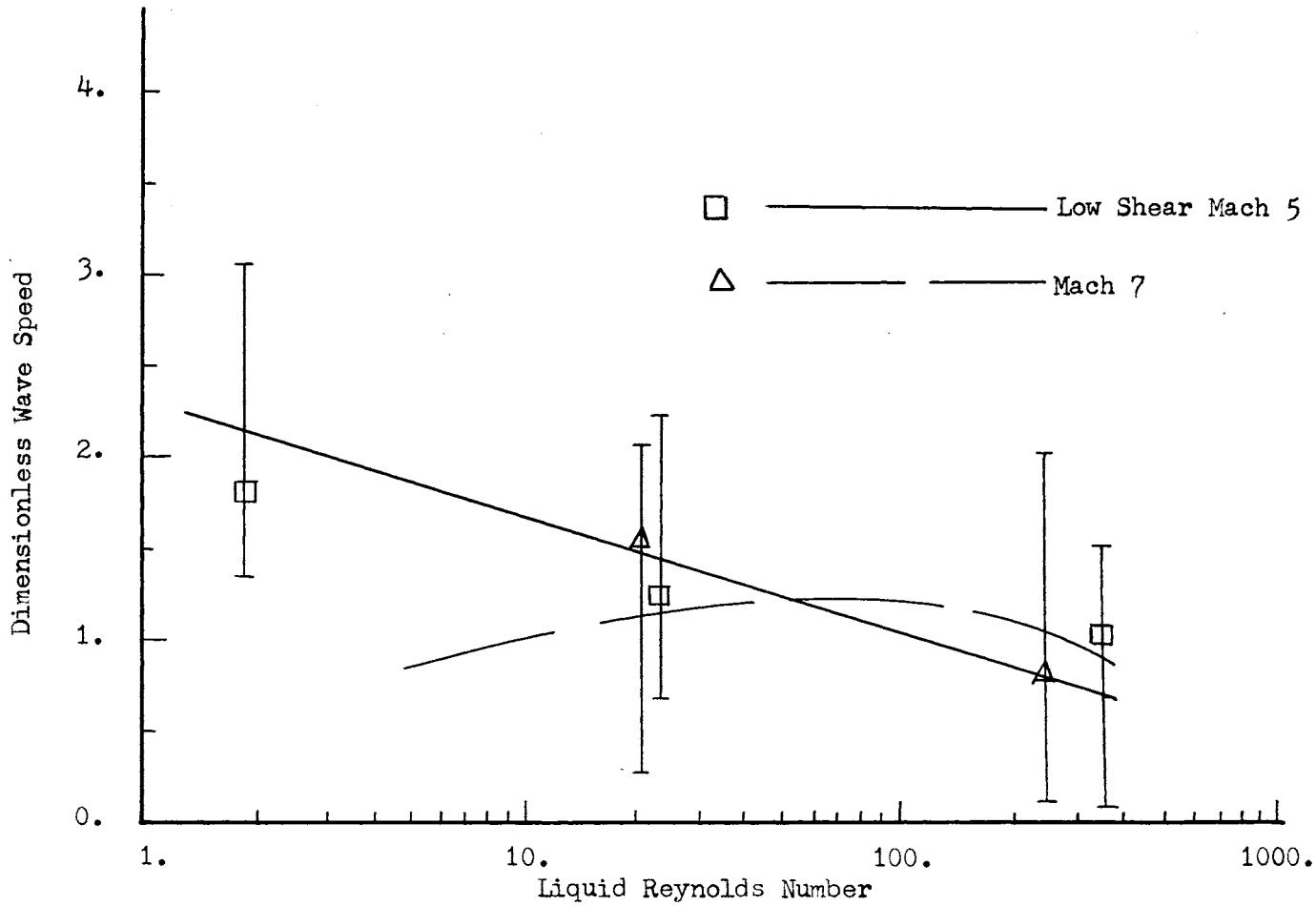

Figure 26. Comparison of Dimensionless Wave Speed for Different Gas Conditions at Similar Liquid Conditions, h = 0.006"

linear surface response model and also indicate that the wave speed decreases with increasing Reynolds number. The decrease in dimensionless wave speed with increasing Reynolds number for each gas condition reflects the increase in the liquid velocity used to nondimensionalize the wave speed data.

The fitted response surface models as well as the measured data for the Mach 7 and the low shear Mach 5 conditions result in approximately the same dimensionless wave speeds at similar liquid conditions. As shown in Figure 92 of Appendix D, the shear stress levels are approximately equal for these conditions and this similarity between the data at the two gas conditions suggests that the shear stress is the dominant gas parameter in determining the interface wave response. However additional experiments with perhaps liquid velocity measurements are necessary before this can be stated as an unqualified conclusion.

Mean Wavelength

The mean wavelength was measured from photographs of the liquid interface taken from the 35 mm movies. The number of waves along the centerline of the model in a three inch length of the interface was counted and the mean wavelength calculated as the average distance between the waves in this length. For all of the experiments the waves are not uniformly spaced along the interface. A series of two or three closely spaced waves followed by more widely spaced waves is typical of the interface. This non-uniformity is not restricted to any specific location on the model (i.e., near the side walls or toward the back). Consequently, it is concluded that the waves which are generated on the

interface are not equally spaced. In spite of this non-uniformity, mean values of the wavelength accompanied with tolerance bands to reflect the scatter in the data are significant data with which to characterize the interface response.

Because of the more highly agitated interface at the high shear Mach 5 condition, it was possible to measure the wavelength data at this gas condition only at three different liquid conditions. This is insufficient data with which to investigate any liquid effects. Consequently, only the data from the other two gas conditions are discussed.

The mean wavelength values for all the low shear Mach 5 experiments in which the data were measured are given in Table IV and it is apparent that the wavelength is a function of the liquid conditions. The response surface model given by equation 3 was utilized to examine the relationship between the data and the liquid Reynolds number and thickness. The results of the regression analysis are given in Table XIX. The standard deviation of the data from the model is 0.01856 and the values of the significant coefficients of the equation are given in Table XX. The assumed critical F-ratio of 2.0 corresponds to a significance level of approximately 80 percent for this analysis. Therefore 80 percent confidence intervals on each of the coefficients are also shown in the table.

Based on this analysis the mean wavelength depends on the liquid thickness and the Reynolds number. The final form of the model for the low shear Mach 5 condition is

$$L = 0.24 + 0.0286\hat{h} + 0.045\hat{R} - 0.011\hat{h}^2.$$

TABLE XIX

ANALYSIS OF VARIANCE FOR MEAN WAVELENGTH
AT LOW SHEAR MACH 5 GAS CONDITION

Source	Sum of Squares	Degrees of Freedom	Mean Square	F-Ratio
Total	.03867	10	.003867	
Regression	.03626	3	.0121	35
Error	.0024	7	.00034	

TABLE XX

MODEL COEFFICIENT VALUES FOR MEAN WAVELENGTH
AT LOW SHEAR MACH 5 GAS CONDITION

Coefficient	Value and 80% Confidence Interval	Standard Error	F-Ratio	Significance Level
b_0	0.24 ± 0.011	0.0076		
b_1	0.0286 ± 0.011	0.0079	12.9	.98
b_2	0.0452 ± 0.007	0.0048	89.1	.999
b_3	-0.011 ± 0.007	0.0046	5.7	.94

In this equation both L and h (within the expression for the normalized thickness parameter) have the units of inches. For a constant value of the thickness this relationship indicates clearly that the wavelength increases with Reynolds number since the significant Reynolds number term has a positive sign. This is consistent with examples which can be cited in Table IV.

The effect of both parameters are apparent in Figure 27. The curves were calculated from the final model form and appropriate data from Table IV are shown to illustrate the fit of the model to the data. Error bands on the curves represent 80 percent confidence levels on future observed values and in all cases these intervals include the observed data. At constant Reynolds number the mean wavelength increases with increasing thickness.

For the Mach 7 gas condition the wavelength data are shown in Table X. The data were analyzed using the response surface model given as equation 3 and the results of the analysis are given in Table XXI. In this analysis the assumed critical F-ratio of 2.0 corresponds to a significance level of 78 percent. The standard deviation using this model is 0.0332 and the significant coefficients, including 80 percent confidence intervals on each, are shown in Table XXII.

The final form of the model for the Mach 7 gas condition is

$$L = 0.37 + 0.061\hat{R} - 0.019\hat{R}^2$$

where L has the dimensions of inches. Based on this model for the range of thickness and Reynolds numbers in these experiments, the wavelength increases with Reynolds number and is independent of the thickness. Based on a comparison of the Reynolds number coefficients, the

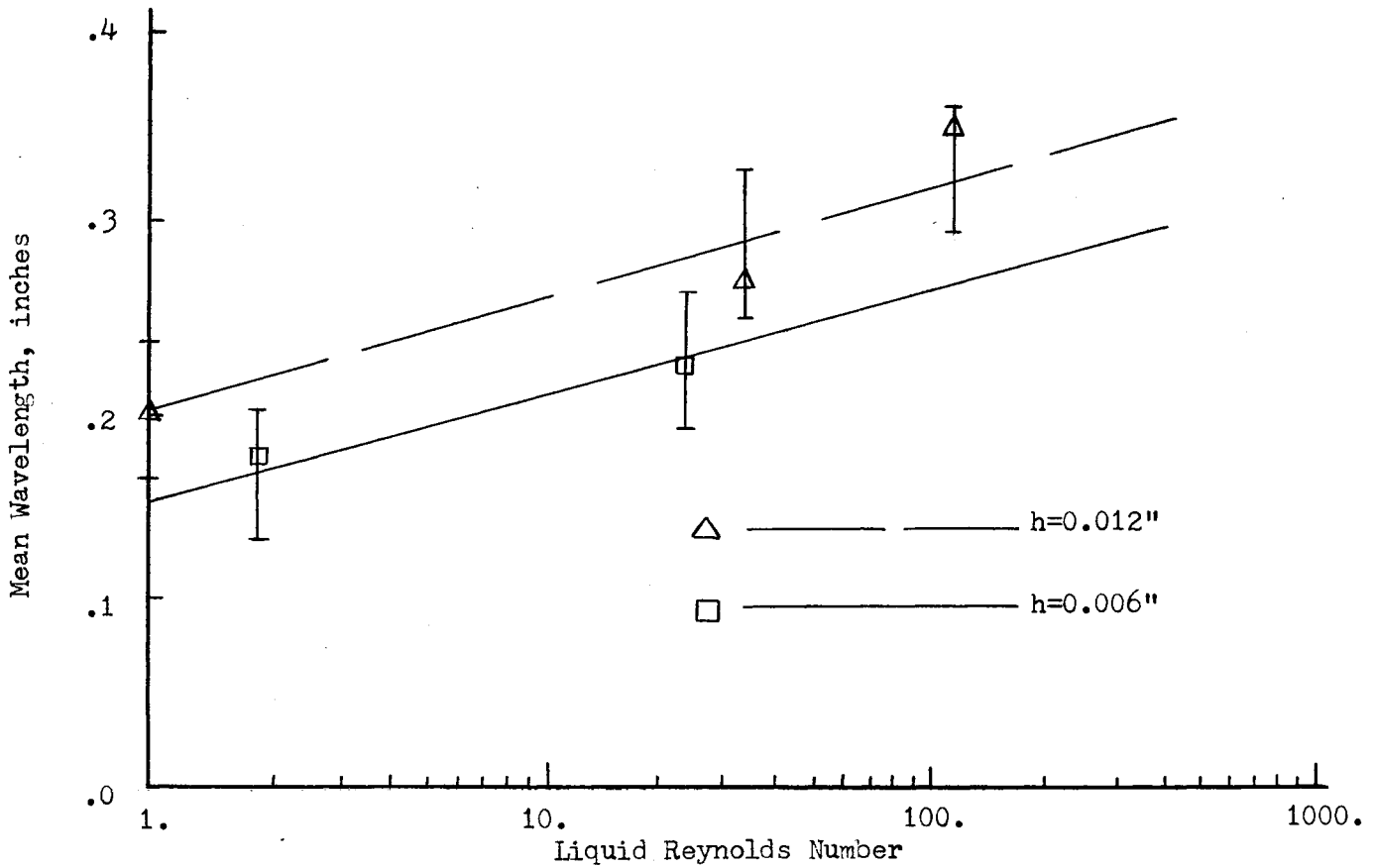

Figure 27. Variation of Mean Wavelength for Constant Liquid Thicknesses at Low Shear Mach 5 Gas Condition

TABLE XXI

ANALYSIS OF VARIANCE FOR MEAN WAVELENGTH
AT MACH 7 GAS CONDITION

Source	Sum of Squares	Degrees of Freedom	Mean Square	F-Ratio
Total	0.0734	8	0.0092	
Regression	0.0672	2	0.0336	32.4
Error	0.0062	6	0.00104	

TABLE XXII

MODEL COEFFICIENT VALUES FOR MEAN WAVELENGTH
AT MACH 7 GAS CONDITION

Coefficient	Value and 80% Confidence Interval	Standard Error	F-Ratio	Significance Level
b_0	0.37 ± 0.028	0.0197		
b_2	0.061 ± 0.0166	0.0115	28.2	.99
b_4	-0.019 ± 0.016	0.0111	2.9	.87

linear Reynolds number term produces the primary variation of the data. The curve and data in Figure 28 illustrate the liquid parameter effects.

Comparison of the data at similar liquid parameters illustrates the effect of the different gas conditions. Figure 29 is a plot of mean wavelength versus Reynolds number for the two gas conditions and a thickness of 0.006 inches. Three measured data points are also shown. The models suggest that for equal liquid conditions the wavelength is larger for the Mach 7 gas condition than for the low shear Mach 5 condition. This is born out by the larger measured wavelength data for the Mach 7 condition.

In summary analysis of the data for the low shear Mach 5 condition reveals that the mean wavelength is dependent on both the thickness and Reynolds number of the liquid. For this gas condition the mean wavelength increases with increasing Reynolds number at constant thickness and also increases with increasing thickness at constant Reynolds number. For the Mach 7 gas condition the wavelength is dependent only upon the Reynolds number and increases with increasing Reynolds number. The mean wavelength for the low shear Mach 5 condition is smaller than that for the Mach 7 condition at similar liquid conditions.

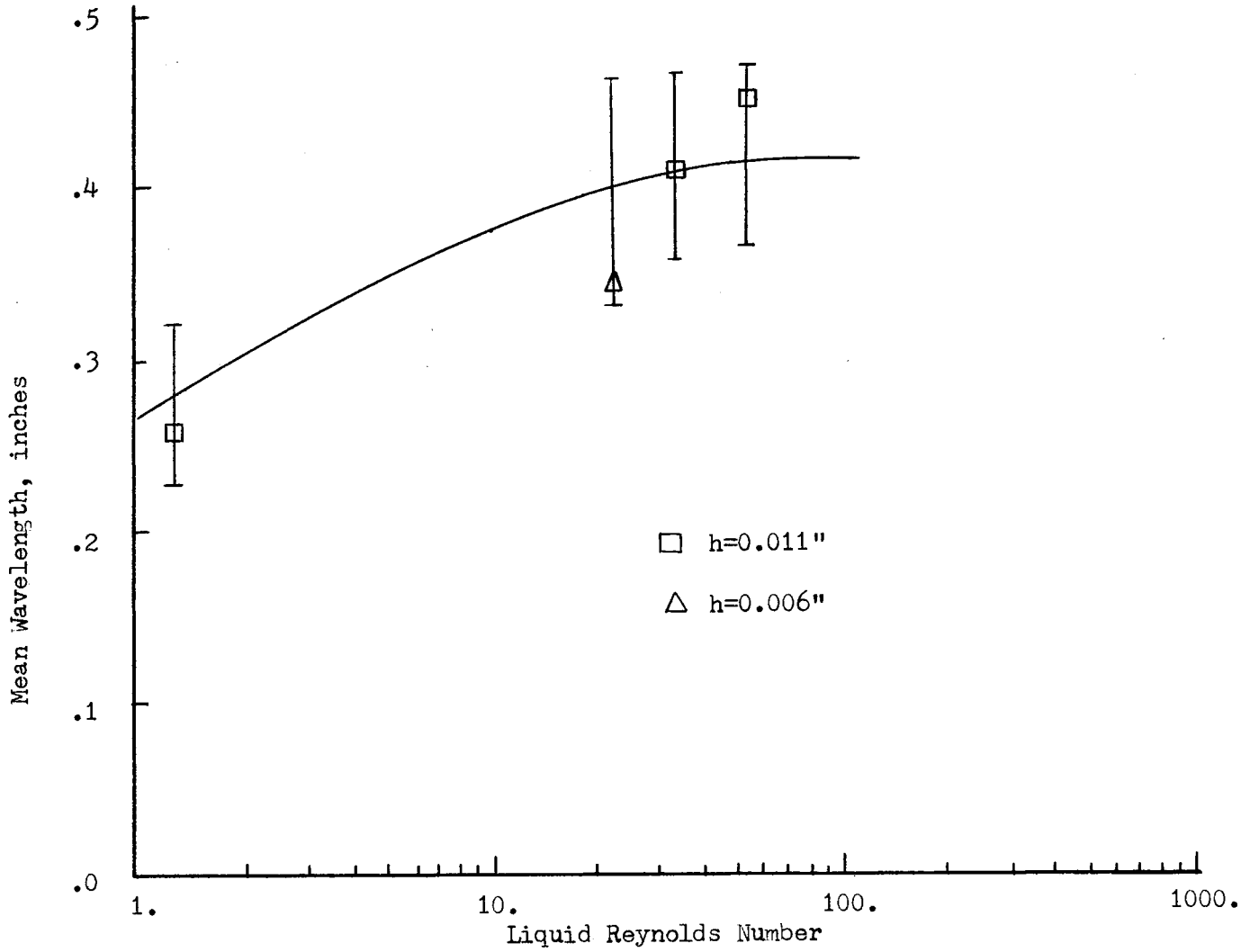

Figure 28. Variation of Mean Wavelength for Constant Liquid Thicknesses at Mach 7 Gas Condition

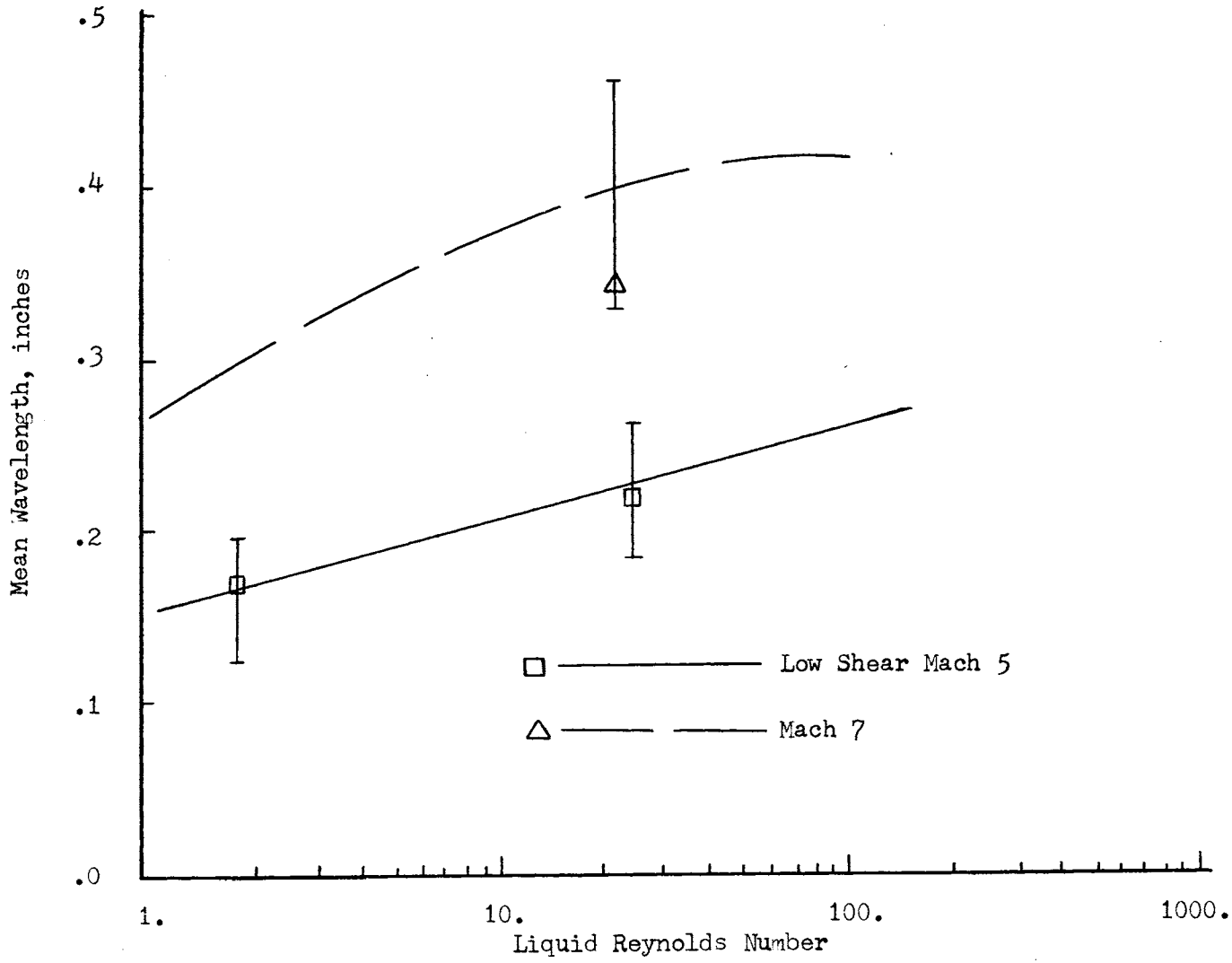

Figure 29. Comparison of Mean Wavelength for Different Gas Conditions at Similar Liquid Conditions, h = 0.006 Inches

CHAPTER IV

DISCUSSION OF WAVE FREQUENCY SPECTRA

The depth gauge located three inches behind the model nose tip provided data on the interface wave profile as a function of time. The output of the depth gauge was recorded on magnetic tape and a six second segment was digitized as described in Chapter II. A Fourier analysis of this digitized data was performed to calculate the frequency spectra of the waves. The spectra were calculated by squaring the Fourier transform of the gauge output for each frequency and normalizing this quantity with the maximum calculated value for each segment of data.

The results of the analysis reveal both the dominant frequency of the interface waves and also the range of wave frequencies which, according to the depth gauge output, exists on the interface at each of the gas-liquid conditions. The gauge calibration shown in Appendix C indicates that the gauge output is nonlinear as a function of the liquid thickness. Therefore it is possible that the amplitude fluctuations of the interface waves are different from the amplitude fluctuations of the gauge output voltage. However since the size of the gauge sensing area is approximately one order of magnitude less than the mean wavelength of the waves, the gauge should in all cases sense the individual waves as they pass. In addition examination of the strip chart records of the gauge output shows that the voltage fluctuations are for

most cases an order of magnitude less than the mean gauge output. Therefore, the nonlinearity of the gauge calibration should not be critical since the data occur over a relatively small range of the output. In view of these factors the assumption is made that the analysis of the voltage output of the gauge satisfactorily represents the interface wave response.

For the low Reynolds number experiments a significant contribution to the frequency spectra occurs in the range from 1 to 10 Hertz. The six second interval of data analyzed is sufficiently long to resolve frequencies in this range. However, the amplitude fluctuations of the waves at these conditions are relatively small and spurious fluctuations from other sources may become significant. In particular pressure and flow rate fluctuations in the liquid expulsion system, variations in the tunnel operation, and vibration of the model are possible sources of extraneous input. Consequently, the low frequency, low Reynolds number data must be considered as tenative pending additional experiments. As a result in the regression analyses for the dominant frequency data, the low Reynolds number data which are considered to be in question are omitted. As an illustration of the reasons for omitting the data, the following example is presented. For a wave frequency of 1 Hertz and wave speeds of 0.5 to 1 foot per second which are typical of the low Reynolds number data, the wavelength must be from 6 to 12 inches. This is not consistent with the observed interface appearance and is difficult to justify physically. The data which are omitted are denoted in the appropriate tables and discussion in this chapter.

Two types of data are produced in the analysis. First, the dominant wave frequency is determined; and second, the range of wave

frequencies is calculated. Therefore the analyses of the frequency data in the remainder of the chapter will be similarly separated.

Variation of Dominant Wave Frequency

The curves which present the calculated Fourier transform of the depth gauge output for the low shear Mach 5 gas condition are presented in Figures 30 through 44. Examination of the curves confirms the presence of a dominant frequency and also illustrates the band of frequencies present at each condition. It is apparent that the dominant frequency varies with varying liquid conditions.

The relationship between the dominant wave frequency and the thickness-Reynolds number conditions at each gas condition was analyzed by using the response surface model given by equation 3. In this case the dominant wave frequency was taken as the dependent variable f and its dependency on the Reynolds number and thickness was examined. For reasons given previously the data for Figures 30, 32, 33, 34, and 35 were omitted from the analyses. The results of the regression analysis are given in Table XXIII. For this analysis the significance level associated with the assumed critical F-ratio of 2.0 is approximately 80 percent. The standard deviation of the data from the model is 12.02 and the significant coefficients including 80 percent confidence intervals are shown in Table XXIV. The final form of the response surface for the low shear Mach 5 gas condition is

$$f = 47.35 + 27.1\hat{R} - 3.18\hat{h}\hat{R}$$

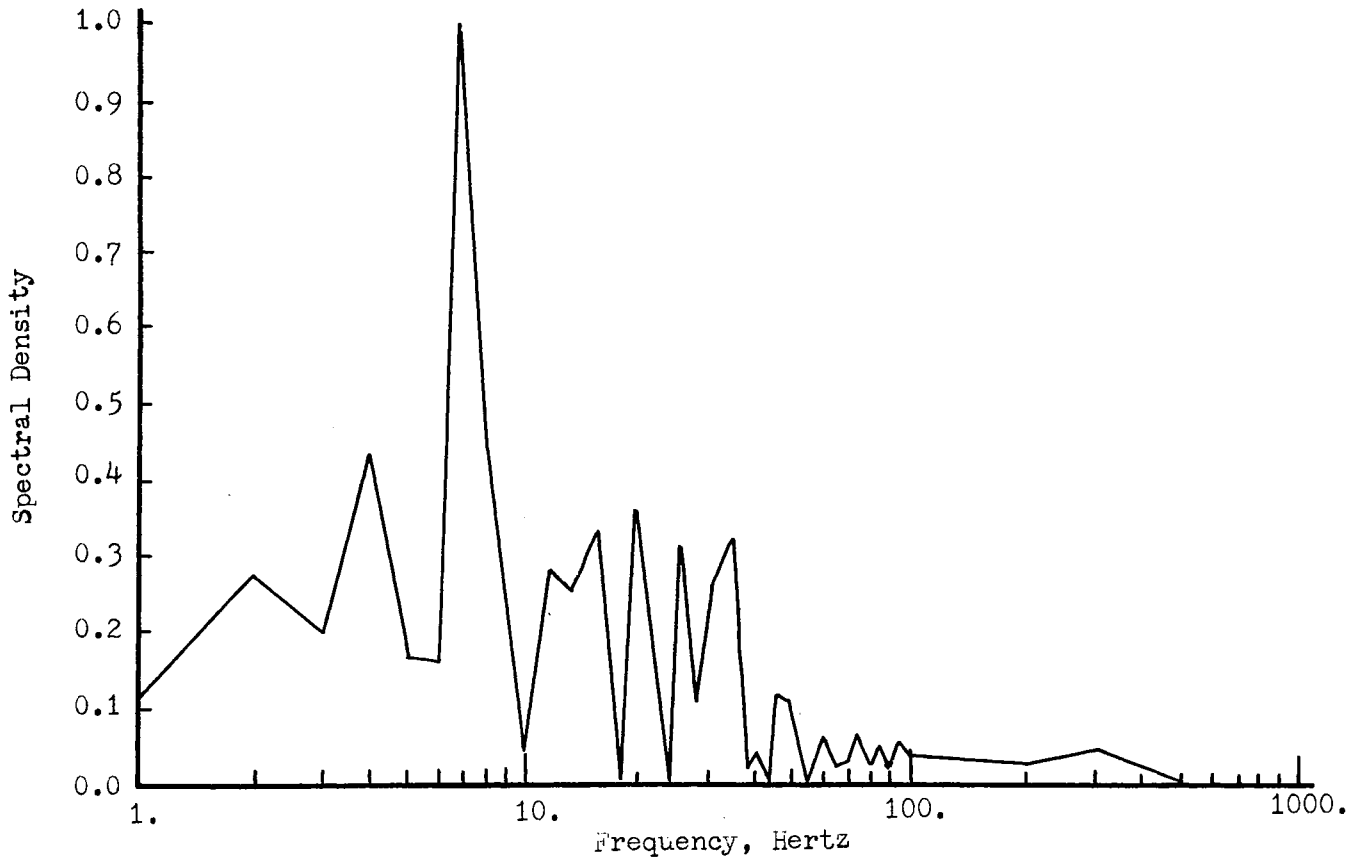

Figure 30. Spectral Density of Amplitude Fluctuation for Reynolds Number = 0.22 at Low Shear Mach 5 Gas Condition

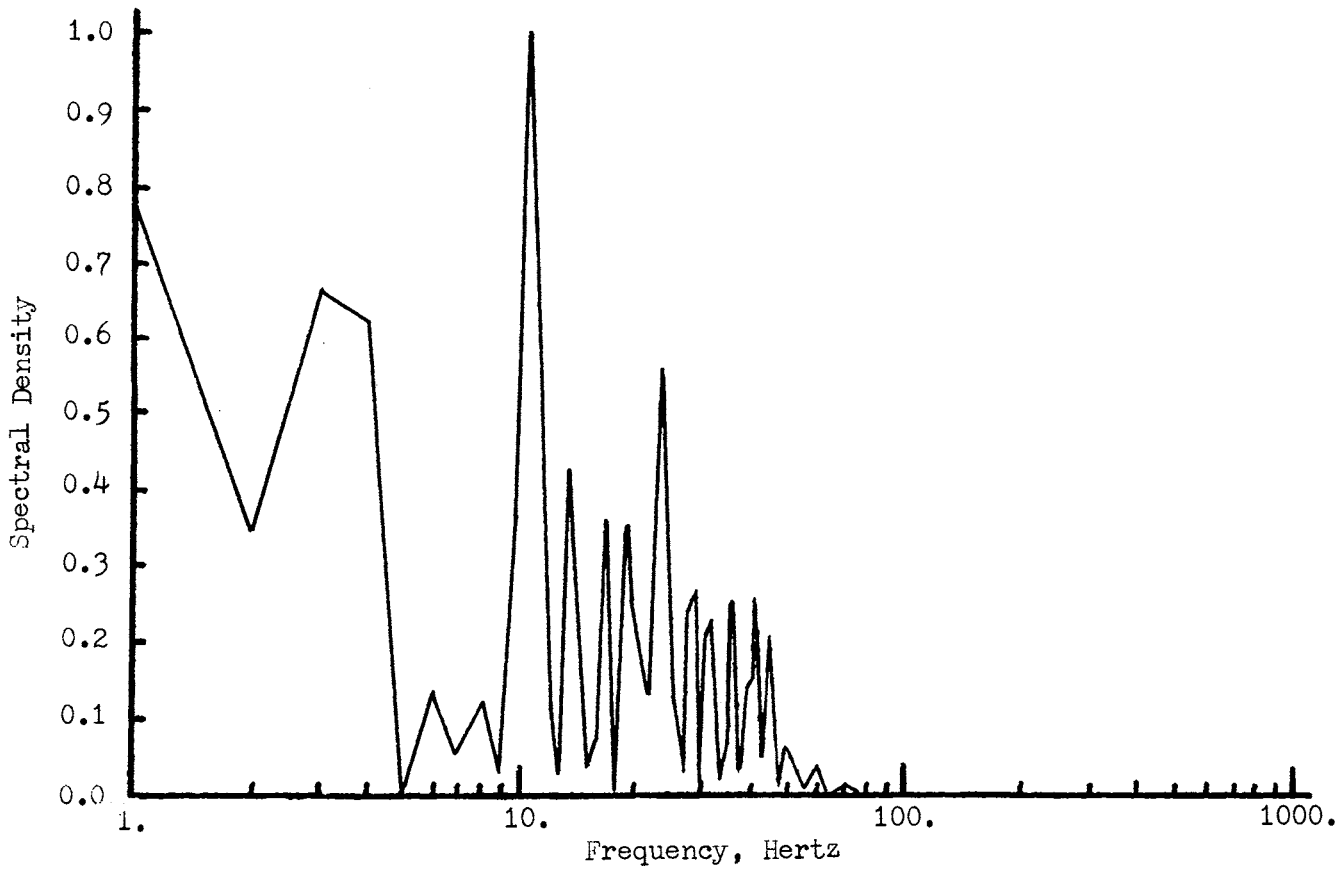

Figure 31. Spectral Density of Amplitude Fluctuation for Reynolds Number = 0.35 at Low Shear Mach 5 Gas Condition

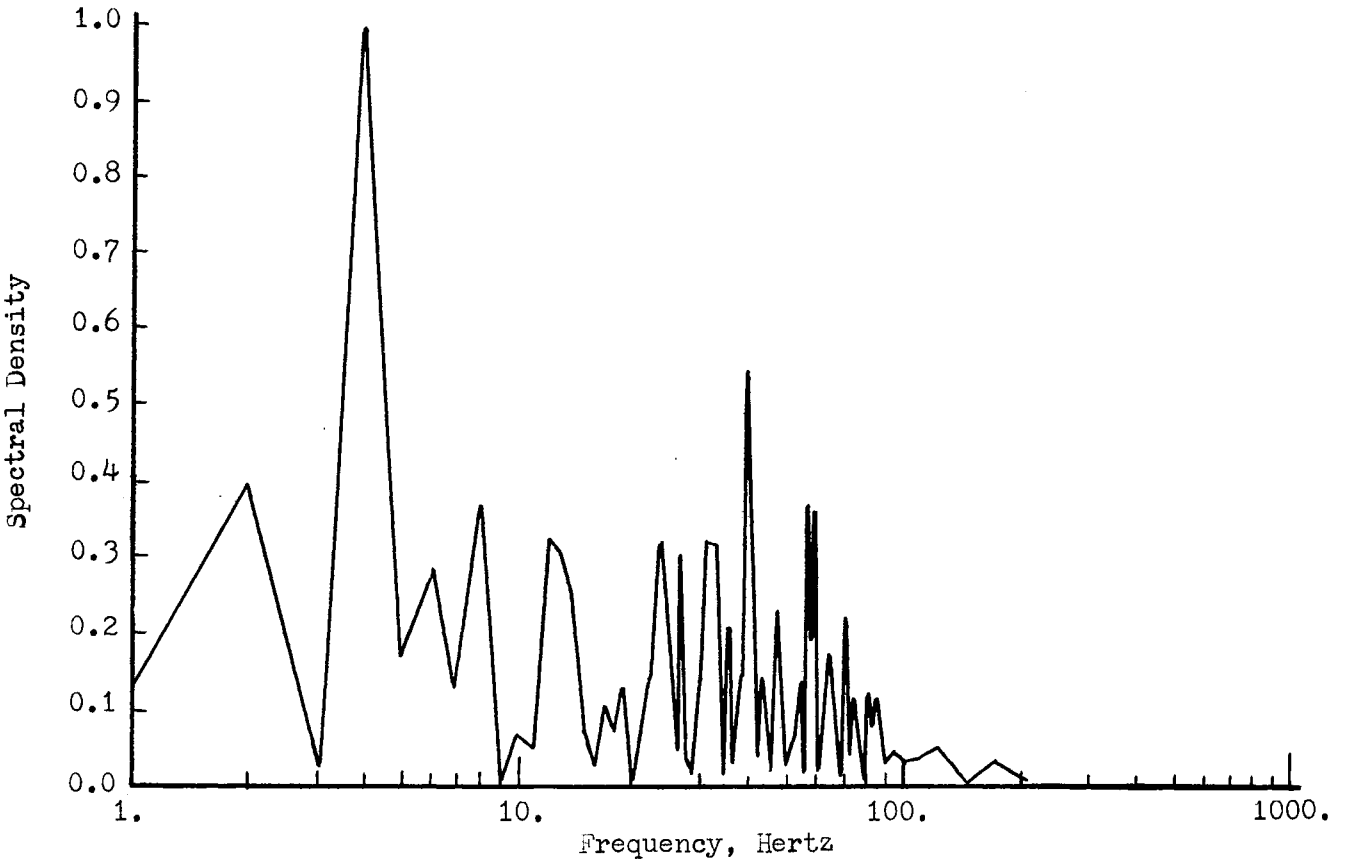

Figure 32. Spectral Density of Amplitude Fluctuation for Reynolds Number = 0.73 at Low Shear Mach 5 Gas Condition

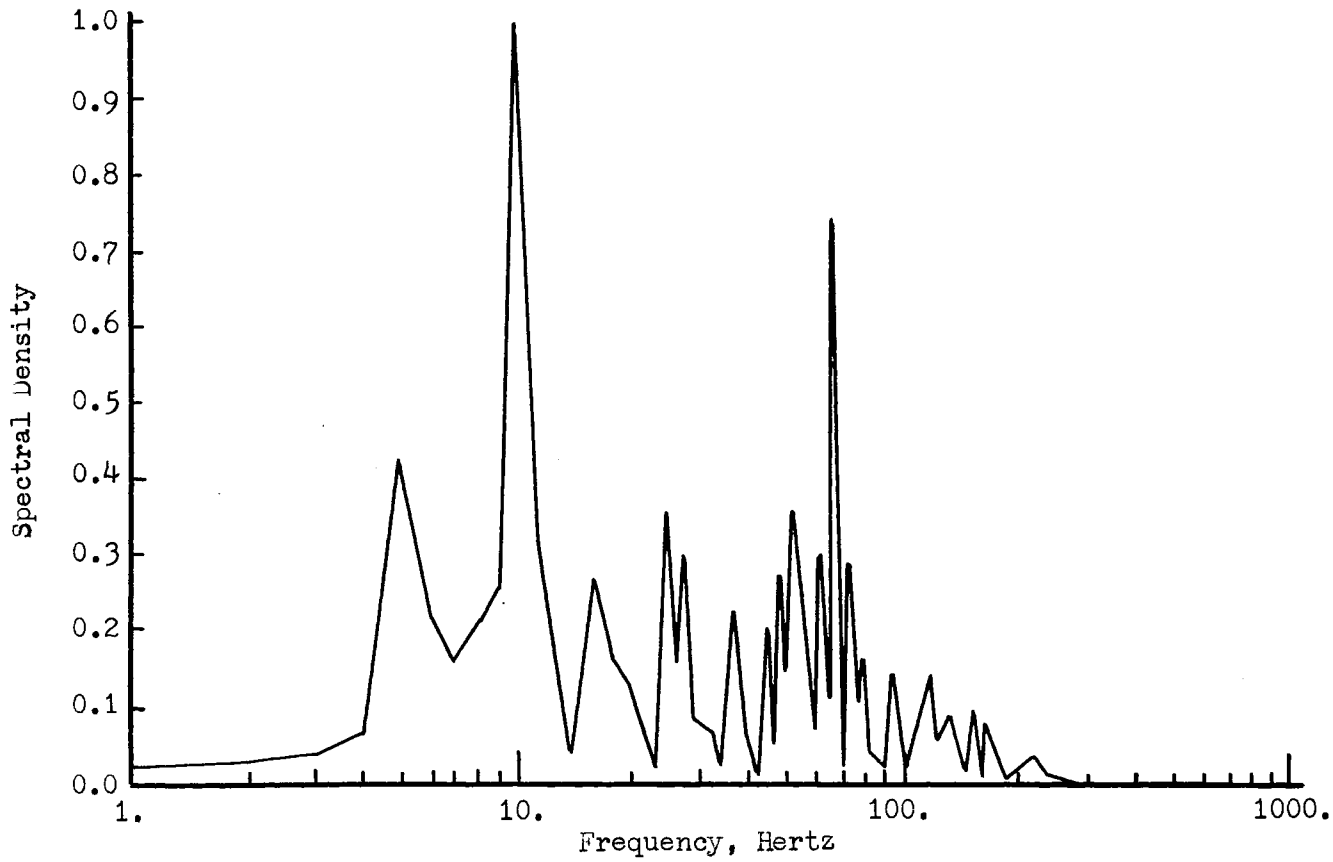

Figure 33. Spectral Density of Amplitude Fluctuation for Reynolds Number = 1.0 at Low Shear Mach 5 Gas Condition

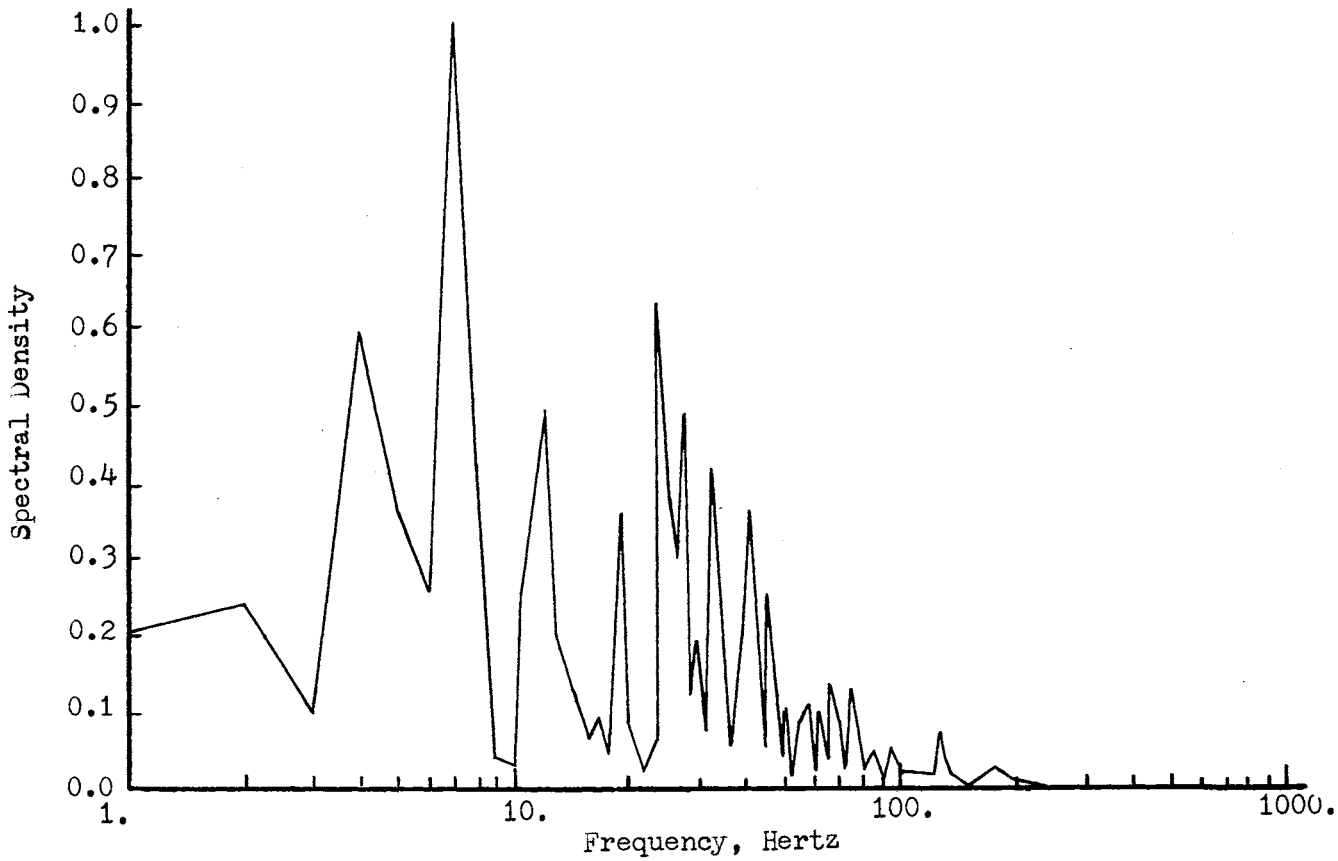

Figure 34. Spectral Density of Amplitude Fluctuation for Reynolds Number = 1.8 at Low Shear Mach 5 Gas Condition

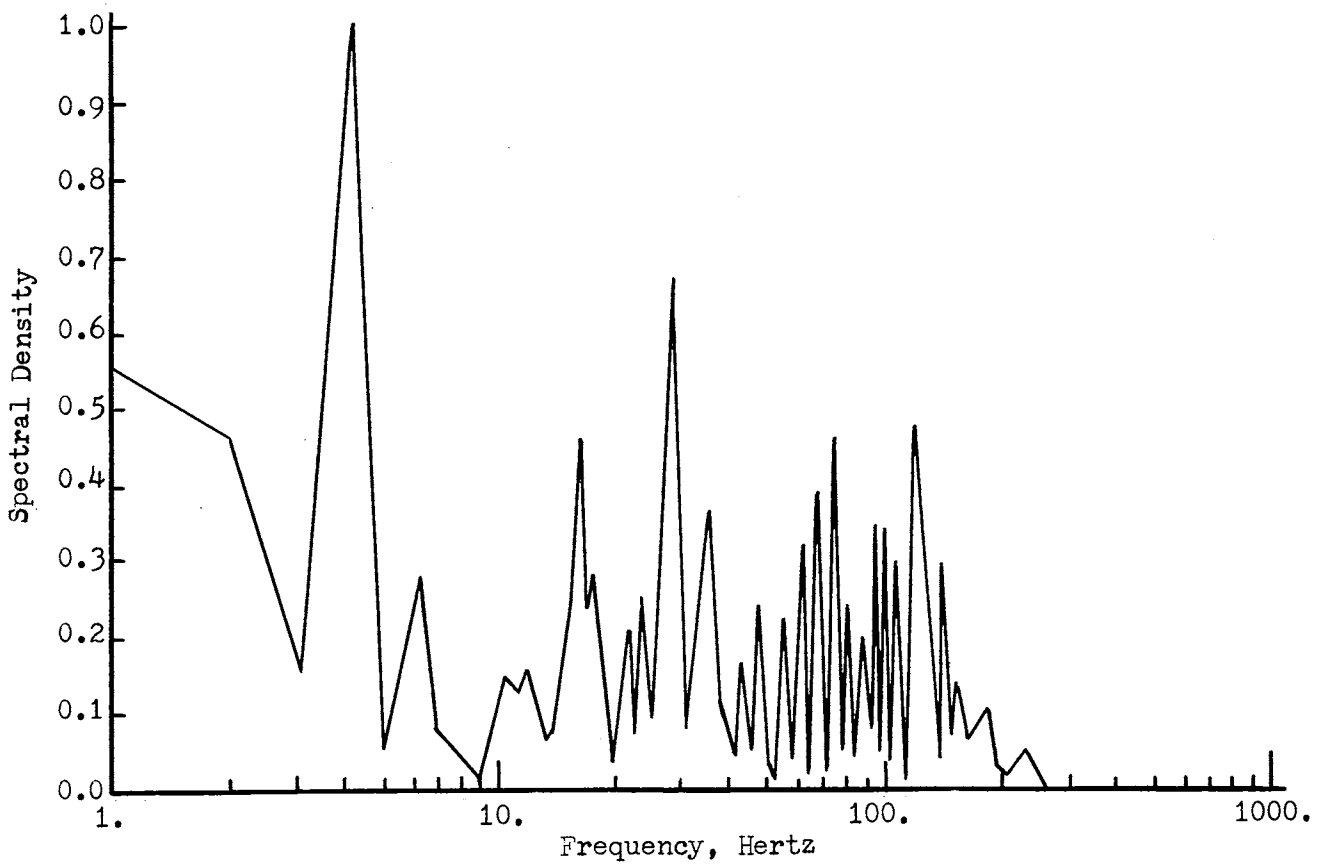

Figure 35. Spectral Density of Amplitude Fluctuation for Reynolds Number = 4.0 at Low Shear Mach 5 Gas Condition

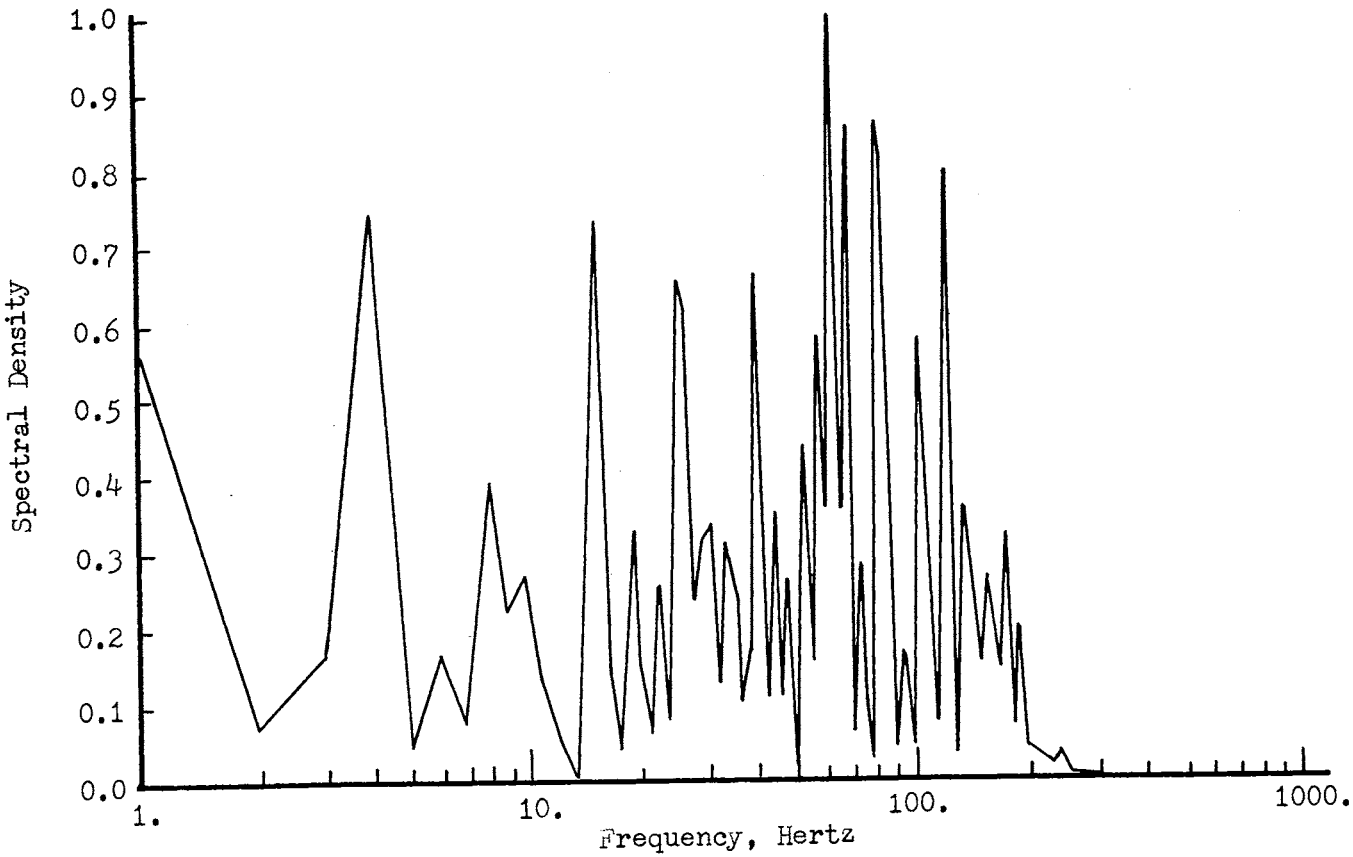

Figure 36. Spectral Density of Amplitude Fluctuation for Reynolds Number = 23. at Low Shear Mach 5 Gas Condition

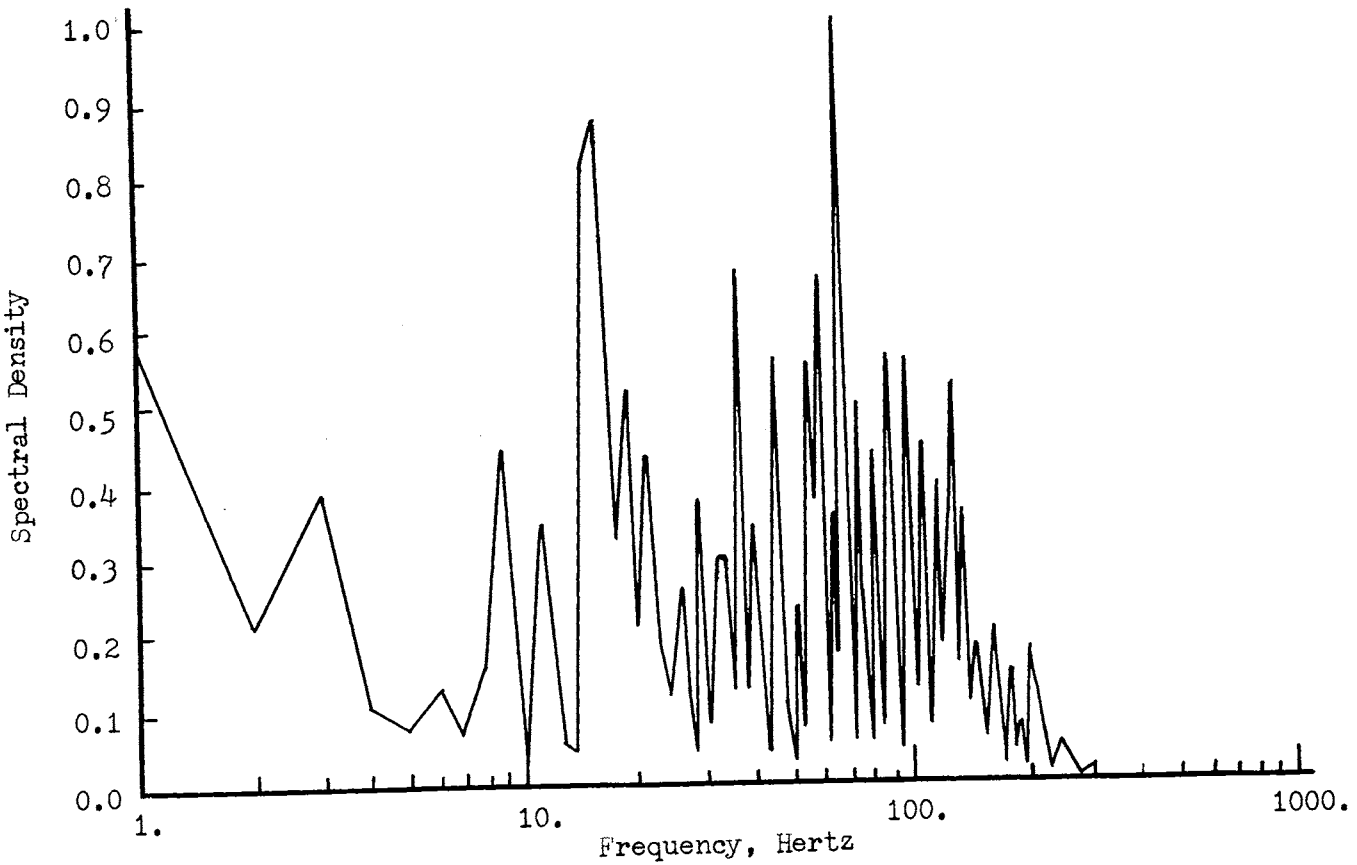

Figure 37. Spectral Density of Amplitude Fluctuation for Reynolds Number = 32. at Low Shear Mach 5 Gas Condition

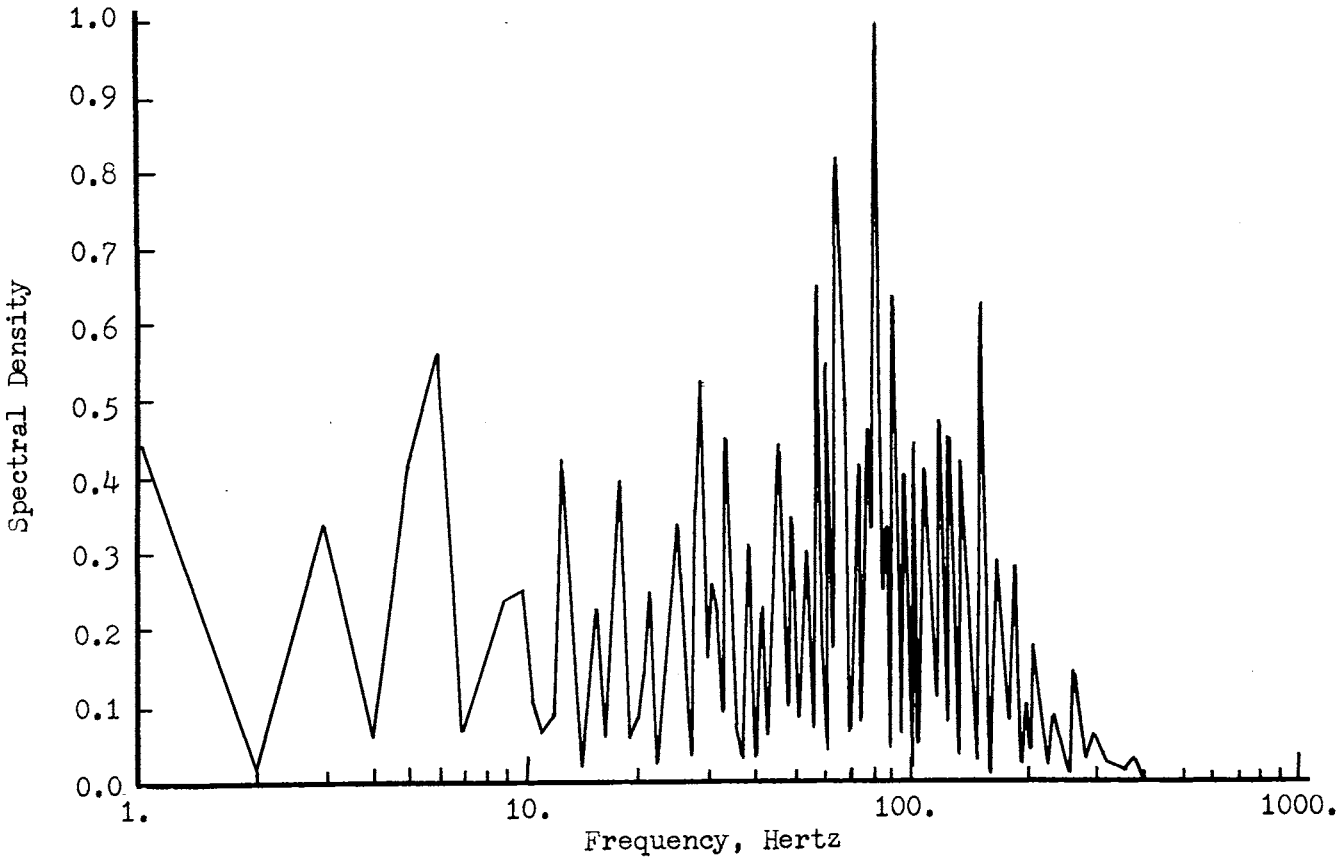

Figure 38. Spectral Density of Amplitude Fluctuation for Reynolds Number = 40. at Low Shear Mach 5 Gas Condition

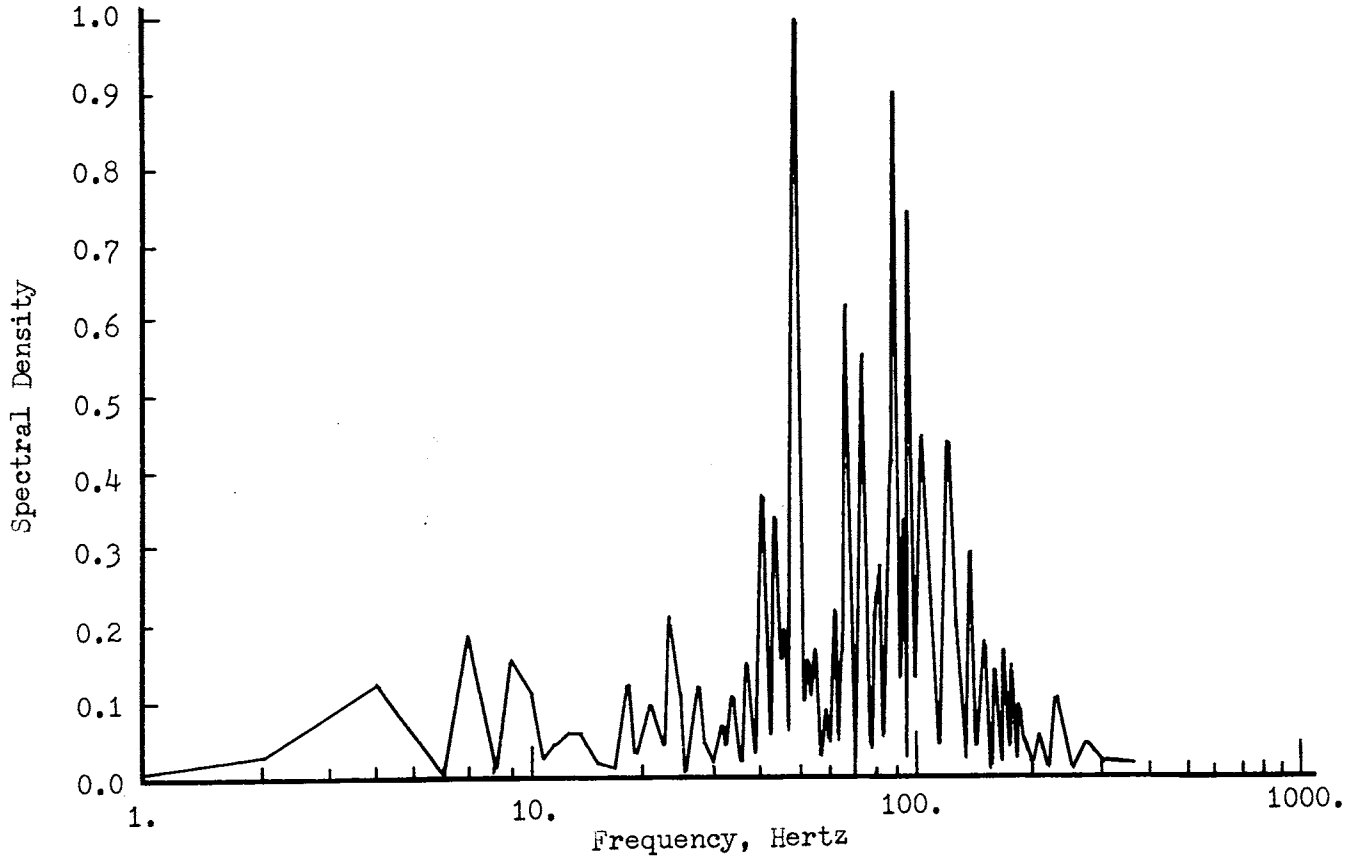

Figure 39. Spectral Density of Amplitude Fluctuation for Reynolds Number = 54. at Low Shear Mach 5 Gas Condition

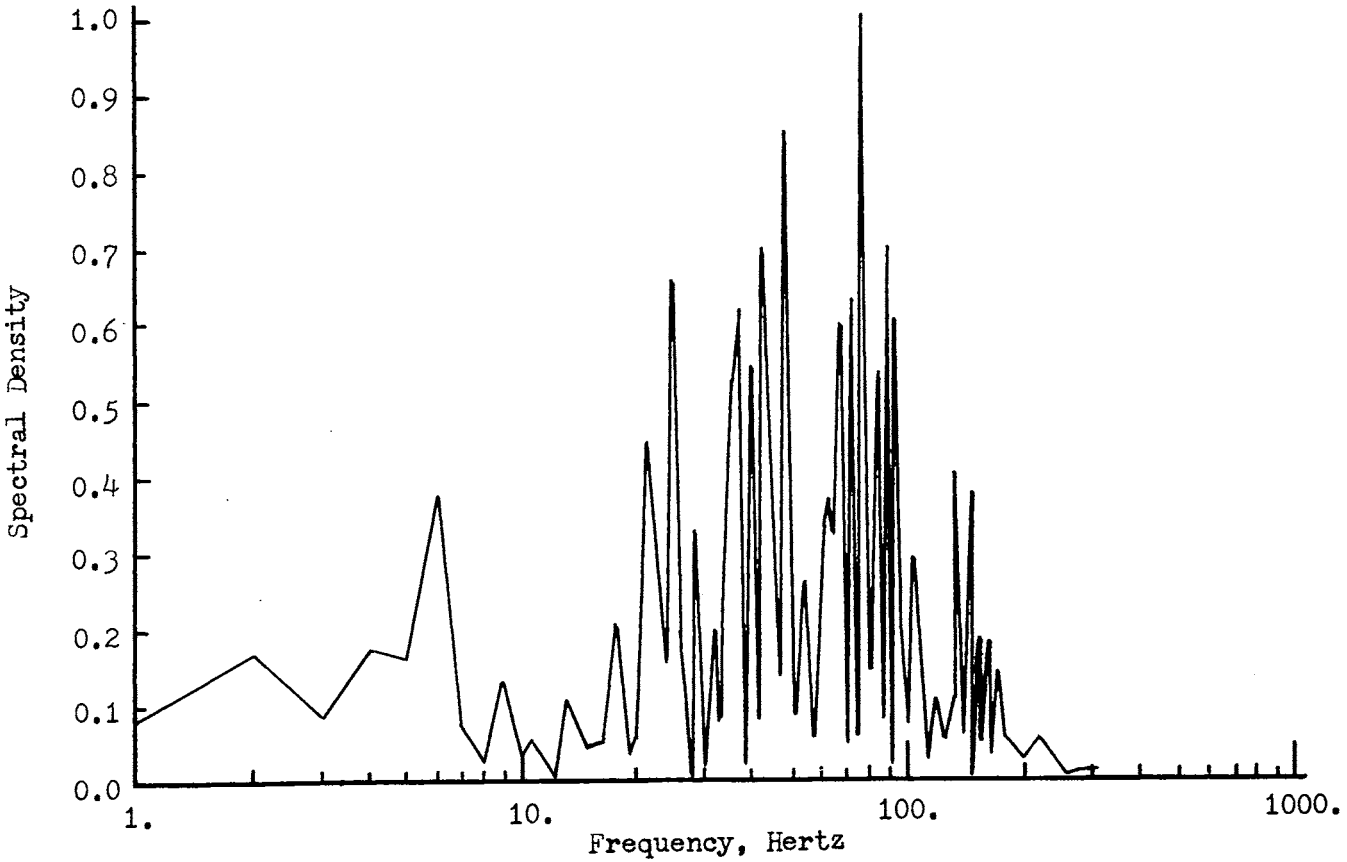

Figure 40. Spectral Density of Amplitude Fluctuation for Reynolds Number = 56. at Low Shear Mach 5 Gas Condition

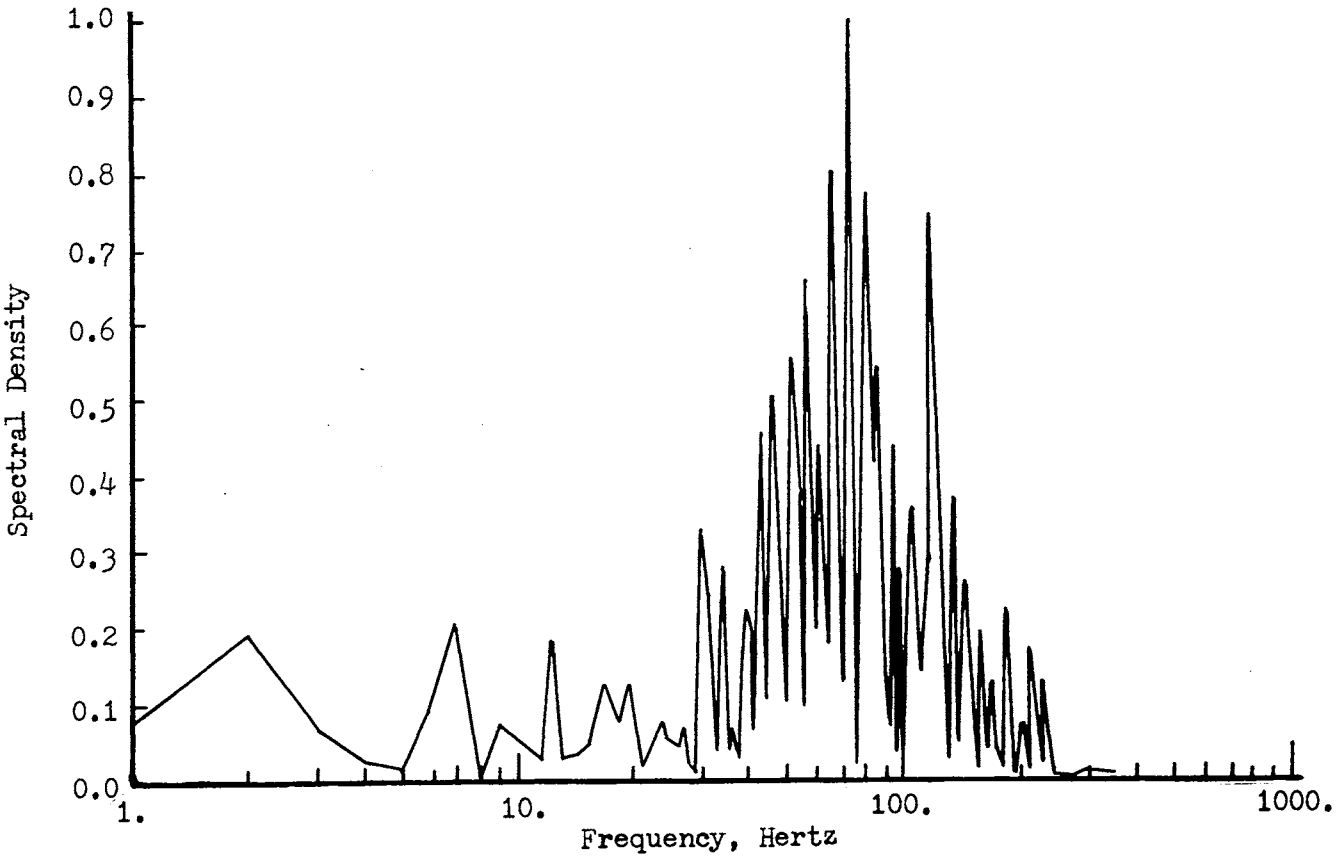

Figure 41. Spectral Density of Amplitude Fluctuation for Reynolds Number = 110. at Low Shear Mach 5 Gas Condition

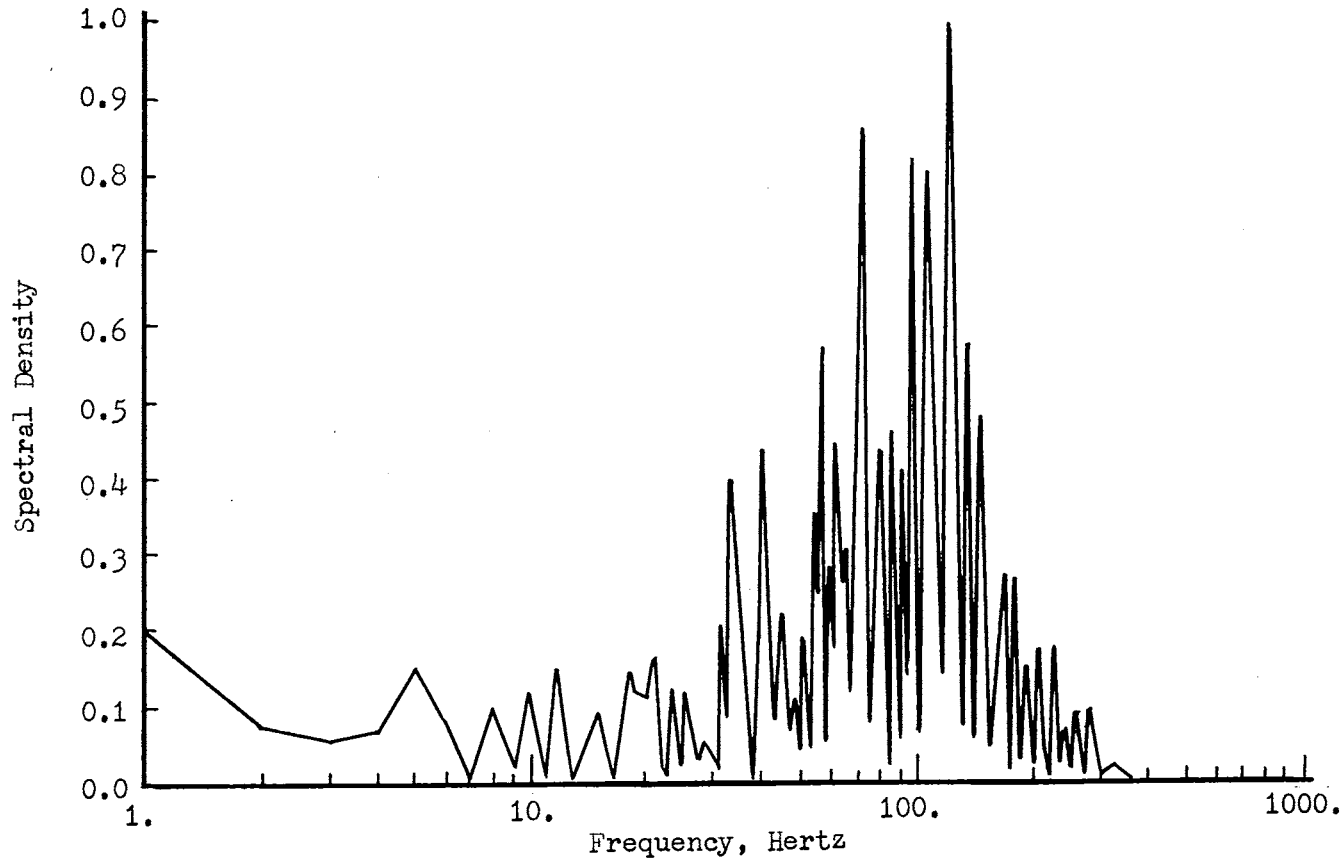

Figure 42. Spectral Density of Amplitude Fluctuation for Reynolds Number = 260. at Low Shear Mach 5 Gas Condition

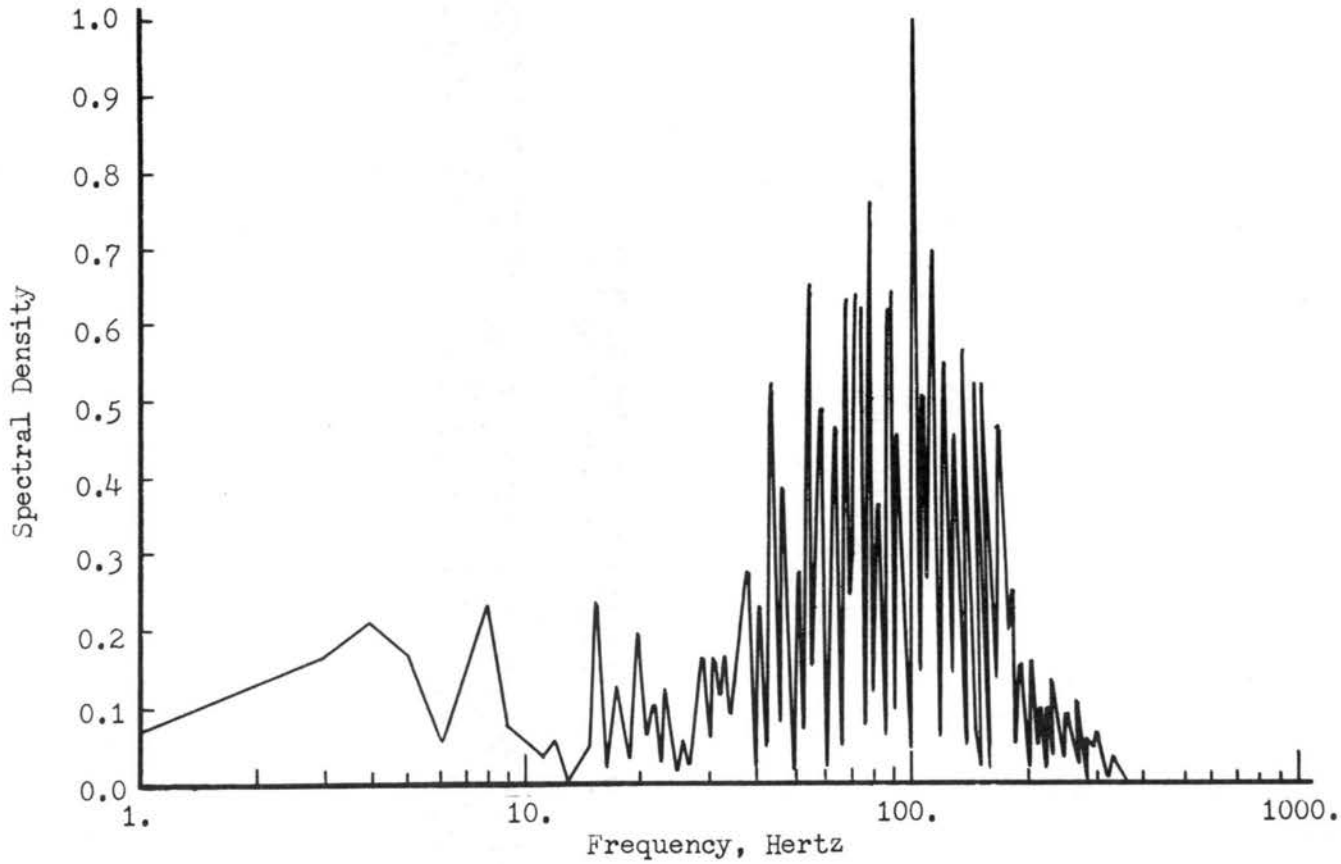

Figure 43. Spectral Density of Amplitude Fluctuation for Reynolds Number = 310. at Low Shear Mach 5 Gas Condition

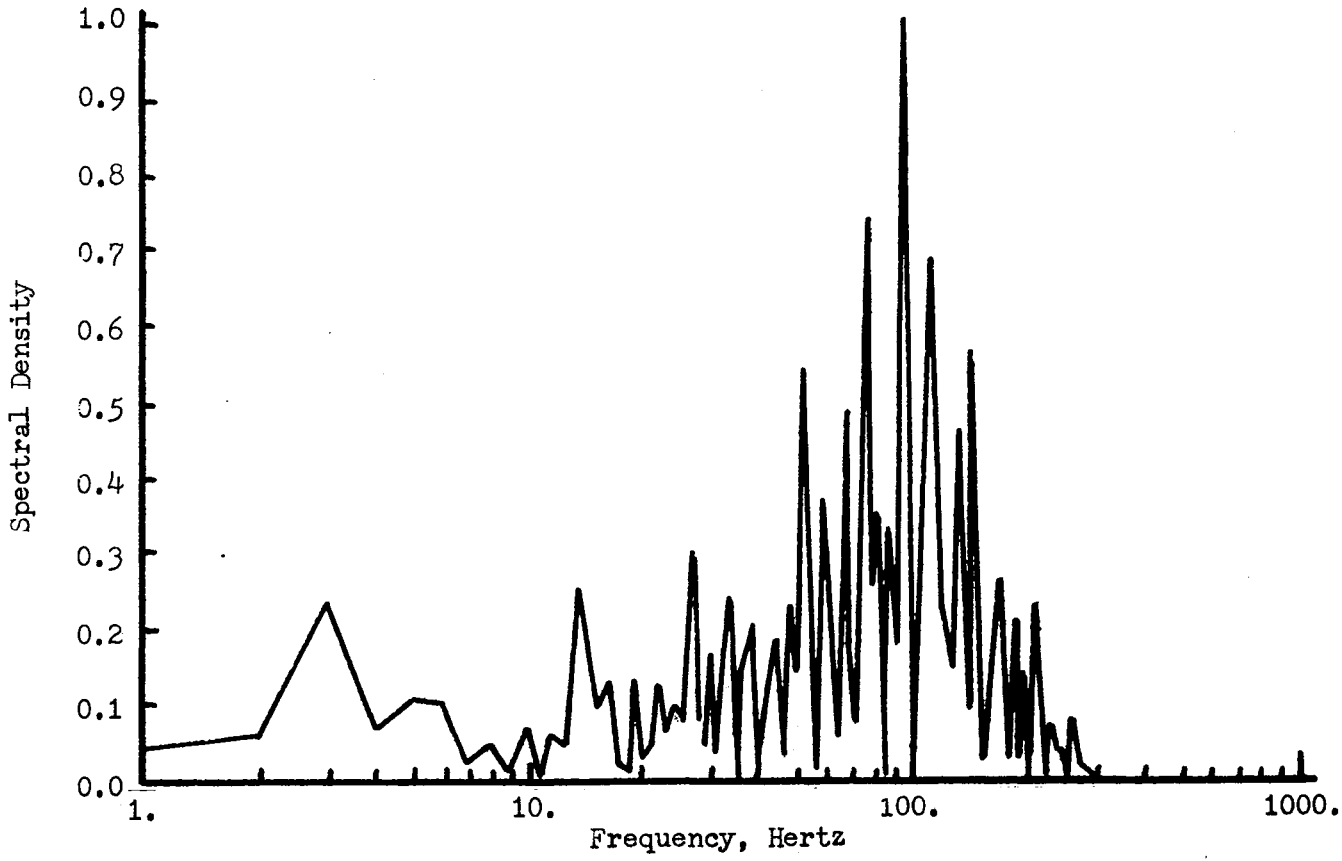

Figure 44. Spectral Density of Amplitude Fluctuation for Reynolds Number = 360. at Low Shear Mach 5 Gas Condition

TABLE XXIII

ANALYSIS OF VARIANCE FOR DOMINANT WAVE FREQUENCY
AT LOW SHEAR MACH 5 GAS CONDITION

Source	Sum of Squares	Degrees of Freedom	Mean Square	F-Ratio
Total	8421	9	935.7	
Regression	7409	2	3704.5	25.63
Error	1012	7	144.6	

TABLE XXIV

MODEL COEFFICIENT VALUES FOR DOMINANT WAVE FREQUENCY
AT LOW SHEAR MACH 5 GAS CONDITION

Coefficient	Value and 80% Confidence Interval	Standard Error	F-Ratio	Significance Level
b_0	47.35 ± 7.77	5.61		
b_2	27.13 ± 5.24	3.79	51.2	.999
b_5	-3.18 ± 2.73	1.97	2.6	.81

where $\hat{h}$ and $\hat{R}$ are defined for all of the data analysis in this chapter by the expressions given in Chapter III for the low shear Mach 5 and the Mach 7 conditions.

The use of this equation is restricted to the range and combination of thickness-Reynolds number conditions shown in Table IV. A comparison of the values of the coefficients for the two variable terms of the equation shows that the linear Reynolds number term produces a larger variation in the frequency than does the interaction term. The curves shown in Figure 45 illustrate the relationship between the dominant frequency and the liquid conditions. Curves are drawn for thicknesses of 0.006, 0.010 and 0.012 inches. The measured data for each of the thicknesses are shown plotted on the curves. The error bars on the curves are 80 percent confidence intervals for this model and represent a prediction for any data observed in additional experiments at this condition.

The agreement between the data and the curves for the corresponding thicknesses illustrates the fit of the data. The data in all cases lie within the confidence interval of the appropriate curves. Based on these data the frequency increases with Reynolds number at constant thickness for all thickness values of this experiment. At Reynolds numbers above 10 the effect of increasing the thickness at constant Reynolds number is to decrease the dominant wave frequency. Below a Reynolds number of 10 the opposite is true. This result is due to the negative sign on the coefficient of the significant interaction term in which the thickness appears.

For the high shear Mach 5 gas condition the frequency spectra are shown in Figures 46 through 58 for the various liquid conditions.

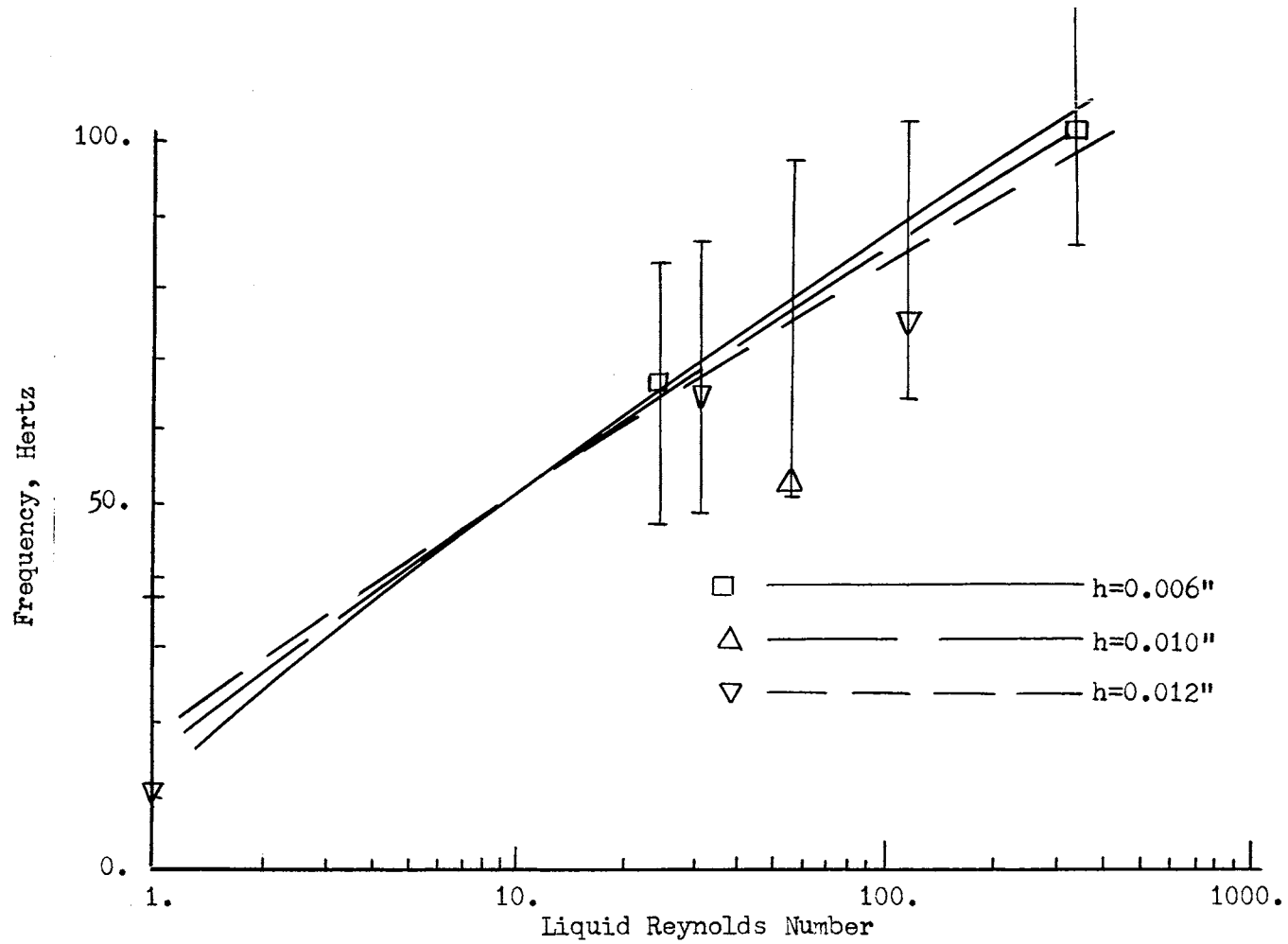

Figure 45. Variation of Dominant Wave Frequency for Constant Liquid Thicknesses at Low Shear Mach 5 Gas Condition

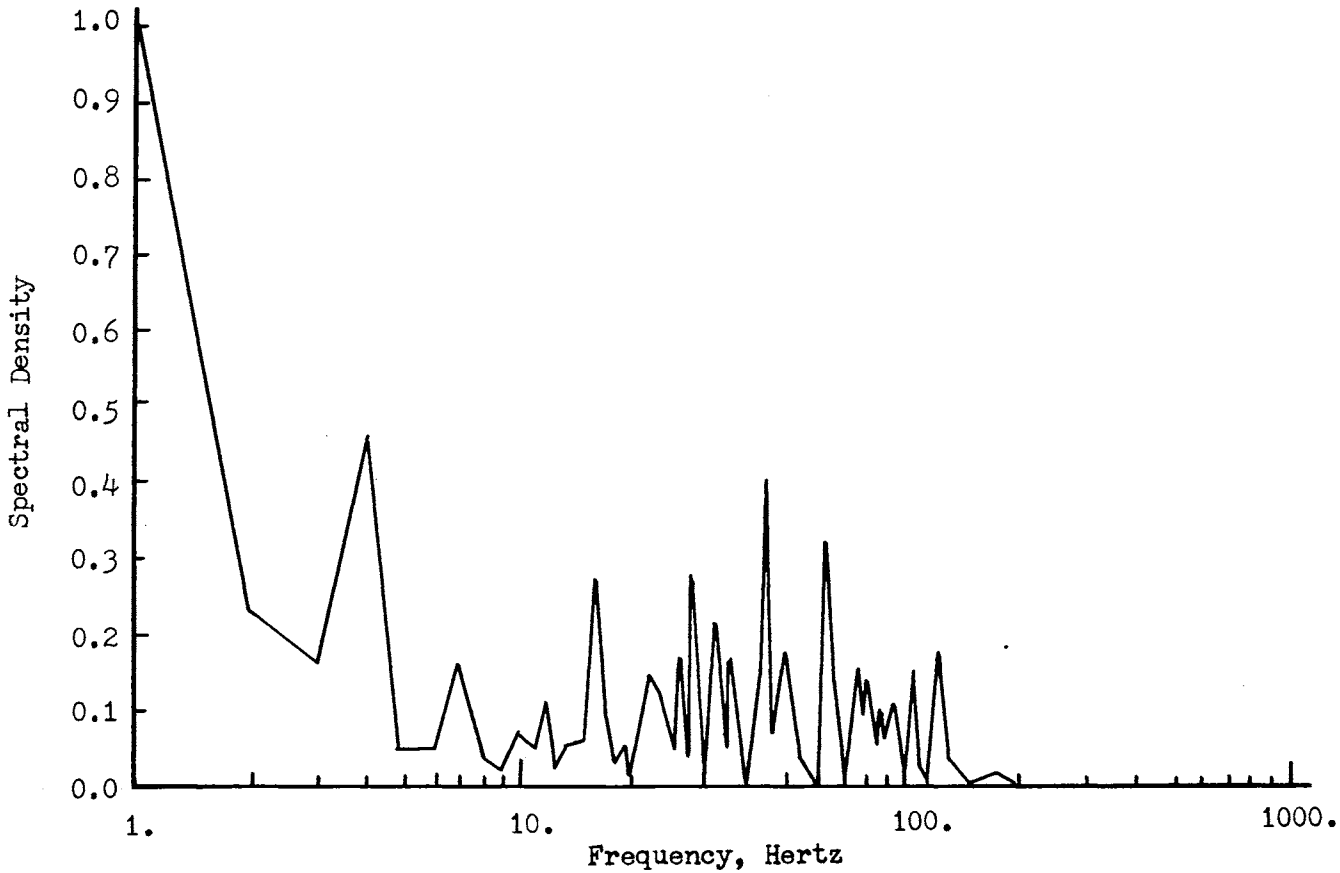

Figure 46. Spectral Density of Amplitude Fluctuation for Reynolds Number = 0.33 at High Shear Mach 5 Gas Condition

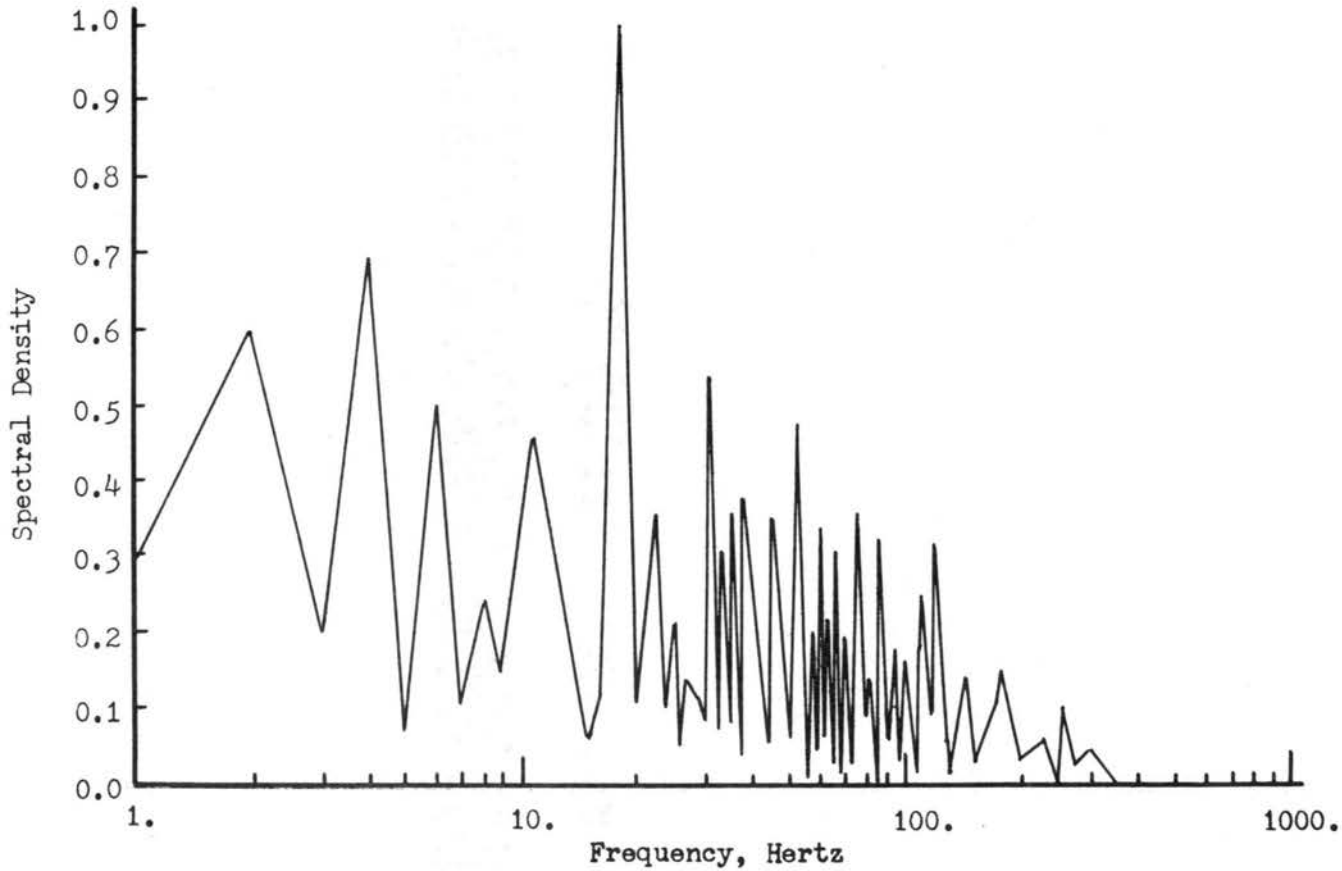

Figure 47. Spectral Density of Amplitude Fluctuation for Reynolds Number = 0.53 at High Shear Mach 5 Gas Condition

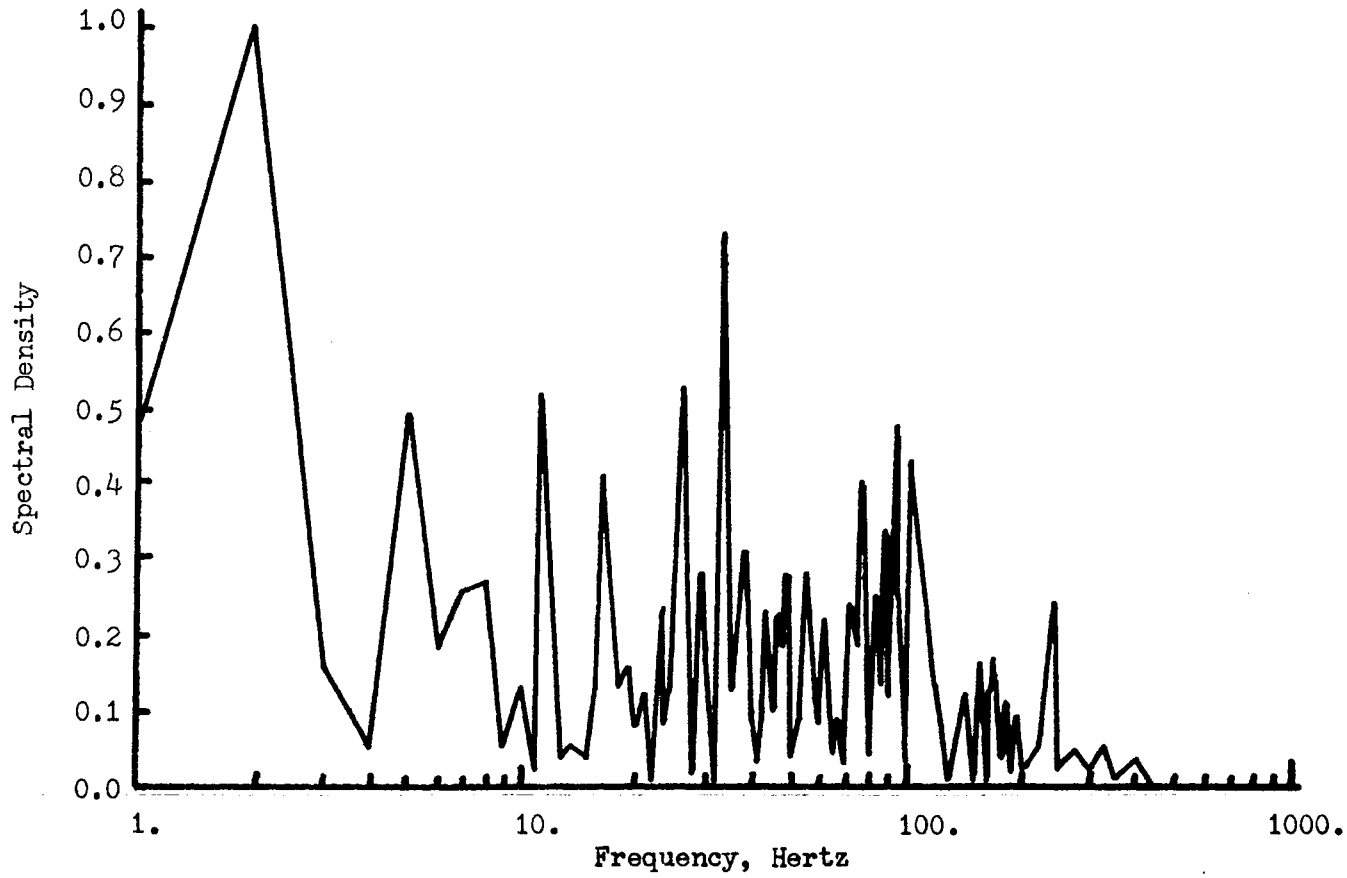

Figure 48. Spectral Density of Amplitude Fluctuation for Reynolds Number = 0.9 at High Shear Mach 5 Gas Condition

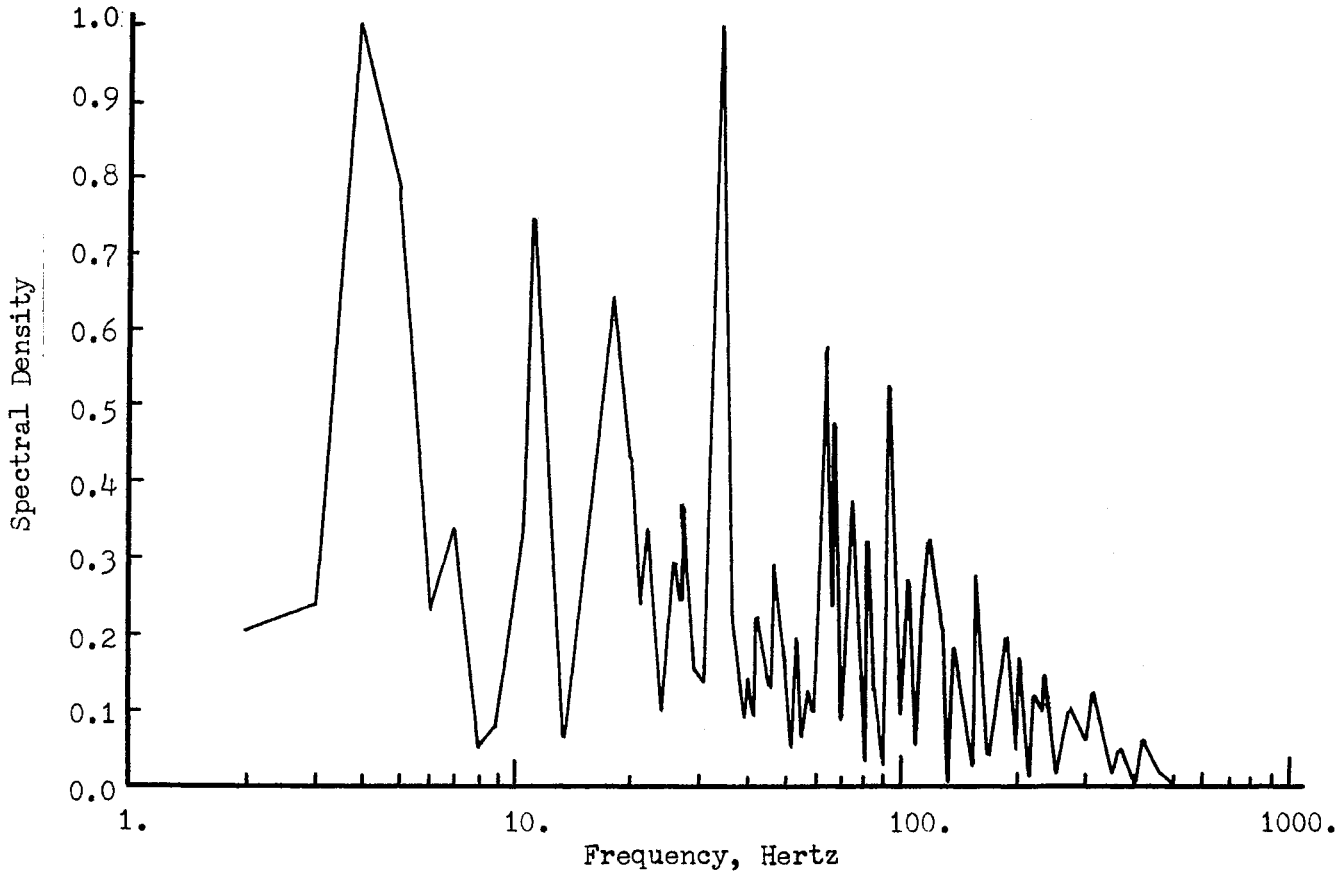

Figure 49. Spectral Density of Amplitude Fluctuation for Reynolds Number = 1. at High Shear Mach 5 Gas Condition

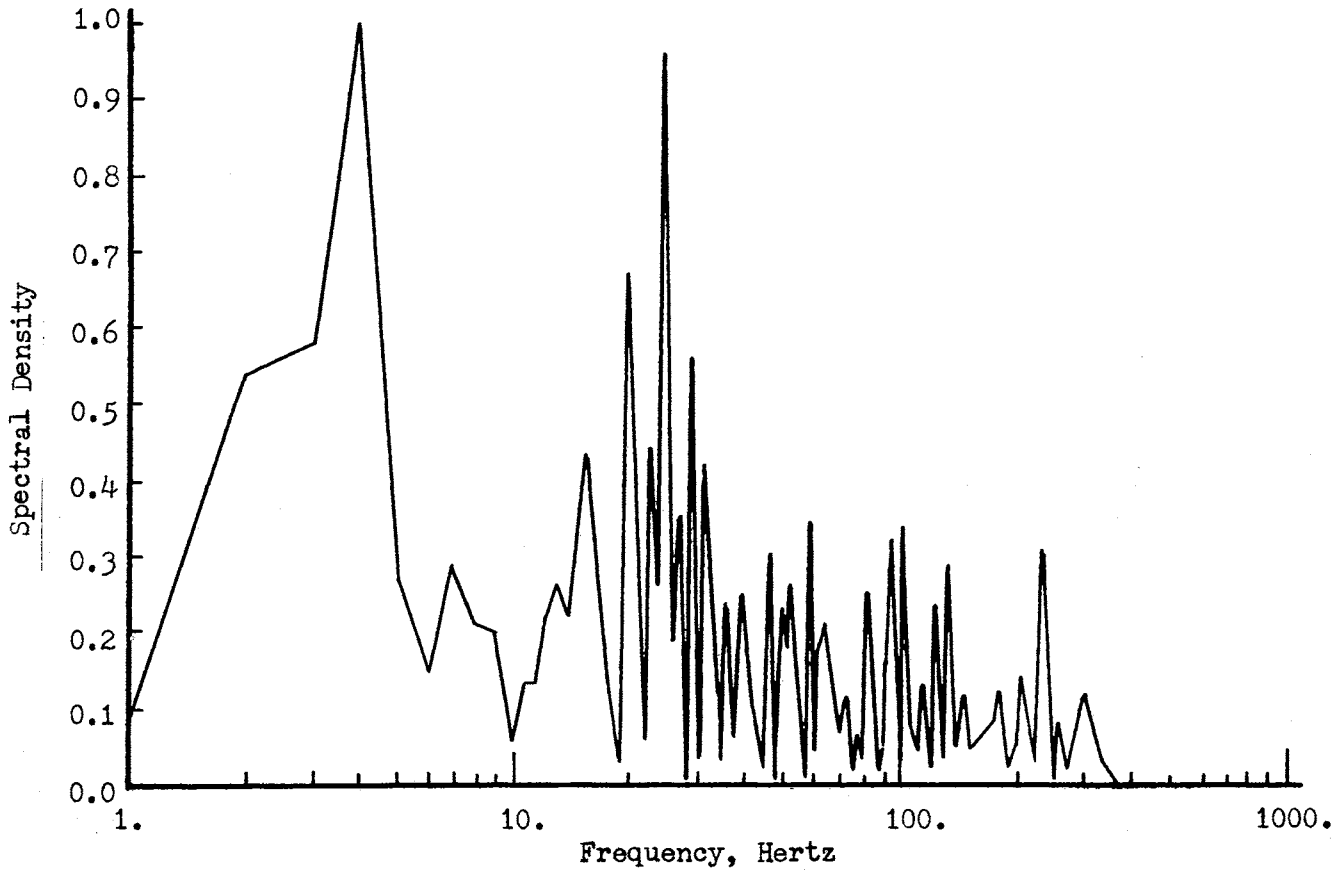

Figure 50. Spectral Density of Amplitude Fluctuation for Reynolds Number = 2.1 at High Shear Mach 5 Gas Condition

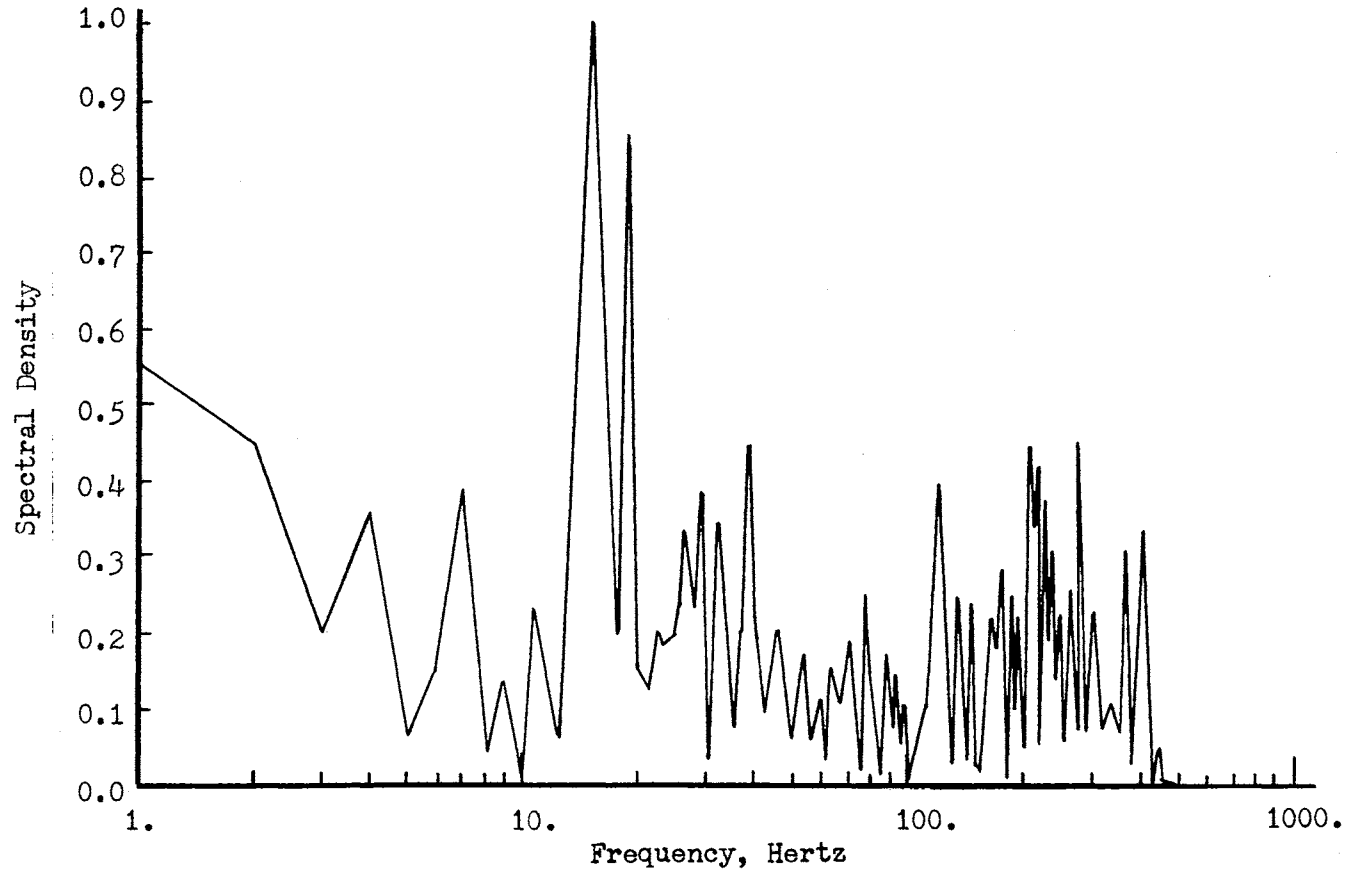

Figure 51. Spectral Density of Amplitude Fluctuation for Reynolds Number = 21. at High Shear Mach 5 Gas Condition

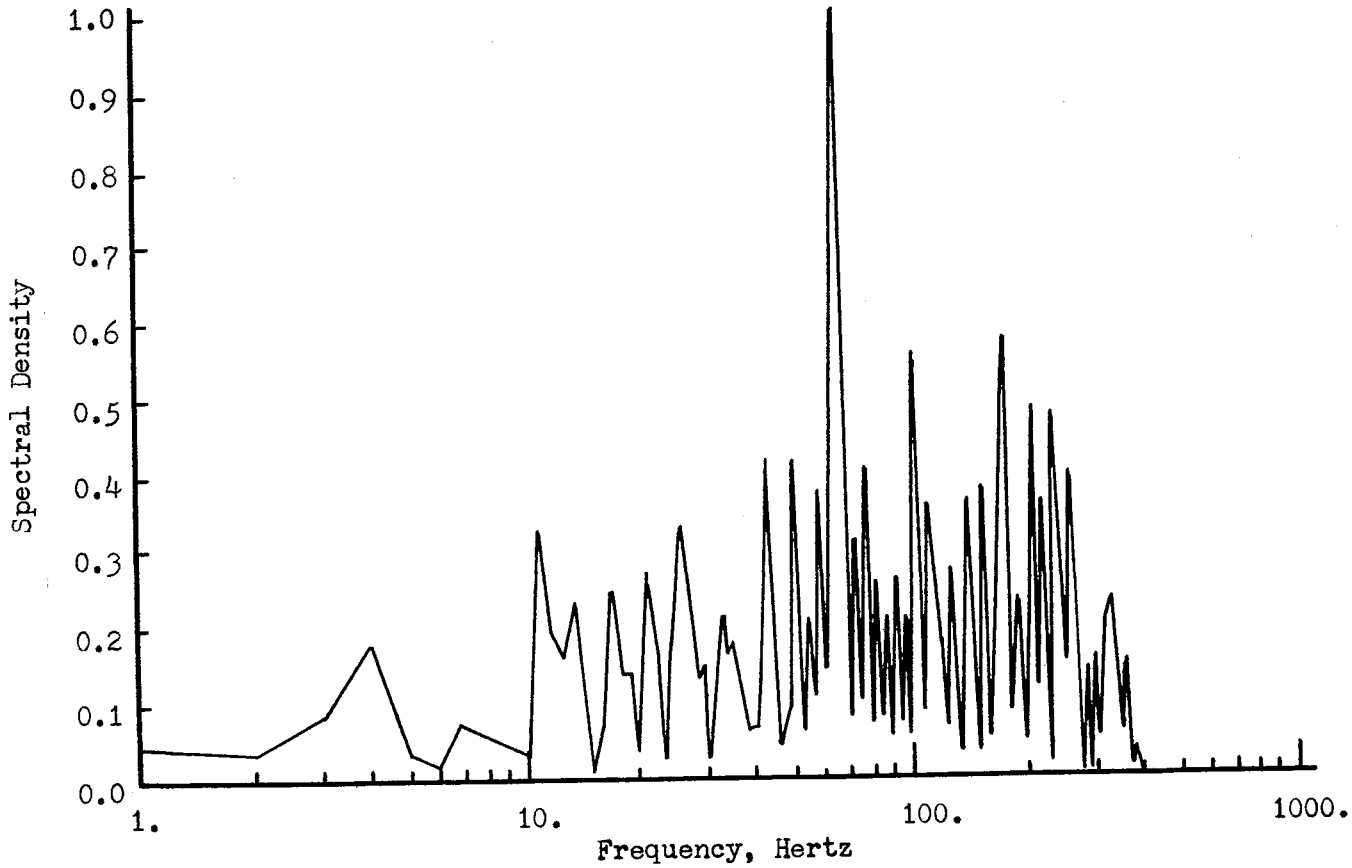

Figure 52. Spectral Density of Amplitude Fluctuation for Reynolds Number = 32. at High Shear Mach 5 Gas Condition

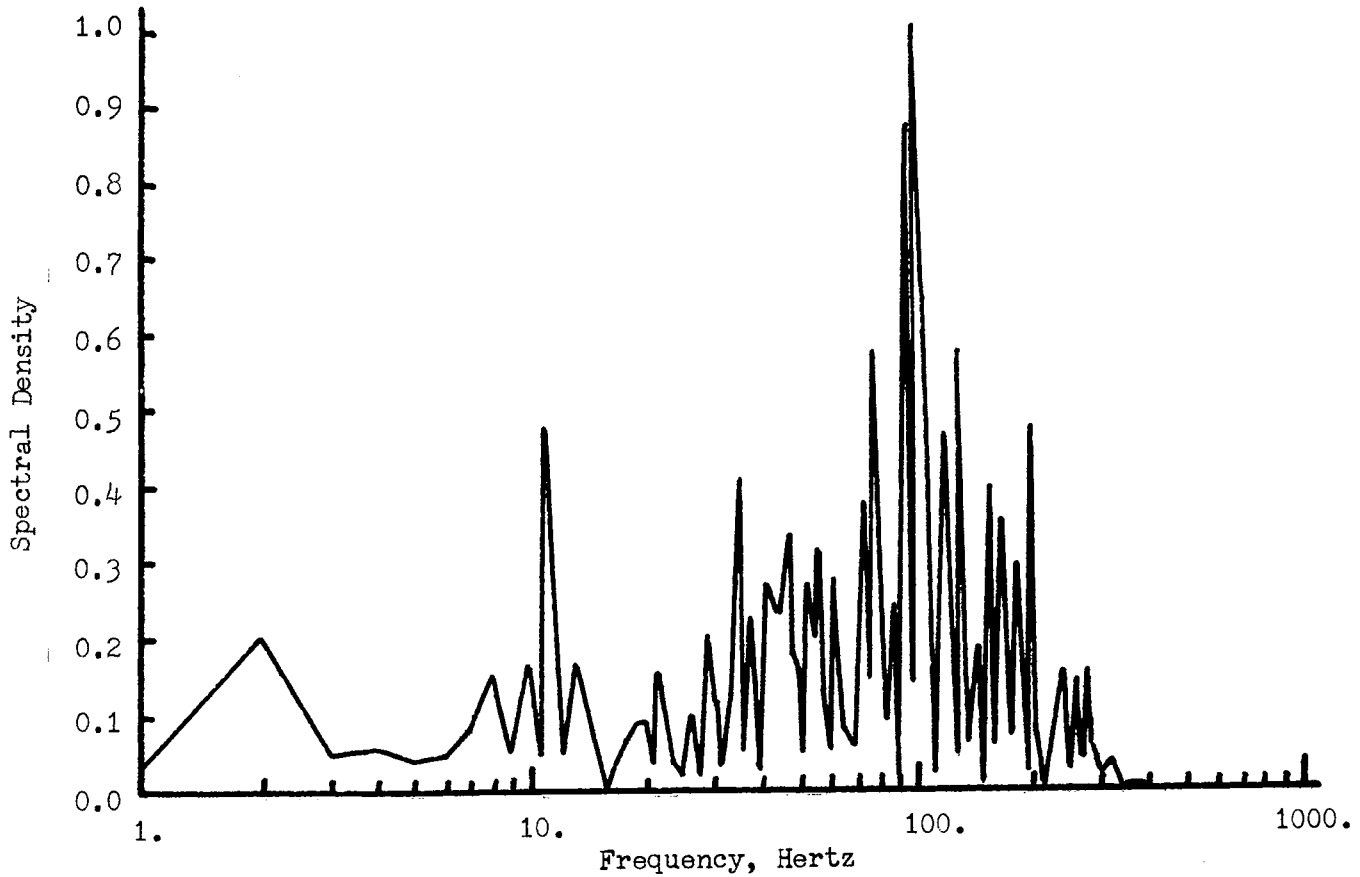

Figure 53. Spectral Density of Amplitude Fluctuation for Reynolds Number = 60. at High Shear Mach 5 Gas Condition

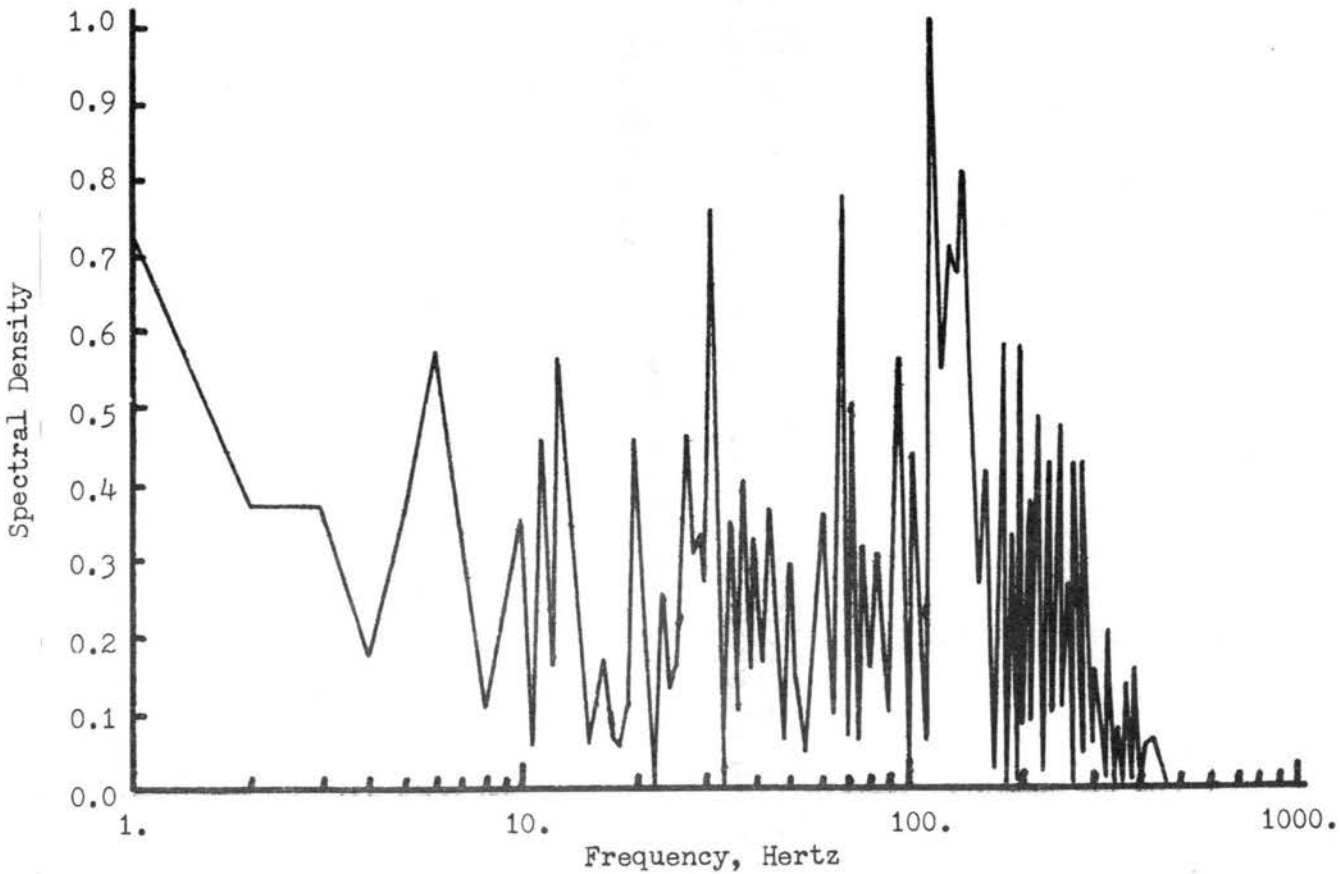

Figure 54. Spectral Density of Amplitude Fluctuation for Reynolds Number = 66. at High Shear Mach 5 Gas Condition

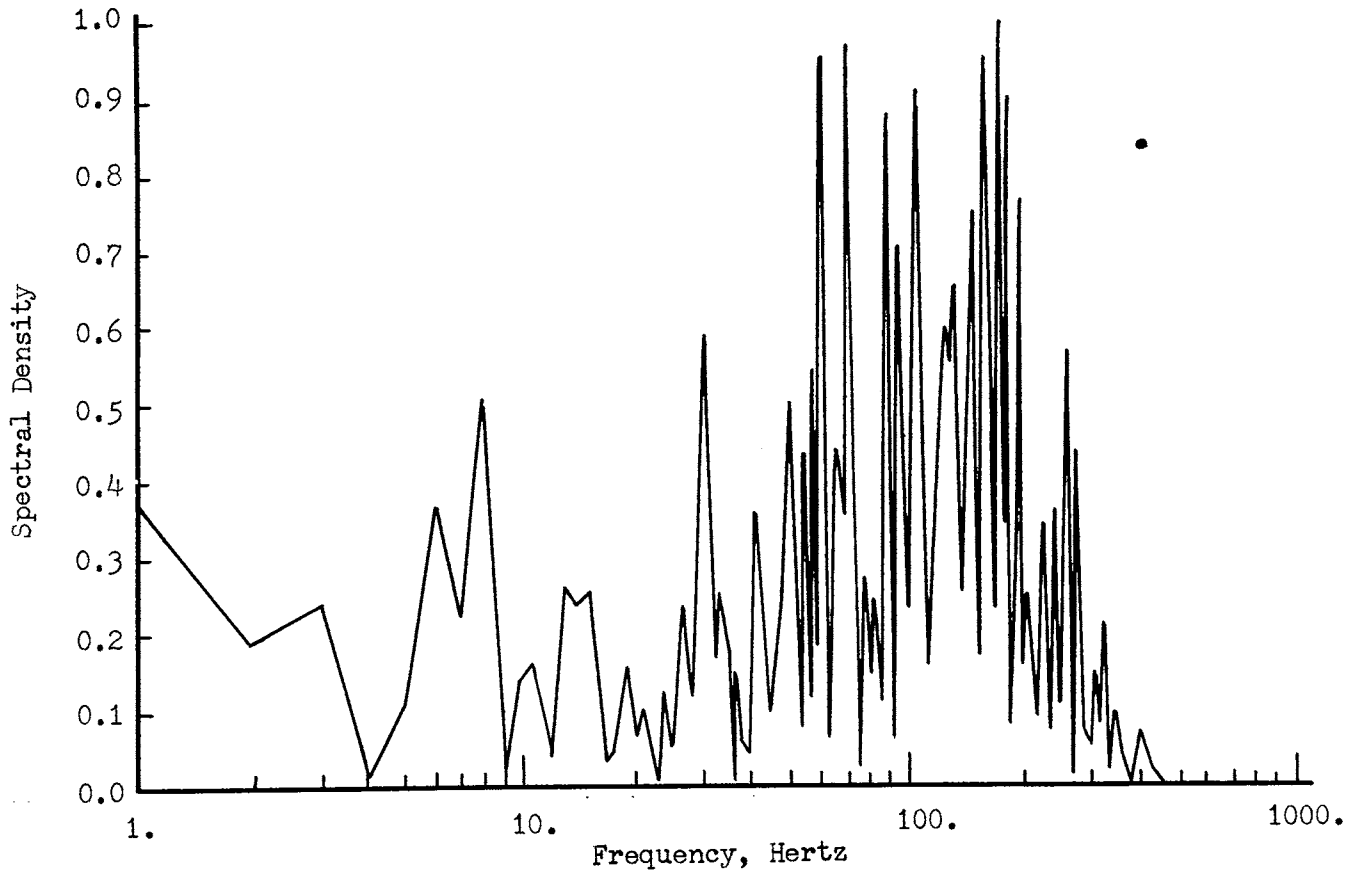

Figure 55. Spectral Density of Amplitude Fluctuation for Reynolds Number = 110. at High Shear Mach 5 Gas Condition

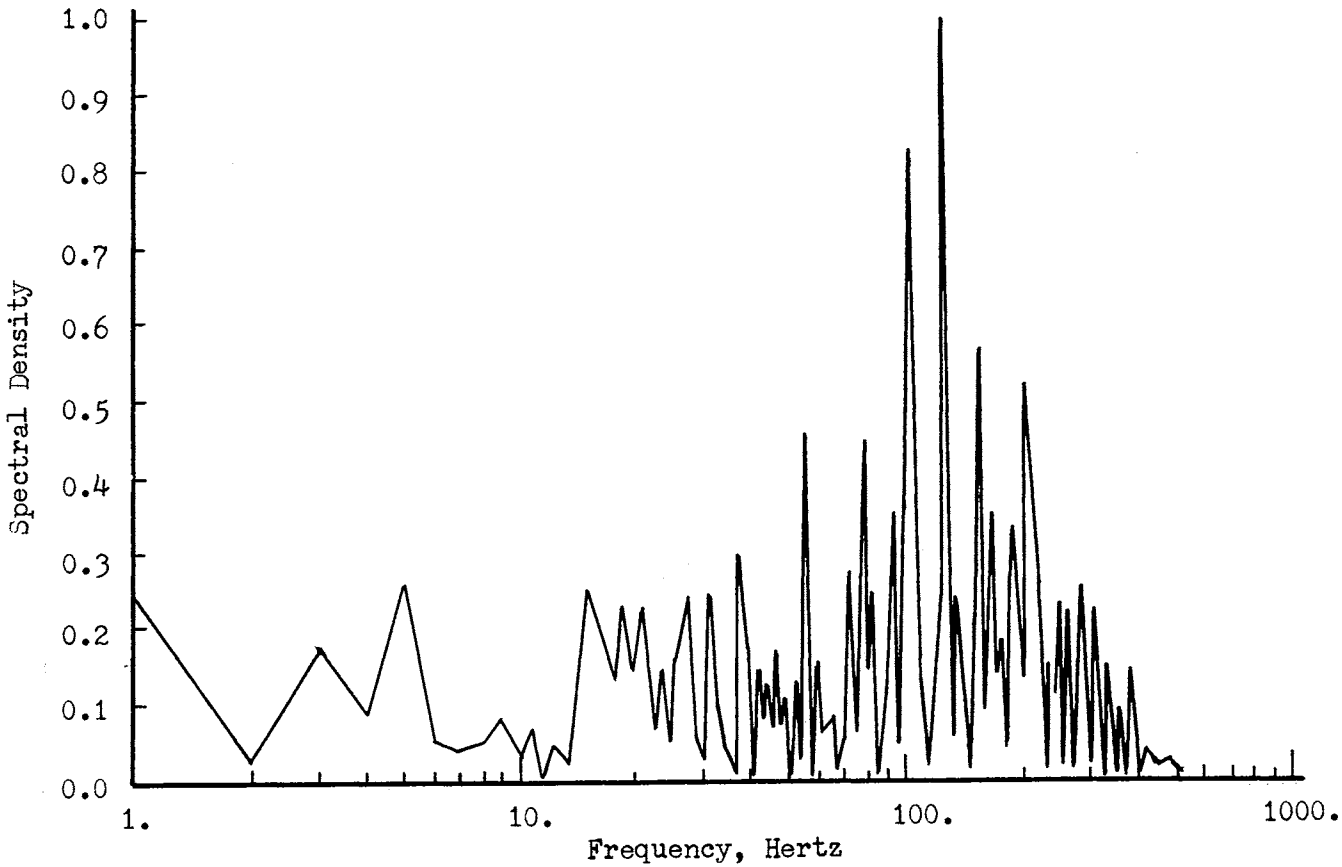

Figure 56. Spectral Density of Amplitude Fluctuation for Reynolds Number = 135. at High Shear Mach 5 Gas Condition

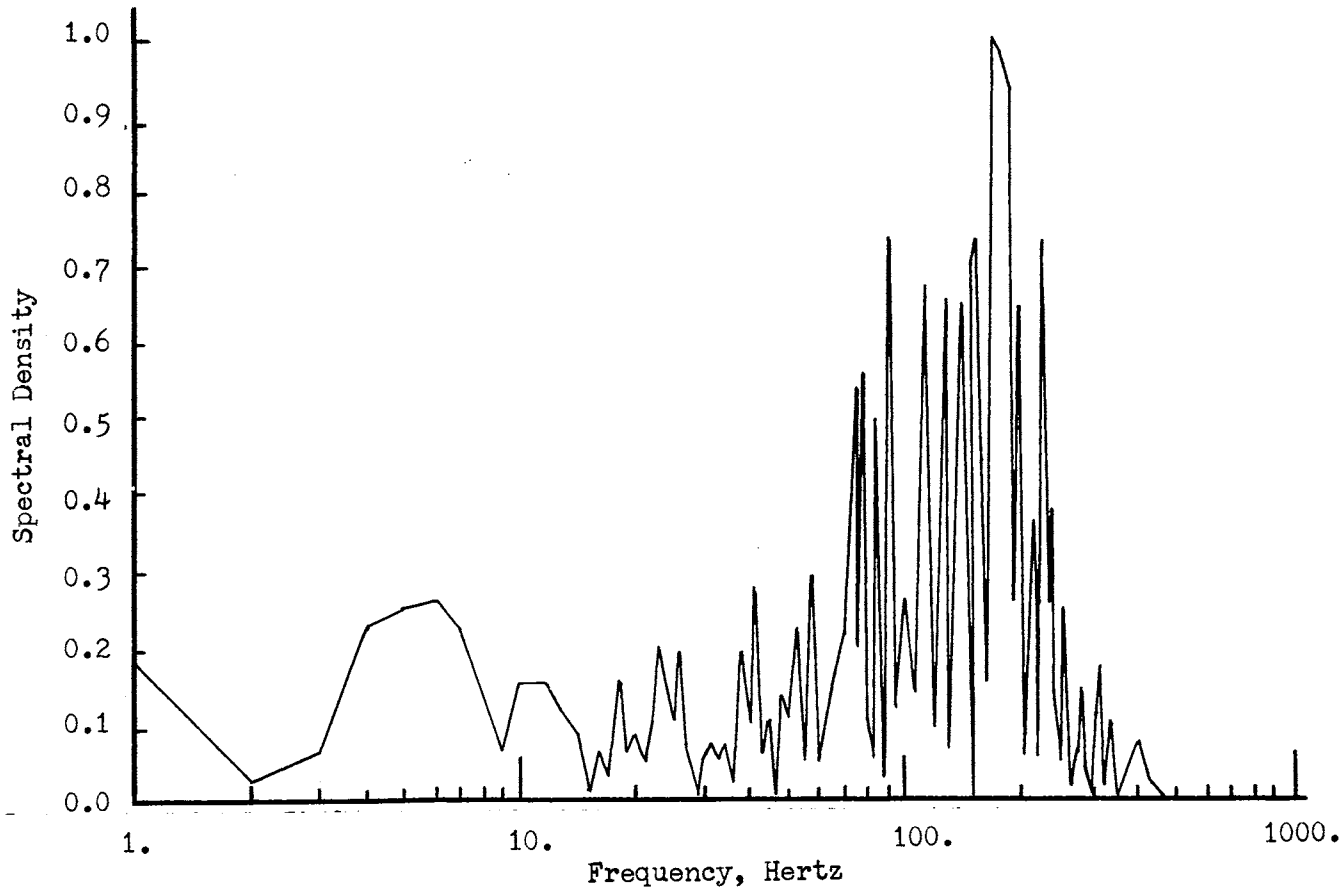

Figure 57. Spectral Density of Amplitude Fluctuation for Reynolds Number = 265. at High Shear Mach 5 Gas Condition

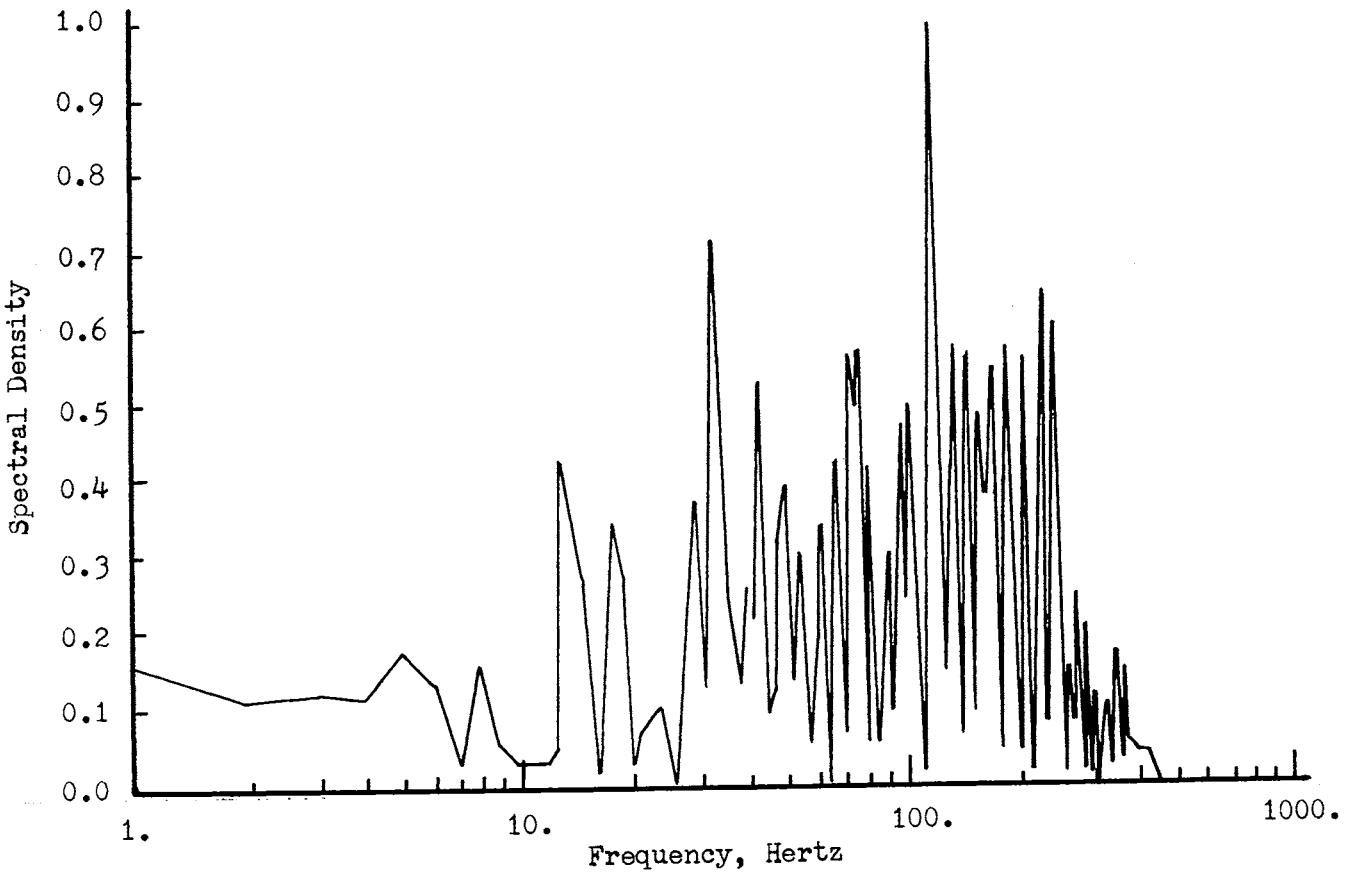

Figure 58. Spectral Density of Amplitude Fluctuation for Reynolds Number = 360. at High Shear Mach 5 Gas Condition

Thirteen spectra are given with data not available for the other two conditions due to malfunction of either the gauge, the bridge electronics, or the recording equipment. Further, because of the uncertainties for the low Reynolds number conditions, the dominant frequency data for Figures 46 and 48 were omitted in the regression analysis and that for Figures 50 and 56 were omitted due to the lack of measured thickness data.

The relationship between the peak frequency and the liquid Reynolds number and thickness was analyzed using a regression analysis to fit the data to the response surface model given by equation 3. The results of this analysis are given in Table XXV. For this analysis the critical F-ratio of 2.0 causes all coefficients with a significance level less than approximately 80 percent to be neglected. The standard deviation of this model is 31.2 and the significant coefficients of the model including 80 percent confidence intervals are given in Table XXVI.

The value of the F-ratio for the coefficient of the linear Reynolds number term in the model (b_2) as well as the value of the coefficient itself indicates a higher significance level for the dependence of the data on this parameter than on the thickness term (b_1) and the quadratic Reynolds number term (b_4). Since the coefficient of the single significant thickness term (the linear effect) is positive, it is clear that the frequency increases with increasing thickness. The fitted form of the response surface for the high shear Mach 5 condition is

$$f = 33.6 + 18.7\hat{h} + 41.0\hat{R} + 16.1\hat{R}^2 .$$

The equation will predict negative frequencies for some combinations of $\hat{h}$ and $\hat{R}$ different from those for which it was calculated and use of the

TABLE XXV

ANALYSIS OF VARIANCE FOR DOMINANT WAVE FREQUENCY
AT HIGH SHEAR MACH 5 GAS CONDITION

Source	Sum of Squares	Degrees of Freedom	Mean Square	F-Ratio
Total	29012	8	3626.4	
Regression	24132	3	8044.0	8.24
Error	4880	5	975.9	

TABLE XXVI

MODEL COEFFICIENT VALUES FOR DOMINANT WAVE FREQUENCY
AT HIGH SHEAR MACH 5 GAS CONDITION

Coefficient	Value and 80% Confidence Interval	Standard Error	F-Ratio	Significance Level
b_0	33.6 ± 27.4	19.58		
b_1	18.7 ± 14.1	10.1	3.4	.88
b_2	41.0 ± 14.0	10.0	16.9	.99
b_4	16.06 ± 13.1	9.41	2.9	.85

equation is restricted to the range and combination of values given in Table VII. The dimension of the frequency is Hertz and similar to all other models the dimension of the thickness is inch. Figure 59 is a plot of the dominant frequency as a function of Reynolds number for thicknesses of 0.004 and 0.012 inches. Plotted on the curves are the observed frequencies for four experimental conditions. The error bars on the curves are 80 percent confidence intervals on the model predictions and in all cases these intervals include the observed data.

From the fitted equation and the curves in Figure 59, it is seen that the dominant wave frequency increases with Reynolds number at constant thickness for these combinations of liquid parameters and likewise increases with thickness for any constant Reynolds number value.

The frequency spectra determined from the Fourier analysis of the depth gauge output for each of the liquid flow rates at the Mach 7 gas condition are shown in Figures 60 through 74. The same trend noted for each of the other gas conditions is present in these data. That is, the location of the dominant wave frequency generally increases with increasing Reynolds number.

The frequency data were analyzed using the response surface model given by equation 3. Because of uncertainties at the low Reynolds conditions the dominant wave data from Figures 60, 62, 63, and 64 were omitted in the regression analysis. The results of the regression analysis are given in Table XXVII. The assumed critical F-ratio of 2.0 corresponds to a 78 percent confidence level for this analysis. The standard deviation of the data from the model is 18.68 and the significant coefficients including the 80 percent confidence intervals are shown in Table XXVIII. Based on the regression analysis results for

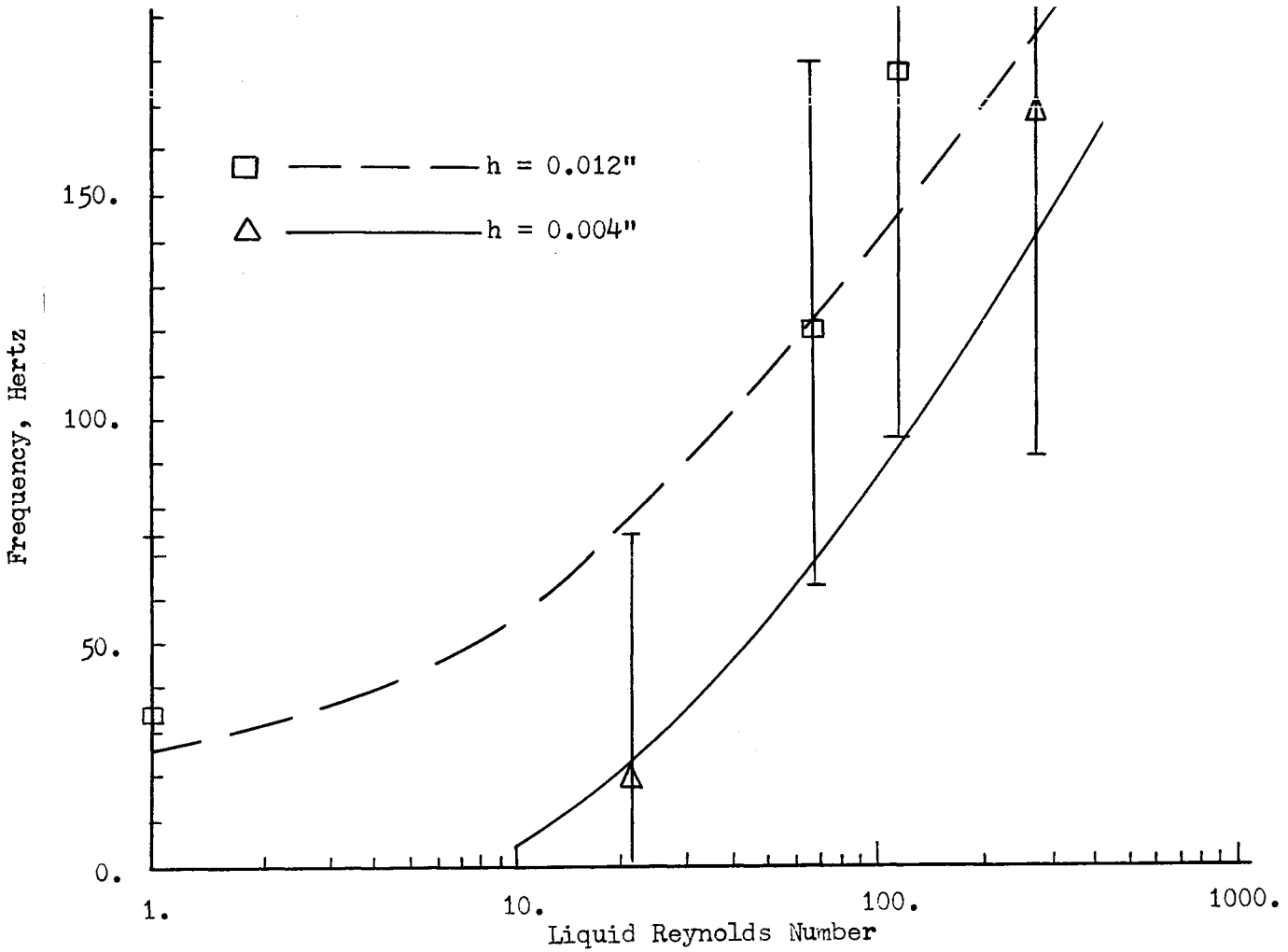

Figure 59. Variation of Dominant Wave Frequency for Constant Liquid Thicknesses at High Shear Mach 5 Gas Condition

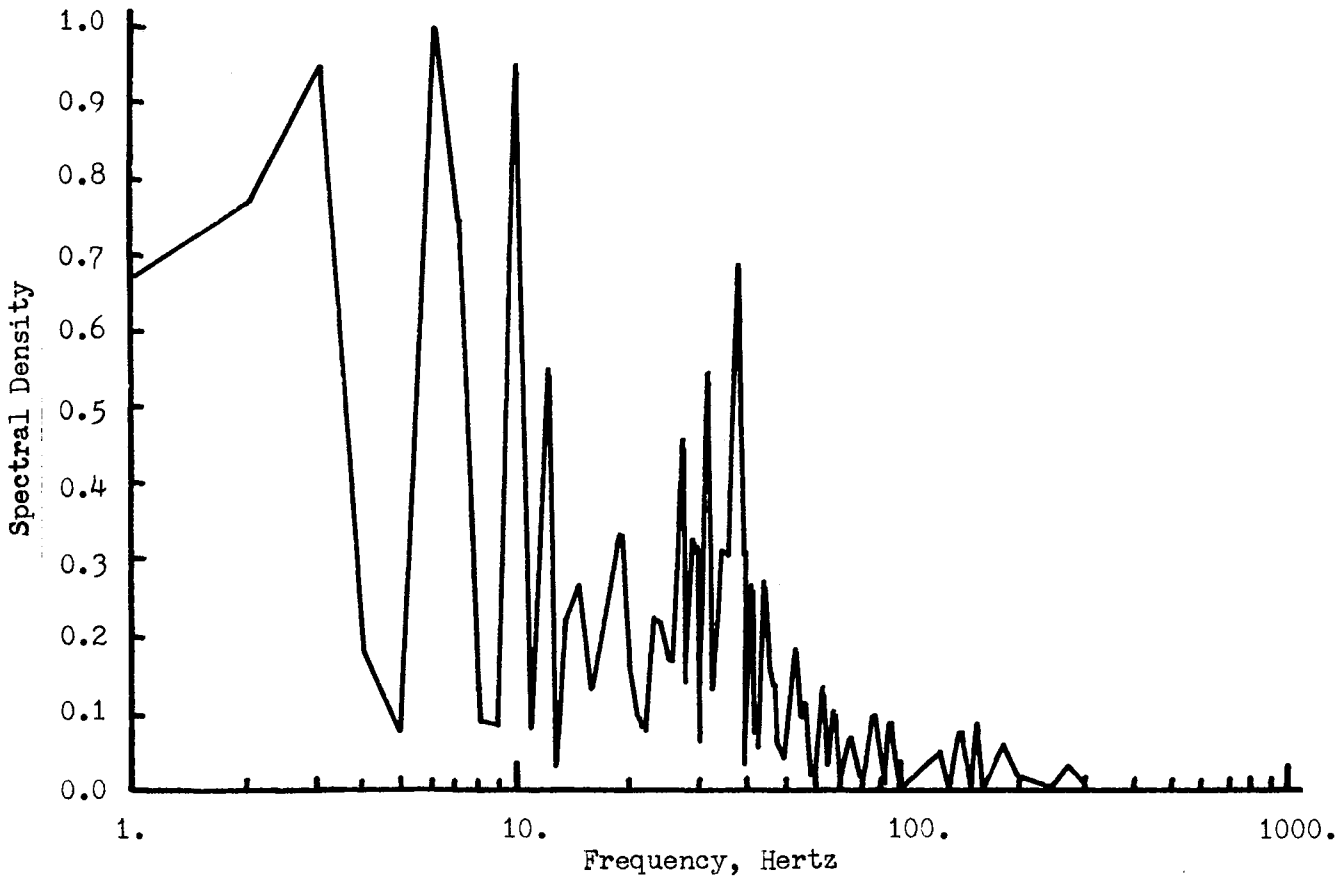

Figure 60. Spectral Density of Amplitude Fluctuation for Reynolds Number = 0.22 at Mach 7 Gas Condition

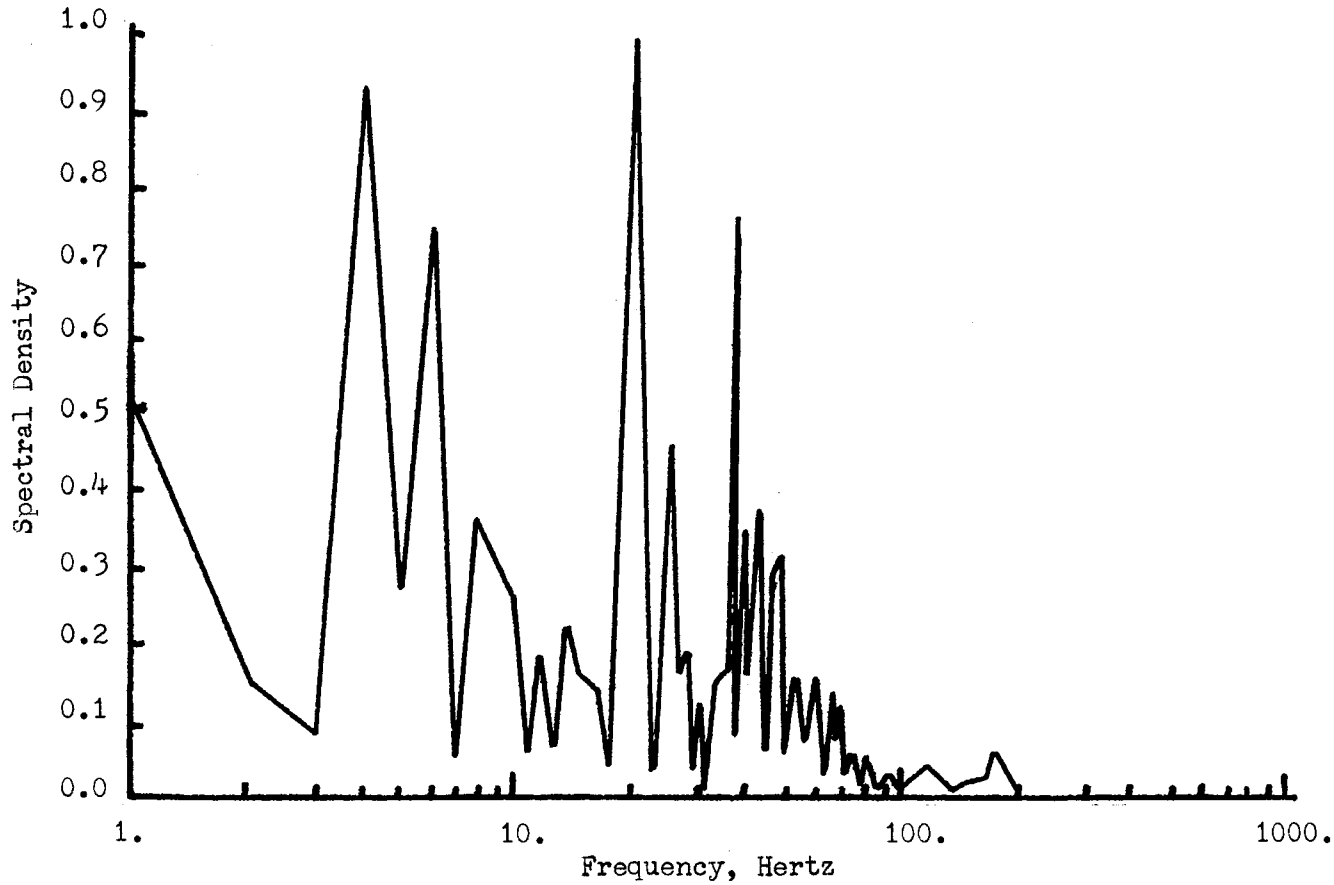

Figure 61. Spectral Density of Amplitude Fluctuation for Reynolds Number = 0.5 at Mach 7 Gas Condition

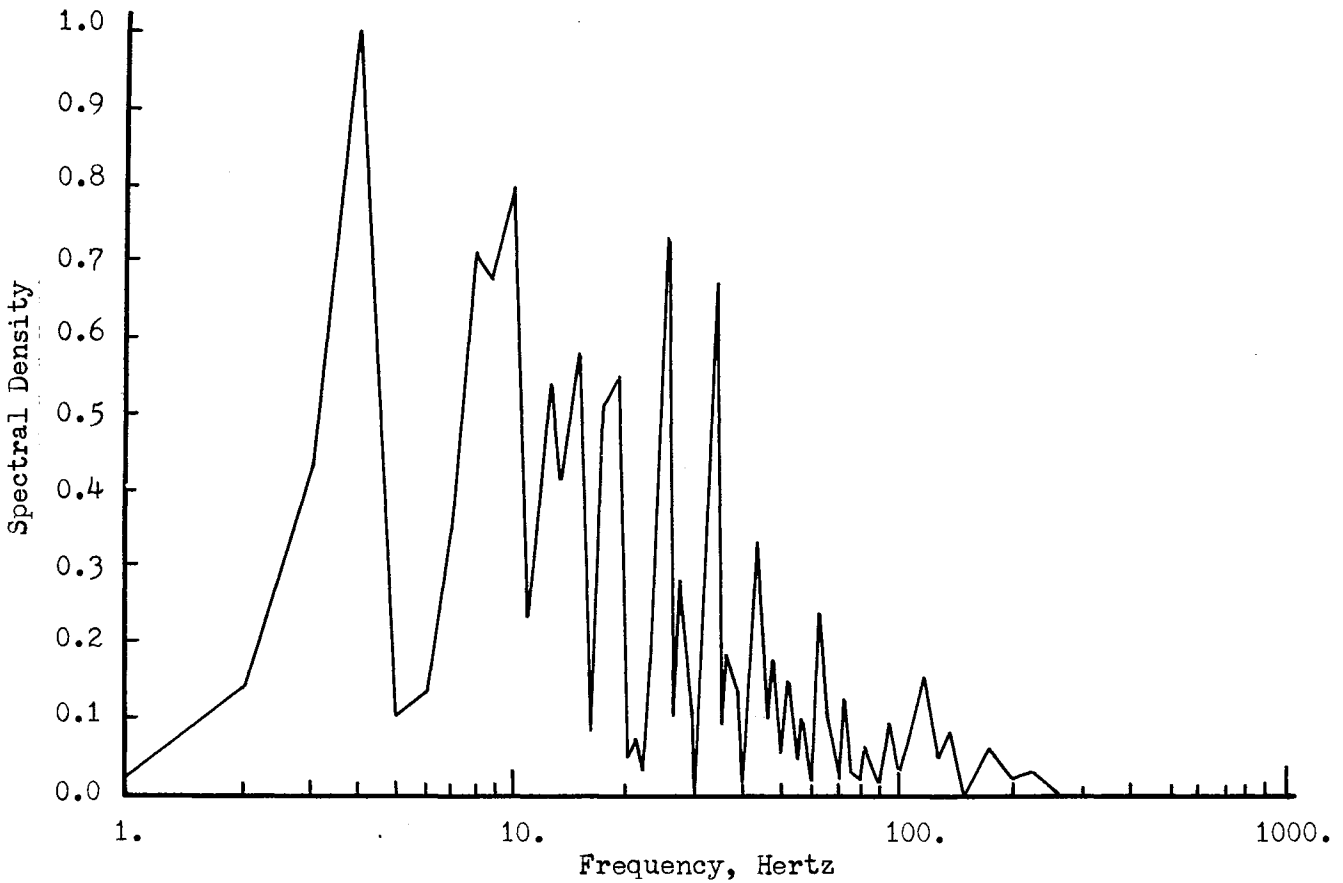

Figure 62. Spectral Density of Amplitude Fluctuation for Reynolds Number = 0.9 at Mach 7 Gas Condition

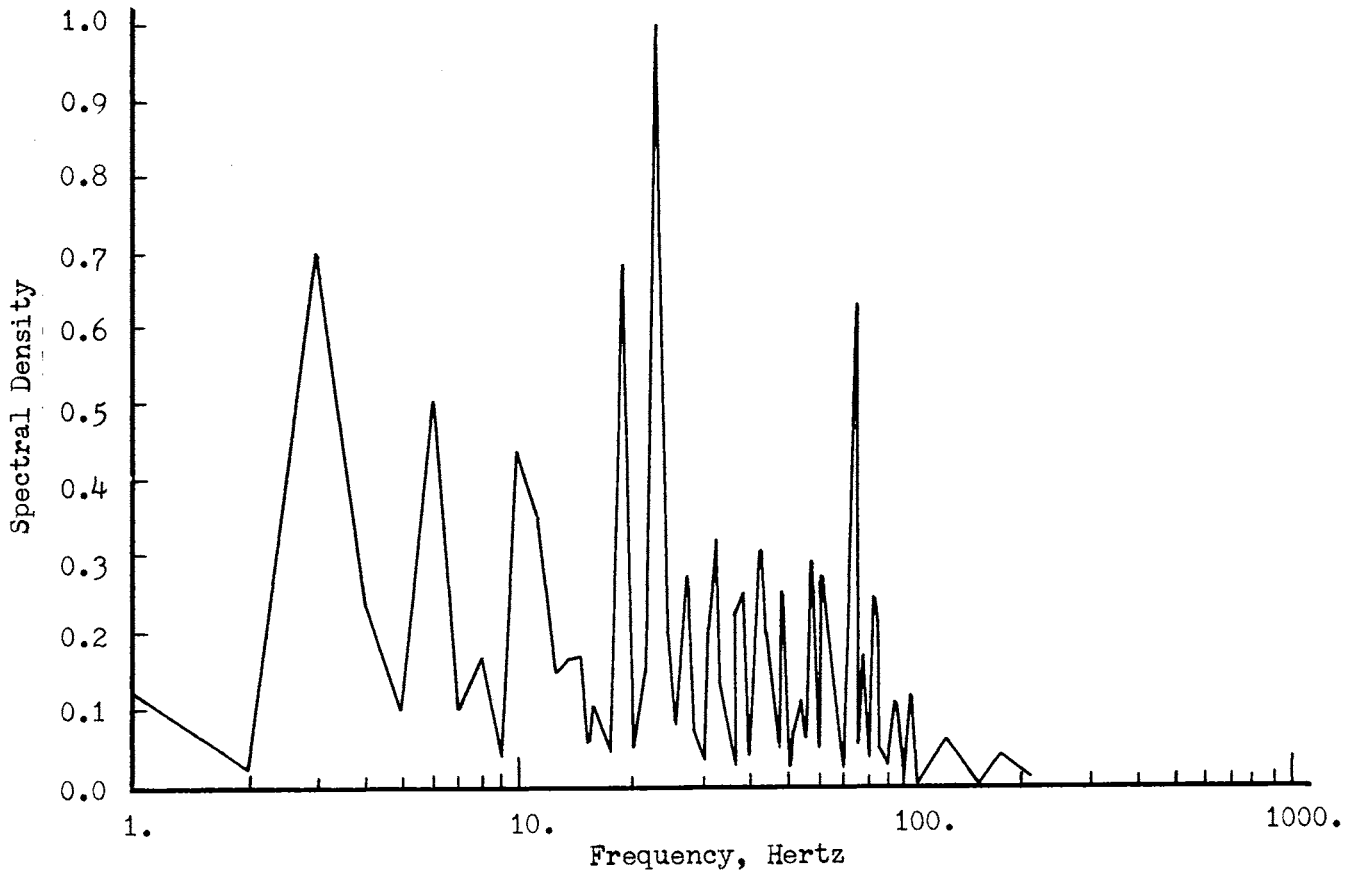

Figure 63. Spectral Density of Amplitude Fluctuation for Reynolds Number = 1.2 at Mach 7 Gas Condition

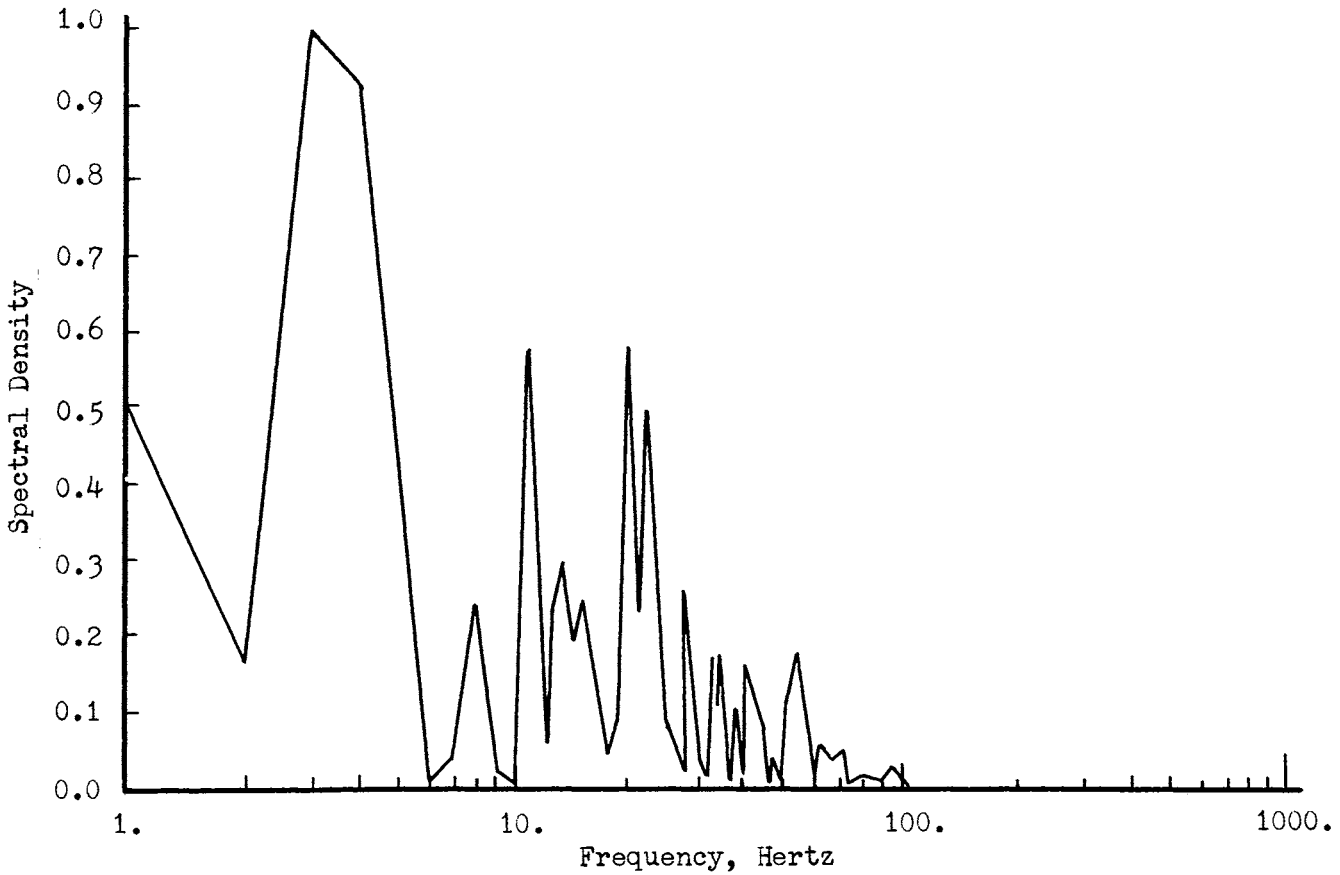

Figure 64. Spectral Density of Amplitude Fluctuation for Reynolds Number = 1.4 at Mach 7 Gas Condition

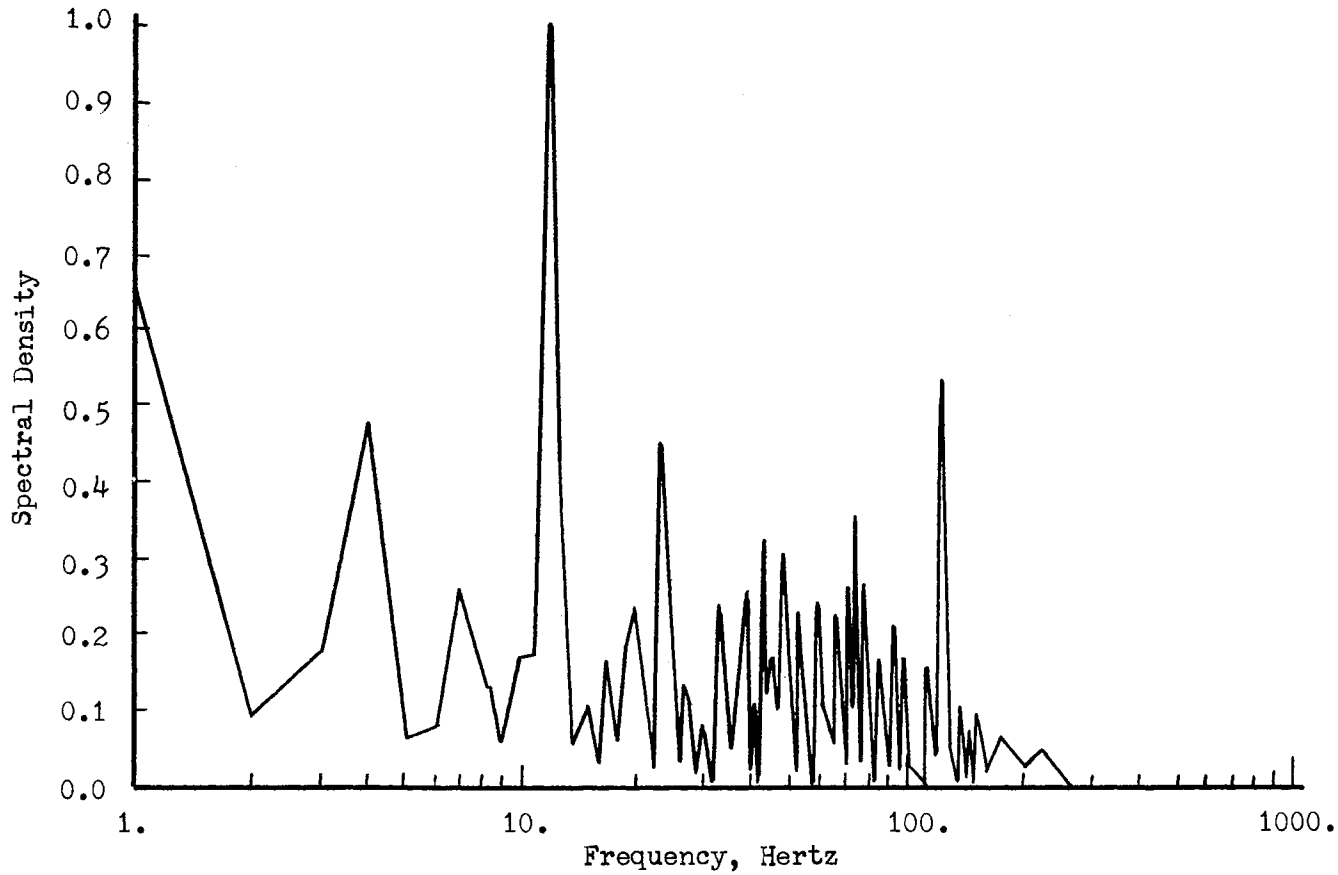

Figure 65. Spectral Density of Amplitude Fluctuation for Reynolds Number = 3.8 at Mach 7 Gas Condition

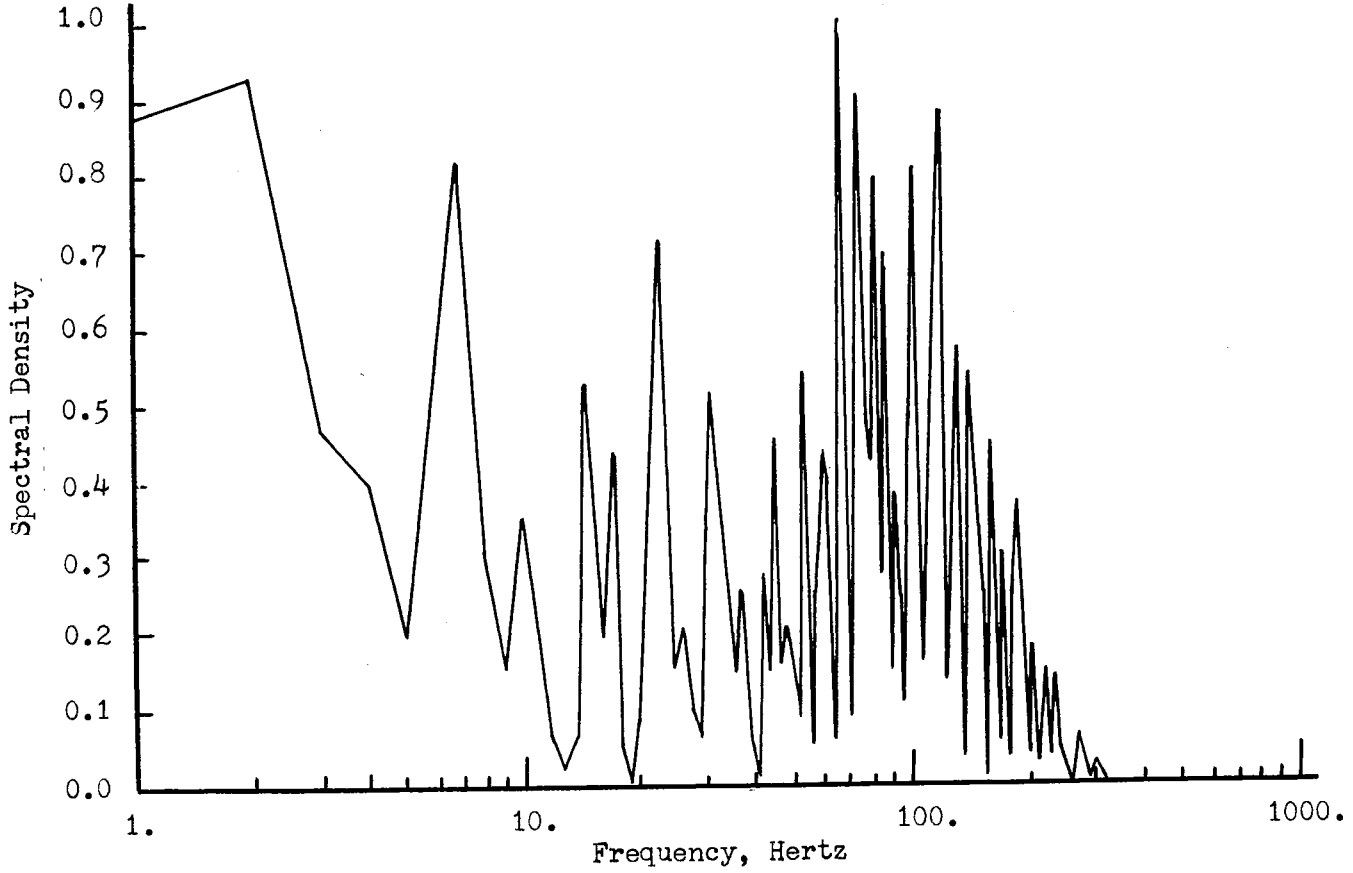

Figure 66. Spectral Density of Amplitude Fluctuation for Reynolds Number = 21. at Mach 7 Gas Condition

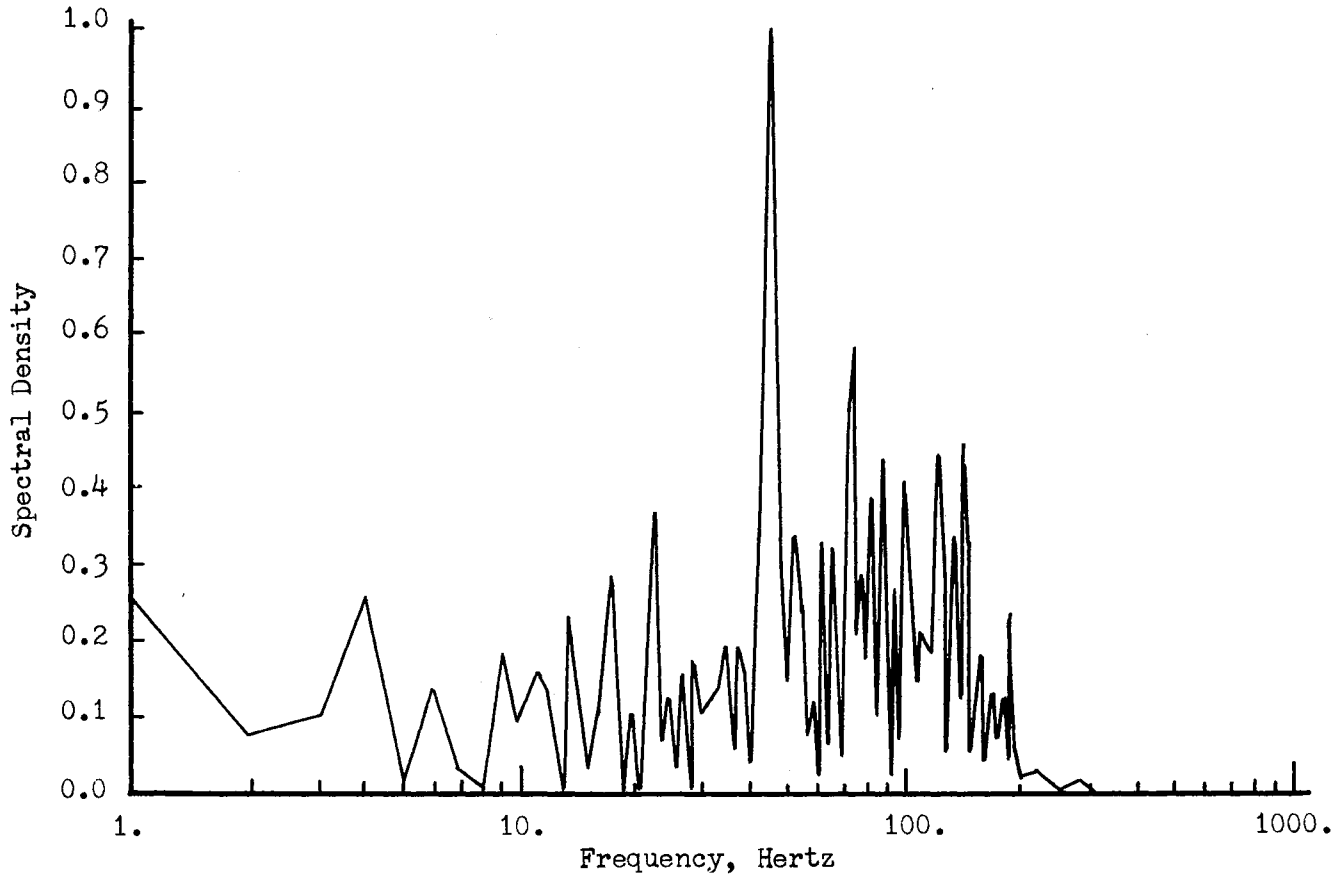

Figure 67. Spectral Density of Amplitude Fluctuation for Reynolds Number = 32. at Mach 7 Gas Condition

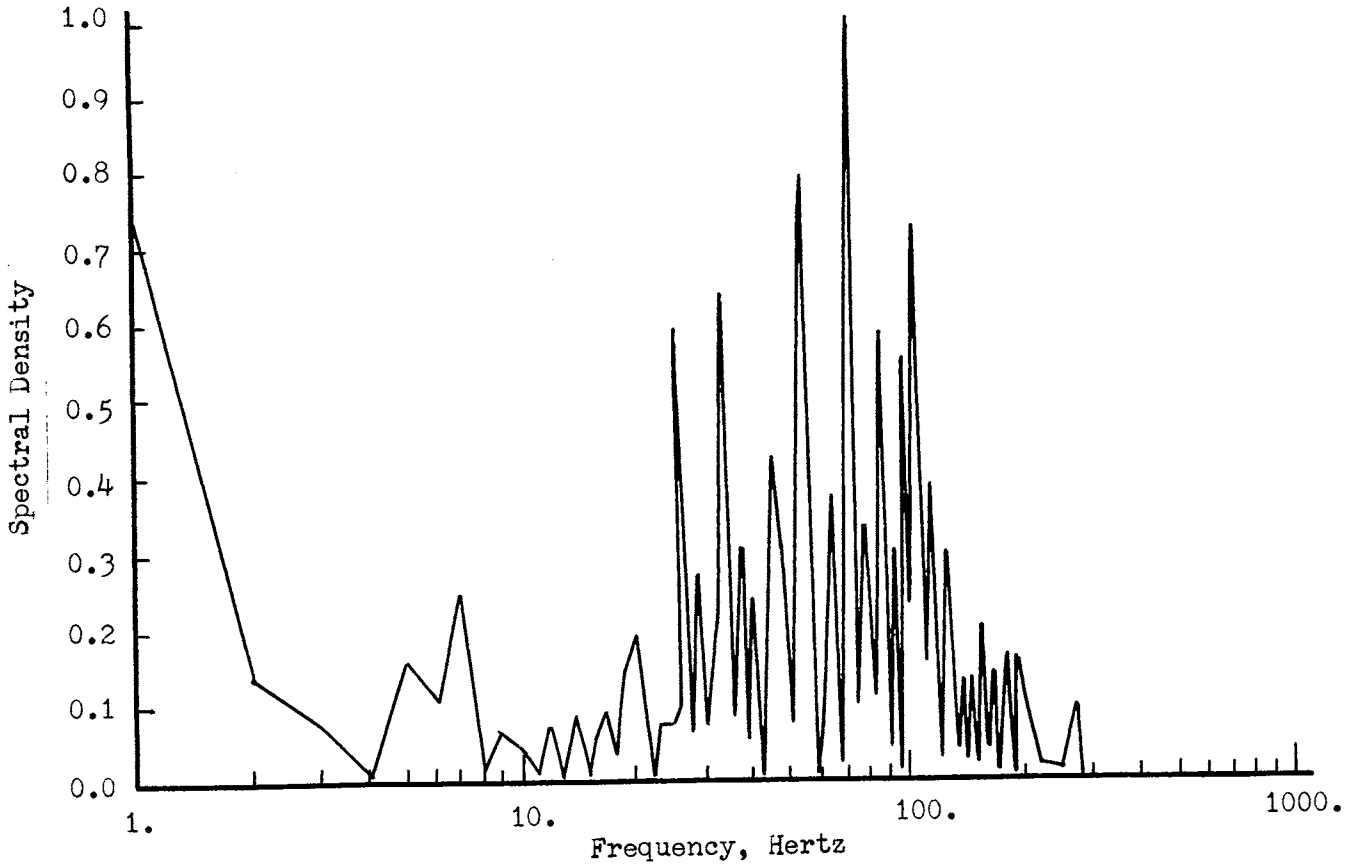

Figure 68. Spectral Density of Amplitude Fluctuation for Reynolds Number = 34. at Mach 7 Gas Condition

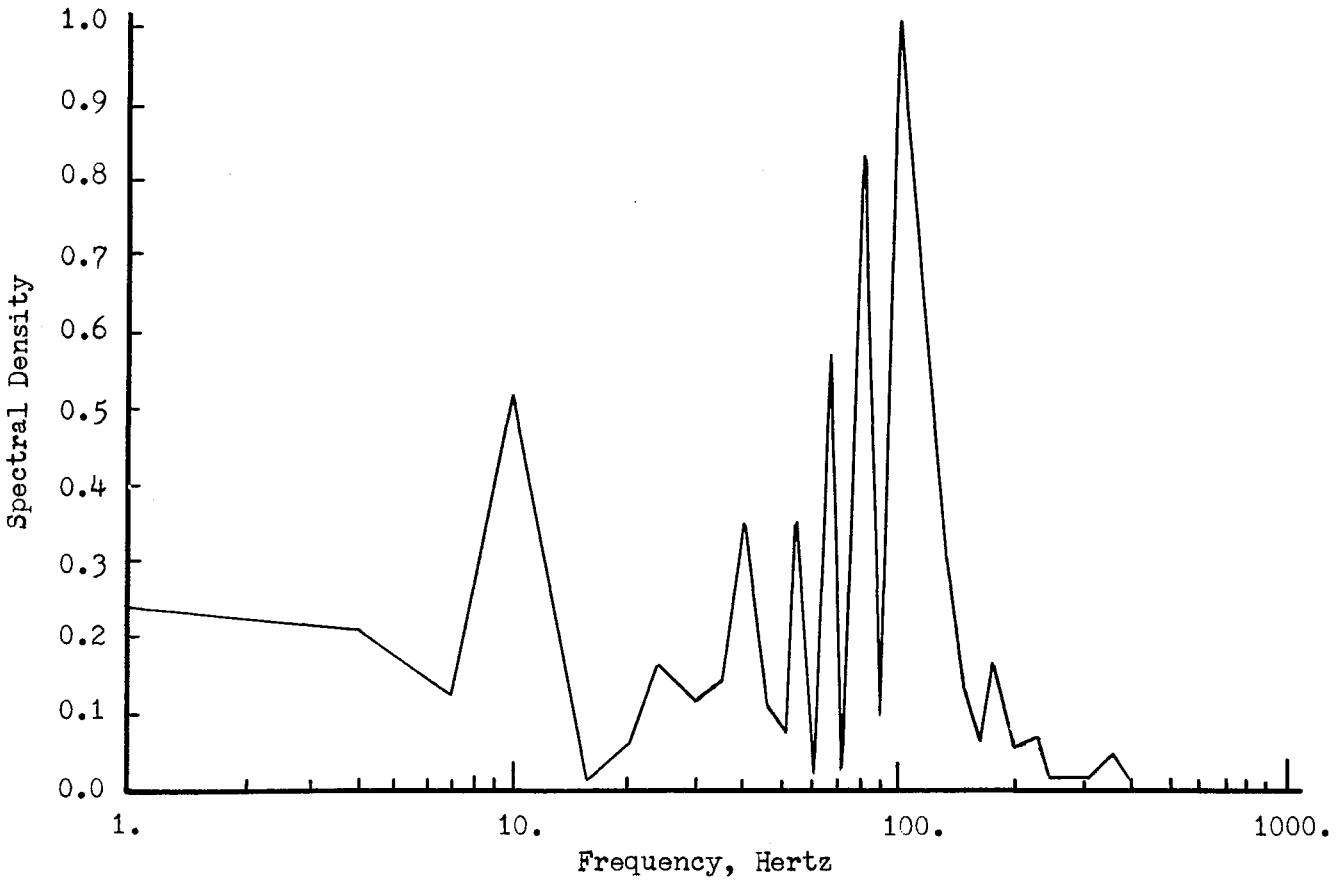

Figure 69. Spectral Density of Amplitude Fluctuation for Reynolds Number = 54. at Mach 7 Gas Condition

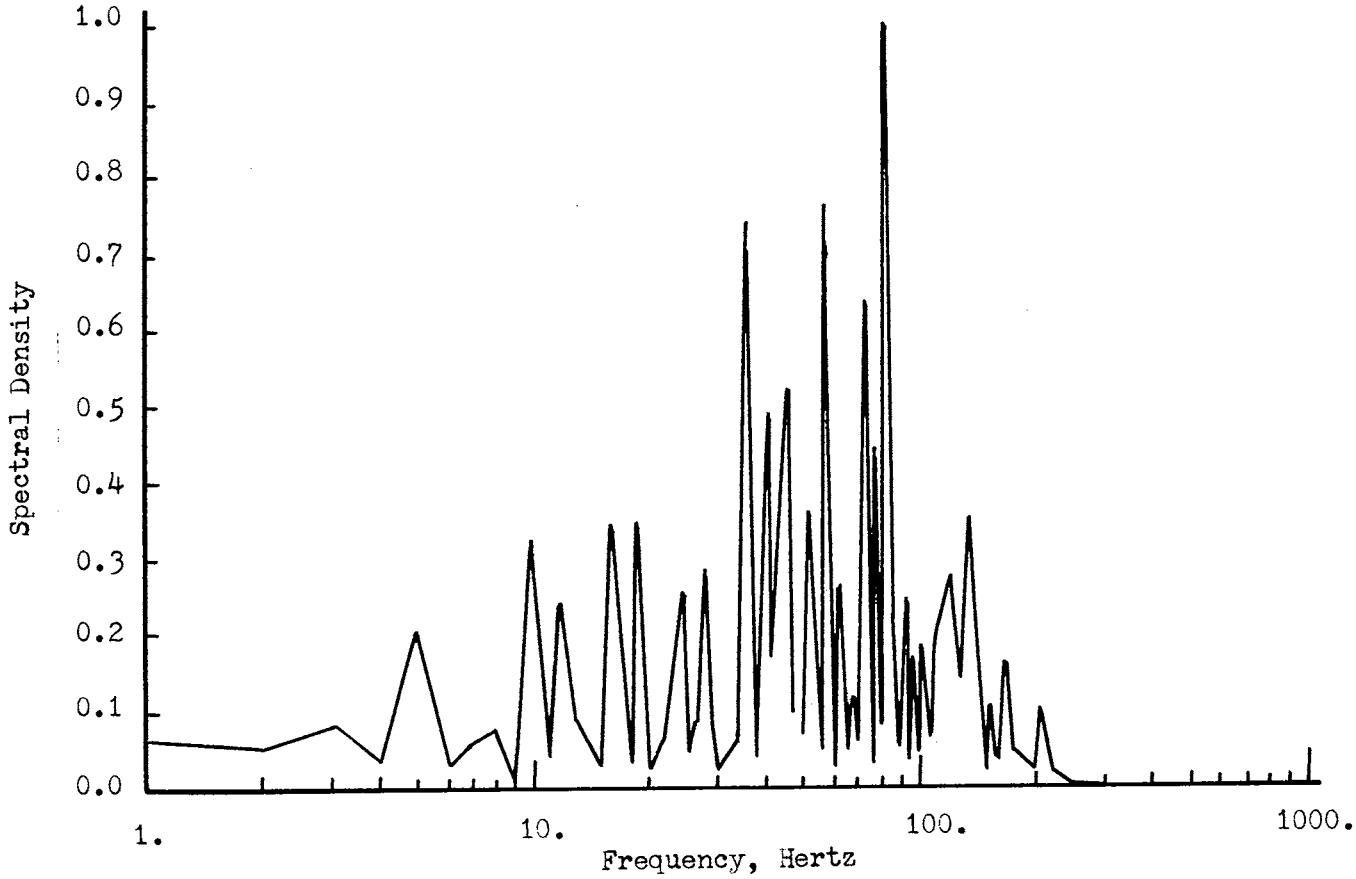

Figure 70. Spectral Density of Amplitude Fluctuation for Reynolds Number = 85. at Mach 7 Gas Condition

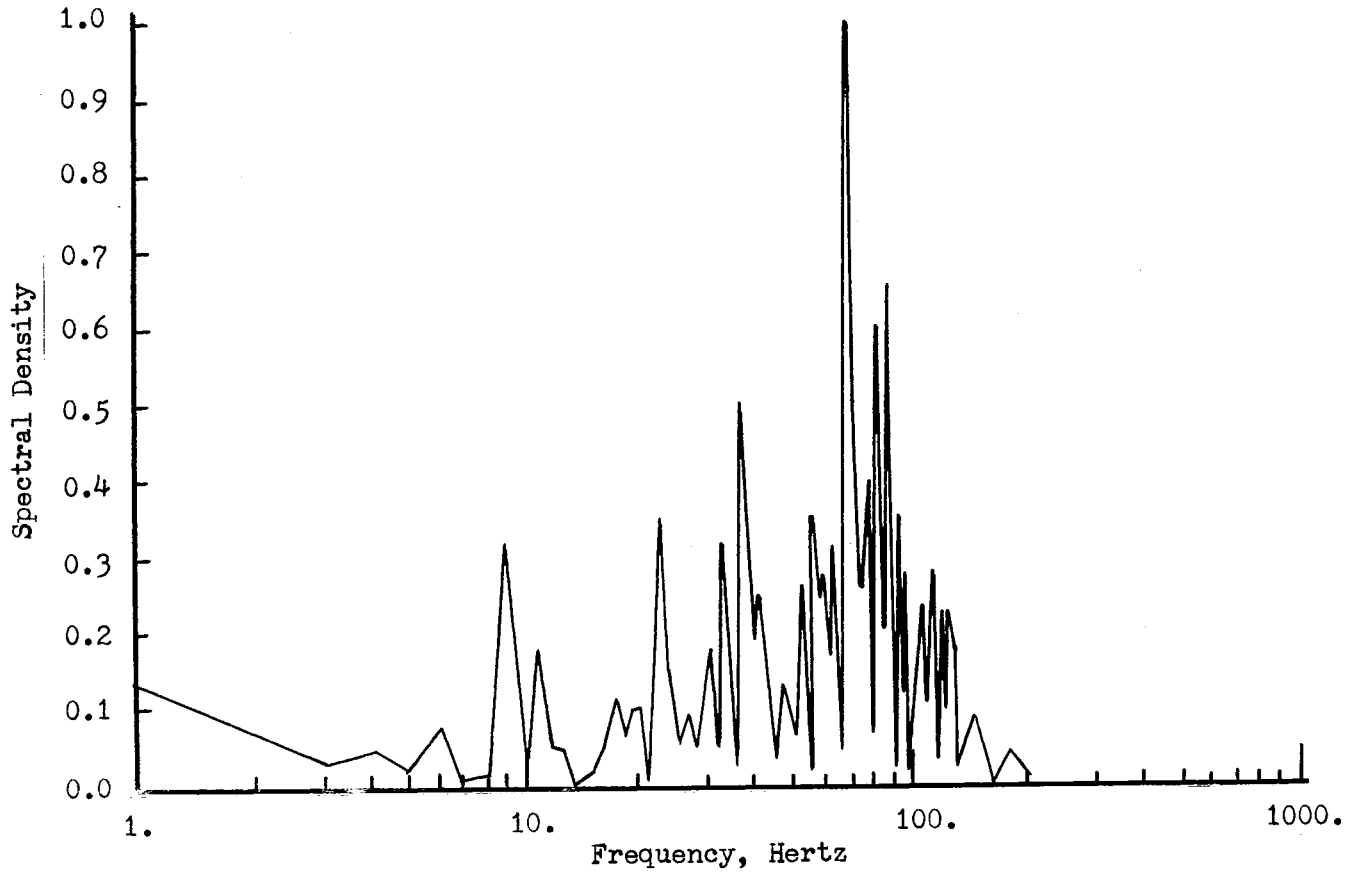

Figure 71. Spectral Density of Amplitude Fluctuation for Reynolds Number = 126. at Mach 7 Gas Condition

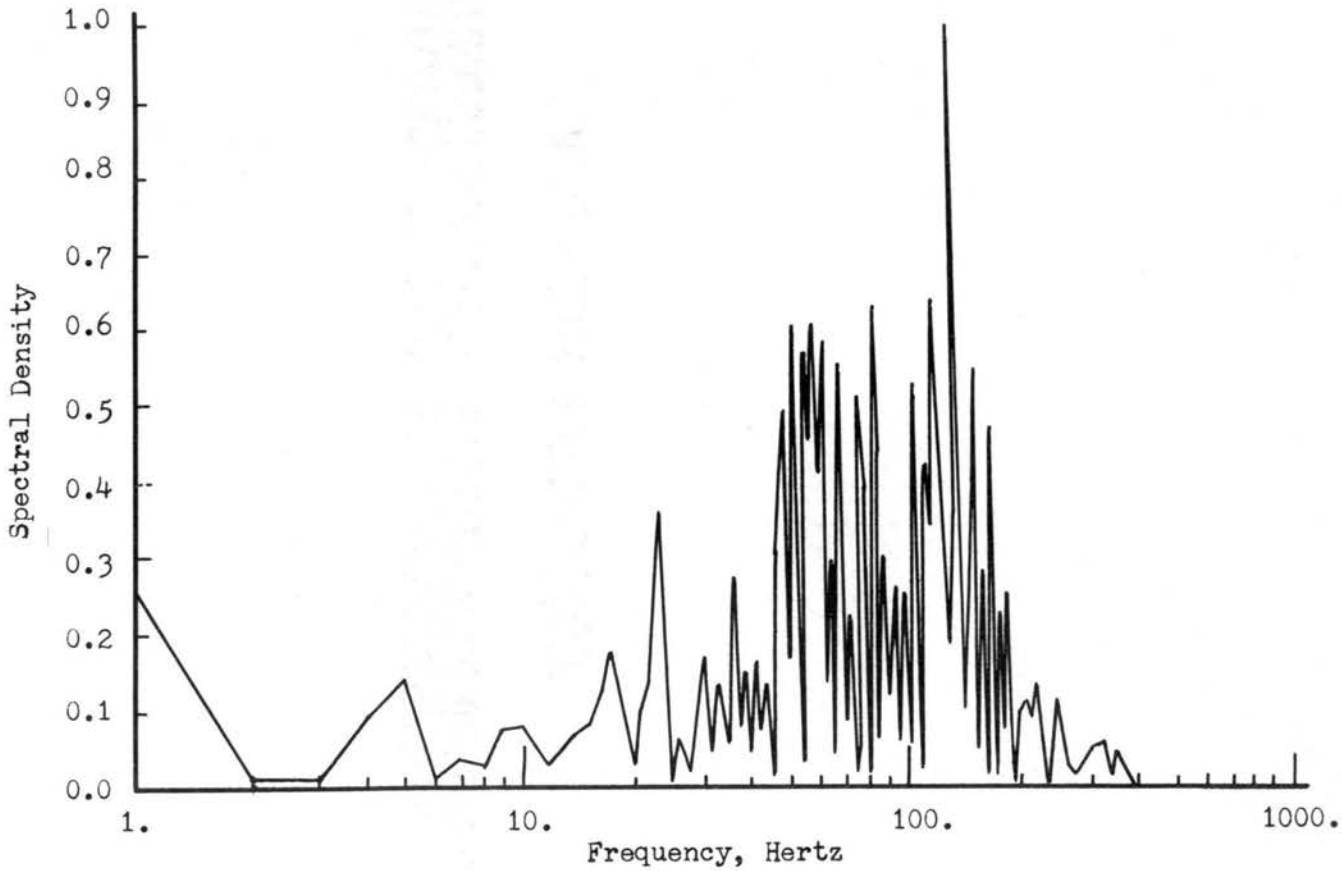

Figure 72. Spectral Density of Amplitude Fluctuation for Reynolds Number = 130. at Mach 7 Gas Condition

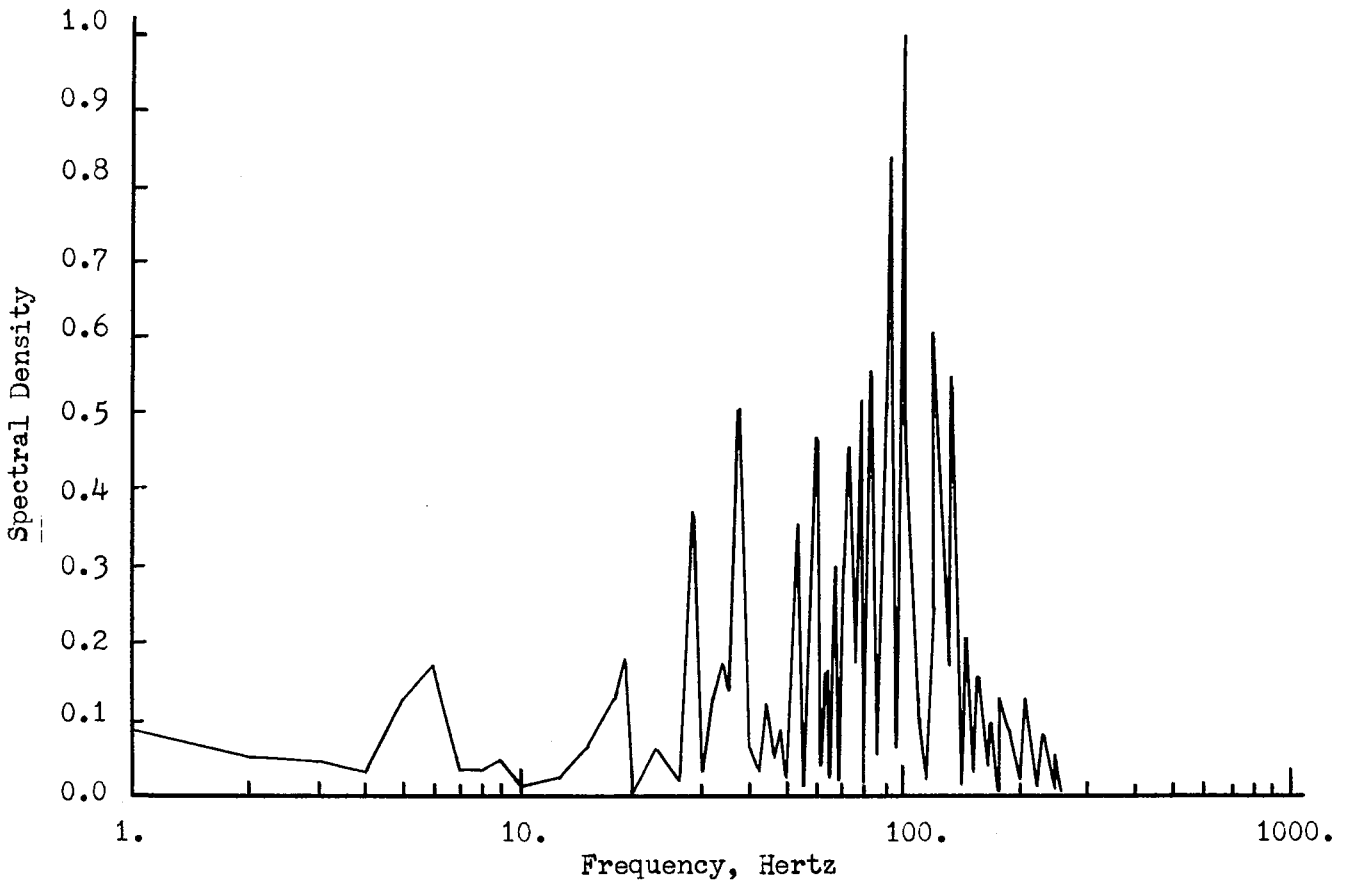

Figure 73. Spectral Density of Amplitude Fluctuation for Reynolds Number = 260. at Mach 7 Gas Condition

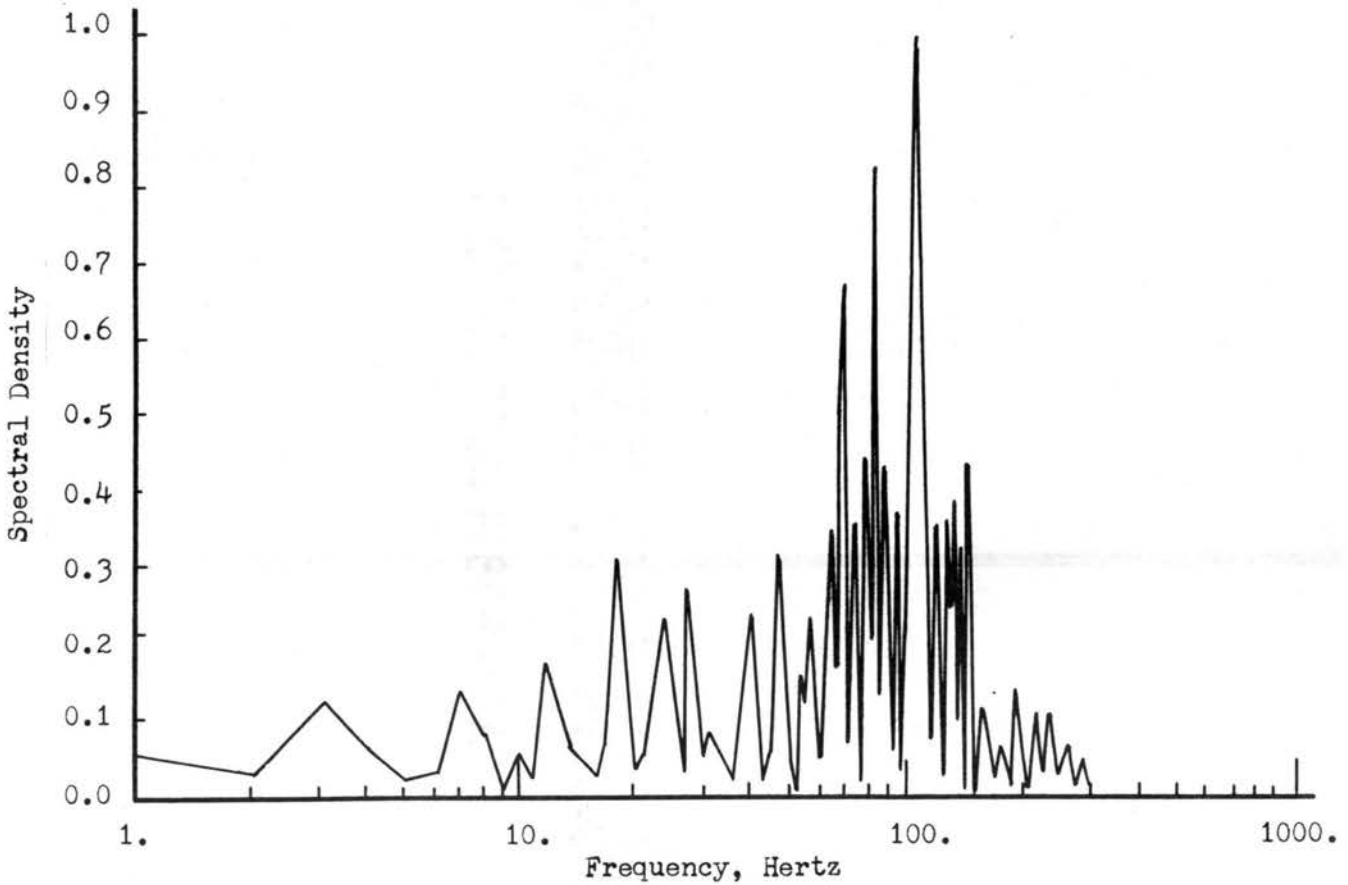

Figure 74. Spectral Density of Amplitude Fluctuation for Reynolds Number = 360. at Mach 7 Gas Condition

TABLE XXVII

ANALYSIS OF VARIANCE FOR DOMINANT WAVE FREQUENCY AT MACH 7 GAS CONDITION

Source	Sum of Squares	Degrees of Freedom	Mean Square	F-Ratio
Total	13169	10	1317	
Regression	10377	2	5188	14.9
Error	2792	8	349	

TABLE XXVIII

MODEL COEFFICIENT VALUES FOR DOMINANT WAVE FREQUENCY AT MACH 7 GAS CONDITION

Coefficient	Value and 80% Confidence Interval	Standard Error	F-Ratio	Significance Level
b_0	54.5 ± 11.5	8.3		
b_1	-6.7 ± 6.37	4.6	2.1	.81
b_2	25.3 ± 9.0	6.5	15.1	.995

this model, the dominant wave frequency is dependent on the Reynolds number at a much higher significance level than the thickness. The final form of the model for the Mach 7 gas condition is

$$f = 54.5 - 6.7\hat{h} + 25.3\hat{R}.$$

The value of the coefficient of the Reynolds number term is much larger than that of the thickness term and this indicates the stronger influence of the Reynolds number on the data. As before negative frequencies are meaningless and use of this equation is restricted to the range and combinations of the data for these experiments.

Figure 75 is a plot of the dominant frequency as a function of Reynolds number for thicknesses of 0.007 and 0.011 inches. Data measured in the experiments are also shown for these two thicknesses. The error bars indicate the 80 percent confidence intervals on the model predictions.

The high significance level in Table XXVIII for the Reynolds number term indicates the certainty of the dependence of the data on this parameter. The form of this dependence can be seen in Figure 75. For both thicknesses the dominant frequency increases with increasing Reynolds number. The effect of thickness, which is shown in Table XXVIII to be significant at a lower confidence level, is to cause a decrease in the wave frequency at constant Reynolds number with increasing thickness. The increase in frequency with Reynolds number is seen from a comparison of Figures 60 through 74 and is consistent with the model.

A comparison of the frequency data at similar liquid conditions reveals the effects of the external gas on the dominant wave frequency.

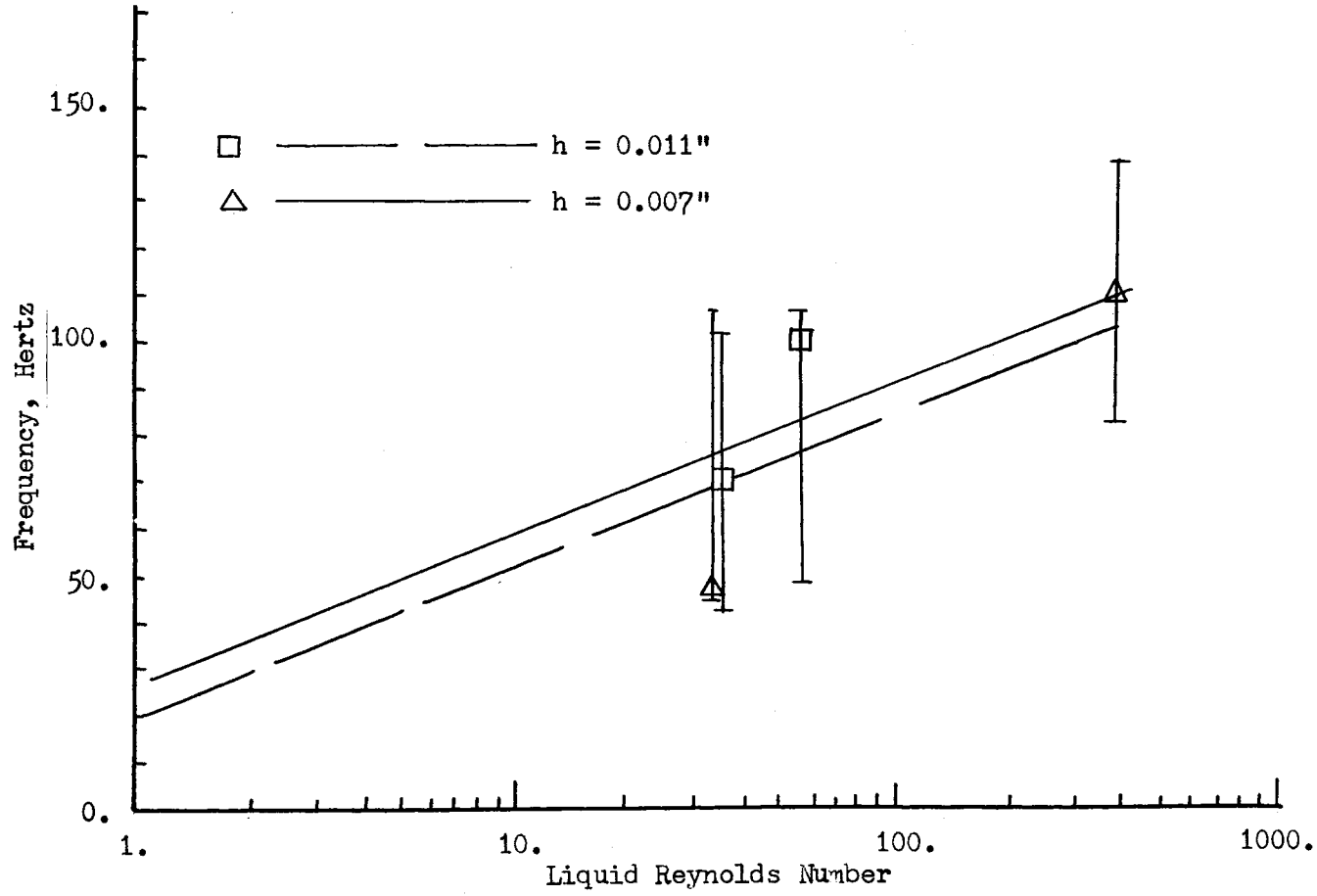

Figure 75. Variation of Dominant Wave Frequency for Constant Liquid Thicknesses at Mach 7 Gas Condition

Figure 76 is a plot of the dominant wave frequency as a function of Reynolds number at a constant thickness of 0.012 inches for each of the three gas conditions. At all Reynolds numbers the regression analyses predict that the highest dominant frequency is associated with the high shear Mach 5 gas condition. For the Mach 7 and the low shear Mach 5 condition the predicted values are very similar. At low Reynolds number conditions the models predict essentially equal frequencies while at higher Reynolds numbers the Mach 7 model predicts the higher values. However as shown on the figure, confidence intervals on each model include for all conditions the predictions on the other model so that one can not be certain based on these models that the data are different. As stated before all three models predict an increase with Reynolds number. Shown plotted on the figure are measured dominant frequencies for the low shear Mach 5 condition and the high shear Mach 5 condition for a liquid thickness of 0.012 inches. The data illustrate the ability of the response surface model to predict the correct trend of the data and also illustrate the scatter in the data.

Examination of the individual data suggests that the high shear Mach 5 condition results in higher dominant frequencies than do either of the other two gas conditions. For the four highest liquid Reynolds number conditions the dominant waves occur at frequencies of 170, 120, 170, and 120 Hertz for the high shear Mach 5 gas condition. For approximately the same Reynolds numbers and film thicknesses the dominant waves occur at frequencies of 75, 120, 100, and 105 Hertz for the low shear Mach 5 condition and at frequencies of 70, 125, 100, and 110 for the Mach 7 condition. This is consistent with the trend predicted by the curves shown in Figure 76.

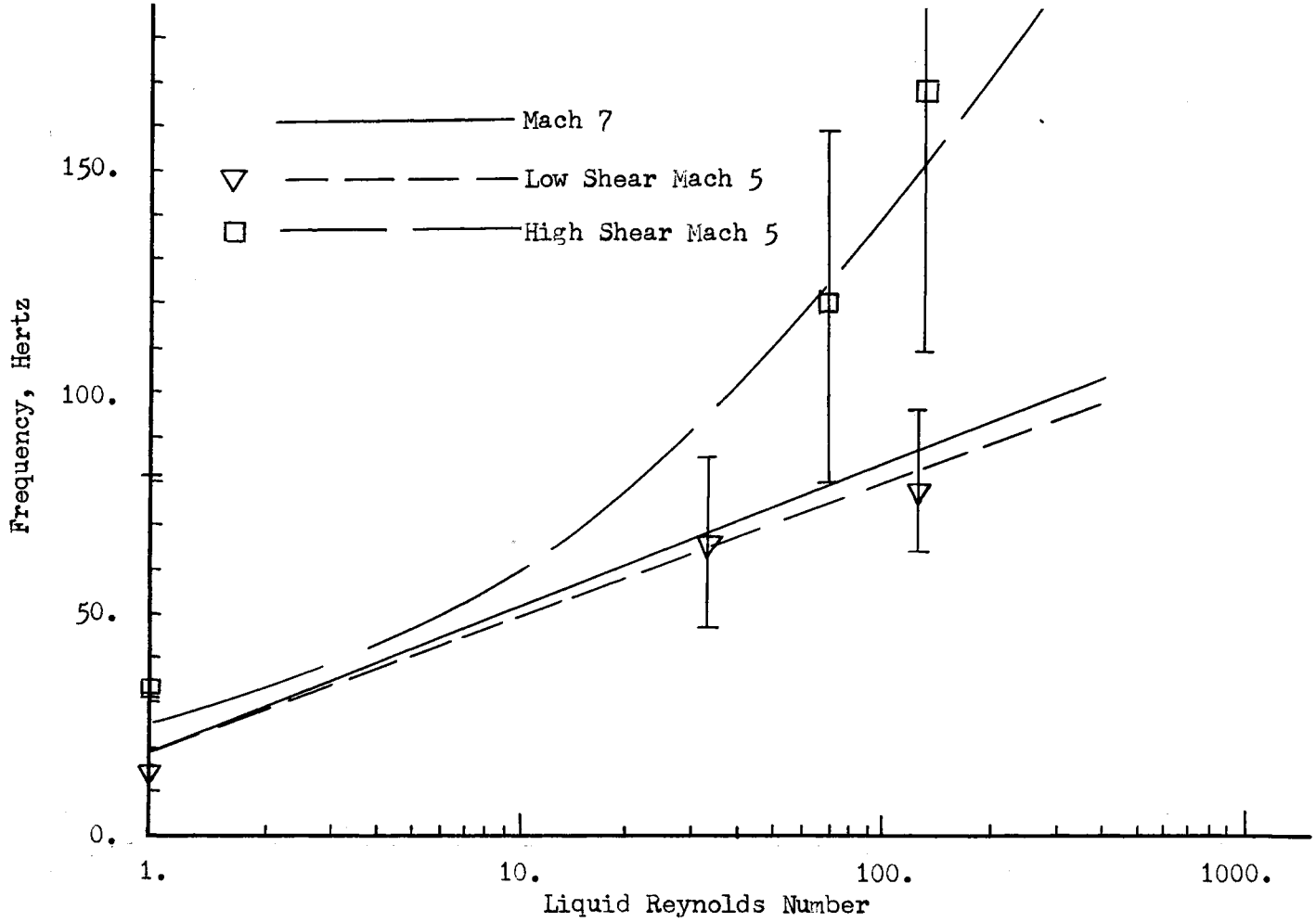

Figure 76. Comparison of Dominant Wave Frequency for Different Gas Conditions at Similar Liquid Conditions, h = 0.012 Inches

In summary the dominant frequency in the wave spectra for each experiment is affected by the liquid thickness and Reynolds number and also by the external gas condition. Based on the regression analyses the dependence on the liquid Reynolds number is accepted at a higher confidence level than the dependence on the thickness for all gas conditions. The dominant wave frequency increases with increasing Reynolds number at constant thickness. This higher frequency at higher Reynolds numbers is consistent with the increase of wave speed with Reynolds numbers reported in Chapter III.

The effects of the higher shear and pressure at the high shear Mach 5 condition are seen in the frequency data. At similar liquid conditions this gas condition generally produces a higher dominant frequency than either of the other two. The Mach 7 and low shear Mach 5 condition produce very similar wave frequencies at similar liquid conditions.

Analysis of Wave Frequency Band

The frequency spectra presented in the previous section all revealed the presence of a particular dominant wave frequency as well as a range of frequencies for each experiment. The variation of the dominant frequency with the liquid and gas conditions was discussed. In this section an interpretation of the range of frequencies is presented.

The presence of waves on the liquid interface which travel at different velocities was discussed in Chapter III. It was also pointed out that the waves were unequally spaced on the interface and varied in size. The conclusion from these observations was that the waves

represent a range of interface disturbances rather than one wave pattern with a single wave speed and wavelength.

The linear stability analyses for a viscous liquid film with an inviscid supersonic gas flow over the interface are discussed in Appendix A. In the analysis of Nachtsheim (1970) as well as that of Nayfeh and Saric (1970), the supersonic gas produces the mean shear in the liquid and supports the pressure perturbations on the interface. The solution of the linearized stability equations for this configuration produces the conditions for which the assumed infinitesimal disturbances on the interface amplify and thereby produce an unstable interface. The behavior of the disturbance growth rate for this model is illustrated in Figure 77. Unstable modes are predicted for all wavenumbers between the two cutoff values α_1 and α_2. Therefore the linear analyses predict a range of unstable wavenumbers rather than a single unstable mode. The unstable waves in this range possess different growth rates, different wave speeds, different wavenumbers (or wavelengths) and therefore different wave frequencies. The previous observation of the unequal wave velocities, uneven wavelengths, and different wave sizes is consistent with the prediction of a range of unstable waves.

For the low shear Mach 5 gas condition the frequency spectra are presented in Figures 30 through 44 in an earlier part of this chapter. Shown in Table XXIX are the maximum and minimum frequencies (upper and lower cutoffs) of the spectra, the dominant frequency and the calculated mean frequency. The calculated mean frequency is determined from the expression

$$f_m = \frac{U_w}{L_m}$$

where f_m is the mean frequency, U_w is the mean wave velocity, and L_m is the mean wavelength. The maximum and minimum frequencies are determined from the spectra data and are the values at each end of the spectra for which the normalized value of the spectral density is approximately 0.1 to 0.15. This value was selected in an attempt to prevent the inclusion of wave frequencies which are in reality 'noise' of the data system.

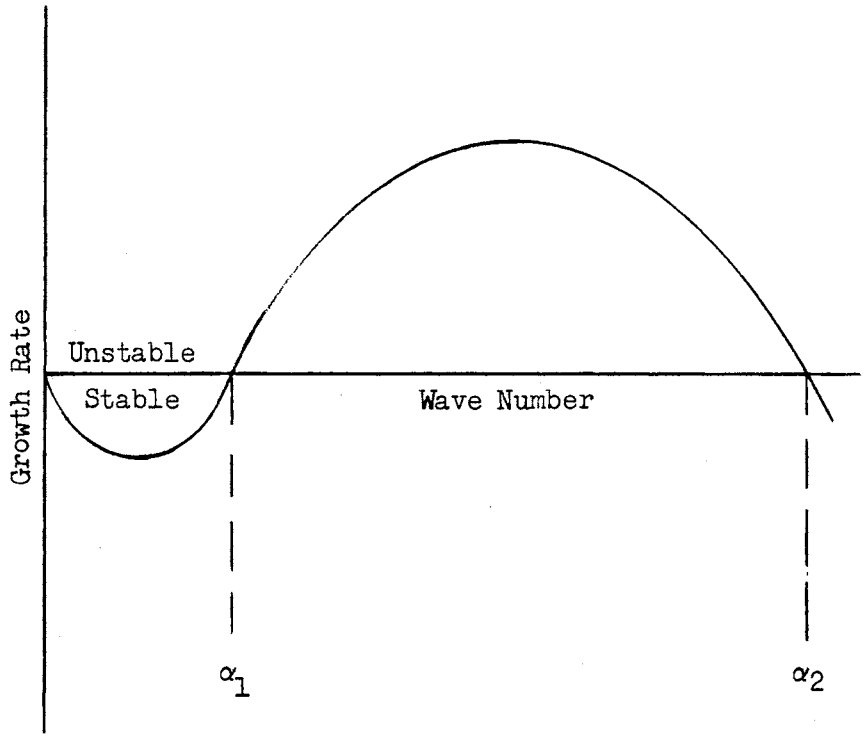

Figure 77. Growth Rate Versus Wave Number

TABLE XXIX

WAVE FREQUENCY BAND FOR LOW SHEAR
MACH 5 GAS CONDITION

Reynolds Number	Thickness, inches	Wave Frequency Band, Hertz		Dominant Frequency Hertz	Calculated Mean Frequency, Hertz
		Minimum	Maximum		
.22	.014		38	7*	30
.35			45	11*	42
.73	.01		80	4*	66
1.	.012		120	11	102
1.8	.006		75	7*	56
4.			170	4*	
23.	.006		190	65	174
32.	.012		210	70	190
40.	.009		250	80	182
54.	.010	18	180	50	172
56.	.016	18	170	75	150
110.	.012	13	225	75	154
255.		13	230	120	
310.		16	250	100	
360.	.006	15	220	105	

*It is not clear that the dominant frequencies at these conditions are not the results of variations in flow parameters or tunnel conditions. Hence, they are not included in dominant frequency regression analyses.

The very low frequency portion of the spectra are not considered to be as reliable as the higher frequencies. Therefore the minimum frequency value is not given for some of the experiments where the data are concentrated in the low frequency region. In others where the data produces higher frequency values and a lower cutoff can be identified well above 10 Hertz, any normalized values of the spectral density above the 0.1 to 0.15 value which exist below 10 Hertz are therefore neglected.

Comparison of the data in Table XXIX reveals several interesting features. The upper cutoff value of the frequency band increases with Reynolds number in the same way as does the dominant frequency. In all cases the calculated mean frequency lies below the upper cutoff frequency. Since the mean value is calculated using mean velocity and wavelength, this is to be expected. The fact that the mean value lies within the frequency band determined from the depth gauge for all experiments lends strong support to the credibility of the frequency band data. At the lower Reynolds number runs the lower cutoff frequencies are not given because of the previously stated uncertainties in these data.

Figure 78 presents a plot of the frequency band as a function of Reynolds number for these experiments. The regions of waves and of no waves are indicated and the lower cutoff line determined from the measured data is not extended to the low Reynolds number conditions. At the low Reynolds number conditions the lower cutoff frequencies calculated using the model of Nayfeh and Saric (1970) are shown. The details on this calculation and the interpretation of the data are presented in Chapter V. The frequencies correspond to the waves which

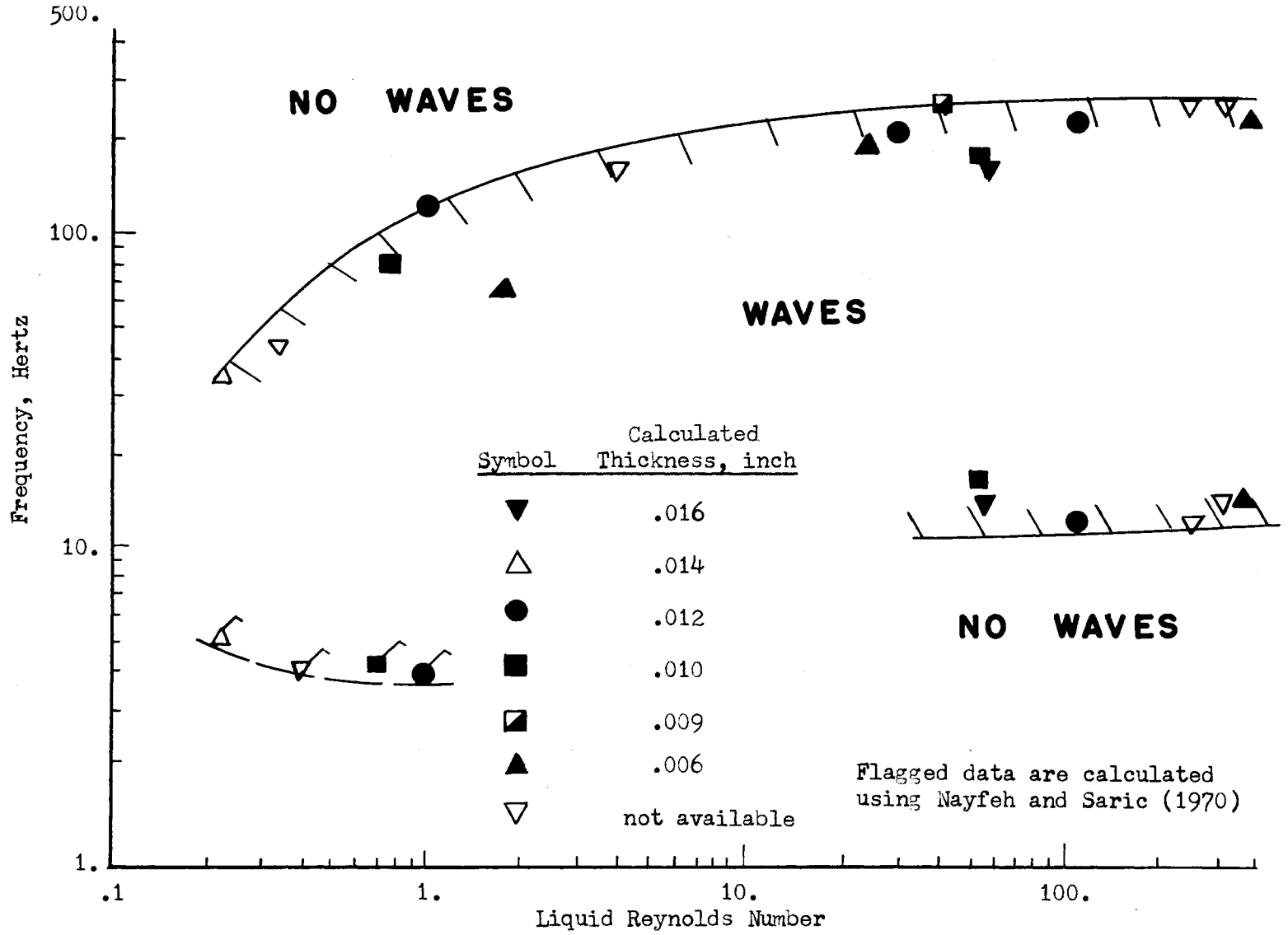

Figure 78. Frequency Band of Interface Waves at Low Shear Mach 5 Gas Condition

possess the lower wavenumber α_1 as shown in Figure 77. From the measured data the cutoff values on the frequency band increase with Reynolds number. The frequency band is consistent with the predictions of linear stability analyses and is also consistent with the observations of the interface waves reported in Chapter III.

For the high shear Mach 5 gas condition the frequency spectra are presented in Figures 46 through 58. Table XXX presents the maximum and minimum values of the frequency band, the dominant frequency, and the calculated mean frequency. Because of the severe limitation of the visual wave data from the photographs at this condition, only a limited number of mean frequency data are presented. For these limited data the calculated mean frequency is less than the maximum cutoff value and is therefore in satisfactory agreement with the gauge data. The upper cutoff value increases with Reynolds number as does the dominant frequency. For the higher Reynolds numbers the lower cutoff frequencies are presented and the frequency band is complete.

Figure 79 presents these data in the form of the frequency bands as a function of Reynolds number. As before the envelope is not complete due to the lack of measured lower cutoff frequency data at the low Reynolds number conditions. Similar to the data in Figure 78 the low Reynolds number lower cutoff data are calculated using the model of Nayfeh and Saric (1970) and are discussed in Chapter V. Regions where waves occur and do not occur are so marked. Similar to the low shear Mach 5 condition, these data are in agreement with the linear theory in that a range of waves with their associated properties are indicated.

The frequency spectra for the Mach 7 gas condition are presented in Figures 60 through 74. The data on the frequency band for this gas

TABLE XXX

WAVE FREQUENCY BAND FOR HIGH SHEAR
MACH 5 GAS CONDITION

Reynolds Number	Thickness, inches	Wave Frequency Band, Hertz		Dominant Frequency Hertz	Calculated Mean Frequency, Hertz
		Minimum	Maximum		
.33			130	1*	72
.53	.011		170	18	
.9			220	2*	
1.	.012		300	33	230
2.1			300	25	
21.	.004		400	17	
32.	.009	11	360	65	345
60.	.013	12	280	95	270
66.	.012		380	120	
110.	.012	10	320	170	
135.		15	280	120	
265.	.004	18	310	170	
360.	.006	14	350	120	

*It is not certain that the dominant frequencies at these conditions are not the results of variations in flow parameters or tunnel conditions. Hence, they are not included in dominant frequency regression analyses.

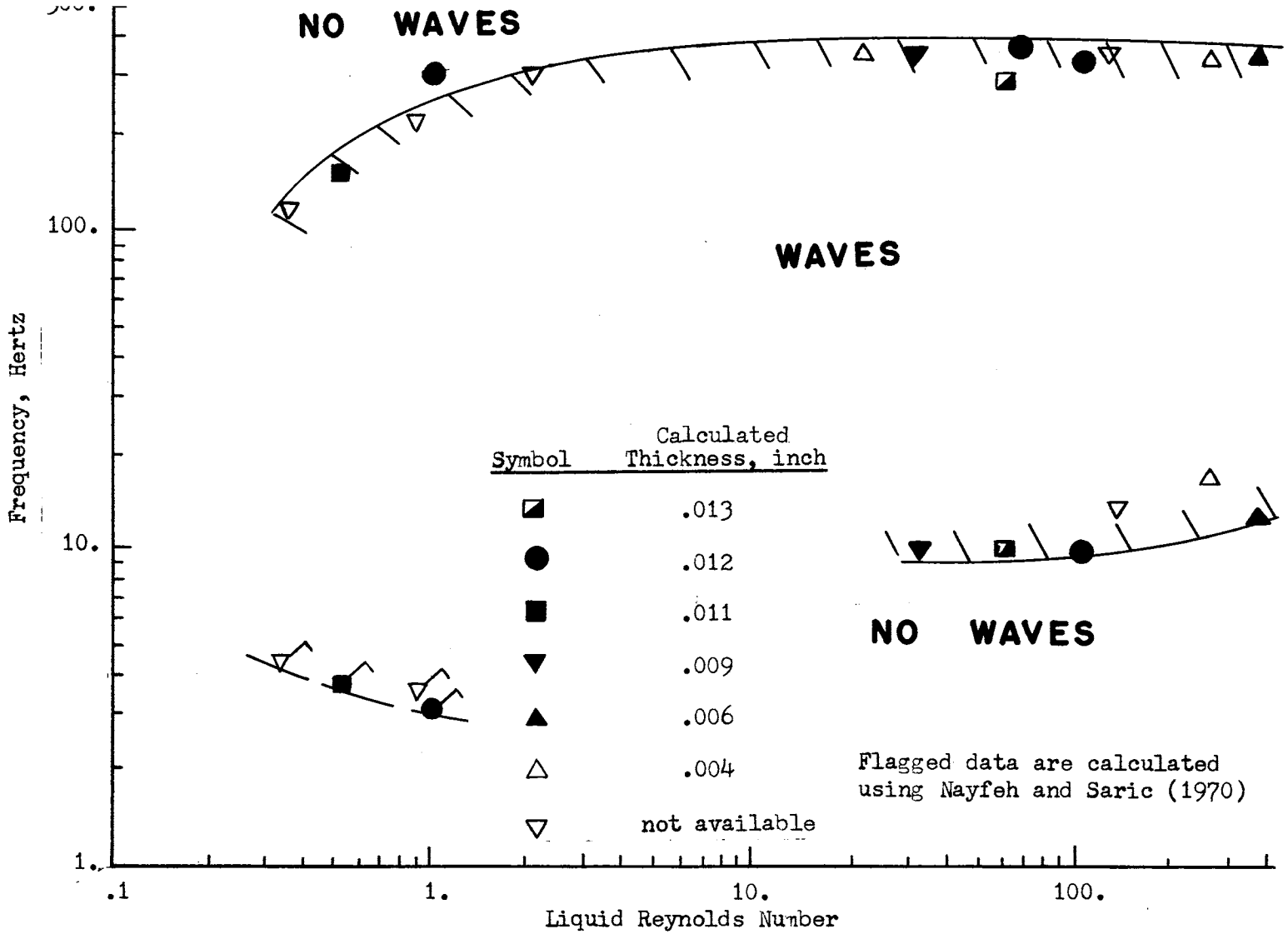

Figure 79. Frequency Band of Interface Waves at High Shear Mach 5 Gas Condition

condition are presented in Table XXXI and the variation of the data is similar to that for both of the previous gas conditions. The calculated mean frequency is for all cases less than the upper cutoff on the frequency band which increases with increasing Reynolds number. The calculated mean frequency agrees extremely well with the frequencies of the gauge output.

Figure 80 is a plot of these data as a function of the liquid Reynolds number. The general appearance of this curve is the same as that for the previous gas conditions. The regions of waves are marked and are partially enclosed by lines drawn through the cutoff values of the frequency band. Calculated low Reynolds number lower frequency cutoff data are also shown.

The data plotted on Figures 78, 79, and 80 may be compared at similar Reynolds numbers to evaluate the effects of the external gas conditions on the frequency bands generated. For the Mach 7 gas condition and the low shear Mach 5 condition, the curves compare very closely. It appears based on these data that the wave frequencies generated at the two conditions are similar. The curve for the high shear Mach 5 condition contains higher frequency waves at the same Reynolds numbers than either of the other two gas conditions. On that basis it is concluded that the high shear Mach 5 condition generates higher frequency waves and this conclusion is consistent with the conclusions in Chapter III of higher wave speed for the high shear Mach 5 condition.

In summary the Fourier analysis of the depth gauge output reveals a band of wave frequencies present on the interface at all gas-liquid conditions. This condition is predicted in linear stability analyses which predict a band of unstable waves. The frequency band shifts to

TABLE XXXI

WAVE FREQUENCY BAND FOR MACH 7 GAS CONDITION

Reynolds Number	Thickness, inches	Wave Frequency Band, Hertz		Dominant Frequency Hertz	Calculated Mean Frequency, Hertz
		Minimum	Maximum		
.22	.01		80	6*	26
.5	.014		80	19	40
.9			110	4*	82
1.2			100	22	78
1.4			55	3*	
3.8	.016		130	12	100
21.	.006		220	65	138
32.	.007	10	190	44	115
34.	.011	20	200	70	105
54.	.011	10	190	100	100
85.	.014	10	160	82	100
126.	.015	11	130	70	117
130.	.003	17	200	125	
260.	.006	18	210	100	
360.	.007	13	220	110	

*It is not certain that the dominant frequencies at these conditions are not the results of variations in flow parameters or tunnel conditions. Hence, they are not included in the dominant frequency regression analyses.

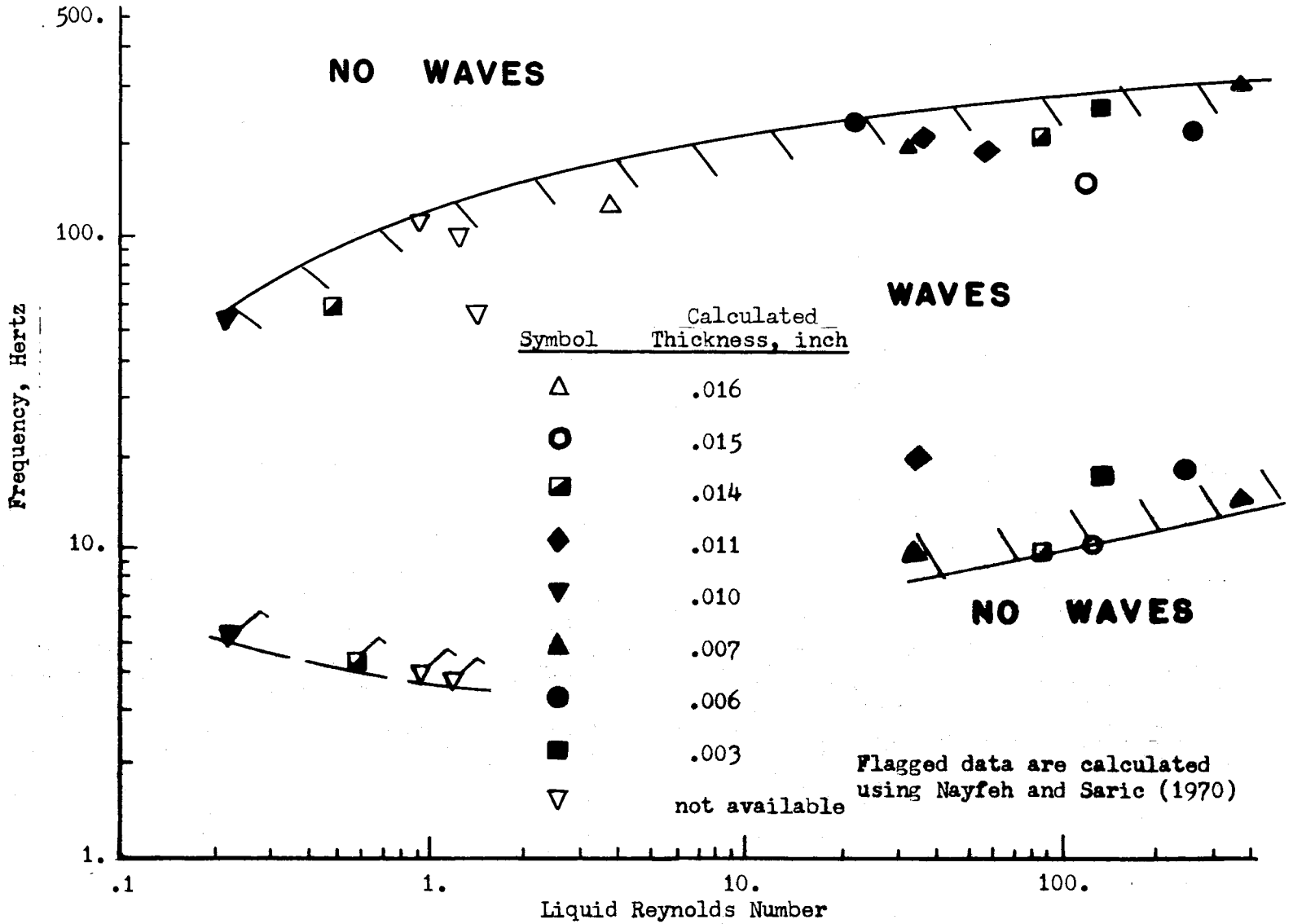

Figure 80. Frequency Band of Interface Waves at Mach 7 Gas Condition

higher frequencies with increasing Reynolds number at each of the three gas conditions. The mean frequency, calculated by dividing the mean wave speed by the mean wavelength, lies within the frequency band for every experiment in which the data were obtained. This agreement lends support to the applicability of the Fourier transform data. The effect of the higher shear Mach 5 condition is apparent from the data. The frequency band shifts to higher frequencies at the high shear condition than at either of the other two. The frequency bands are remarkably similar at equal Reynolds numbers for the low shear Mach 5 and the Mach 7 gas conditions.

CHAPTER V

COMPARISON WITH LINEARIZED THEORY AND OTHER EXPERIMENTS

The data reported in these experiments are taken from visible, finite amplitude waves. Consequently, one might anticipate that nonlinear effects of the disturbances are significant and that a linear analysis would not successfully predict and correlate these data. In the linear analyses the infinitesimal waves have an exponential growth rate and interaction of the periodic waves is neglected. For the experimental data neither of these conditions is satisfied. Consequently, the linear analyses are most appropriately utilized to predict the onset of unstable behavior together with wave speed and growth rate information for the very initial stages of wave formation. However if one assumes that the finite disturbances observed in the experiments have grown from initially infinitesimal waves, then one would expect to observe finite waves on the interface at those conditions for which linear waves are unstable. Therefore the experimental liquid-gas conditions may be compared with the predicted condition of instability calculated from an appropriate linear analysis.

Various linear analyses on the stability of liquid films are discussed in Appendix A and it is shown there that the specific boundary conditions chosen make the different analyses distinctive. The correlation and interpretation of the data from these experiments with any of the analyses must be done with a consideration of the particular

boundary conditions employed. For most of the experiments reported in this study, it is concluded that the waves observed on the liquid interface move faster than the liquid. The physical model of Nachtsheim (1970) as well as that of Nayfeh and Saric (1970) is applicable only to 'fast' waves and incorporates boundary conditions which most closely describe the actual experimental configuration. Both models include an inviscid external gas whose essential effects are to provide the mean shear flow in the liquid and to exert pressure perturbations on the interface which are in phase with the wave slope. The results of these analyses are that wavenumbers which lie between two cutoff values represent unstable waves as indicated by the sketch shown in Figure 77. The results presented by Nachtsheim are for fixed values of the Weber and Froude number whereas in these experiments neither of these parameters is constant. As a result, the analysis of Nayfeh and Saric, which incorporates the same boundary conditions but allows variation of the Weber and Froude numbers in the calculations, is used to provide some comparison for the data.

The solution of Nayfeh and Saric is a perturbation solution in powers of the dimensionless wavenumber α ($\alpha = 2\pi h/\lambda$) and includes as a boundary condition the supersonic pressure perturbation. The perturbation expansion for the stream function is carried to four terms. Because of the form of the results of the solution, the analysis is restricted to the region where the product of the wavenumber and the Reynolds number is less than one. Consequently only the lower cutoff wavenumber can be predicted by the analysis for the range of liquid Reynolds numbers in these experiments. The model predicts unstable behavior for wavenumbers in excess of a lower cutoff wavenumber given by

$$\alpha_1^2 = C_f(M^2 - 1)^{\frac{1}{2}}[\zeta_1 - (\zeta_1^2 + \zeta_2)^{\frac{1}{2}}]$$

where

$$\zeta_1 = \frac{15}{4}[WC_f(M^2 - 1)^{\frac{1}{2}} - \frac{49}{168}]$$

$$\zeta_2 = -\frac{15G}{2}$$

$$W = \frac{\sigma}{\rho U_1^2 h}$$

$$G = \frac{gh}{U_1^2}$$

$$C_f = \frac{\tau}{\rho_e U_e^2}$$

In these expressions τ is the mean gas shear stress which may be determined from Figure 92 of Appendix D, M is the gas Mach number at the outer edge of the boundary layer, and ρ_e and U_e are the gas density and velocity at the outer edge of the boundary layer. These last three parameters are calculated using the method described in Appendix D. The remaining liquid parameters are the liquid surface tension σ, the density ρ, the interface velocity U_1, and the thickness h.

For each of the three gas conditions the lower cutoff wavenumber, α_1, was calculated for low liquid Reynolds numbers. The results of these calculations are shown in Figure 81. The proper interpretation of the calculations is that points above the curves (i.e., higher wavenumber values) represent unstable behavior of the waves. Although the upper cutoff wavenumber is not predicted by this analysis, preliminary

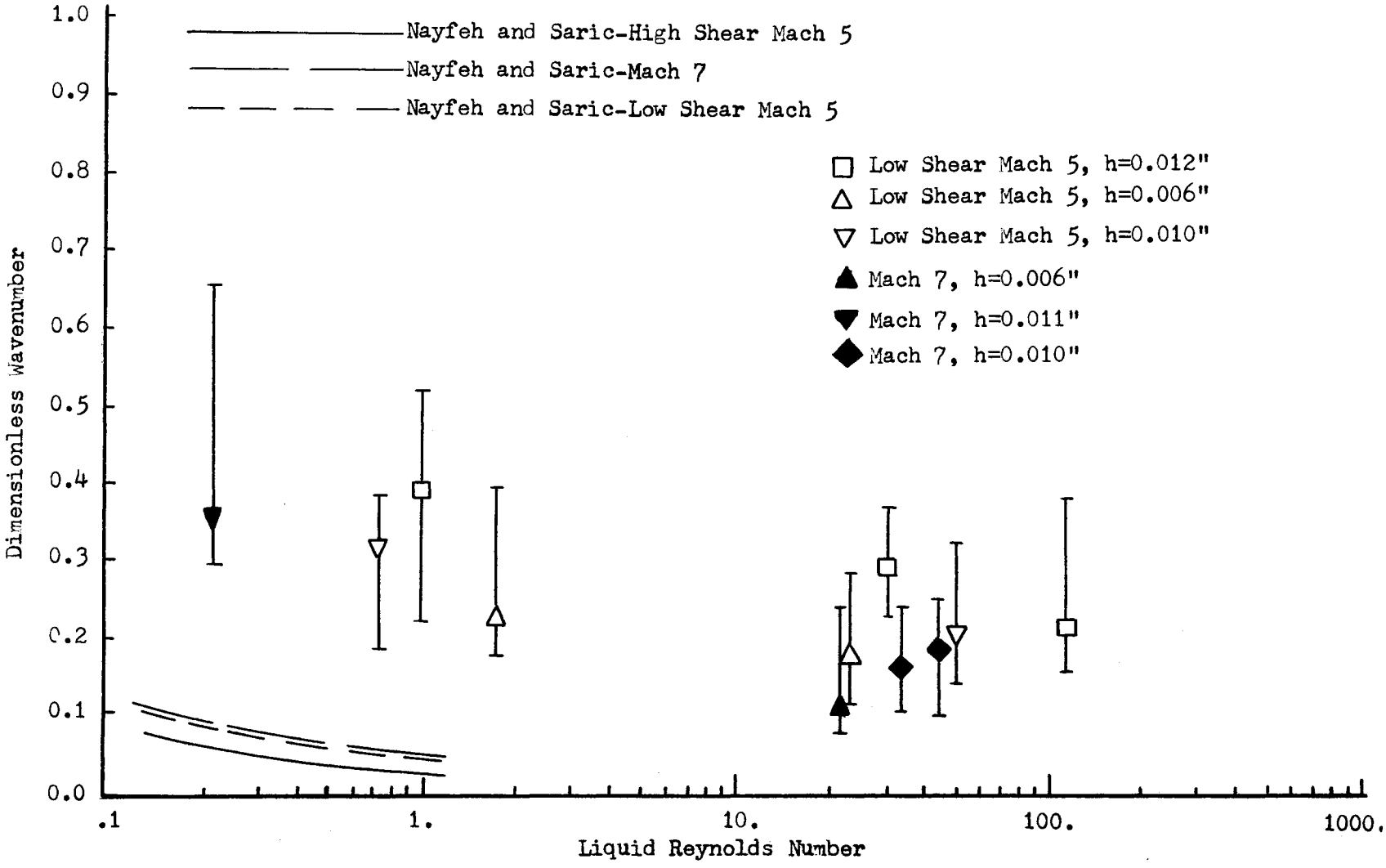

Figure 81. Dimensionless Wavenumber for Low Shear Mach 5 and Mach 7 Gas Conditions

calculations using a numerical solution of the full Orr-Sommerfeld equation have shown that the upper cutoff value is of order 1 and larger. Refinement of this computer analysis will permit a more definitive calculation in the future for the upper cutoff; however the calculations are sufficient to show that the predicted upper cutoff values are in excess of the data measured in these experiments.

Also shown in Figure 81 are the experimentally determined mean wavenumbers as a function of Reynolds number for selected thicknesses at the low shear Mach 5 condition and the Mach 7 condition. The movie coverage of the third gas condition was not of sufficient quality such that these data could be obtained. The bars shown on the measured data represent the variation of the wavelengths measured on the photographs and the uncertainty in the measured thickness. The mean wavelength as well as the maximum and minimum spacing of waves was measured on the photographs and this range in the wavelength data contributed to the ranges shown in the figure.

For both gas conditions the mean dimensionless wavenumber decreases as the Reynolds number increases at constant thickness. With the experimental scatter taken into account, the wavenumbers at the Mach 7 condition appear from these limited data to be smaller at equal Reynolds numbers and thicknesses. This conclusion reflects the larger wavelength values for the Mach 7 condition as discussed in Chapter III which, since they appear in the denominator, result in lower wavenumbers.

As discussed in Chapter III, the waves are not always uniformly spaced on the liquid interface. However, an examination of the photographs of the interfaces revealed that the scatter in the wavelength

data is not sufficiently large such that the associated wavenumbers are less than the calculated cutoff values.

Based on a comparison of these calculated and measured wavenumbers, it is concluded that the measured wavenumbers are in excess of the cutoff values calculated using the inviscid, supersonic gas model. Therefore the waves are observed on the interface at conditions for which the linearized stability model predicts unstable behavior. Moreover for a fixed gas condition the calculations show that the cutoff wavenumber decreases with increasing Reynolds number for constant thickness and this trend also exists for the measured data. While the agreement between the calculated and measured wavenumbers is considered acceptable, this is not a sufficient test of the stability model. One can only conclude that waves are seen at liquid-gas conditions for which this particular linear model predicts waves and that none of the data contradict the model. The irregularly spaced waves with finite amplitudes are sufficiently different from the assumed infinitesimal wave forms to preclude any stronger conclusion.

The wave speed data discussed in Chapter III show that the waves move at speeds which are dependent on both the film thickness and Reynolds number. For all the interface conditions the presence of waves which are traveling at velocities different from other nearby waves is noted. It is also shown that for the low and moderate Reynolds numbers the waves travel faster than the calculated interface velocity and that the shape of the wave and the mean wave speed are dependent upon the level of shear and pressure exerted by the gas on the interface. The waves are of finite amplitude, particularly for the low fluid viscosity, high Reynolds number conditions in which the amplitude

is estimated to be of the same order as the film thickness. Further, the waves interact with adjoining waves and in some cases two waves merge to form a single wave. Consequently, it is clear that the interface disturbances are not similar to the infinitesimal wave form assumed in the linear stability theory. Because of the fundamental differences in the assumed forms of the interface disturbances in the model and those which are observed in the experiments, any additional comparisons between calculated and observed characteristics of the waves are considered inappropriate.

In Tables IV and X the dimensionless wave speed data are shown for the low shear Mach 5 and the Mach 7 conditions. For several of the experiments at Reynolds numbers near 100 and above, the wave speed is calculated to be less than one, indicating that the wave is moving slower than the calculated interface velocity. To the author's knowledge, this is the first reported observation of waves at these Reynolds number values for which the dimensionless wave speed is calculated to be less than one.

Several explanations of this observation can be offered. First, there is the possibility that the wave speed is actually greater than one because of inaccuracies in the calculation of the interface velocity. The calculated interface velocity is the reference term in nondimensionalization. For these conditions the liquid thickness is a minimum for all of the experiments and the wave size and amplitude appear from the movies to be a maximum. Consequently, the interface velocity calculation which is made by assuming a linear velocity profile in the liquid may not be appropriate. No measurement of the interface velocity was made and the calculation is not correct if the

profile is not linear. The combined inaccuracy due to the finite waves and a nonlinear profile may result in a calculated interface velocity sufficiently in excess of the actual value to cause the calculated dimensionless wave speed to be less than one.

Second, it was shown by Craik (1966) that nonlinear effects of finite amplitude waves produce an effect on the wave speed. He performed a nonlinear analysis on the stability of a thin film with a subsonic gas flow over the interface and showed that finite amplitude effects can result in a dimensionless wave speed less than one. In particular his results indicated that the value would be between 0.5 and 1. This could be a major effect in these experiments because the wave amplitude, based on the wave appearance in the movies, is a maximum and since the films are thinnest, the finite wave effects are a maximum.

The third possible interpretation of these 'slow' waves is the possibility that they have grown from the type of waves discussed by Miles (1960). This type of linear instability is referred to as a Tollmein-Schlichting instability and according to Miles is only operative for dimensionless wave speeds less than one. Miles found that a necessary condition for instability is

$$R > 203$$

and

$$\frac{1}{W} + \frac{1}{\alpha^2 F} < \frac{1}{3}$$

where W and F are the liquid Weber and Froude numbers respectively. As mentioned previously the 'slow' waves are first observed in the

experiments at Reynolds numbers near 100 which is significantly lower than the first inequality determined by Miles. Also, the second inequality is satisfied for only about half of the slow wave cases. Consequently, the data are not in substantial agreement with the conditions stated by Miles as necessary for the existance of the Tollmein-Schlichting waves. An additional factor to be recognized in this interpretation is that Miles' results are based on a linear analysis and the observed waves are of finite amplitude.

The trends and interpretation of the data from these experiments may also be compared with the experiments of other investigators. For example experiments on the breakup of liquid sheets in a supersonic gas stream were reported by Sherman and Schetz (1970). Although the primary objectives of their experiments were different from those reported here, some wave observations were reported. The same type of non-periodic, finite wave structure as that reported here was observed. The precise thickness and Reynolds numbers were not stated; but measured wave speeds of 4.9, 6.1, and 8.2 feet per second were observed for carbon tetrachloride, 30% glycerol/water, and water respectively. The magnitude of these wave velocities is the same as that reported at the higher Reynolds numbers in the present experiments, and the waves described by Sherman and Schetz were three-dimensional.

The experiments reported by Craik (1966) are of some interest although they were conducted at atmospheric pressure and the external gas flow was subsonic. Craik observed for certain Reynolds numbers waves moving slower than the liquid interface velocity while for higher Reynolds number, waves traveling faster than the liquid were observed. For Reynolds numbers based on the interface velocity and film thickness

of approximately 50 and above, the waves were three-dimensional in character. The dimensionless wave speed varied from 1.75 to 3.84 for the 'fast' waves which occurred at liquid Reynolds number from approximately 30 to 50. The dimensionless wave speeds were near 0.75 for the 'slow' waves which occurred at Reynolds numbers below 30. The fast waves were straight-crested and apparently sinusoidal whereas the slow waves were non-periodic. Thus Craik found for the conditions of his experiments slow waves present at Reynolds numbers as low as 2 with a film thickness of approximately .005 inches. In contrast, for the very low Reynolds number conditions of the experiments reported here, the dimensionless wave speeds were a maximum and decreased with increasing Reynolds number. Hence, one can conclude that the supersonic gas flow plays a significant and unique role in the characteristics of the liquid interface. In particular, a source of energy in the supersonic gas flow is the pressure perturbation which is in phase with the wave slope and thus creates a supersonic wave drag.

Linearized stability analyses predict unstable behavior of the liquid interface for a range of wavenumbers as is illustrated in Figure 77. For that particular sketch, the model predicts instability for all waves whose wavenumbers lie between the two cutoff values α_1 and α_2. Each of the waves between these two values has a distinct wavelength and wave speed value. Consequently, for each constant external gas and liquid condition which produces unstable behavior, the model predicts a band of wave frequencies which are unstable.

In Chapter IV the wave frequencies calculated from the Fourier analysis of the depth gauge output are presented. For each of the experiments the waves on the interface are represented by a band of

frequencies with an upper and lower cutoff value. However, a measured lower cutoff value is not defined for some of the lower Reynolds number conditions due to difficulties in reliably measuring very low frequency (i.e., 1 to 10 Hertz) data.

As discussed earlier in this chapter the model of Nayfeh and Saric (1970) may be utilized to predict the lower cutoff wavenumber for Reynolds numbers below approximately one. The equations for the wavenumber α, the growth rate αc_i, and the dimensionless propagation velocity c_r, are solved using numerical techniques. For the condition where the growth rate is zero, the lower cutoff wavenumber and propagation velocity are determined from the numerical solutions. The lower cutoff frequency corresponding to this cutoff wavenumber is therefore

$$n = \frac{U_w}{\lambda}$$

where U_w and λ are the dimensional wave speed and wavelength respectively and are calculated from the wavenumber and dimensionless wave speed by the relationships

$$U_w = c_r U_1 \qquad\qquad \lambda = \frac{2\pi h}{\alpha} \quad .$$

At each of the gas conditions the calculated lower cutoff frequencies for Reynolds numbers of one and below are shown in Figures 78, 79, and 80 in Chapter IV. The calculated values for all gas conditions are in the range from 3 to 6 Hertz. The calculated data are of the same order of magnitude as the measured data at higher Reynolds numbers and are slightly lower than the higher Reynolds number data. Consequently, one can conclude that the model of Nayfeh and Saric

predicts lower cutoff frequencies consistent with those measured in these experiments at slightly higher Reynolds numbers.

The presence of a range of frequencies of the interface waves is consistent with the type of unstable behavior predicted by the analyses. For the higher Reynolds numbers the upper cutoff frequency shifts to higher values and reflects the increased wave speed. This is consistent with the trend predicted by the linear analyses and is the expected result. For the more severe Mach 5 gas condition the measured upper cutoff frequency occurs at higher values for similar liquid conditions. This result is also expected and it is likewise consistent with the analyses since the higher pressure represents an increased energy input in the pressure perturbation boundary condition. Therefore, the wave frequency results agree with the linear analysis by first predicting a range of unstable waves and second by illustrating the relative effects on the wave frequency band of changing the liquid and the gas conditions.

In experiments with a subsonic external gas at atmospheric pressure flowing over a liquid film approximately 4 inches thick, Plate et al. measured the energy density spectrum of the interface waves. The peak energy density was found to exist at frequencies from 7 to 11 Hertz. The frequency of the spectral peak also was shown to increase as the external wind speed was increased. In contrast to the somewhat diffuse spectrum observed for all the conditions in these supersonic experiments, the distribution reported by Plate et al. showed a very distinct peak with no frequencies above approximately 20 Hertz. Consequently, consistent with the wave speeds reported by Craik as being lower than those for the supersonic gas case, the frequency for the

spectral density peak is also generally lower for the subsonic external gas. The liquid thicknesses in the experiments of Plate et al. are typically two orders of magnitude greater than those reported here. Hence, one can conclude that the characteristics of the waves generated on the interface are dependent on the condition of the external gas and perhaps the liquid thickness. Further one can conclude that supersonic external gas flow over a very thin liquid film results in a more agitated state of the interface than does low velocity subsonic gas flow over a relatively thick film.

CHAPTER VI

SUMMARY, CONCLUSIONS, AND RECOMMENDATIONS

Summary

This research was primarily an experimental study of the waves on a liquid interface adjacent to a supersonic gas flow. The results are related to the protection of an object from the severe heating associated with high speed entry into the earth's atmosphere. This protection is provided by a liquid sheath over the body and the technique is called transpiration cooling. The wave characteristics were examined on a blunt-nose, zero-degree wedge in a hypersonic wind tunnel. The nose tip of the model was porous with liquid expelled through the tip and spread back over the model by the gas flow. The objectives of this program were: (1) to characterize the response of a liquid film interface interacting with a supersonic gas flow and (2) to evaluate the dependence of interface wave properties on the liquid thickness and Reynolds number and on the gas shear stress and Mach number.

The experiments were conducted in the eighteen inch hypersonic wind tunnel at Sandia Laboratories in Albuquerque, New Mexico. Two free stream Mach numbers, 5 and 7.3, were utilized. Two stagnation pressures were employed at the Mach 5 condition resulting in a low shear and a high shear level and producing a total of three gas test conditions. As stated the test model was a blunt, zero-degree wedge and sides possessing sharp leading edges were attached to the model.

The model was six inches wide, twelve inches long and was equipped with a one inch diameter cylindrical nose tip. A 75 degree arc of this cylinder was made of porous stainless steel. The liquid was forced out the porous nose tip by a high pressure expulsion system and was swept back over the model by the shear stress exerted by the supersonic gas flow.

Glycerin-water mixtures ranging from 100 percent water to 100 percent glycerin were utilized and the resulting variation of viscosity in addition to control of the flow rate permitted an independent variation of the liquid Reynolds number and the liquid thickness. The liquid film thickness was varied from 0.003 inches to 0.016 inches while the Reynolds number was varied from 0.22 to approximately 360. The liquid temperature was measured during each run by thermocouples embedded in thin copper discs which were mounted flush with the model surface and insulated from the model by small teflon rings.

The data measured in the experiments were the mean wave speed, mean wavelength and the frequency spectra of the waves. The interface response was recorded with a 300 frame-per-second 35 millimeter camera as well as a 16 millimeter camera operating at 400 frames per second on selected tests. The wave speed and wavelength data were taken from the 35 mm movie film. A liquid depth gauge, consisting of two 0.010 inch thick Kovar plates separated by 0.002 inch of quartz glass, was mounted into the model such that an edge of the plates and glass was flush with the model surface. This gauge provided an indication of the mean liquid depth in addition to the transient wave profile at the gauge location. The depth gauge signal was recorded on an FM tape recorder and the transient portion of the signal was Fourier analyzed to determine the frequency spectrum of the waves.

No smooth liquid interface was observed for any test condition. At the lowest Reynolds numbers relatively small three-dimensional horseshoe type waves were observed. As the Reynolds number was increased, the waves became larger but generally retained their three-dimensional appearance. The amplitude of the high Reynolds number waves appeared to be larger than that of the low Reynolds number waves. At the highest Reynolds number the interface appearance was one of intense agitation, particularly for the high shear Mach 5 condition, and the wave speed data were difficult and in some cases impossible to obtain.

For each gas condition the measured dimensional mean wave speed data were fit to a response surface model using a regression analysis. For the low shear Mach 5 condition the analysis with a quadratic model confirmed that the mean wave speed depends on both the liquid Reynolds number and thickness. Generally the Reynolds number dependence is found to be significant at a higher confidence level and the mean wave speed increases with Reynolds number. At the Mach 7 condition the mean wave speed data were fit to the same response surface model and the results indicate that the mean wave speed depends on both the film thickness and Reynolds number. The mean wave speed at this gas condition also increases with increasing Reynolds number. Because of the limited quantity of data at high shear Mach 5 condition the mean wave speed data were fit to a linear response surface model rather than a quadratic model. The analysis showed that the wave speed is dependent on both the Reynolds number and the thickness and that the wave speed increases with Reynolds number. A comparison of the wave speeds at similar liquid conditions for the low shear Mach 5 and the Mach 7 gas

conditions shows that the mean wave speeds at both conditions are approximately equal and the data are not conclusive in determining which of the two gas conditions produces a higher mean wave speed. Calculations indicate the shear stress for the low shear Mach 5 condition and that for the Mach 7 condition are approximately equal with both lower than the high shear Mach 5 condition. The wave speeds at selected liquid conditions for the high shear Mach 5 condition are faster than those at similar liquid conditions at the other gas conditions.

The dimensionless mean wave speed data, formed by dividing the dimensional mean wave speed by twice the mass average liquid velocity, were fit to response surface models for all three gas conditions. In all cases the data depend on both the liquid Reynolds number and thickness. The dimensionless wave speed for all three gas conditions decreases with increasing Reynolds number and reflects the higher liquid velocity at higher Reynolds numbers. The mean wavelength data for both the low shear Mach 5 and the Mach 7 condition were also found to be a function of the liquid parameters. The wavelength increases with Reynolds number for both conditions and at similar liquid conditions the mean wavelength at the Mach 7 condition is larger than that at the low shear Mach 5 condition.

The Fourier analysis of the transient depth gauge data revealed several interesting results. Based on regression analysis using the quadratic model, the dominant wave frequency increases with increasing Reynolds number at each gas condition. In addition a band of frequencies was observed at all test conditions and the cutoff frequencies which define this band also increase with increasing Reynolds number. Further, the high shear Mach 5 condition in general results in the

dominant wave frequency being located at higher values for comparable liquid conditions than the other two gas conditions. The band of wave frequencies is consistent with linear analyses which predict a range of unstable waves.

Some of the experimental data were compared with the results of a linear stability analysis. The particular model used for the analysis was an inviscid supersonic gas flowing over a viscous, thin, liquid film with the waves resulting in a perturbation in the gas pressure at the interface. The measured mean wavelength data are for the low shear Mach 5 and the Mach 7 conditions clearly in excess of the lower cutoff wavenumber value calculated from the analysis. Since the theory predicts instability for wavenumbers above this value, it is concluded that the waves are observed at wavenumbers which according to the model are unstable.

Conclusions

The objectives of this research were to characterize the interface response of a liquid film interacting with a supersonic gas flow and to examine the dependence of the wave characteristics on the liquid and gas parameters. However, to accomplish these objectives, it was necessary to provide some development on the model and data acquisition system. Consequently, the conclusions regarding these are presented first and are followed by the conclusions regarding the wave data.

Model and Data Acquisition System

1. The model and flow expulsion system provide a satisfactory means with which to study the interface stability characteristics of a

liquid film in a supersonic gas flow. The data obtained during these experiments demonstrate that the model coverage is satisfactory and that the liquid flow is sufficiently uniform so that the interface waves have no discernable mean motion other than directly along the plate. The porous nose material provides a smooth uniform creeping liquid flow over the tip and the demonstrated range of flow rate and liquid viscosity provide a wide range of Reynolds number conditions.

2. The acquisition of data by a 35 millimeter camera is satisfactory and the movie film provides clear details of the wave shape, speed, and general interface response.

3. The capacitance depth gauge offers a means of obtaining information on the frequency spectra of the waves on the interface. The data from these experiments demonstrate the ability of the gauge to sense the instantaneous height of the liquid as a function of time. The technique also offers possibilities for accurately measuring the mean film thickness. However, the gauge is sensitive to temperature variations, and further development of the gauge is necessary to improve the accuracy of this measurement. This sensitivity to temperature resulted in variations estimated at $\pm$ 25 percent in the mean liquid thickness measurements for these experiments.

Interface Characteristics

4. For the particular liquid-gas conditions of these experiments, a smooth interface does not exist. Finite amplitude waves are formed at all liquid thickness-Reynolds number conditions for the three supersonic gas conditions. One can conclude that stabilizing effects of the liquid such as surface tension, viscous dissipation, and the gravity

force are not sufficient to prevent infinitesimal waves from rapidly growing to a finite amplitude condition.

5. At liquid Reynolds numbers (based on twice the mass average velocity and the mean thickness) near one and below, the disturbances on the interface are three-dimensional, horseshoe-shaped waves. These waves, as measured by their lateral span and the length of the trailing parts of the waves, are relatively small. For the high Reynolds number values from 100 to 360 the three-dimensional waves are irregular and the interface in general appears highly agitated. Compared to the low Reynolds number conditions, these waves are much larger. Therefore, an increase in the Reynolds number results in an increase in the amplitude and size of the finite amplitude waves which appear from a study of the photographic data to be neutrally stable.

6. The waves are unevenly spaced on the interface and do not possess a single propagation speed. One concludes therefore that the data represent a range of finite amplitude waves and are therefore consistent with the results of linear stability analyses which predict a range of unstable waves.

7. The wave frequency spectra show a dominant wave frequency within a band of frequencies. Consequently, it is concluded, consistent with the previous conclusion of unevenly spaced waves with unequal propagation velocities, that the waves are not regularly spaced on the interface.

8. The dominant wave frequency occurs at increasingly higher values as the Reynolds number increases at constant thickness for each of the three gas conditions. The upper cutoff frequency for the band of waves also occurs at higher values. Therefore, the higher Reynolds

number results in higher wave frequencies on the interface and since the mean wavelength increases with Reynolds number, the increase in frequency is caused by the increase in wave speed at the higher Reynolds numbers.

9. The mean wave speed depends on both the liquid thickness and Reynolds number for all gas conditions. In all cases the dimensional wave speed increases with increasing Reynolds number at constant thickness while the dimensionless wave speed decreases with increasing Reynolds number. Therefore one concludes that the decrease in dimensionless wave speed results from the interface velocity increasing faster with increasing Reynolds number than does the measured wave speed.

10. The interface wave characteristics, including the wave speed, wavelength, and wave frequency, are dependent on the magnitude of the shear stress and pressure exerted by the gas on the liquid. For constant liquid Reynolds number and thickness, the wave speed and wave frequencies increase with higher gas shear and pressure while the wavelength decreases. Therefore one concludes that the gas shear stress and pressure are significant parameters in determining the interface response.

11. The low shear Mach 5 gas condition and the Mach 7 gas condition resulted in similar shear and pressure levels on the liquid with the free stream Mach numbers different. The wave data on the characteristics are inconclusive in determining which of the two gas conditions consistently produces higher wave speed and frequencies. A calculation of the gas boundary layer properties reveals that the gas Mach numbers at the outer edge of the boundary layer are equal due to

the blunt body effects of the model. Consequently, the effects of the gas Mach number must be evaluated by additional experiments.

12. The observed experimental wavenumbers are found to be in excess of the cutoff wavenumbers calculated using the inviscid supersonic gas model of Nayfeh and Saric (1970). Since the model predicts instability for wavenumbers above the cutoff value, the data therefore agree with the predictions of unstable behavior for this particular model.

13. The calculated band of wave frequencies is conceptually consistent with the results of linear stability analyses which predict a range of unstable wave behavior. The high shear Mach 5 condition results in higher upper cutoff values for the frequency band than either of the other gas conditions. This trend is also consistent with the linear analyses which incorporate the higher pressure at the high shear condition as a boundary condition.

Recommendations

Based on the data, observations, and conclusions that have resulted from the experiments herein, several recommendations are made which can provide additional understanding of the interactions between a liquid film and a supersonic gas flow. As discussed previously, the basic concept of using this type of model to study the interface behavior has been demonstrated. However, there are certain features which can be modified.

The uniform model coverage by the liquid and the lack of any mean lateral wave motion is evidence that if shock waves existed across the model, they did not produce significant adverse pressure gradients. However, schlieren photographs and pressure measurements on the model

would provide unquestionable evidence of the absence or presence of shocks originating from the model side walls. In addition, the pressure distribution is an input to the boundary layer calculations and any improvement in the pressure distribution will improve the accuracy of this calculation. Therefore it is recommended that schlieren photographs and static pressure measurements on the model be made.

The depth gauge is a satisfactory means of measuring the frequency of the waves on the interface but several improvements in the gauge can be made. Development of a means of compensating the temperature variation of the gauge is recommended. One possibility for this is a small thermocouple mounted directly into the gauge elements and is coupled with a temperature compensation bridge circuit.

With further development of the depth gauge, it is recommended that experiments be conducted with two or more depth gauges installed in the model. This would require that a capacitance bridge circuit be available for each gauge. Data on the growth of the disturbances provide positive conclusions regarding stable or unstable behavior of the interface. With the temperature compensation and a calibration technique such as that used in these experiments, two gauges would also provide data on the mean liquid depth as a function of the location on the model. Gauge calibration would also premit a more meaningful normalizing of the frequency spectra data.

The data taken in these experiments represent the liquid response for a limited range of gas Mach number and shear stress. It is recommended that additional experiments be performed for a wider range of these parameters. In particular, gas conditions which produce different

Mach numbers at the edge of the gas boundary layers are recommended to evaluate the effect of the gas Mach number on the interface waves.

Experiments at gas conditions which produce a turbulent boundary layer over the entire model, except of course in the nose tip region, are recommended. Additional experiments in which the gas boundary layer undergoes a transition from a laminar to turbulent flow on the model are recommended. These experiments would provide direct comparisons of how the state of the boundary layer affects the interface response.

A final recommendation is made regarding performing this type of experiments with a different model design. As a part of the development of the model configuration used in the experiments reported herein, experiments were performed at the gas conditions described in Table I using a sphere cone model. The nose tip of the model was made of porous stainless steel and the liquid was swept back over the 5-degree half-angle cone by the gas shear. The model was unsatisfactory for these gas conditions because the gravity force normal to the model axis caused an uneven film thickness around the model. For the higher viscosity fluids the liquid did not cover the top of the cone at the model base. However, for higher gas shear conditions it is anticipated that the model coverage will be more uniform. Consequently, it is recommended that experiments using a cone model be performed at higher shear gas conditions for both laminar and turbulent gas boundary layers.

A SELECTED BIBLIOGRAPHY

Benjamin, T. Brooke. "Shearing Flow Over a Wavy Boundary." J. Fluid Mech., Vol. 6 (1959), 161-205.

Chandrasekhar, S. Hydrodynamic and Hydromagnetic Stability, Oxford: Oxford University Press, 1961.

Chapman, Dean and H. K. Larson. "The Lunar Origin of Tektites," NASA TN D 1556, 1963.

Chang, I-Dee and Paul E. Russell. "Stability of a Liquid Layer Adjacent to a High-Speed Gas Stream." Phys. Fluids, Vol. 8 (1965), 1018-26.

Cohen, Leonard S. and Thomas J. Hanratty. "Generation of Waves in the Concurrent Flow of Air and a Liquid." A. I. Ch. E. Jour., Vol. 11 (1965), 138-44.

Craik, Alex D. D. "Wind-Generated Waves in Thin Liquid Films." J. Fluid Mech., Vol 26 (1966), 369-92.

Eaton, R. R. "Numerical and Experimental Surface Pressure Distributions and Shock Shapes on 15-Degree Cones at Angles of Attack." Sandia Laboratories Report SC-DR-69-259, (1969).

Jeffreys, H. "On the Formation of Water Waves by Wind." Proc. Royal Soc., Vol. 107 (1925), 189.

Kelvin, Lord. "Hydrokinetic Solutions and Observations." Mathematical and Physical Papers, iv, Hydrodynamics and General Dynamics, Cambridge, (1910), 69-85.

Kline, S. J. and F. A. McClintock. "Describing Uncertainties in Single-Sample Experiments." Mech. Engr., (1953), 3-8.

Kendall, Robert M. and Eugene P. Bartlett. "Nonsimilar Solutions of a Multicomponent Laminar Boundary Layer by an Integral-Matrix Method." AIAA Jour., Vol. 6 (1968), 1089-97.

Lin, C. C. The Theory of Hydrodynamic Stability, Cambridge: Cambridge Univerisity Press, 1967.

Miles, John W. "The Hydrodynamic Stability of a Thin Film of Liquid in Uniform Shearing Motion." J. Fluid Mech., Vol 8 (1960), 593-610.

Miles, John W. "On the Generation of Surface Waves by Shear Flows." J. Fluid Mech., Vol. 13 (1962),433-48.

Moretti, G. and G. Bleich. "Three-Dimensional Flow About Blunt Bodies." AIAA Jour., Vol. 9 (1967),1557-62.

Nachtsheim, Phillip R. "Stability of Crosshatched Wave Patterns in Thin Liquid Films Adjacent to Supersonic Streams." (Accepted by Phys. Fluids, 1970).

Nayfeh, Ali Hasan and William S. Saric. "Stability of a Liquid Film." (Submitted to AIAA Jour., 1970)

Plate, E. J., D. C. Chang, and G. M. Hidy. "Experiments on the Generation of Small Water Waves by Wind." J. Fluid Mech., Vol. 35 (1969), 625-56.

Rakich, John V. "Calculation of Hypersonic Flow Over Bodies of Revolution at Small Angles of Attack." AIAA Jour., Vol. 3 (1964).

Reynolds, W. C. "Hydrodynamic Stability of the Liquid Layer on a Small Object in High Altitude Reentry." Sandia Laboratories Report SC-CR-67-2636, (1967).

Rogovaya, I. A., V. M. Olevskii, and N. G. Runova. "Measurement of the Thickness and Profile of Liquid Films." Izv. Akad. Nauk., SSSR, Pribory i Teknika Eksperimenta, No. 1 (1966), 183-85.

Sherman, Allan and Joseph Schetz. "Breakup of Liquid Sheets and Jets in a Supersonic Gas Stream." AIAA Paper No. 70-89, (Presented at AIAA 8th Aerospace Sciences Meeting), (1970).

Snedecor, G. W. and W. G. Cochran. Statistical Methods, 6th ed. Ames: Iowa State University Press, 1968.

Squire, H. B. "On the Stability of the Three-Dimensional Disturbances of Viscous Flow Between Parallel Walls." Proc. Roy. Soc., Vol. 142 (1933), 621-28.

APPENDIX A

FORMULATION OF PROBLEM AND REVIEW OF LITERATURE

In formulating an experimental program to study the interface behavior of a liquid film, it is useful to consider the manner in which stability theories have been formulated and to examine the particular boundary conditions used to determine their applicability in interpreting the resulting experimental data. The physical problem of interest is one in which a liquid film flows over a solid surface and the interface of the film interacts with a gas stream flowing over the liquid.

Derivation of Governing Equations

In principle the complete linear stability problem for the two fluid system, which can be expressed as two fourth-order differential equations for a two-dimensional disturbance, must be formulated. The four boundary conditions and four matching conditions which are required to complete the problem are as follows: (a) both velocity components must be zero in each fluid at the walls which bound the fluids or they must be finite at large distances from the interface if the fluids are unbounded (four boundary conditions), (b) both components of velocity must be continuous across the interface between the two fluids (two matching conditions), (c) the shear stress must be continuous across the interface (one matching condition), and (d) the

normal stress must be continuous across the interface (one matching condition). Because of the mathematical complexity of solving this complete problem, the stability of the two fluids is generally assumed to be partially uncoupled and a single fourth order equation is solved for the stability characteristics of the particular fluid of interest. As a result, two features of the complete formulation are neglected. First, the matching conditions on both velocity components across the interface are no longer satisfied; and second, the stability of the gas is not influenced by the liquid which is the fluid of interest.

In this approach the stability of the outer fluid is of interest only to the degree that the perturbations in the gas properties which will affect the stability of the liquid are included in its stability analysis. Specifically, the presence of the outer fluid is acknowledged only by the expressions for the shear stress and pressure perturbations which are then imposed on the interface as boundary conditions for the liquid problem. Solutions of the gas problem for configurations which are applicable to this problem have been provided by Benjamin (1959), Miles (1962), and Nachtsheim (1970).

By reducing the complete stability analysis to that of the liquid only, the problem is treated in two parts. First, appropriate expressions for the shear and pressure perturbations are developed and second, the stability problem for the liquid is solved.

Consistent with this, the literature will be reviewed by formulating the liquid stability analysis and utilizing available expressions for the surface stress perturbations appropriate to the problem considered. The analyses to be considered may all be examined in a framework consistent with the sketch shown in Figure 82. Throughout

this section the nomenclature is taken consistent with this sketch and the origin of the Cartesian coordinates is located at the undisturbed gas-liquid interface.

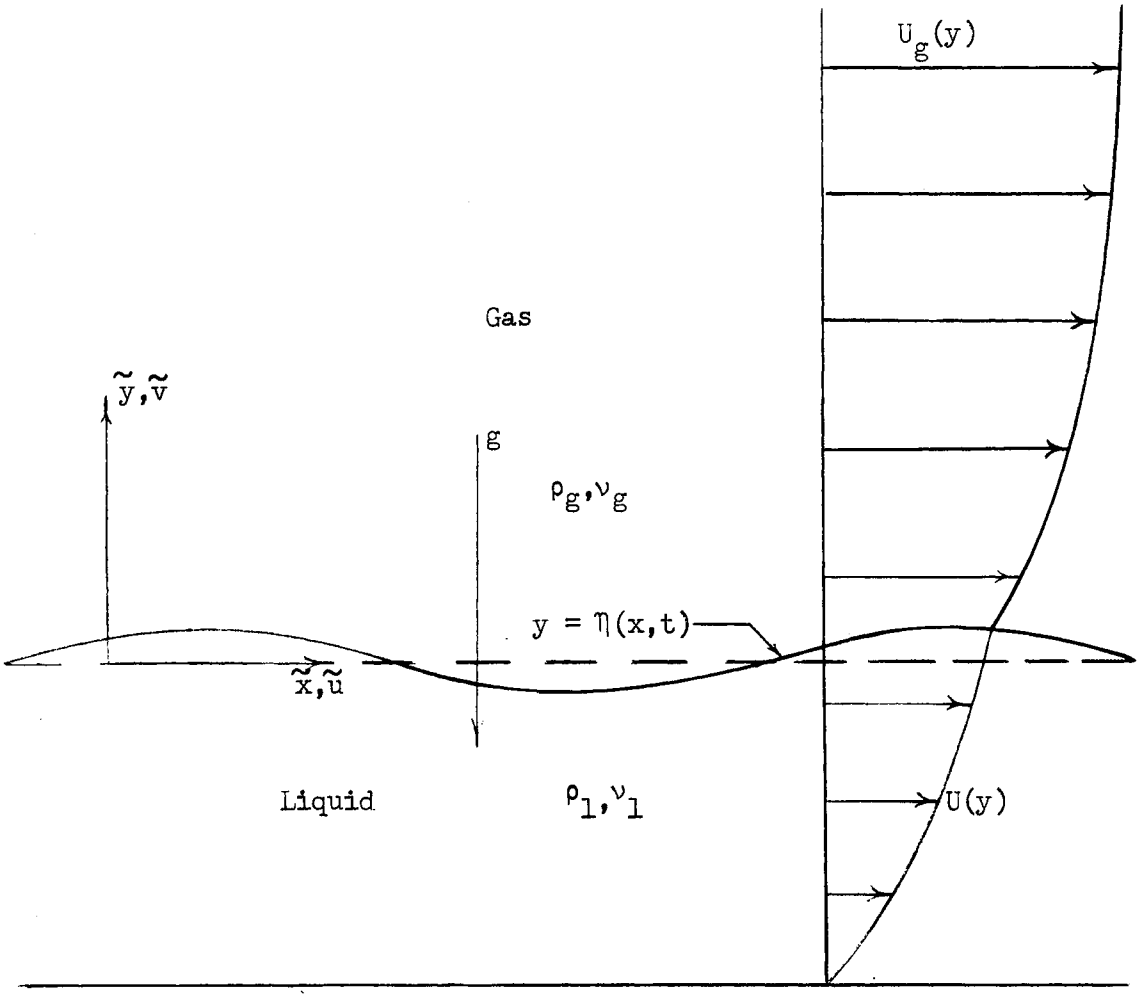

Figure 82. Sketch of Flow Configuration

The physical problem is one in which both the liquid and the gas are arbitrary functions of the mean velocity which has a component only in the x-direction. The density and viscosity of each fluid are assumed constant and the liquid velocity at the interface is defined as U_1. A body force g acts on the film normal to the undisturbed interface. To consider the stability of such a system, one assumes that the system is slightly disturbed from equilibrium by superposing infinitesimal disturbances. If the assumed disturbance amplifies, the system is unstable. If the disturbance is damped, the system is stable. Lin (1967) presents Squire's proof that the problem of three dimensional disturbances is equivalent to a two-dimensional problem at a lower Reynolds number. Consequently, the critical Reynolds number is given by the two-dimensional analysis. Therefore, it is sufficient to consider a two-dimensional wavelike perturbation of the liquid interface as indicated in Figure 82. The perturbation is given in dimensionless form by

$$y = \eta(x,t) = \delta \mathrm{Re}[\ e^{i\alpha(x-ct)}\ ] \tag{5}$$

where Re implies the real part of the expression in the brackets, α is the real, dimensionless wave number and c is the complex dimensionless wave velocity expressed in the usual form by $c = c_r + ic_i$. The amplification of the disturbance is given by αc_i and its phase velocity by c_r. The amplitude of the wave is assumed to be sufficiently small such that the motion equations may be linearized by neglecting all terms which are quadratic in the perturbation quantities. The continuity equation is satisfied by introducing a dimensionless perturbation stream function of the form

$$\psi(x,y,t) = \mathrm{Re}[\ \varphi(y)\,\delta\, e^{i\alpha(x - ct)}\ ] \qquad (6)$$

where Re implies the real part of the expression in the brackets. Thus the dimensionless perturbation velocity components are given by

$$u = \psi_y = \varphi_y\eta \qquad\qquad v = -\psi_x = -i\alpha\varphi\eta$$

where the x and y subscripts indicate differentiation with respect to x and y respectively.

When these relationships are substituted into the equations of motion for the liquid film and the resulting equations are linearized and non-dimensionalized, one obtains the Orr-Sommerfeld equation.

$$\varphi_{yyyy} - 2\alpha^2\varphi_{yy} + \alpha^4\varphi = i\alpha R\,[\ (U - c)\ (\varphi_{yy} - \alpha^2\varphi) - U_{yy}\varphi\ ] \qquad (7)$$

In this equation the Reynolds number is formed with the liquid interface velocity and liquid thickness and U is the dimensionless velocity profile in the liquid. This equation or an appropriate approximation must be solved using four boundary conditions to determine the stability of a particular flow. Since the boundary conditions are homogeneous, an eigenvalue problem results where the complex phase velocity c is the eigenvalue and is a function of the wavenumber and Reynolds number. The product of the wavenumber and the imaginary component of the phase velocity is the amplification rate of the disturbance while the real component is the velocity of the traveling wave. From the solution of this equation conditions may be deduced for which the film is unstable ($c_i > 0$) as well as those for neutral stability ($c_i = 0$) and film stability ($c_i < 0$).

Derivation of Boundary Conditions

To complete the formulation of the problem, the four boundary conditions must be specified. Consistent with the dimensionless form of the Orr-Sommerfeld equation, the boundary conditions are also formulated in dimensionless form with the following expressions utilized in the non-dimensionalization procedures.

$$u = \frac{\tilde{u}}{U_1} \qquad v = \frac{\tilde{v}}{U_1} \qquad x = \frac{\tilde{x}}{h} \qquad y = \frac{\tilde{y}}{h}$$

$$p = \frac{\tilde{p}}{\rho U_1^2} \qquad \tau = \frac{\tilde{\tau}}{\rho U_1^2} \qquad U = \frac{\tilde{U}}{U_1}$$

$$t = \frac{\tilde{U}_1}{h} t$$

The Reynolds number is defined by

$$R = \frac{U_1 h}{\nu} .$$

For a linear velocity profile in the liquid, this definition is consistent with equation 1. Two of the boundary conditions are expressed for the liquid-solid interface while the remaining two are derived at the gas-liquid interface. At the wall both components of the disturbance velocity must vanish. Therefore,

$$\text{(i)} \qquad u = 0 \qquad v = 0 \qquad y = -1 \qquad (8)$$

The remaining two boundary conditions which are satisfied are the continuity of normal stress and of shear stress at the interface. Because of the surface disturbance, the interface is not in general located at $y = 0$ but rather is located at $y = \eta(x,t)$. Therefore, these boundary

conditions must be written at the actual interface location and subsequently related by a Taylor series expansion to the mean interface location (y = 0). The continuity of shear stress across the interface may be expressed as

$$\tau_g(\eta) = \tau_l(\eta) \tag{9}$$

$$\left[\tau_o + \frac{1}{R}(u_y + v_x)\right]_g = \left[\frac{1}{R}(U_y(\eta) + u_y + v_x)\right]_l .$$

After expanding about y = 0, the equation becomes

$$\left[\tau_o + \frac{1}{R}(u_y + v_x)\right]_g = \left[\frac{1}{R}(U_y + \eta U_{yy} + u_y + v_x)\right]_l . \tag{10}$$

The mean shear relationship is defined by

$$\tau_o = \frac{1}{R} U_y \tag{11}$$

and the dimensionless perturbation shear stress in the gas caused by the interface disturbance is denoted by

$$\hat{\tau}_g = \frac{1}{R}(u_y + v_x) . \tag{12}$$

After substitution of these two expressions into equation 9, the equation for the continuity of shear stress becomes

(ii) $$\chi\eta = U_{yy}\eta + u_y + v_x \tag{13}$$

where

$$x\eta = R\,\hat{\tau}_g \quad .$$

A similar procedure may be applied to the expression for continuity of normal stress. With σ denoting the liquid surface tension, the pressure balance is written in dimensionless form as

$$P_g = P_l - \frac{\sigma}{\rho U_l^2 h}\,\frac{1}{r} \tag{14}$$

where r is the local radius of curvature of the interface. The pressure in the gas may be expressed as

$$P_g = \left(-P_o + \frac{2}{R}v_y\right)_g \tag{15}$$

at $y = \eta(x,t)$. Assuming the pressure may be divided into a primary and a perturbation component, one may write

$$P_o(\eta) = P(\eta) + p(\eta). \tag{16}$$

This equation must be expanded in a Taylor series to $y = 0$. The results after substitution into equation 15 are,

$$P_g = -P - \frac{dP}{dy}\eta \quad - p + \frac{2}{R}\frac{\partial v_g}{\partial y} \tag{17}$$

or

$$P_g = -P - \lambda\eta$$

where λ is the perturbation pressure in the gas defined by

$$\lambda\eta = \frac{dP}{dy}\eta + p - \frac{2}{R}\frac{\partial v_g}{\partial y} \quad . \tag{18}$$

Applying the same procedure to the liquid

$$P_1 = -P - \frac{dP_1}{dy}\eta - p + \frac{2}{R}\frac{\partial v_1}{\partial y} \quad . \tag{19}$$

Combining equations 14, 17, and 19,

$$-P - \lambda\eta = -P - \frac{dP_1}{dy}\eta - p + \frac{2}{R}\frac{\partial v_1}{\partial y} - \frac{\sigma}{\rho U_1^2 h}\eta_{xx} \tag{20}$$

where the local radius of curvature has been evaluated by

$$\frac{1}{r} = \frac{\dfrac{\partial^2\eta}{\partial x^2}}{\left[\,1 + \left(\dfrac{\partial\eta}{\partial x}\right)^2\,\right]^{3/2}} \sim \eta_{xx} \quad .$$

Thus the final form for this boundary condition is

$$\text{(iii)} \quad P - \frac{hg}{U_1^2}\eta + \frac{\sigma}{\rho U_1^2 h}\eta_{xx} - \frac{2}{R}\frac{\partial v_1}{\partial y} = \lambda\eta \tag{21}$$

where

$$\frac{dP_1}{dy} = \frac{-hg}{U_1^2} \quad .$$

The final equation necessary for this problem is one that relates the kinematic condition of the interface to the vertical perturbation velocity component at the interface. That is

$$v = \frac{Dy}{Dt} = \frac{\partial y}{\partial t} + U\frac{\partial y}{\partial x} \quad . \tag{22}$$

Therefore for $y = \eta(x,t)$,

(iv) $$v = \eta_t + U\eta_x \quad . \tag{23}$$

To be consistent with the governing differential equation, the boundary conditions must be written in terms of the perturbation stream function. The results are:

$$\varphi = 0 \qquad \varphi_y = 0 \qquad y = -1 \tag{24-a}$$

$$\varphi_{yy} + \alpha^2\varphi + U_{yy} = \chi \qquad y = 0 \tag{24-b}$$

$$\varphi_{yyy} - 3\alpha^2\varphi_y - i\alpha R[\,(U - c)\varphi_y + G + T\alpha^2 - \varphi U_y\,] = i\alpha R\lambda \qquad y = 0 \tag{24-c}$$

$$c = U + \varphi \qquad y = 0 \tag{24-d}$$

The parameters G and T are the inverse Froude and Weber numbers respectively and are defined as

$$G = \frac{hg}{U_1^2} \qquad T = \frac{\sigma}{\rho U_1^2 h} \quad .$$

Equation 7, the Orr-Sommerfeld equation, together with equations 24-a through 24-d as boundary conditions, complete the general formulation of the problem. The functions χ and λ, which may be complex or real depending on the gas flow, are the shear stress and pressure perturbations in the gas caused by the waves on the interface.

Solutions of Governing Equations

The analyses which have been formulated and are related to these experiments may be examined separately by considering the specific boundary conditions employed. Although not directly related to these experiments, the classical Rayleigh-Taylor problem warrants a brief description. In this problem a body force acts on the fluids and causes the instability. If the body force acts from the lighter to the heavier fluid, the system is stable; if it acts in the opposite direction, the system is unstable. The solution is presented in detail in several textbooks including that of Chandrasekhar (1961). For the experiments reported in this thesis, the body force acts normal to the mean liquid interface from the gas to the liquid. As a result the body force is stabilizing and the Rayleigh-Taylor instability is not present and will not be discussed further.

Liquid in Uniform Shearing Motion with no External Gas Perturbations

Miles (1960) considered the problem of a thin film of liquid in uniform shearing motion with no effects of an external gas on the surface wave formation considered. The liquid flow was considered incompressible, two-dimensional, and laminar and only those waves with propagation velocities on the interface less than the liquid interface velocity were considered. Miles posed the solution of the resulting Orr-Sommerfeld equation as an asymptotic solution for large values of the Reynolds number with the following boundary conditions.

$$\text{(i)} \quad \varphi = \varphi_y = 0 \qquad y = -1$$

$$\text{(ii)} \quad \varphi_{yy} + \alpha^2\varphi = 0 \qquad y = 0$$

$$\text{(iii)} \quad \varphi_{yyy} - 3\alpha^2\varphi_y - i\alpha R\left[(U - c)\varphi_y + G + T\alpha^2 - \varphi \right] = 0 \qquad y = 0$$

$$\text{(iv)} \quad c = U + \varphi \qquad y = 0$$

When (ii) and (iii) above are compared with their counterparts in the general boundary condition expressions (Equations 24-b and 24-c), it is obvious that both the shear stress and pressure perturbations are neglected ($\chi = \eta = 0$). This type instability is due to the transfer of energy from the primary motion of the fluid to the disturbance and is called the Tollmein-Schlichting instability. Miles found that a sufficient condition for stability was that either the Weber number be less than 3 or that the Reynolds number based on the interface velocity and film thickness be less than 203. Because of the lack of an external gas interacting with the interface, this analysis does not represent the entire problem of interest; but for sufficiently high liquid Reynolds numbers this instability may be present.

Inviscid Liquid and External Gas

When an external gas is included in the formulation of the problem, there are potentially different sources of instability. In particular, the surface waves cause perturbations in the normal and shear stresses exerted by the gas on the liquid. Consider first the case where both fluids possess uniform but unequal velocity and both are considered incompressible, inviscid and infinite in extent. Since the viscosity

of the liquid (as well as that of the gas) is zero, the inviscid Orr-Sommerfeld equation governs the stability characteristics and the shear stress perturbation boundary condition cannot be satisfied. However, the pressure perturbation boundary condition must be satisfied and in fact has been determined explicitedly from a solution of the external gas equations. The appropriate boundary conditions are

$$\text{(i)} \qquad \varphi = 0 \qquad\qquad y \to -\infty$$

$$\text{(iii)} \qquad \varphi_y(c - U) - G - T\alpha^2 = -\frac{\alpha^2}{C_f} \qquad y = 0$$

where C_f is defined by the mean shear

$$\tau_o = C_f \rho_g U_g^2 .$$

$$\text{(iv)} \qquad c = U + \varphi \qquad\qquad y = 0$$

This is the classic Kelvin-Helmholtz instability for incompressible flow which is described in Chandrasekhar (1961). The mechanism which provides energy to the instability is the pressure perturbation. The pressure for the uniform external flow is 180 degrees out of phase from the interface displacement. The pressure pushes down in the wave troughs and sucks up at the crests as shown in Figure 83. Stability at the interface results when

$$(U_g - U_l)^2 < \frac{2(\rho_g + \rho_l)}{\rho_g \rho_l} [\sigma g(\rho_l - \rho_g)]^{\frac{1}{2}} .$$

If the liquid is assumed to be of finite thickness h, the conclusions for stability conditions are unchanged but the wave speed and amplification rate are altered by the constant factor $(\coth \alpha h)^{\frac{1}{2}}$.

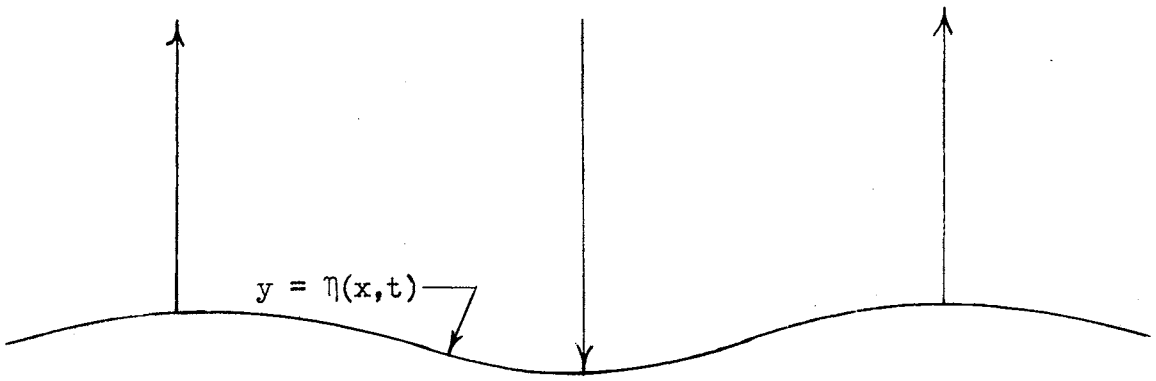

Figure 83. Perturbation Pressure Distribution for a Kelvin-Helmholtz Instability

Chang and Russell (1965) have considered a similar problem except that the liquid layer is assumed initially quiescent and compressibility effects are included in the external gas for both subsonic and supersonic flow. Since both fluids are assumed to be inviscid as before, the only boundary condition which is altered is the pressure perturbation term. Thus the boundary conditions are

(i) $\varphi = 0$ $\qquad y \to -\infty$

(iii) $\varphi_y(c - U) - G - T\alpha^2 = -\dfrac{\alpha^2}{C_f(1 - M^2)^{\frac{1}{2}}}, \quad M < 1$

$y = 0$

$= -\dfrac{\alpha^2}{C_f(M^2 - 1)^{\frac{1}{2}}}, \quad M > 1$

(iv) $c = U + \varphi$ $y = 0$

where C_f is defined as before. The compressibility effects in the external gas are seen in the right hand side of the normal pressure equation (condition iii).

With a subsonic uniform external gas and an inviscid liquid of infinite depth, Chang and Russell found two cutoff wave numbers for the case where the body force (acceleration) is directed from the gas to the liquid. All waves with wave numbers below the lower value or above the higher value are stable due to the stabilizing effects of surface tension and the body force. However, if the body force is directed from the liquid to the gas, then both the Rayleigh-Taylor and Kelvin-Helmholtz mechanisms are in operation and only the surface tension is stabilizing. Therefore, only one cutoff wavenumber exists and waves are stable only for wavenumbers greater than this value.

With a supersonic external gas the condition is always one of instability regardless of the effects of surface tension. This instability is due to the action of the pressure perturbation on the interface whereby the pressure is in phase with the wave slope and evidences itself as supersonic wave drag.

Viscous Liquid and Inviscid External Gas

Chang and Russell (1965) extended their analysis to consider the case of a low Reynolds number liquid with an inviscid external gas. In this case the complete fourth order Orr-Sommerfeld equation must be solved and the complete set of four boundary conditions is required. By neglecting the perturbation of the frictional force between the liquid interface and the gas viscous boundary layer ($X = 0$ in equation

24-b), the required boundary conditions are

(i) $\varphi = \varphi_y = 0$ $\qquad y \to -\infty$

(ii) $\varphi_{yy} + \alpha^2\varphi + U_{yy} = 0$ $\qquad y = 0$

(iii) $\varphi_{yyy} - 3\alpha^2\varphi_y - i\alpha R\,[\,(U - c)\varphi_y + G + T\alpha^2 - \varphi U_y\,]$

$$= -\frac{\alpha^2}{C_f(1 - M^2)^{\frac{1}{2}}}, \qquad M < 1$$

$y = 0$

$$= -\frac{\alpha^2}{C_f(M^2 - 1)^{\frac{1}{2}}}, \qquad M > 1$$

(iv) $c = U + \varphi$ $\qquad y = 0$

The perturbation of the shear stress between the liquid interface and the gas boundary layer is neglected as shown in condition (ii) while the pressure perturbation is the same as that for the inviscid external gas. For this formulation the results for the subsonic external gas are unaltered from those of the inviscid liquid case wherein a lower and an upper cutoff wavenumber for instability is found. The effect of the liquid viscosity is to attenuate the growth rate of the waves.

For the supersonic external gas condition the results are significantly different from the inviscid liquid case. For the low Reynolds number limit, the stabilizing effects of surface tension are recovered. The liquid will always be stable if the body force is directed from the gas to the liquid and will also be stable for the body force directed from the liquid to the gas for disturbances with wave numbers $\alpha > \alpha_c$

where

$$\alpha_c = \left(\frac{-\rho_1 g}{\sigma}\right)^{\frac{1}{2}} .$$

Nachtsheim (1970) recently treated the configuration somewhat similar to that of Chang and Russell. The viscous liquid is of finite depth h. However, in contrast to Chang and Russell's assumption of an initially stationary liquid, the liquid is assumed to possess a linear velocity profile and to be fully established. An inviscid, compressible, supersonic gas flows over the interface. The body force acts perpendicular to the interface from the gas to the liquid. Nachtsheim considered three dimensional disturbances for which the gas flow is supersonic in the direction normal to the wave fronts. Consistent with the assumed inviscid external gas, shear stress disturbances at the interface are neglected and only the pressure perturbation is considered. By considering the stability of the gas, Nachtsheim generated the expression for the pressure perturbation. The boundary conditions in Nachtsheim's analysis may be put into the two-dimensional formulation used herein by using Squire's transformation. They are

(i) $\varphi = \varphi_y = 0$ $\qquad y = -1$

(ii) $\varphi_{yy} + \alpha^2 \varphi = 0$ $\qquad y = 0$

(iii) $\varphi_{yyy} - 3\alpha^2 \varphi_y - i\alpha R \left[(U - c)\, \varphi_y + G + T\alpha^2 - \varphi \right] = \dfrac{\alpha^2}{\frac{C_f}{2}(M^2-1)^{\frac{1}{2}}}$ $\qquad y = 0$

(iv) $c = U + \varphi$ $\qquad y = 0$

where C_f is defined as

$$\tau_o = \tfrac{1}{2} C_f \rho_g U_g^2 .$$

Nachtsheim obtained a numerical solution of the eigenvalue problem and in addition performed a two term Taylor expansion for small liquid film Reynolds numbers. He found in his numerical results an upper and a lower cutoff wave number for instability and found for each value of the parameter $C_f/2\ (M^2 - 1)^{\frac{1}{2}}$ a critical value of the Reynolds number beyond which the flow is always stable. That is, one passes from a region of instability to stability as the Reynolds number is increased for fixed values of the Froude number, Weber number and wave number. Nachtsheim explains this interesting result by stating that the only force representing the action of the supersonic gas stream (pressure perturbation) is the force proportional to the interaction parameter defined as

$$\frac{1}{(C_f/2)\ R\ (M^2 - 1)^{\frac{1}{2}}}$$

where

$$\frac{1}{(C_f/2)\ R} = \frac{\rho_g U_g^2}{\rho_l U_l^2} .$$

As R increases, the parameter becomes smaller and the relative importance of the gas pressure on the interface decreases. Nachtsheim concludes that whatever decreases this interaction parameter tends to stabilize the liquid film. Additional interpretation of this result may be gained by considering the relationship between the shear and

Reynolds number. For the assumed linear velocity profile

$$\tau = \rho\left(\frac{\nu}{h}\right)^2 R \quad .$$

The stated condition that both the Weber and Froude numbers are constant implies that both the interface velocity and film thickness are constant. Therefore, the condition of increasing Reynolds number requires that the mean shear decrease and is therefore stabilizing. The disturbance pressure is in phase with the wave slope and therefore exerts a supersonic wave drag on the interface.

Viscous Liquid and External Gas

Craik (1966) considers essentially the same physical problem as those previously discussed. However, one important feature that is added is the external gas is viscous. Hence the shear stress perturbation exerted by the gas on the interface must be included. The thickness of the film is h and the liquid possesses a linear velocity profile. The stability analysis of the viscous film requires the solution of the complete Orr-Sommerfeld equation and the appropriate boundary conditions are:

(i) $\varphi = \varphi_y = 0$ $\qquad y = -1$

(ii) $\varphi_{yy} + \alpha^2\varphi = -R\Sigma$ $\qquad y = 0$

(iii) $\varphi_{yyy} - 3\alpha^2\varphi_y - i\alpha R\left[(U - c)\varphi_y + G + T\alpha^2 - \varphi U_y \right] = i\alpha R\Pi$ $\qquad y = 0$

(iv) $c = U + \varphi$ $\qquad y = 0$

To evaluate the surface stress perturbations Craik uses expressions derived by Benjamin (1959) in his theoretical study of shearing gas flows over a simple-harmonic wavy surface. These results are

$$\Pi = \frac{\alpha}{RC_f}\left[I - (3)^{\frac{1}{2}} s + i(2C_f - s)\right]$$

$$\Sigma = \frac{2\beta I}{(3)^{\frac{1}{2}} C_f}\, \rho \frac{i\pi}{3} (\alpha R)^{-4/3}$$

where

$$s = 0.644\, \Delta I \qquad \Delta = \frac{I}{C_f} \left(\frac{\mu_g}{\mu_1}\right)^{2/3} (\alpha R)^{-2/3} \alpha^2$$

$$I = \int_0^\infty \left(\frac{U}{U_\infty}\right)^2 e^{-\alpha y}\, d(\alpha y)$$

$$\frac{2\beta}{(3)^{\frac{1}{2}}} = 372\, I \left(\frac{\nu_g}{\nu_1}\right)^{2/3} \left(\frac{\rho_g}{\rho_1}\right)^{1/3} .$$

Real parts of Π and Σ correspond to components of normal and tangential stress in phase with the wave displacement while the imaginary parts correspond to components in phase with the wave slope. Craik solves the Orr-Sommerfeld equation by the series

$$\varphi(y) = \sum_0^\infty A_n y^n$$

for the conditions where

$$\alpha^2 \ll 1,\ \alpha R < O(1),\ \alpha R\,|c| < O(1).$$

He found the condition for instability as

$$P_r + \frac{3T_i}{2\alpha h} > \rho g + \frac{\sigma\alpha^2}{h^2}$$

where P_r is the real component of pressure perturbation and T_i is the imaginary component of shear stress perturbation. Thus for a very thin film (small values of h), the shear stress perturbation becomes the dominant mechanism causing the instability; while for thicker films the pressure perturbation is the dominant feature. Craik explains this phenomenon physically by considering the phasing of the two perturbation components. The pressure perturbation, P_r, is in phase with the wave displacement and attempts to deform the interface in the same manner as the normal Kelvin-Helmholtz mechanism. The shear stress component, T_i, is in phase with the wave slope and it has the effect of accelerating the liquid on the windward slopes while retarding that on the leeward slopes. This latter mechanism tends to displace fluid from the wave troughs to the crests and is more effective for thin films.

Free Molecular External Gas

Reynolds (1967) considers the stability of a liquid film exposed to hypersonic free molecular flow. The viscosity and density of the liquid are assumed constant and the velocity profile in the liquid is linear. For the free molecular gas flow, Reynolds expresses the perturbation pressure and stress conditions in explicit form. Consequently, the boundary conditions for this analysis are:

(i) $\varphi = \varphi_y = 0$ $\qquad y = -1$

(ii) $\varphi_{yy} + \alpha^2\varphi = -i\alpha Rs$ $\qquad y = 0$

$$\text{(iii)} \qquad \varphi_{yyy} - 3\alpha^2\varphi_y - i\alpha R\left[(U - c)\varphi_y + G + T\alpha^2 - \varphi\right] = i\alpha QR \qquad y = 0$$

$$\text{(iv)} \qquad c = U + \varphi \qquad y = 0$$

where

$$Q = a_p \frac{\rho_\infty U_\infty^2}{\rho_1 U_1^2} \sin 2\theta_o$$

$$s = -a_t \frac{\rho_\infty U_\infty^2}{\rho_1 U_1^2} \cos 2\theta_o \, .$$

These boundary conditions are then specializations of those given by Craik whereby $\Pi_r = \Sigma_r = 0$ in his analysis produces these boundary conditions.

The constants a_p and a_t are near unity and θ_o is the angle of the incident flow with the interface. By including the shear stress perturbations, Reynolds considers a problem similar to that of Craik with the particular perturbation expressions applicable to the free molecular flow. He concludes that the shear stress perturbations must be included and determines that the 'Craik-Benjamin' mechanism will be dominant for thin films when θ_o approaches 90 degrees. Reynolds presents a solution for both small αR (after Craik) and large αR (after Miles) and find a cutoff wave number above which the disturbance is stable.

Nayfeh and Saric (1970) present an analysis on the stability of a film with an inviscid external gas flow with the solution taken as a long wave approximation. An arbitrarily oriented body force is included and the Orr-Sommerfeld equation is solved by a perturbation solution

in the wavenumber. Specific boundary conditions for the various types of external flow are considered and the results are compared with those from previously reported analyses. The axial body force is found to be stabilizing if directed opposite to the external flow; otherwise, it is destabilizing. For the supersonic inviscid external gas, the results are compared with those of Nachtsheim. Two cutoff wavenumbers are calculated and wavenumbers above the higher value or below the lower value represent stable waves.

Experimental Investigations

There have been several experimental investigations of gas-flow generated waves of a liquid interface reported. The majority of the experiments were performed with a subsonic air flow over the liquid; however, in one experimental study a supersonic gas flow was produced over the interface. The more recently reported experiments are discussed in detail.

Experiments of Cohen and Hanratty (1965)

Cohen and Hanratty employed a closed channel 12 inches wide, 1.015 inches high, and 21 feet long to study the waves which appear on a liquid interface with subsonic air flow over the liquid. Water-glycerin mixtures were employed to vary the viscosity and the liquid thickness was varied from 0.07 to 0.3 inches. The liquid Reynolds number, based on the average liquid velocity and thickness of the film, was varied from 21 to 590. They reported a critical air velocity above which waves were found to exist on the interface. The first waves to appear were two-dimensional and extended across the entire width of the

channel. At a higher gas velocity the waves changed to a three-dimensional 'pebbled' structure. For both wave structures, it was stated explicitly that the wave velocities were larger than the maximum liquid velocity but much smaller than the average gas velocity. For the two-dimensional waves the wave speed was approximately 1.2 feet per second with a wavelength of approximately 1.2 inches. The variation of wave speed with Reynolds number was not reported. For the three-dimensional waves the wave speed was measured at 0.9 to 1.27 feet per second and the wavelength from 0.39 to 0.5 inches. Cohen and Hanratty compared the measured data for the two-dimensional waves with calculations using the gas models of Jeffreys (1925) and of Miles (1962) and Benjamin (1959). The conclusion was that both models satisfactorily predict the wave speed and wavelength at wave inception. For three-dimensional waves the Miles-Benjamin model was found to satisfactorily predict the measured data. However, the emperical sheltering coefficient of the Jeffreys model had to be reduced by an order of magnitude from the 0.3 value used for the two-dimensional wave inception data to obtain agreement for the three-dimensional wave transition data.

Experiments of Plate, Chang, and Hidy (1969)

Using a wind-water tunnel, Plate, Chang, and Hidy investigated the generation and growth of small water waves by a turbulent wind. Air flowed over a smooth inlet plate approximately 12 feet long onto a body of initially quiescent water 4.5 inches deep and 45 feet long. The liquid depth was greatly in excess of that produced in the experiments reported in this research as well as that of all other experiments

reported here. Free stream air velocities from 12 to 42 feet per second were employed and waves were generated at all air velocities. The first waves to appear were two-dimensional in appearance with crests nearly perpendicular to the flow. As the wind speed increases the appearance of a rhombic wave pattern made up of small capillary waves superimposed over the first undulations was reported. A further increase in the air speed caused a return to a more two-dimensional pattern. A capacitance gauge consisting of a 32-gauge, Nyclad insulated, magnet wire combined with a capacitance bridge circuit was employed to measure the water surface displacement. A sensitivity which permitted the detection of surface undulations with amplitudes of less than ten microns was reported. Using this device they were able to measure the density of the potential energy of the Fourier component associated with a particular frequency.

With the 'critical fetch' defined as that distance where the surface undulations became visible, Plate et al. found that prior to this distance the wave spectra was diffuse in the low range frequency. Beyond the critical fetch the spectrum sharpened to a particular frequency. With increasing distance the energy reached an equilibrium limit and for further increases in distance the energy density shifted to lower frequencies. Plate, et al. concluded there was no indication that the waves were produced by direct interaction of the water surface with the air turbulence and used the viscous shearing mechanism of Miles (1962) to interpret the data. The growth rates agreed with the estimates from Miles analysis to within an error of 61 percent or less.

Experiments of Craik (1966)

Craik employed a 11.4 inch wide, 46 inch long channel to study the liquid interface behavior and produced water film thicknesses from approximately 0.008 inches to 0.063 inches. The subsonic airflow over the interface was provided by a large fan. For constant airflow he reported the following sequence for decreasing liquid flow rate; (a) a pebbled surface, (b) regular waves, (c) smooth surface, (d) wavy surface, (e) dry patches. The waves of case (b) were faster than the interface velocity (fast waves) while those of (d) were slower (slow waves). With the air flow sufficiently large, region (c) disappeared altogether. Craik concluded from the presence of case (c) that there is a non-zero thickness for which a water film is most stable for certain gas flow conditions.

At liquid Reynolds numbers in the range from approximately 30 to near 50, Craik observed the fast waves. For Reynolds numbers from near 2 to 30, he observed slow waves with the external gas conditions similar for both ranges of Reynolds number. Three-dimensional, fast waves were reported at the same gas conditions for Reynolds numbers from near 50 to 75.

For conditions just beyond the transition from a stable film to the fast waves, the dimensionless wave speed, formed with the interface velocity, varied from 1.75 to 3.84 while for the slow waves, the dimensionless wave speed was essentially constant at 0.8.

Experiments of Sherman and Schetz (1970)

To the author's knowledge the only experiments reported with a supersonic gas flow over the liquid are those of Sherman and Schetz.

The model was 7 inches long, had a 20 degree half wedge angle at the leading edge and was exposed to a Mach 2.2 flow. The initial inch of the model was solid while the next five inches were made of porous stainless steel through which water and glycerin-water mixtures were expelled. High speed movies and photomicrographs were used to record the surface response. However, since the purpose of the experiments was to study the sheet breakup, only limited data on the wave formation of the interface were taken. They reported the observation of three-dimensional waves and reported typical measured wave speeds, but no correlations with liquid parameters were reported.

Summary

The details of the boundary conditions for the various liquid film stability analyses are discussed in a previous section. However, a brief summary and comparison of the various analytical formulations can provide insight into the physical mechanisms which are included in the analyses and are therefore responsible for the instabilities.

Miles (1960) considers the stability of a liquid film in uniform shearing motion which arises as a result of the mean shear stress exerted by the airflow. However, the pressure and shear perturbations at the interface are assumed to be negligible. The instability for this configuration occurs at relatively large liquid Reynolds numbers (i.e., > 200) due to the transfer of energy from the basic liquid flow to the disturbance. The results of this analysis are of interest in interpreting the high Reynolds number data of these experiments.

Chandrasekhar (1961) considers the stability of an inviscid, incompressible liquid moving at a velocity U_1 with a second inviscid,

incompressible fluid moving at a velocity U_2 over the interface. The instability which results is due to the pressure perturbation in the gas being 180 degrees out of phase with the interface displacement. As a result, the pressure pushes down in the wave troughs and sucks up at the peaks. The liquid surface tension is the only stabilizing influence. This instability is the normal Kelvin-Helmholtz instability.

Chang and Russell (1965) extend the inviscid, incompressible Kelvin-Helmholtz model to include the effects of a viscous liquid with both subsonic and supersonic external gases considered. However, the external gas is inviscid and the liquid is assumed to be infinitely deep and initially quiescent. The liquid is suddenly subjected to a disturbance which is periodic in time. For the supersonic external flow, the liquid is unstable for all wavenumbers in the inviscid limit. The introduction of viscosity for the liquid results in a cutoff wavenumber above which disturbances are stable. The instability is a result of the pressure perturbation in the external gas which is in phase with the wave slope and results in a supersonic wave drag on the interface.

The models of Nachtsheim (1970) and of Nayfeh and Saric (1970) are similar except that the latter model includes a body force oriented at an arbitrary angle to the interface and the former includes the body force normal to the interface. The external gas is assumed inviscid and supersonic. The pressure perturbation at the interface is included whereas the shear stress perturbation is neglected. These analyses show that increasing the Mach number is stabilizing whereas increasing the liquid Reynolds number or the mean shear exerted by the gas is destabilizing. The solution of Nayfeh and Saric is a perturbation

expansion in powers of the wavenumber and is expanded to include four terms. Because of the inclusion of the supersonic gas perturbation acting on the interface, the results of this analysis are used for comparison with the low Reynolds number experimental data.

Craik (1966) considers the stability of a liquid film and includes both shear stress and pressure perturbations exerted by the gas on the interface. Of the analyses reviewed here, this is the only one which includes a viscous gas perturbation effect on the interface of the liquid. The expressions for the shear and pressure perturbations are taken from Benjamin's (1959) analysis of a shearing gas flow over a simple-harmonic wavy surface. Craik finds that the shear stress perturbation has a very pronounced effect on the stability characteristics of the interface. For very thin films, the shear stress, which is in phase with the wave slope, is the dominant source of the instability.

APPENDIX B

MODEL DESIGN

The model used in preliminary experiments to evaluate the general experimental principal and the liquid expulsion system was a sphere-cone combination. The five degree half angle cone was equipped with a one inch diameter nose tip which was made of porous stainless steel. Tips were made from material of two different permeability coefficients, 5×10^{-10} and 1×10^{-10} square inches. The permeability coefficient was measured around the tip and found to vary by less than 7 percent thus assuring a satisfactorily uniform flow throughout the tip. The nose tip attached onto the five degree half angle conical stainless steel model to give a total model length of twelve inches. Six thermocouples were used to measure the liquid temperatures.

The cone model was successful in demonstrating the experimental principal. However, wave characteristic data could not be obtained for several reasons. First, because of the increasing circumference along the model, the liquid film thickness decreased back along the model. Second, the effect of gravity normal to the cone axis caused a non-uniform thickness around the model. Particularly for the high viscosity-low Reynolds number condition, the model was not covered along the top at the back of the cone.

To remove these objections, the two dimensional wedge model was designed and utilized for all of the data reported in this research.

A run was made with no side plates on the model; and, as expected, the pressure gradients caused the liquid to flow off the sides. It was therefore necessary to attach side plates to the model.

Three different side designs were utilized in an attempt to provide the largest area of the model surface on which satisfactory two dimensional flow characteristics in the fluid could be observed.

The sides used initially were three inches tall with a sharp leading edge along the front surface. The side was designed such that it could be attached to the model side at practically any position. Initially, the side was mounted symmetrically on the model with its leading edge 0.5 inches in front of the model nose tip. The movie film clearly showed the effects of shocks originating near the intersection of the side walls and the nose tip. These shocks originated from both side walls and spread outward from the sides and back over the model surface. The shocks intersected on the model centerline at a point approximately six inches behind the nose tip. In addition the liquid was seen to detach from the side walls for a short distance. Because of these effects the acquisition of wave characteristic data was limited to the front five inches of the model in an area one to two inches on either side of the centerline.

In an attempt to eliminate the effects of these shocks, several alterations were made in the manner in which the sides attached to the wall. The leading edge was recessed to a position 0.25 inches in front of the model nose and the sides were shimmed out at several different angles. In addition the sides were dropped to a position such that the walls extended 0.125 inches above the model surface. None of these

alterations caused any detectable change in the presence or location of the shocks.

The remaining two types of side wall were designed as an attempt to remove or minimize the effects of the shocks and also in order to permit the model to be run at an angle of attack in the tunnel. The initial design tried was five inches tall with a sharp edge around the entire wall except for the back edge. The front was cut on a 2.5 inch radius. This design was totally unsatisfactory for several reasons. First, the side loads on the large area walls resulted in significant vibration and lateral movement of the model. Second, the liquid detached very near the leading edge from the sides and covered a region approximately three inches wide along the model centerline. The final design was similar to that just described except that it was two inches tall and the front edge was cut on a one inch radius. This side wall was used for all experiments reported here and no effects in the liquid due to the presence of shocks could be detected in the photographic film coverage.

APPENDIX C

DEPTH GAUGE CALIBRATION

The mean output of the depth gauge is an indication of the liquid film thickness provided a satisfactory calibration can be obtained. The system used for calibration of the gauge is sketched in Figure 84. A cubical container with one face open was fitted with a micrometer through the center of the side opposite the open face. The container was attached beneath the plate in which the depth gauge was mounted as shown in the figure. A 0.25 inch diameter hole through the plate directly above the micrometer permitted the pointer to be advanced through the plate to the height of the liquid interface above the plate. To perform the calibrations, the container was filled with the particular liquid to be calibrated and was overfilled until the desired thickness of liquid existed above the plate surface. Surface tension effects cause a liquid to jump toward an object when it is brought sufficiently close to the interface from outside the liquid. However, since the micrometer is mounted within the liquid, this phenomena is totally removed. The plate with the container and micrometer mounted was leveled very carefully in order that the liquid thickness above the micrometer be equal to that over the gauge located approximately one inch away.

The actual model plate and depth gauge utilized in the experiments were attached to the liquid container and micrometer. The entire

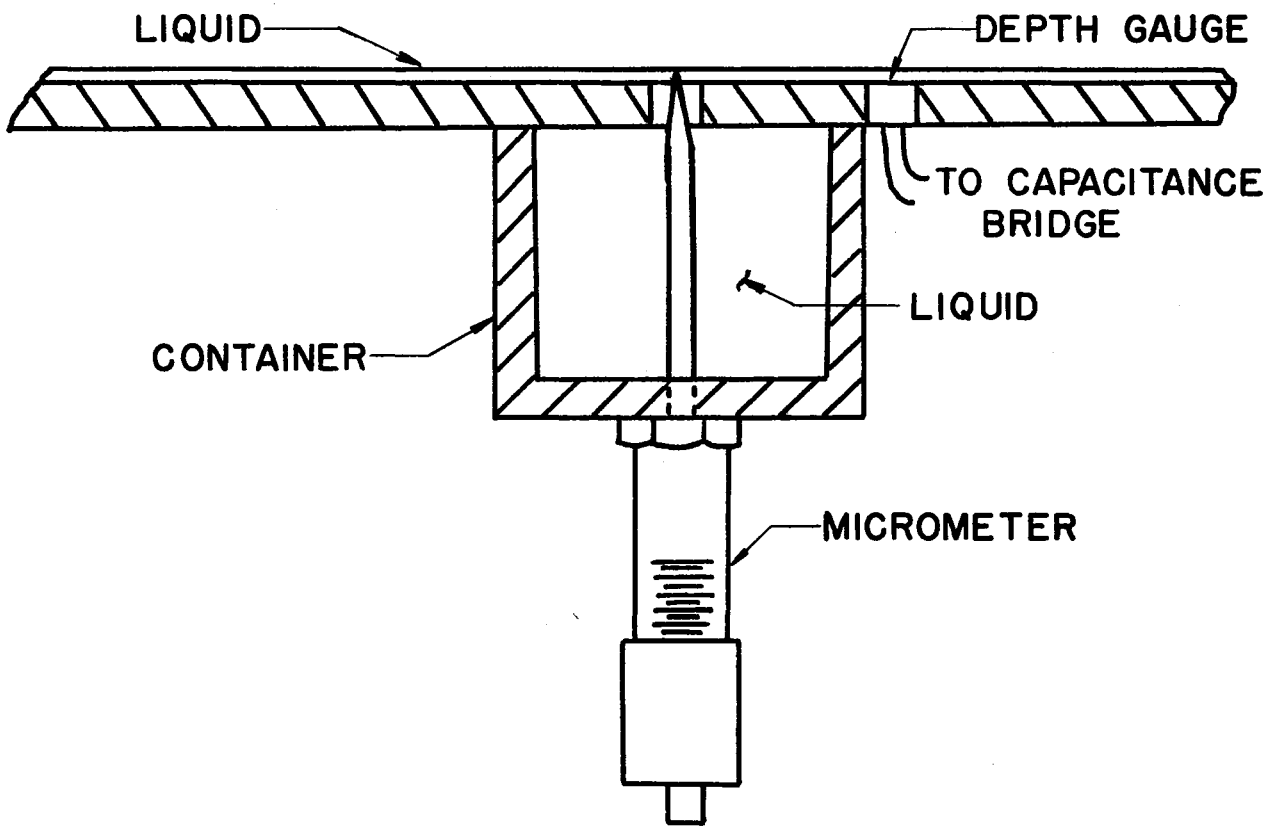

Figure 84. Apparatus for Depth Gauge Calibration

system was leveled very carefully and the depth gauge nulled. With no liquid on the plate a metal bar with a flat surface was placed over the micrometer opening. A resistance meter was connected to the metal bar and to the micrometer handle which were electrically insulated from each other by the paint on the plate. When the micrometer pointer was brought into contact with the metal bar, the ohmeter indicated a short circuit and provided a non-liquid zero reference condition for the micrometer. As the container was overfilled, the liquid spread out over the depth gauge to an equilibrium height above the plate surface and the micrometer pointer was advanced to the liquid interface location. The liquid depth was determined by subtracting the non-liquid null micrometer reading from the reading at the particular depth. The liquid depth was correlated with the output of the gauge which was connected to the same bridge electronics as during the experiments. Efforts to estimate the repeatability of the micrometer indicated an error of less than .0005 inches in repeatedly locating the interface. Samples of each of the particular fluids used in the experiments were used to provide the gauge calibration which was performed at the measured test model temperatures. A small blower was utilized to heat the entire calibration system to the desired test temperature with a thermometer used for the temperature measurement.

Figures 85 through 90 are the calibration curves for the depth gauge with each of the fluids used. During the calibration a variation in gauge output for a given thickness at different liquid temperatures clearly demonstrated the temperature sensitivity of the gauge. Consequently, two factors influence the overall accuracy of the calibration. The scatter of the data at a particular temperature and the uncertainty

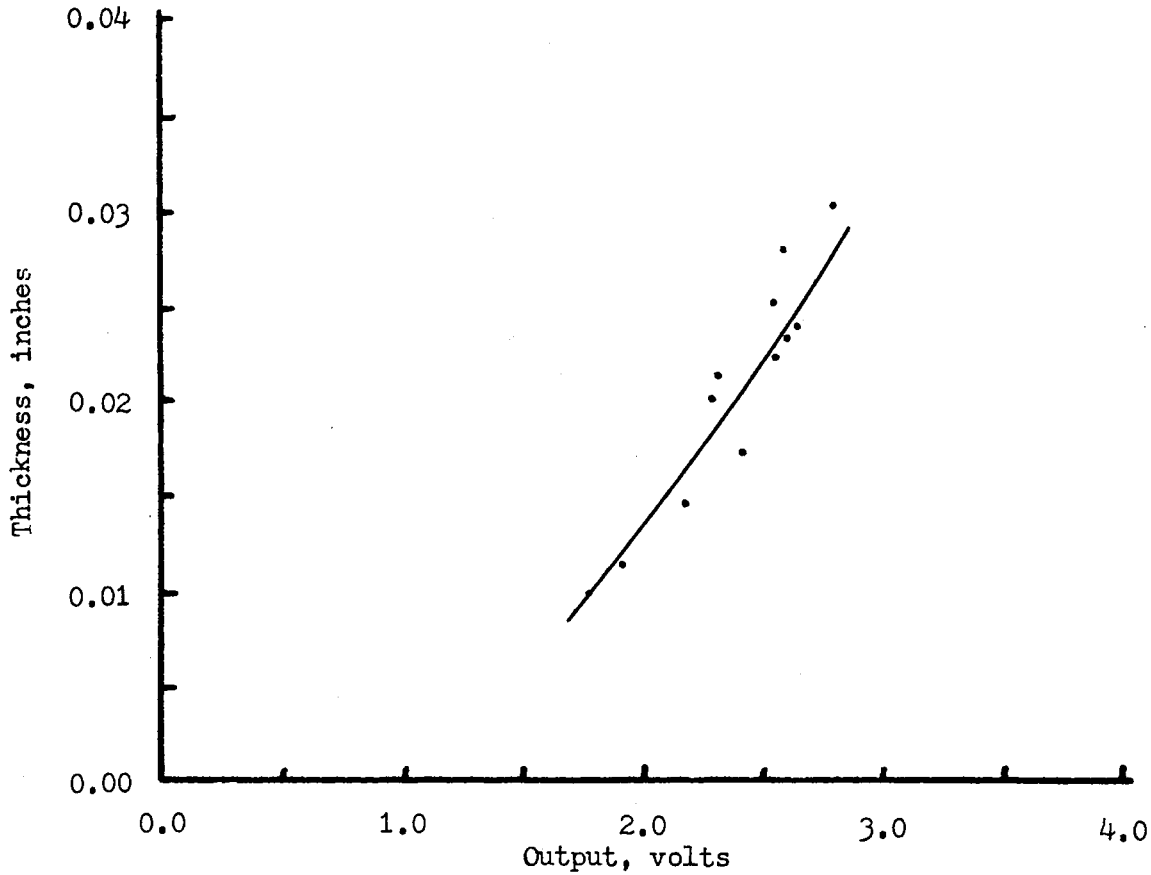

Figure 85. Depth Gauge Calibration Curve for Fluid F

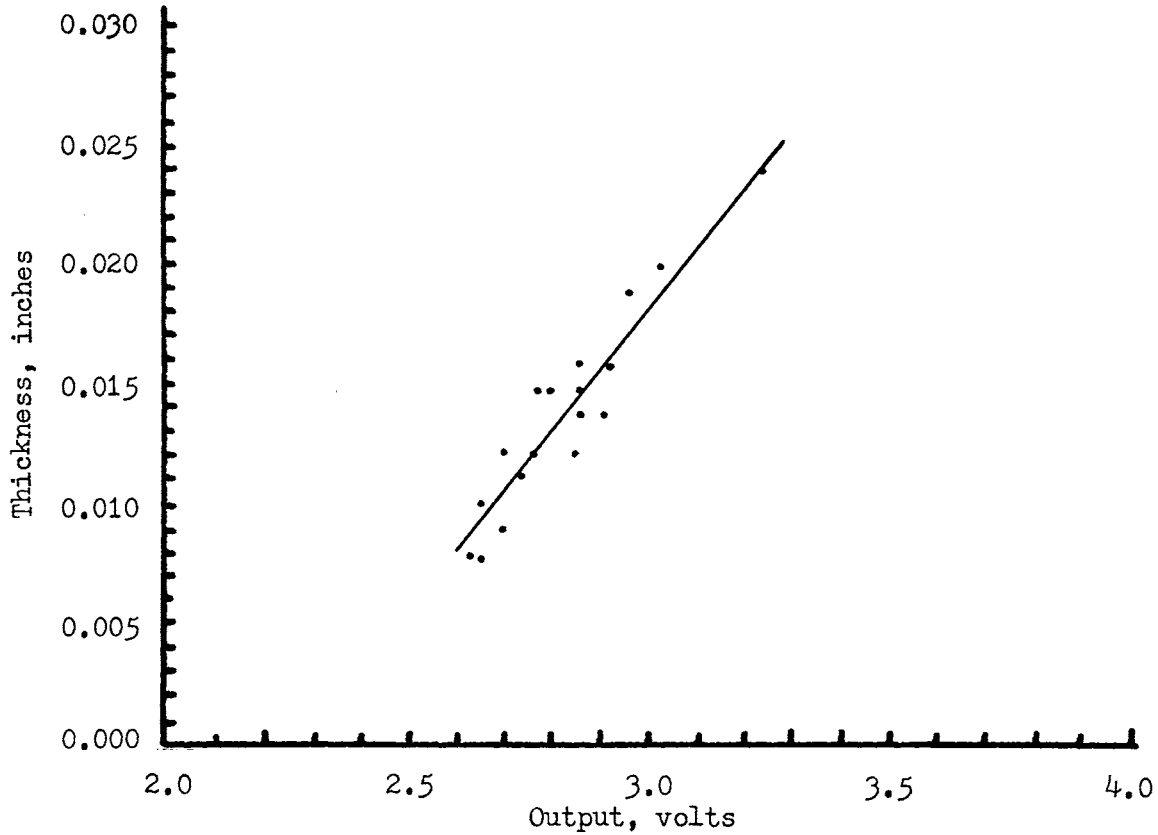

Figure 86. Depth Gauge Calibration Curve for Fluid E

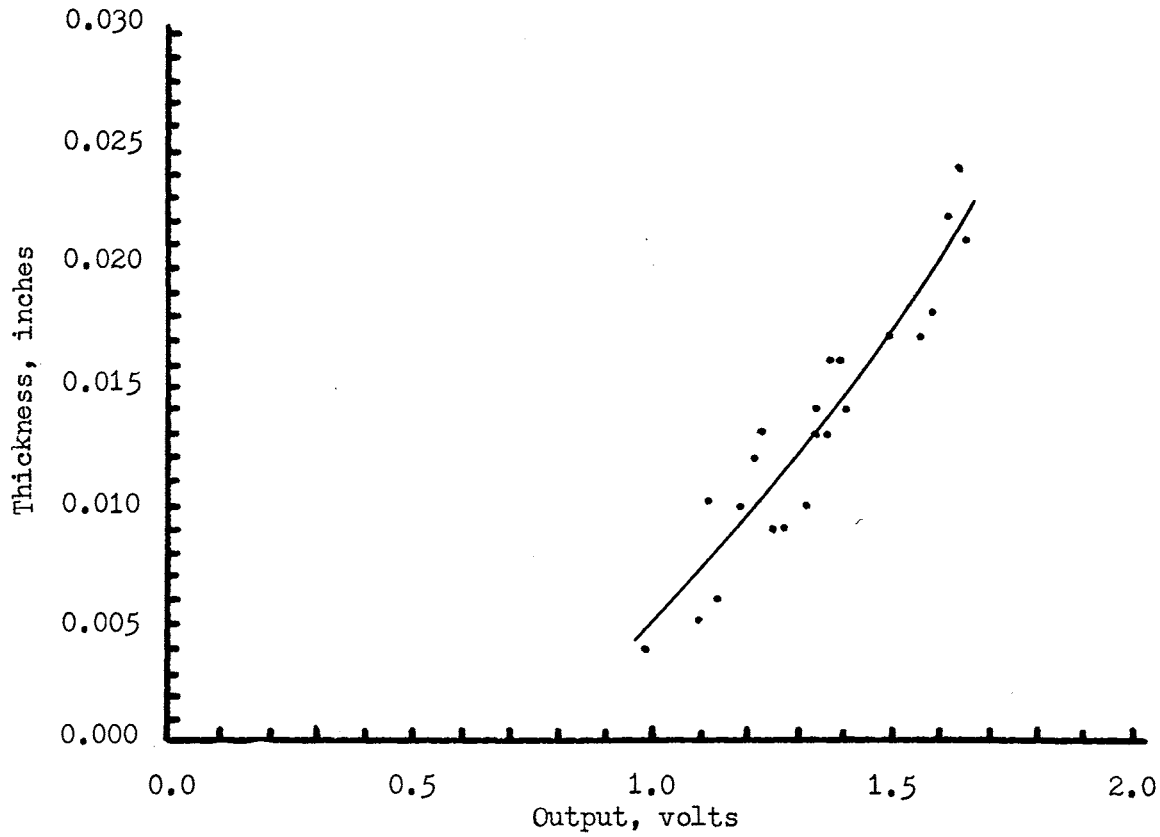

Figure 87. Depth Gauge Calibration Curve for Fluid D

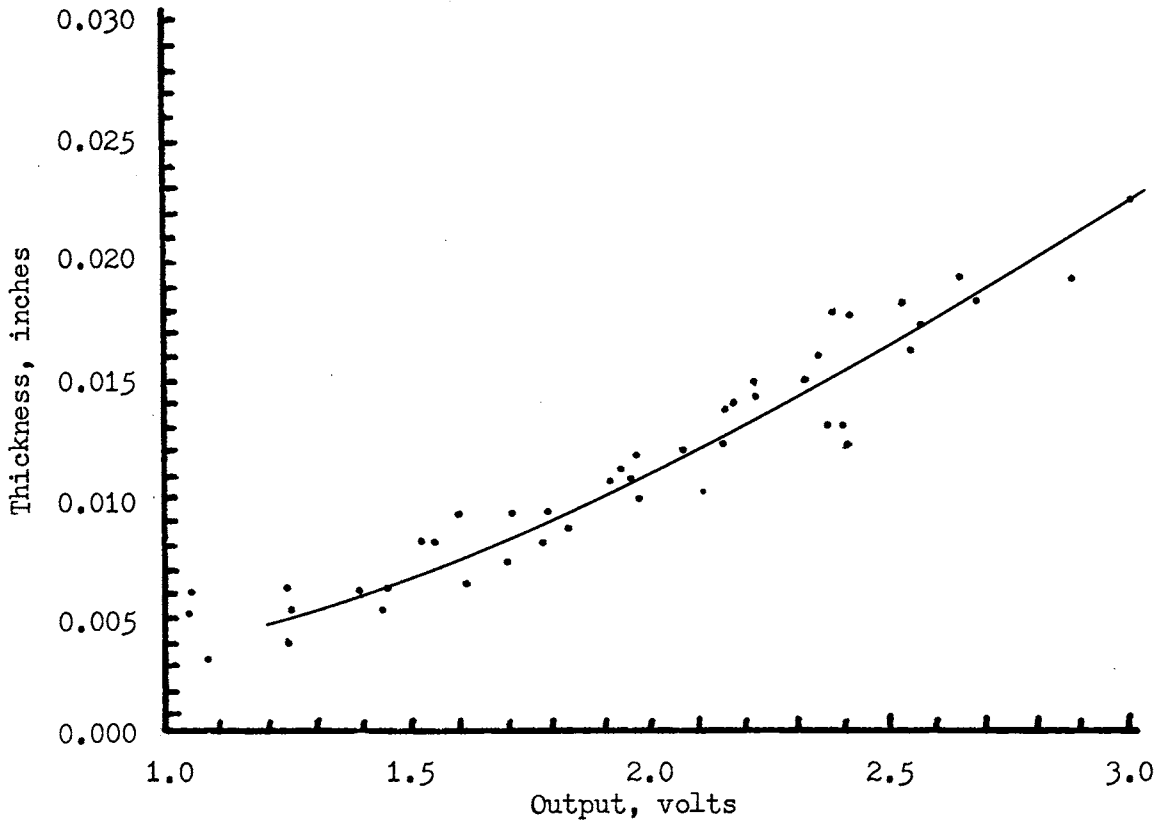

Figure 88. Depth Gauge Calibration Curve for Fluid C

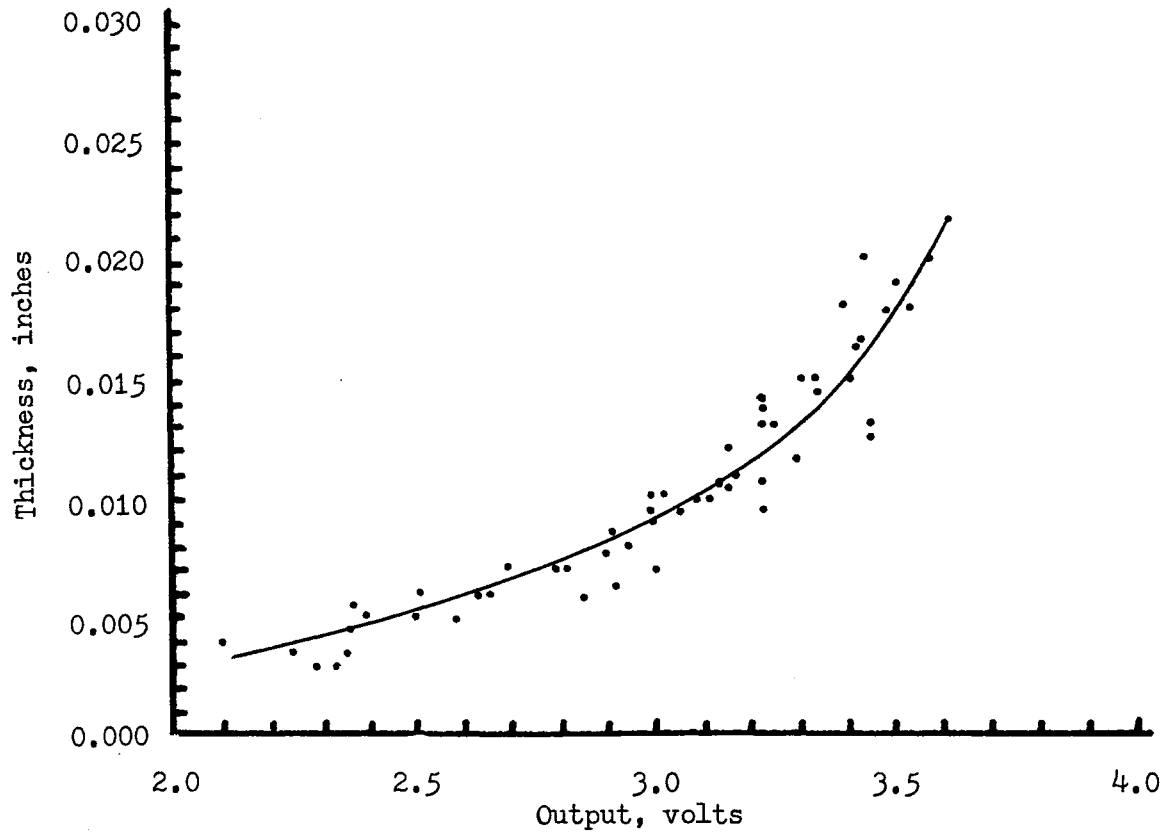

Figure 89. Depth Gauge Calibration Curve for Fluid B

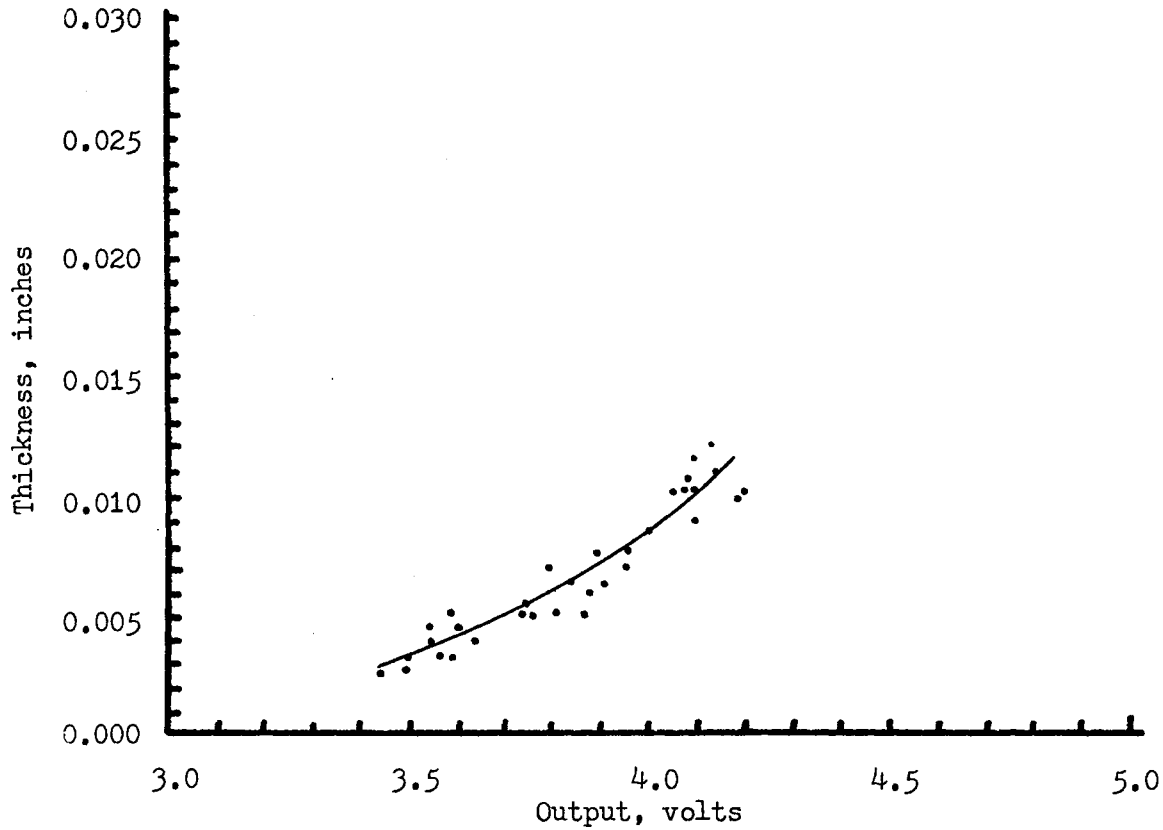

Figure 90. Depth Gauge Calibration Curve for Fluid A

of the actual operating temperature in view of the apparent temperature dependence both contribute to uncertainty in the depth gauge data.

APPENDIX D

DESCRIPTION OF THE LIQUID THICKNESS CALCULATION AND COMPARISON WITH THICKNESS MEASUREMENT

The velocity profile in the liquid and the film thickness are determined using three sequential numerical calculations. First, the pressure distribution on the model is calculated; second, the properties of the gas boundary layer are calculated; and third, the properties of the liquid film are calculated.

The pressure distribution on the model is determined by combining the results of two calculation techniques--one for the subsonic flow in the stagnation region of the model and the other for the supersonic flow about the afterbody of the model. In the subsonic region the numerical technique described by Moretti and Bleich (1967) was utilized. The elliptic equations for this region are converted to hyperbolic equations by assuming a time dependent solution. For the given body shape and free stream conditions, the conditions throughout the shock layer and the shock shape are assumed. A two-term Taylor expansion about time t_0 is performed and the properties are calculated for time $t_0 + \Delta t$ using the explicit numerical scheme. The calculations are continued until the properties at all points throughout the region have reached a steady state condition. The calculations are performed throughout the subsonic region and are extended past the sonic line to provide initial conditions for the supersonic flow calculations on the afterbody.

In the supersonic region a standard method of characteristics technique is used. In particular the program developed by Rakich (1964) is used. Eaton (1969) has compared the pressure distribution determined by these techniques with some experimental data for a Mach number of 5.25 and concluded that the data were in agreement to within 12 percent. The calculated pressure distribution for each of the three tunnel conditions is shown in Figure 91.

With the pressure distribution determined in this manner and the nominal tunnel conditions, the gas boundary layer properties are calculated using a numerical method for the solution of non-similar, laminar, compressible boundary layers. Multi-component laminar boundary layer equations are solved using an integral-matrix technique as described by Kendall and Bartlett (1968). In this method no similarity assumptions are made in the transformation applied to the equations and the non-similar terms remain. The series of algebraic relations produced are solved by general Newton-Raphson iteration which proceeds until the error terms in the momentum, energy and species equations are less than some prescribed acceptable limit. A thermal boundary condition of the model--such as constant temperature or an adiabatic wall--is assumed to provide the boundary condition for the energy equation which is solved as a part of the boundary layer solution. Kendall and Bartlett examine the accuracy of the calculations by comparison of the shear function profiles with available results for incompressible and compressible similar boundary layers with various positive and negative pressure gradients. Comparisons are also made with non-similar incompressible boundary-layer problems with uniform blowing and uniform sunction on a flat plate. For all comparisons

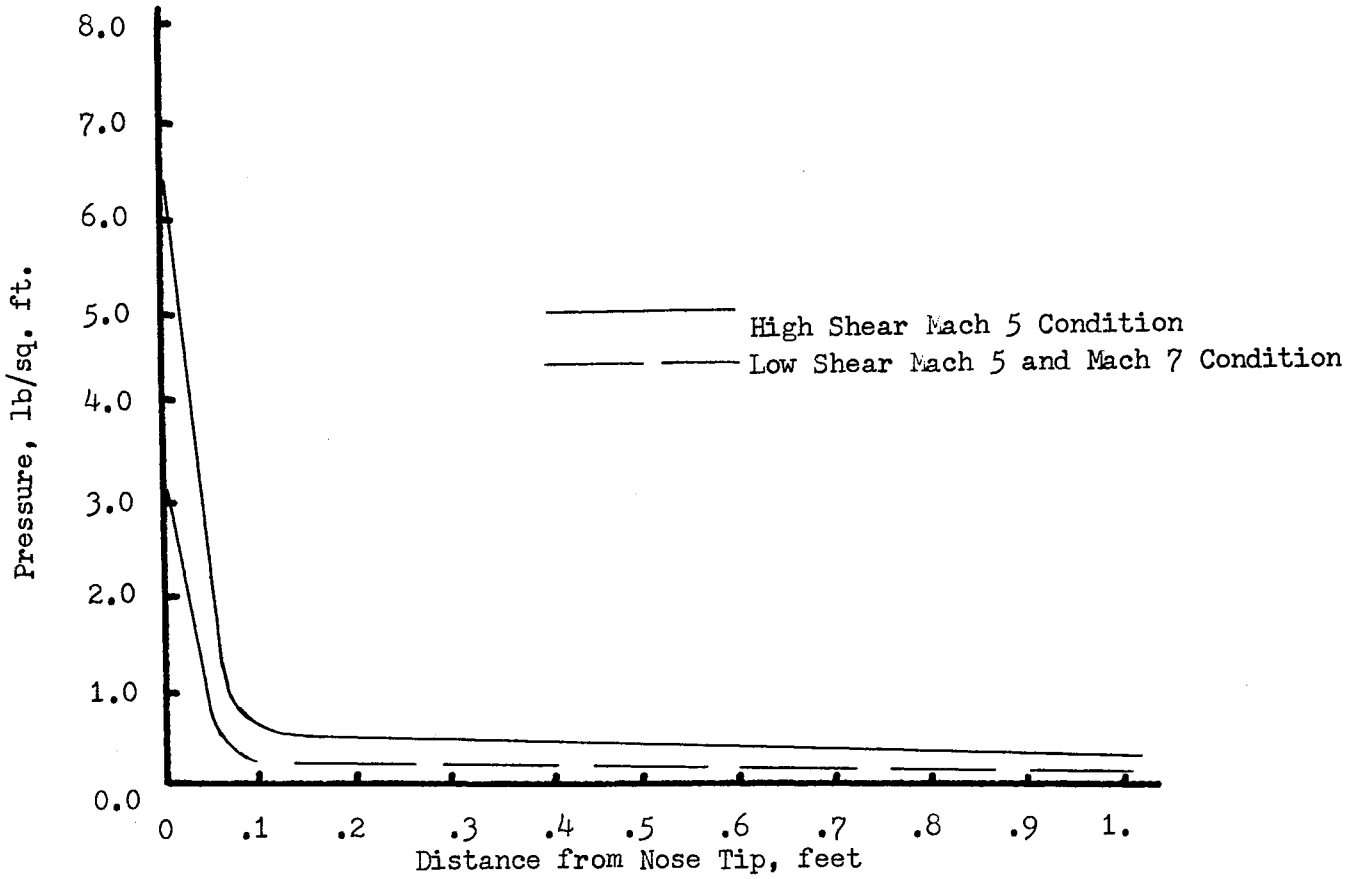

Figure 91. Calculated Pressure Distribution on Model

favorable results are found. For each of the three gas conditions and the previously calculated pressure distributions, the boundary layer conditions, including the shear parameter evaluated at the wall, are calculated. Figure 92 presents the calculated shear stress distribution on the model surface for each of the three gas conditions assuming no mass transfer at the interface.

The final calculation in the series is that which determines the properties and parameters of the liquid film. The calculation for these parameters is essentially the same as that utilized for the gas boundary layer calculations. The method is modified to include the incompressible liquid film and the pressure and shear stress distributions as boundary conditions at the liquid interface. The proper flow rate is injected through the model surface at the position corresponding to the porous section of the nose tip. Variable liquid properties as well as vaporization from the gas-liquid interface are considered. The liquid film thickness and the velocity profile in the liquid are calculated as a function of the position along the model surface.

In addition to this calculation the thickness was also measured with the depth gauge. In the tables of data presented in Chapter III both the calculated and measured values are presented. A comparison of the two quantities indicates generally satisfactory agreement and one is tempted to conclude that the results of each of the methods verify the other. However, an examination of factors affecting the accuracy of each of the two independently determined pieces of data is necessary for their proper interpretation.

The calculated thickness data are the result of three sequential numerical calculations as just described. The ultimate accuracy of the

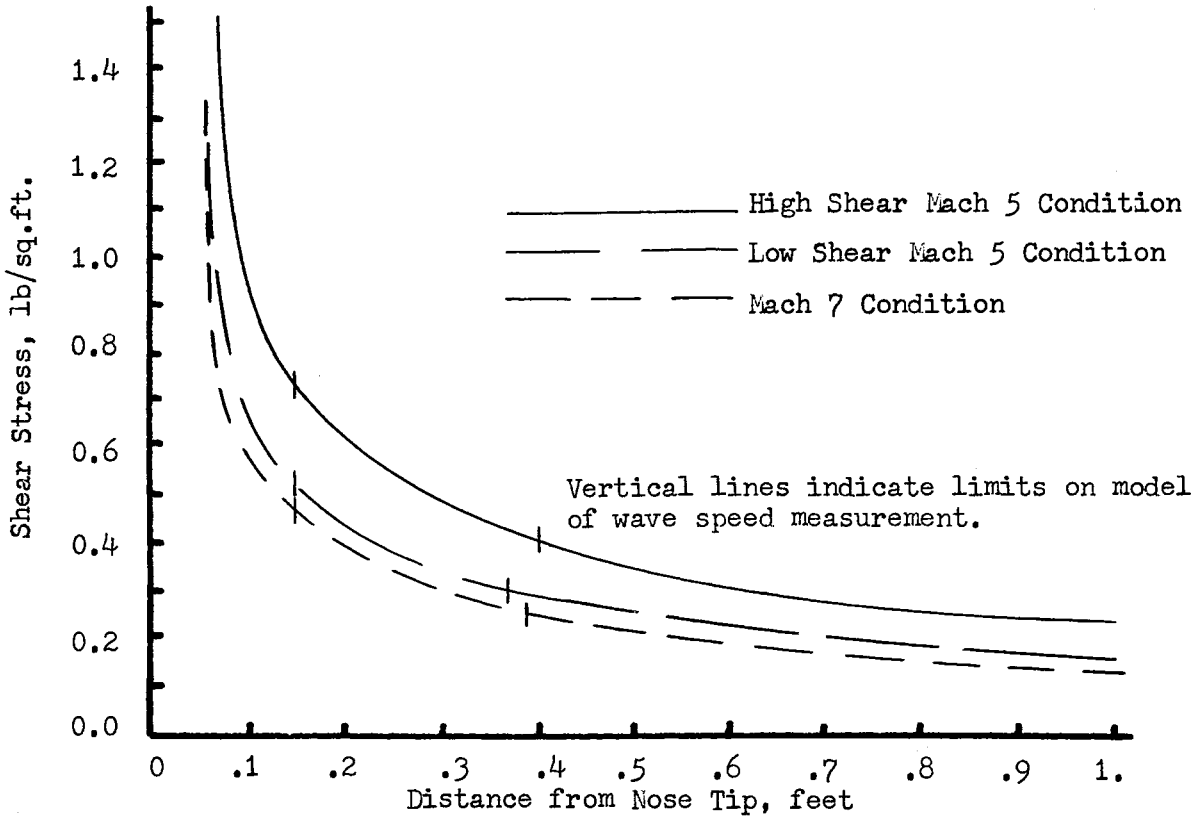

Figure 92. Calculated Shear Distribution on Model

liquid thickness and interface velocity determined using these composite calculations has not been verified. Certain factors which can affect the accuracy of the calculations as they are utilized in these experiments should be discussed. The calculations for the runs using 100 percent water are made by first making the gas boundary layer calculations for gas over water with no effects of the interface waves included in the calculations. The shear stress distribution and mass transfer across the interface are calculated. However, for all other glycerin-water mixtures the boundary layer calculations are made assuming gas flow over a solid surface and with the model at an assumed constant temperature. No mass transfer across the interface is included due to the lack of accurate thermochemical property data for the various mixtures.

An additional factor is that the gas is assumed to undergo an isentropic expansion along the model surface. A comparison between the calculated properties resulting from an isentropic expansion and those from a non-isentropic expansion for a 5-degree cone revealed a negligible difference between the shear stress levels. However, the isentropic expansion assumption should be included as a possible source of inaccuracy for the wedge model.

For the liquid calculations the physical properties of the liquid are assumed constant at the measured temperature for each run. The temperature gradient across the liquid is not known and any inaccuracy resulting from the constant temperature assumption is therefore unknown. In addition no vaporization from the liquid interface is included for any calculations except the water runs. Since water has a higher vapor pressure than glycerin, it can be hypothesized that water

evaporates from the films of water-glycerin mixtures and a thinner film results together with a variation in the properties (particularly the viscosity). The combined uncertainty in temperature and liquid composition can alter the properties sufficiently to cause some inaccuracy in the resulting calculations.

The measured thickness values depend directly upon the accuracy of the gauge calibration. The calibration curves shown in Appendix C for the six different fluids were determined at nominal measured test temperatures. For each curve the scatter in the calibration data produces a variation about the mean of approximately $\pm$ 25 percent. Consequently, the measured thickness must be considered to possess as a minimum this variation. When this scatter in the calibration is considered, the thickness measurements agree with the calculated values in the majority of the cases.

There are two additional known factors which can produce errors in the measured values. First, the variation of operating temperature will cause a shift in the gauge null and produce a voltage output. The high intensity lamps shining on the model for photographic lighting purposes were turned on approximately 45 seconds prior to the tunnel start and resulted in slight model heating. This null shift was accounted for in the data reduction but in all tests the model temperature varied during the run and no accurate means to remove this null variation was included in the system. The second factor which may affect the accuracy of the thickness measurement is the lack of calibration of the gauge with the original paint on the model. During the experiments it was necessary to remove the paint from the model and to apply a new coating of paint. The gauge was calibrated after the

experiments and consequently, no calibration with the original paint was performed. Since the gauge was renulled after the paint change, the paint change did not affect the null of the gauge; but any effect on the gauge sensitivity due to the paint change was not determined.

The measured thickness data are used throughout the data reduction in all instances where a thickness parameter is required. The choice of the measured rather than the calculated value is based on a comparison of the uncertainties inherent in each procedure which are discussed in the preceding paragraphs. Whereas the overall effects of the assumptions made in the series of calculations can not be assessed in a quantitative sense, the $\pm$ 25 percent variation assigned to the measured data is based on repeated calibration of the gauge. While the calibrations were not performed in the actual dynamic test environment, they represent measurements taken on different days with the bridge system balanced as in the experiments and the gauge operating at the measured nominal test temperature.

APPENDIX E

CALCULATION OF UNCERTAINTIES RESULTING FROM USE OF MEASURED DATA IN CALCULATIONS

As in any experimental study the data measured and presented herein are subject to the various uncertainties of imprecise measurement. In particular the flow rate, wave speed, and the thickness are measured and used in the data reduction and analysis. In order to reflect the expected accuracy of the measurements together with any subsequent effect on the conclusions, an analysis of the uncertainties is performed. The procedure described by Kline and McClintock (1953) was used.

In the data reduction dimensionless wave speed was calculated using the relationship

$$C = \frac{U_w}{2\,Q\,/\,hl}$$

where U_w is the wave speed, Q is the liquid flow rate, l is the model width, and h is the liquid thickness. Kline and McClintock show that the second power equation

$$S_c = \left[\frac{\partial C}{\partial U}(S_u)^2 + \frac{\partial C}{\partial Q}(S_q)^2 + \frac{\partial C}{\partial h}(S_h)^2 \right]^{\frac{1}{2}} \qquad (25)$$

may be used to calculate the uncertainty interval for the dimensionless wave speed C. In this equation S_c is the uncertainty in the resulting wave speed and S_u, S_q, and S_h are the uncertainties in the measured

wave velocity, flow rate and thickness respectively. This equation may be normalized using the equation for the dimensionless wave speed with the results

$$\frac{S_c}{C} = \left[\left(\frac{S_u}{U_w}\right)^2 + \left(\frac{S_q}{Q}\right)^2 + \left(\frac{S_h}{h}\right)^2\right]^{\frac{1}{2}}$$

where the indicated partials have been performed. To illustrate the calculation, consider the following conditions. For the condition of a liquid Reynolds number equal to 54 shown in Table IV, the following presents a description of the measured variables together with the associated expected uncertainties in each parameter.

$Q = 27.6$	$S_q = 1.4$
$U_w = 4.0$	$S_u = 0.5$
$h = 0.016$	$S_h = 0.004$

Substituting these values into the foregoing equation, one obtains

$$\frac{S_c}{C} = \left[\left(\frac{.5}{4}\right)^2 + \left(\frac{1.4}{27.6}\right)^2 + \left(\frac{.004}{.016}\right)^2\right]^{\frac{1}{2}}$$

$$\frac{S_c}{C} = \left[.0156 + .00257 + .0625\right]^{\frac{1}{2}}$$

$$\frac{S_c}{C} = 28.4\%$$

Consequently, the dimensionless wave speed, including the uncertainty, is $C = 1.32 \pm .37$. This calculation was made for each of the experiments at the three gas conditions and the results are included in Tables IV, VII, and X.

APPENDIX F

CALCULATION OF MEAN WAVE SPEED

The wave speed data were determined by measuring the wave displacement in a known time interval on the 35 mm film. Numerous wave speeds were measured in this fashion and the mean wave speed was calculated by computing the arithmatic average of these data. In order to evaluate the degree to which this calculation represents a true statistical mean for the data, the measurements were repeated for selected cases with different size samples and the resulting means compared. The analysis utilized to determine if the calculated value represents the true mean is the standard hypothesis test of the assumption that the means for unequal sample sizes are equal. This comparison is given by Snedecor and Cochran (1968). The comparison is made by calculating the t-statistic with the relationship

$$t = \frac{\bar{X}_1 - \bar{X}_2}{s_{\bar{X}_1 - \bar{X}_2}}$$

where $\bar{X}_1$ and $\bar{X}_2$ are the calculated sample means and $s_{\bar{X}_1 - \bar{X}_2}$ is the variance of the difference in the means given by

$$s_{\bar{X}_1 - \bar{X}_2} = \left[s^2 \frac{n_1 + n_2}{n_1 n_2}\right]^{\frac{1}{2}} .$$

The sample sizes are n_1 and n_2 and s^2 is the pooled variance of the two

samples. The calculated t value is compared with tabulated values to test the hypothesis of equal means.

For the low shear Mach 5 run which produced a Reynolds number of 54 as shown in Table IV, the two samples produced the following results.

$$n_1 = 40 \qquad n_2 = 87$$

$$\bar{X}_1 = 4.42 \text{ fps} \qquad \bar{X}_2 = 4.28 \text{ fps}$$

The calculated quantities are for 125 degrees of freedom

$$s^2 = .1717$$

$$s_{\bar{X}_1 - \bar{X}_2} = .0792$$

$$t = \frac{.14}{.0792} = 1.766$$

From tables given in Snedecor and Cochran, the probability of a t-statistic this large if the means are equal is P = .08. Therefore, there is a 1 in 12 chance that a calculated mean difference of this size will occur if the means are in fact equal. A 95% confidence interval on the difference in the means of the two samples is

$$-.016 \leq \bar{X}_1 - \bar{X}_2 \leq .296 .$$

For the low shear Mach 5 run which produced a Reynolds number of 30 shown in Table IV, the two samples produced the following results

$$n_1 = 39 \qquad n_2 = 70$$

$$\bar{X}_1 = 4.296 \qquad \bar{X}_2 = 4.233$$

The calculated quantities are for 107 degrees of freedom

$$s^2 = 0.2084$$

$$s_{\bar{X}_1 - \bar{X}_2} = 0.0912$$

$$t = 0.702$$

A probability of a t-statistic this large for equal means is P = 0.49 which amounts to a 1 in 2 chance that the sample means would differ by this amount if they represent the same means. The 95% confidence interval on the difference of the means is

$$-0.009 \leq \bar{X}_1 - \bar{X}_2 \leq 0.025.$$

For the high shear Mach 5 run which produced a Reynolds number of 21 shown in Table XI, the two samples produced the following results

$$n_1 = 22 \qquad n_2 = 48$$

$$\bar{X}_1 = 5.957 \qquad \bar{X}_2 = 5.95 \ .$$

The calculated quantities are for 68 degrees of freedom

$$s^2 = 0.269$$

$$s_{\bar{X}_1 - \bar{X}_2} = 0.1335$$

$$t = 0.0524 \ .$$

The probability of a t-statistic this large for equal means is essentially P = 1.0. The 95% confidence interval on the difference in the means is

$$-0.26 \leq \bar{X}_1 - \bar{X}_2 \leq 0.274 \ .$$

The general conclusion from these three comparisons is that the smaller sample size satisfactorily represents the true statistical mean of the wave speed.

An additional effect which may be examined is the relationship between the measured wave speed and the location of the wave on the model. This effect may be examined by utilizing a standard regression analysis technique such as that described in Chapter 6 of Snedecor and Cochran. The mathematical model for the regression analysis is

$$U_W = a + bx + E$$

where x is the distance along the model measured from the tip of the model in feet and U_W is the wave speed in feet per second. The measured data may be fit to the equation to estimate values of the constants a and b. The analysis also provides the means of testing the hypothesis that the coefficient of the variable x is zero and that the wave speed does not depend on the location of the wave. The test is made by calculating the t-statistic from the relationship

$$t = \frac{\hat{b} - 0}{s_b}$$

where $\hat{b}$ is the estimated value of b and s_b is the variance of the estimated value. Both parameters are calculated in the regression analysis and the resulting t value is compared with tabulated values to test the hypothesis that b is zero and to assign a significance level to the dependence of U_W on x.

An example will illustrate the procedure. The measured wave speeds as a function of the position on the model are analyzed for the

low pressure Mach 5 experiment which produced a liquid Reynolds number of 54 as shown in Table IV. The pertinent parameters which result from the regression analysis are

$$a = 4.53$$

$$b = -.937$$

$$t = .986$$

$$\text{degrees of freedom} = 85$$

The resulting relationship is

$$U_w = 4.53 - 0.937x$$

which shows that the wave speed decreases with distance. However, comparison of the calculated t-value reveals a significance level of 0.65 for the dependence of the wave speed on the location. Statistically speaking, this value is relatively low and suggests that a t value this large would result in about 1 out of every 3 samples even if the data were independent of x. The wave speed data for this example were measured at locations from 0.2 to 0.36 feet.

Additional experiments were analyzed to determine the dependency of the wave speed on the location and the results are given in Table XXXII. Included in the table is the location of the waves on the model for each of the examples.

Examination of the fitted equations and the significance levels illustrate the 'apparent' contradiction which exists in the data. Several equations reveal an increase in wave speed with distance while others reveal a decrease in the speed. For certain of these the significance level is high and for others relatively low with no association

of a high significance level noted for either the predicted increase or decrease in the wave speed.

TABLE XXXII

RESULTS OF REGRESSION ANALYSIS OF WAVE SPEED AND WAVE LOCATION

Gas Condition	Reynolds Number	Fitted Equation	Significance Level	Location of Data Measurement, feet
Low Shear Mach 5	1.0	U = 1.684 + .28x	0.5	.15 to .26
	1.8	U = -.034 + 4.2x	0.9	.16 to .24
	23.	U = 3.33 - .548x	0.5	.17 to .34
	54.	U = 4.53 - .937x	0.65	.2 to .36
	56.	U = 4.5 - 2.5x	0.975	.18 to .35
High Shear Mach 5	21.	U = 6.55 - 2.94x	0.8	.15 to .26
	60.	U = 4.0 + 5.014x	0.95	.17 to .4
Mach 7	126.	U = 3.78 + 1.25x	0.6	.19 to .38

The contradictions in the data are interpreted as resulting from the different wave speeds which occur on the interface. In some cases 'slow' waves are measured near the front and 'fast' waves are measured further back. For other runs the random wave selection resulted in the opposite. Because of this phenomena and due to the interaction effects of nearby waves, the data are interpreted only as mean data which illustrate the interface behavior for mean gas conditions.

Figure 92 reproduces the calculated shear stress distribution for the three gas conditions for the section of the model on which the wave speed data were taken. Shown by brackets on each gas condition are the limits of the model for which data was taken. From this the variation in shear stress over the sampled distance is apparent and one could anticipate some effect on the wave speed. For the reasons discussed the data are interpreted as mean wave speeds.

VITA

Billy Wayne Marshall

Candidate for the Degree of

Doctor of Philosophy

Thesis: AN EXPERIMENTAL INVESTIGATION OF A LIQUID FILM ON A HORIZONTAL FLAT PLATE IN A SUPERSONIC GAS STREAM

Major Field: Mechanical Engineering

Biographical:

Personal Data: Born in Magnolia, Arkansas, July 22, 1936, the son of Mr. and Mrs. J. F. Marshall.

Education: Graduated from Magnolia High School, Magnolia, Arkansas, in May, 1954; attended Southern State College in Magnolia, Arkansas, in 1954 and 1955; received the Bachelor of Science degree from Louisiana State University in 1958 with a major in Mechanical Engineering; received the Master of Science degree from the University of Missouri at Rolla in 1961 with a major in Mechanical Engineering; completed requirements for the Doctor of Philosophy degree at Oklahoma State University in May, 1971.

Professional Experience: Engineer, McDonnell Aircraft Company, Summer 1958; Instructor in Mechanical Engineering, University of Missouri at Rolla, 1958-1961; Engineer, Aluminum Company of America, Summer, 1960; Staff Member, Sandia Laboratories, 1961-present.